Final Report
October 2001 – August 2006

SOLID STATE ENERGY CONVERSION ALLIANCE (SECA)
SOLID OXIDE FUEL CELL PROGRAM

Performed under DOE/NETL Cooperative Agreement
DE-FC26-01NT41245

Submitted to
United States Department of Energy
National Energy Technology Laboratory
Pittsburgh, PA

GE Energy

Hybrid Power Generation Systems

19310 Pacific Gateway Drive

Torrance, CA 90502

DISCLAIMER

ABSTRACT

This report summarizes the work performed for Phase I (October 2001 – August 2006) under Cooperative Agreement DE-FC26-01NT41245 for the U. S. Department of Energy, National Energy Technology Laboratory (DOE/NETL) entitled “Solid State Energy Conversion Alliance (SECA) Solid Oxide Fuel Cell Program”. The program focuses on the development of a low-cost, high-performance 3-to-10-kW solid oxide fuel cell (SOFC) system suitable for a broad spectrum of power-generation applications. During Phase I of the program significant progress has been made in the area of SOFC technology. A high-efficiency low-cost system was designed and supporting technology developed such as fuel processing, controls, thermal management, and power electronics. Phase I culminated in the successful demonstration of a prototype system that achieved a peak efficiency of 41%, a high-volume cost of $724/kW, a peak power of 5.4 kW, and a degradation rate of 1.8% per 500 hours. . An improved prototype system was designed, assembled, and delivered to DOE/NETL at the end of the program. This prototype achieved an extraordinary peak efficiency of 49.6%.

TABLE OF CONTENTS

ABSTRACT iii
TABLE OF CONTENTS iv
TABLE OF ABBREVIATIONS v
EXECUTIVE SUMMARY vi
1 INTRODUCTION 1
2 OVERVIEW 1
EXPERIMENTAL APPROACH, RESULTS AND DISCUSSION BY TASK 2
3 SYSTEM DESIGN AND ANALYSIS 2
4 COST ESTIMATE 18
5 STACK DEVELOPMENT 46
6 FUEL PROCESSING 66
7 CONTROL SYSTEM DEVELOPMENT 112
8 THERMAL MANAGEMENT SUBSYSTEM 133
9 ELECTRICAL SYSTEM 142
10 PROTOTYPE ASSEMBLY 155
11 PROTOTYPE TEST 164
12 NETL PROTOTYPE 199
13 CONCLUSIONS 215

TABLE OF ABBREVIATION

ASR:	Area Specific Resistance
ATR:	Autothermal Reforming
BOM:	Bill of Materials
BOP:	Balance of Plant
CFD:	Computational Fluid Dynamics
CPOX:	Catalytic Partial Oxidation
CSD:	Conceptual System Design
CTE:	Coefficient of Thermal Expansion
CTQ:	Critical to Quality
DC:	Direct Current
DFP:	Design for Performance
DFR:	Design for Reliability
DFSS:	Design for Six Sigma
DOE:	United States Department of Energy
DOE:	Design of Experiments
DTC:	Design to Cost
FMEA:	Failure Mode and Effects Analysis
GE:	The General Electric Company
GE-EER:	GE Energy and Environmental Research
GE HPGS:	GE Hybrid Power Generation Systems
GEPS:	GE Power Systems
GR&R:	Gage Repeatability and Reproducibility
IPD:	Ion Plasma Deposition
LSL:	Lower Specification Limit
LSM:	Lanthanum Strontium Manganite
NETL:	DOE National Energy Technology Laboratory
OCV:	Open Circuit Voltage
PID:	Proportional-Integral-Derivative Control
POX:	Partial Oxidation
PSD:	Prototype System Design
QC:	Quality Control
QFD:	Quality Function Deployment
RBD:	Reliability Block Diagram
S/C:	Steam-to-Carbon Ratio
SEM:	Scanning Electron Microscope
SOFC:	Solid Oxide Fuel Cell
SR:	Steam Reforming
USL:	Upper Specification Limit
YSZ:	Yttria-stabilized Zirconia

EXECUTIVE SUMMARY

This report summarizes the work performed for Phase I (October 2001 – September 2005) under Cooperative Agreement DE-FC26-01NT41245 for the U. S. Department of Energy, National Energy Technology Laboratory (DOE/NETL) entitled "Solid State Energy Conversion Alliance (SECA) Solid Oxide Fuel Cell Program". The program focuses on the development of a low-cost, high-performance 3-to-10-kW solid oxide fuel cell (SOFC) system suitable for a broad spectrum of power-generation applications. The overall objective of the program is to demonstrate a modular SOFC system that can be configured to create highly efficient, cost-competitive, and environmentally benign power plants tailored to specific markets. When fully developed, the system will meet the efficiency, performance, life, and cost goals for future commercial power plants.

Phase I of the SECA program was extremely successful with major advances in SOFC technology made in the areas of performance, stack design, manufacturing, and power output. A high-efficiency low-cost system was designed and supporting technology developed such as fuel processing, controls, thermal management, and power electronics. Phase I culminated in the successful demonstration of a prototype system that achieved a peak efficiency of 41%, a high-volume cost of $724/kW, a peak power of 5.4 kW, and a degradation rate of 1.8% per 500 hours. All of the SECA minimum requirements were exceeded with the exception of transient cycle degradation. A summary of the Phase I results versus the SECA requirements are as follows:

PERFORMANCE PARAMETER	REQUIREMENTS	RESULTS
DC Efficiency	35%	41%
Estimated Cost	<$800/kW	$724/kW
DC Peak Power	3-10 kW	5.4 kW
Steady State Degradation	<2% per 500 hrs	1.8% per 500 hrs
Thermal cycle	1	3
Power Cycle	9	15
Cycle Degradation	<1%	1.8%
Availability	80%	90%
Test Time	1500 hrs	1720 hrs

An improved prototype system (75% reduction in system volume) was built and delivered to NETL. Preliminary testing of this prototype before delivery indicated an extraordinary peak efficiency of 49.6% with a net power output of 3.27 kW.

1 INTRODUCTION

This report summarizes the work performed during Phase I (October 2001 – August 2006) under Cooperative Agreement DE-FC26-01NT41245 for the U. S. Department of Energy, National Energy Technology Laboratory (DOE/NETL) entitled “Solid State Energy Conversion Alliance (SECA) Solid Oxide Fuel Cell Program”. The program focuses on the development of a low-cost, high-performance 3-to-10-kW solid oxide fuel cell (SOFC) system suitable for a broad spectrum of power-generation applications. The overall objective of the program is to demonstrate a modular SOFC system that can be configured to create highly efficient, cost-competitive, and environmentally benign power plants tailored to specific markets. When fully developed, the system will meet the efficiency, performance, life, and cost goals for future commercial power plants.

2 OVERVIEW

The SOFC system under development for Phase I of the SECA program is a 5 kW stationary power module targeted for residential applications. The system consists of all the required components for a self-contained unit, including fuel cell stack, fuel processing subsystems, fuel and oxidant delivery subsystem, thermal management subsystem, and various control and regulating devices. The system was designed to be modular and so that it can be integrated to form a larger system. Figure 2.1shows an example of the concept system.

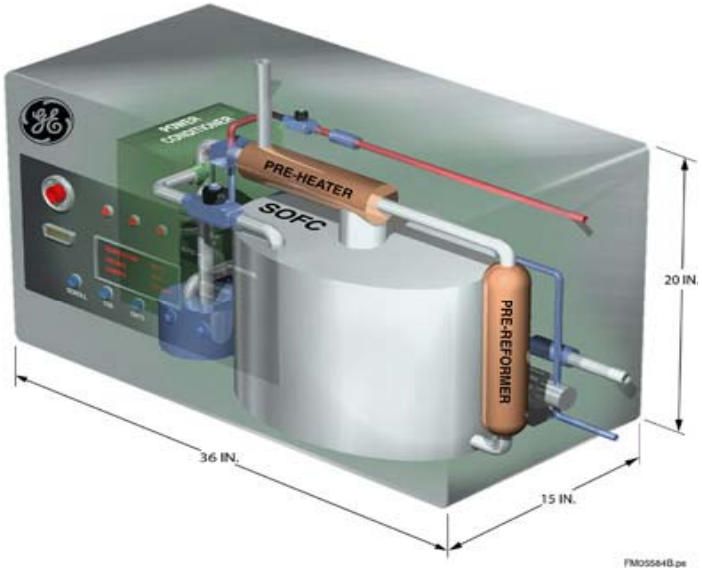

Figure 2.1 SECA System Concept

The general features of the SECA SOFC program are summarized in Figure 2.2. Phase I culminated in a demonstration of a modular SOFC system suitable for operation under different conditions. A specified application will be selected at the beginning of Phase II. Phase II will result in a demonstration of a packages system for the specified application. Phase III will result in field testing of a packaged system for the specified application for extended periods to demonstrate operating characteristics required for commercial power plants.

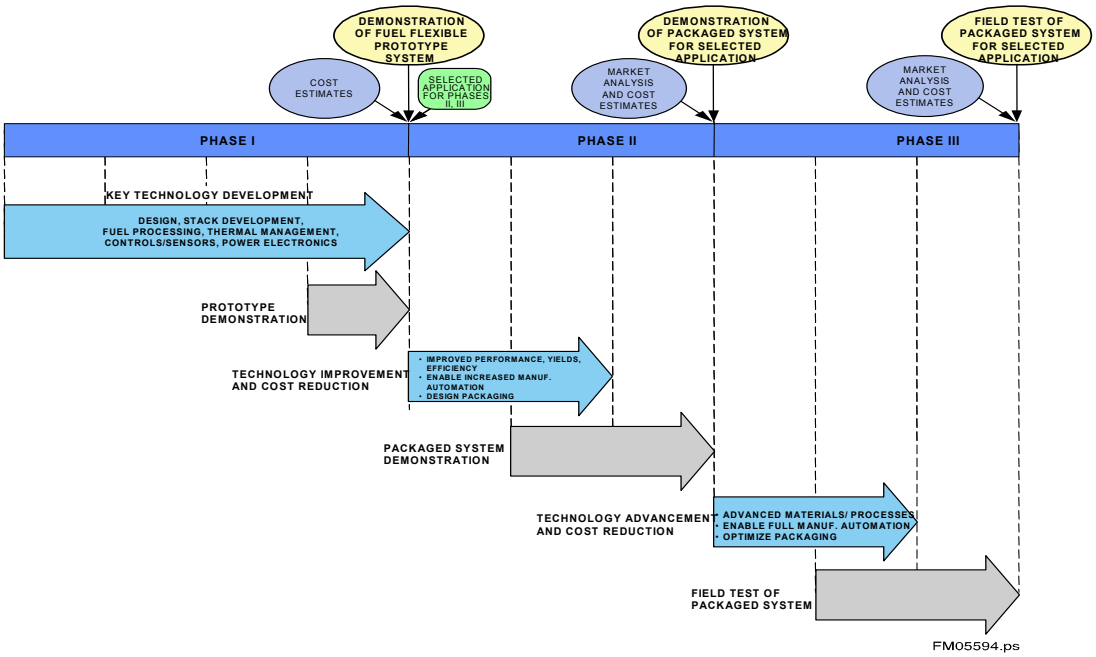

Figure 2.2 Key SECA Program Features

EXPERIMENTAL APPROACH, RESULTS AND DISCUSSION BY TASK

Each of the eight major subtasks will be discussed in detail covering the initial design and analysis through the final testing of the components in the prototype system. The results from the Phase I prototype system test will also be discussed and compared with the SECA minimum requirements.

3 SYSTEM DESIGN AND ANALYSIS

Throughout the course of the program, the Aspen Plus computer software was used to assist with system design and analysis. Aspen Plus system simulation models were developed to help predict flowrates, pressures, temperatures, and stream compositions throughout both the conceptual system design (CSD) and the preliminary system design (PSD). During both the conceptual system design and preliminary system design tasks, the Aspen models were primarily set-up to run in “design” mode (as opposed to “simulation”

mode), which essentially allowed component performance parameters to "float" in order to meet specified design criteria. For instance, the outlet temperature of air from the cold-side of the cathode air preheater is automatically adjusted by the model to meet a required stack operating temperature (inlet or outlet temperature specification). This method of setting up the Aspen simulation model is extremely useful in helping to identify the performance requirements of individual components.

3.1 CONCEPTUAL SYSTEM DESIGN DESCRIPTION

During the conceptual design, numerous design concepts were developed and trade studies conducted to evaluate these concepts on the basis of efficiency, cost, reliability, and technical risk within the four years of the Phase I program. The most promising design was then selected for further study during the preliminary design portion of the program. The design concept that was chosen was a simple-cycle system without recycles using an autothermal reformer (ATR) for pre-processing of the fuel prior to entering the anode of the fuel cell stack. The merits of this design will be discussed in greater detail in the following sections.

3.2 PRELIMINARY SYSTEM DESIGN DESCRIPTION

Figure 3.1 represents a simplified schematic of the system configuration selected for study during preliminary system design. Methane, air, and steam are supplied to an ATR fuel processor, which provides reformate to the stack. The air and steam lines to the ATR are pre-heated through the use of heating elements that extract heat from the stack's cathode-air exhaust line. Since sufficient preheating of these lines is expected, the integral heat exchanger originally specified for the ATR fuel processor was removed. The preheat air line contains a bypass line thereby allowing a method of controlling the temperature of the mixed stream entering the ATR fuel processor. Preheating within the steam line is accomplished by using a vaporizer placed immediately downstream of the cathode air preheater and a superheater placed upstream of the combustor.

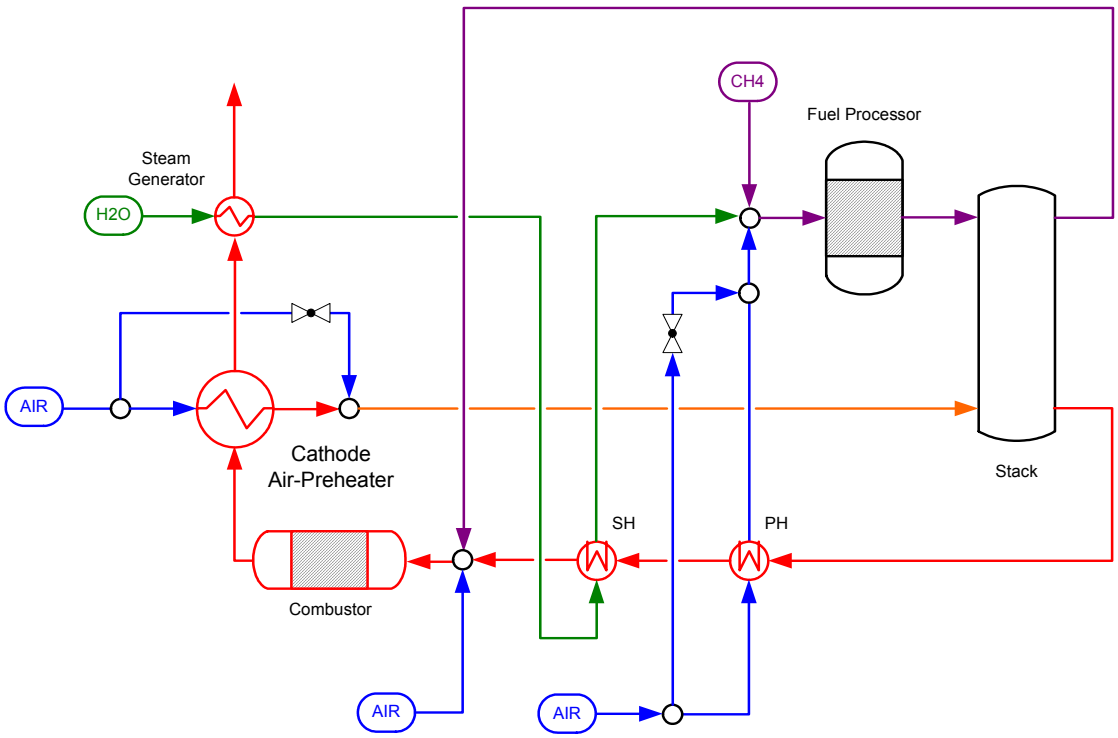

Figure 3.1 Simplified system schematic.

The cathode air-preheater recuperatively heats the inlet air to the stack (cathode side) by using the heat contained within the stack's cathode exhaust line. A combustor is placed directly upstream of the hot side of the cathode air preheater to recover heat from any remaining unburned combustibles in the exhaust stream, thereby raising the temperature difference across the hot and cold sides of the cathode air preheater.

3.2.1 Assumptions

Appropriate assumptions were developed and reviewed such as stack operating temperature, stack temperature rise, level of internal reforming, etc. The values chosen were representative values and should not be viewed as "default" operational setpoints. The results of this analysis were used as a guide when developing performance requirements to be included within component specifications.

3.2.2 Stack Operating Envelope

Single-cell test data was used early in the program to develop an "operating envelope" for the stack. The data from this single-cell test is shown in Figure 3.2. Of the data sets shown below, the data corresponding to a fuel utilization of 50% and a H_2 concentration of 64% (FU50%H64%) was chosen to

represent the upper voltage limit of stack performance. A lower voltage limit of 0.6 V was chosen for all current densities shown below.

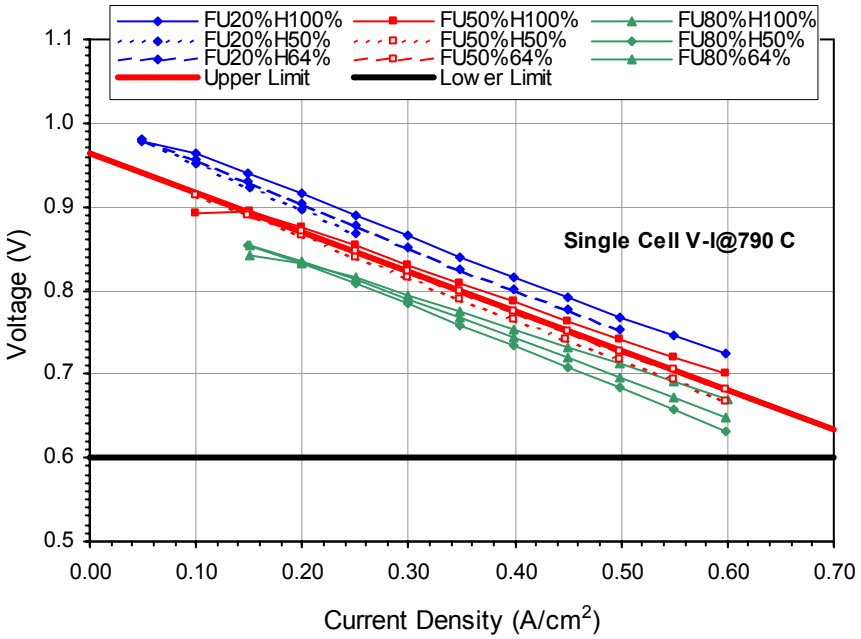

Figure 3.2 Single-cell test data used to set stack performance parameters.

Aspen analyses were completed over an entire range of current densities ranging from 0.1 to 0.6 A/cm^2. For analysis purposes, the operating voltage corresponding to any current density was set to values ranging from 0.6 V (minimum) up to the maximum voltage shown in Figure 3.2 for data set FU50%H64% (heavy line shown in red). For instance, at a current density of 0.3 A/cm^2, Aspen analyses were completed with operating voltages set to 0.6, 0.7, 0.8, and 0.83 volts. It is a general assumption that the actual operating voltage will fall within this range of values.

3.2.3 Performance Analysis Results

The performance analysis results provided ranges of expected flows, pressures, temperatures, etc. for the major components within the system. These results were used as a starting point for developing component specifications. It was not intended to be all inclusive, since certain components may require additional information to properly develop their component specifications.

3.3 COMPONENT CHARACTERIZATION

Component specifications created during the conceptual design phase of the program were reviewed for compatibility with the system performance results

(Section 3.2.3), and modified as appropriate. Specifications for longer lead-time components, which had been sourced during the conceptual design phase (i.e. main air compressor, cathode air preheater, inverter), were checked to ensure that they were still valid. In most cases, it was confirmed that previously written specifications for the longer lead-time components were still valid. In some cases, however, it was felt that the previously written specifications were overly conservative resulting in oversized equipment. In other cases, the opposite was true. In general, system performance estimates were updated to reflect any limitations of previously ordered components.

The information contained within Section 3.2.3 provided component owners with the necessary data to begin searching for components to be used for the prototype system. When component performance data became available, appropriate component models were developed to allow inclusion into Aspen. The inclusion of these component performance models into Aspen allowed Aspen to be run in "simulation" mode, where the performance of the system at "off-design" or "part-load" conditions can be assessed.

Much of the performance data used to characterize component performance was based directly on test data. This is true for the ATR fuel processor, the cathode air blower/compressor, the stack, and the inverter. In the absence of direct testing, component performance data was obtained from vendor supplied performance charts. In many cases (i.e. valves), these performance charts were developed from vendor laboratory testing. In other cases (i.e. heat exchangers), performance charts were developed from vendor proprietary computer programs. In the absence of either test data or vendor supplied performance charts, component performance estimates were based on the results from basic analysis techniques.

3.4 PROTOTYPE SYSTEM SIMULATION MODEL

As the program moved through the preliminary design stage and into the prototype development stage, Aspen models of the system were refined and updated. A simplified schematic of the prototype system, with all components laid out in their proper locations is shown below. It is noted that a catalytic burner was down-selected for the tail-gas combustor, and was modeled by Aspen as an equilibrium reactor. Compared to the schematic shown in Figure 3.1, the schematic below in Figure 3.3 incorporates a number of changes to the system layout, mainly to accommodate system packaging issues. These changes include; 1) elimination of a steam superheating section, 2) placement of the fuel processor air preheater downstream of the combustor, 3) elimination of quench air line prior to combustor.

A separate steam superheating section was eliminated since analysis determined that we could obtain sufficient superheat with the steam generator in its current location. The fuel processor air preheater consists of a coil wrapped around the catalytic combustor and may be considered integral to the combustor. From a modeling standpoint, the placement of the fuel processor air preheater

before, after, or integral to the combustor has almost negligible effect on system performance, therefore it's placement was for packaging convenience. Lastly, the quench air line prior to the combustor was eliminated. The purpose of this line was to provide supplemental cooling to the combustor to protect the catalyst from over-temperature conditions. Previous analysis limited combustor temperatures, but after consultation with the catalyst vendor it was determined that the combustor can tolerate a sufficiently high temperature to support this system design.

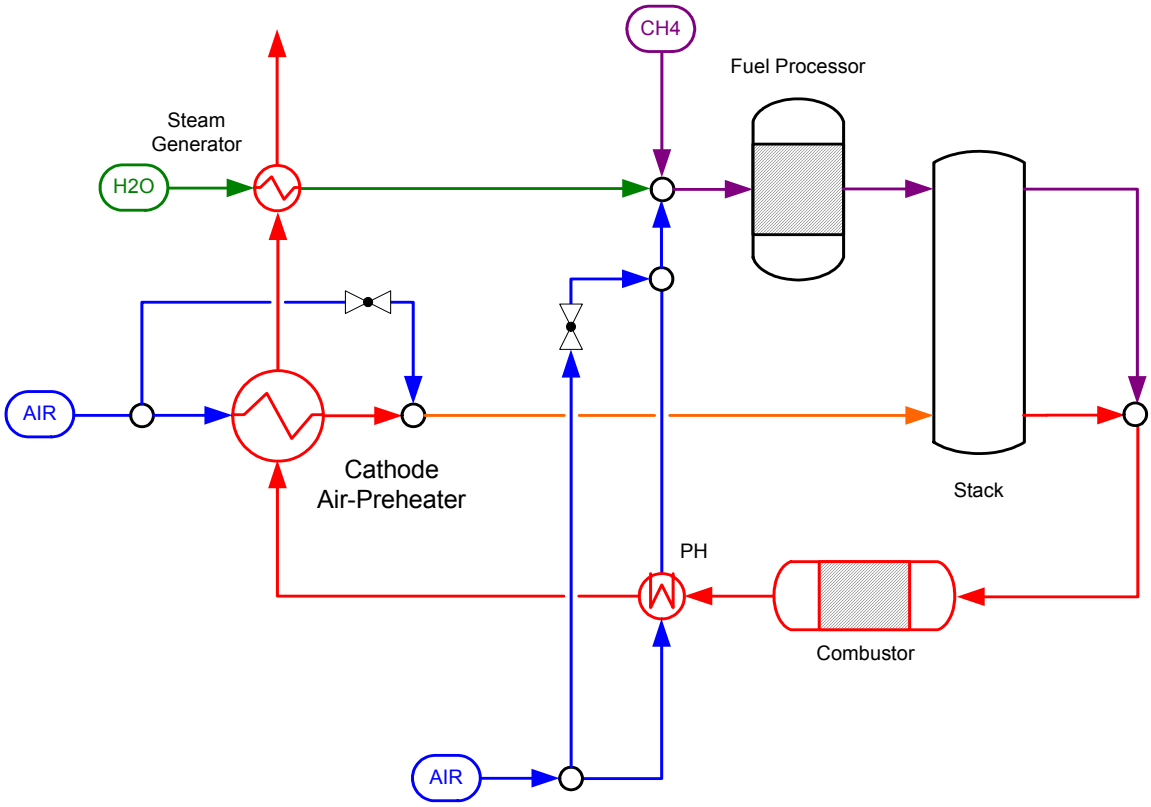

Figure 3.3 Simplified schematic of final prototype system.

3.5 PROTOTYPE SYSTEM TRADE STUDIES

A number of trade studies were completed to determine the sensitivity of the system to various operating parameters. The three primary parameters of interest include the cell operating voltage, cell current density, and fuel utilization. The figures below present the results from a number of these trade studies. These studies were completed to help answer "what-if" type questions regarding stack performance variations and to provide guidelines for setting stack performance targets. Additional studies were later completed, taking into account actual stack operating test data to provide projected system performance estimates.

Figure 3.4 shows the effect of cell voltage and current density on net system efficiency. Net system efficiency is defined as the net AC power

produced by the system divided by the LHV of the fuel delivered to the system. The results shown in Figure 3.4 were for a constant fuel utilization of 80%. The range of operating voltages at each current density is consistent with the values shown in the operating envelope of Figure 3.2.

The most significant result was the strong dependence of system efficiency on cell operating voltage and the apparent insensitivity of system efficiency to current density (for a particular operating voltage). This result is somewhat misleading, since in reality, operating voltage is strongly dependent on current density and higher operating voltages are expected at lower current densities. For instance, at a current density of 0.6, the maximum operating voltage within the "operating envelope" is 0.68. At a current density of 0.3, the maximum operating voltage within the "operating envelope" is 0.84.

From the figure below, it is clear is that, regardless of current density, a minimum operating voltage of about 0.66 (with a fuel utilization of 80%) was required if the prototype system was expected to meet or exceed 35% system efficiency. If the stack was able to achieve operating performance (i.e. operating voltage vs. current density) along the upper bounds of the operating envelope (Figure 3.2), a net system efficiency of 46% could be expected at a current density of 0.3. For the range of current densities shown, a 7% increase in system efficiency is expected for a 0.1 V increase in operating voltage. System performance is expected to deteriorate at current densities below 0.3 due to the increasing effects of stack enclosure heat loss on reducing stack temperature.

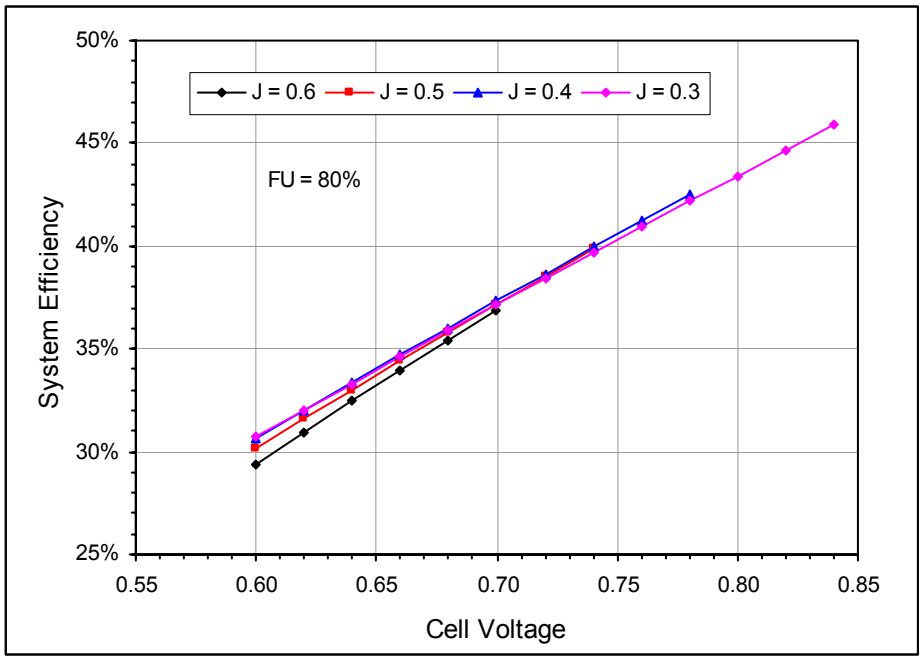

Figure 3.4 Effect of cell voltage on system efficiency.

Figure 3.5 shows the effect of cell voltage and current density on net system AC power. Net system AC power is defined as the amount of AC power available for external use, and is calculated after accounting for inverter losses and other parasitic power requirements (i.e. compressors, pumps, actuators, etc.) required by the system. At a current density of 0.6, the maximum operating voltage within the "operating envelope" is 0.68. If the stack was able to meet this operating condition, a peak power of 7800 Watts (net AC) could be expected from the system. The results are shown assuming a fuel utilization of 80%. Decreasing the fuel utilization will accordingly decrease the net AC power produced by the system.

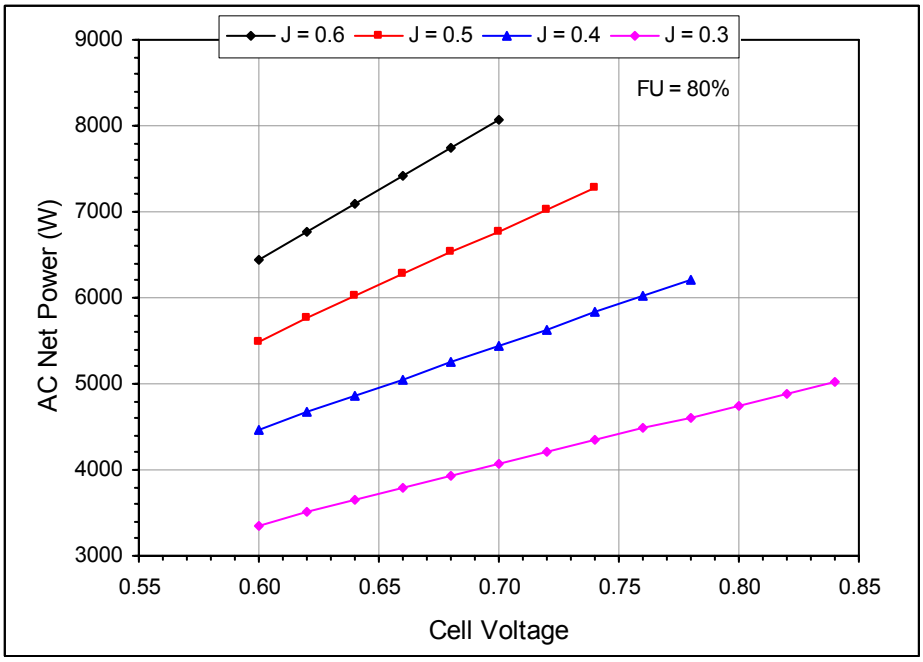

Figure 3.5 Effect of cell voltage on AC net power.

The analysis results of Figure 3.4 and Figure 3.5 clearly show how important it was to improve the stack operating performance if the system is expected to meet its target efficiency goals of 35%. The other major drivers that effect system efficiency are inverter losses and parasitic power consumption. Of the parasitic power consumption, the major loss is the cathode air delivery blower/compressor. Efforts were made during the duration of the program to minimize losses associated with both of these components.

From a system standpoint, minimization of the parasitic power consumption requirements was focused on minimizing the pressure drop throughout the system, which in turn, lowered the power requirements for the cathode air blower. All major components were evaluated with regards to their contribution to the overall system pressure drop, and where feasible, design efforts were made to lower their design pressure drop. Figure 3.6 shows early estimates for system pressure drop as a function of cell operating voltage and

current density at a constant fuel utilization of 80%. As expected, pressure drop is reduced as cell operating voltage increases due to decreasing air flow requirements.

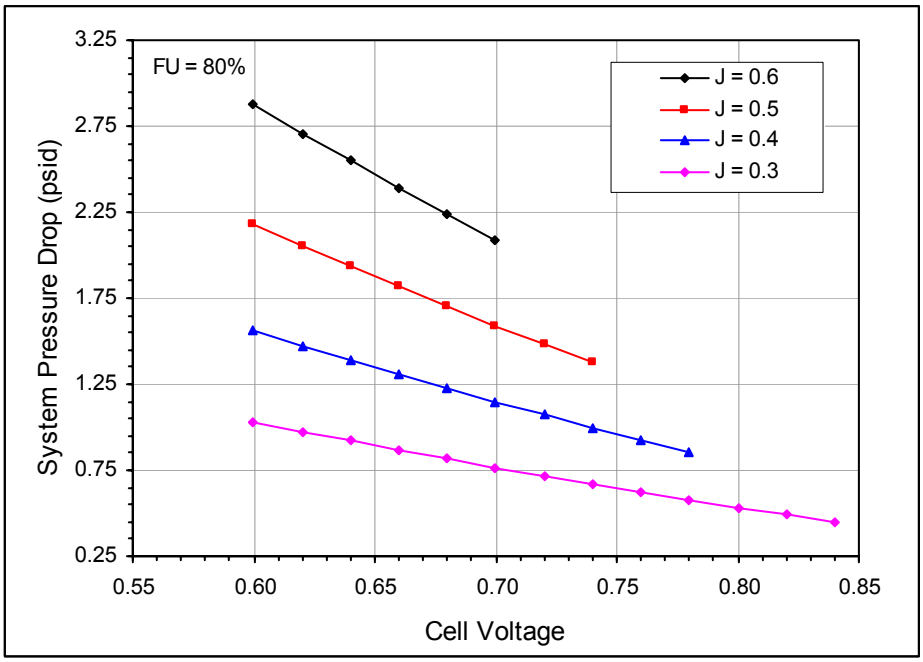

Figure 3.6 Effect of cell voltage on system pressure drop.

Figure 3.7, shows the system efficiency as a function of fuel utilization and operating voltage for current densities of 0.3 and 0.6. The uppermost line on the plot is for a current density of 0.3 and operating voltage of 0.84. The lowest set of lines on the plot is for current densities of 0.3 and 0.6, with operating voltage at 0.6. At an operating voltage of 0.6, a 10% decrease in fuel utilization results in a ~3.7% drop in system efficiency. At an operating voltage of 0.84, a 10% decrease in fuel utilization results in a 6% decrease in system efficiency. It should be noted that cell operating voltage and fuel utilization are not independent parameters, and dropping the fuel utilization will generally tend to increase the operating voltage of a cell. The increase in cell voltage will tend to offset the drop in system efficiency, however, the effect is considered to be minor from a system standpoint.

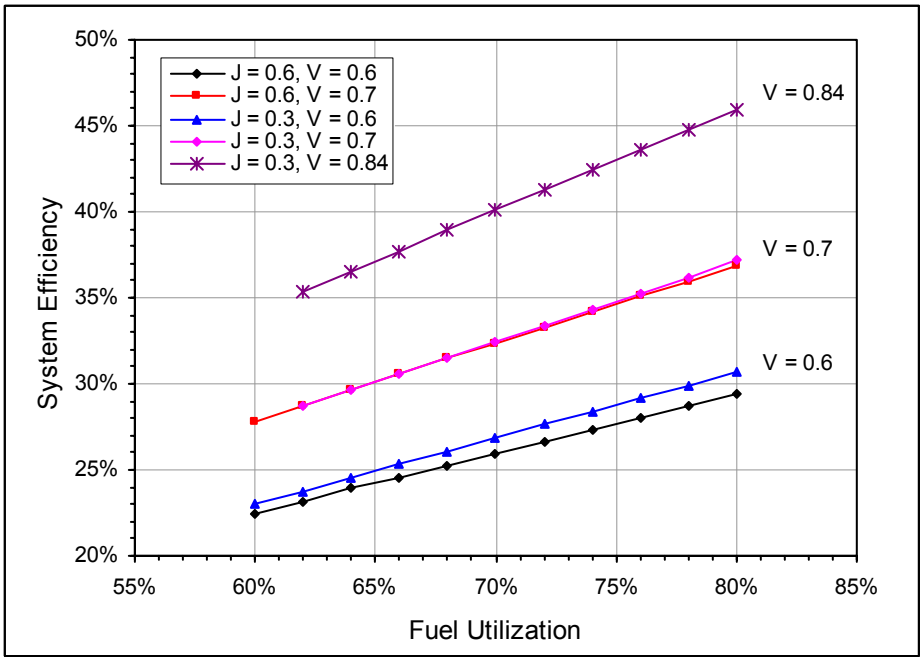

Figure 3.7 Effect of fuel utilization on system efficiency.

3.6 SYSTEM PERFORMANCE BASED ON STACK/CELL TEST DATA

Leading up to testing of the prototype system, a significant amount of stack and cell testing had been completed. The results of this testing are generally reported elsewhere in this report. Figure 3.8, however, shows a representative sample of some of these test results. The figure shows cell voltage and current density plotted within the context of the "operating envelope", defined earlier in Figure 3.2. Results are shown for a 4-cell stack, a 10-cell stack, and for a single cell that exhibited superior performance (denoted "super cell").

The results shown in Figure 3.8 were plugged into the Aspen system model to enable estimates of projected system performance. These estimates are shown in Figure 3.9. Using stack performance data for the 10-cell stack, a maximum system efficiency of ~42% and a maximum power of ~4600 W was calculated. Using 4-cell stack data, a maximum system efficiency of ~42% and a maximum power of 6200 W was calculated. The maximum power estimate of 6200 W seems to represent a peak, as evidenced by the slope of the curve at this power level. Finally, using the "super cell" data, a maximum system efficiency of ~44.5% and a maximum power level of 8600 W is calculated. The maximum power point using the "super-cell" test data is beyond the bounds of the operating envelope, but nonetheless demonstrated the capability of the system to handle higher power levels.

The projections shown in Figure 3.9 were the most current projections of what was expected from the system leading up to prototype testing. At that time, the projected system efficiencies exceeded the SECA requirement of 35% using

current cell technology. Further improvement in system efficiency was expected as stack technology matures.

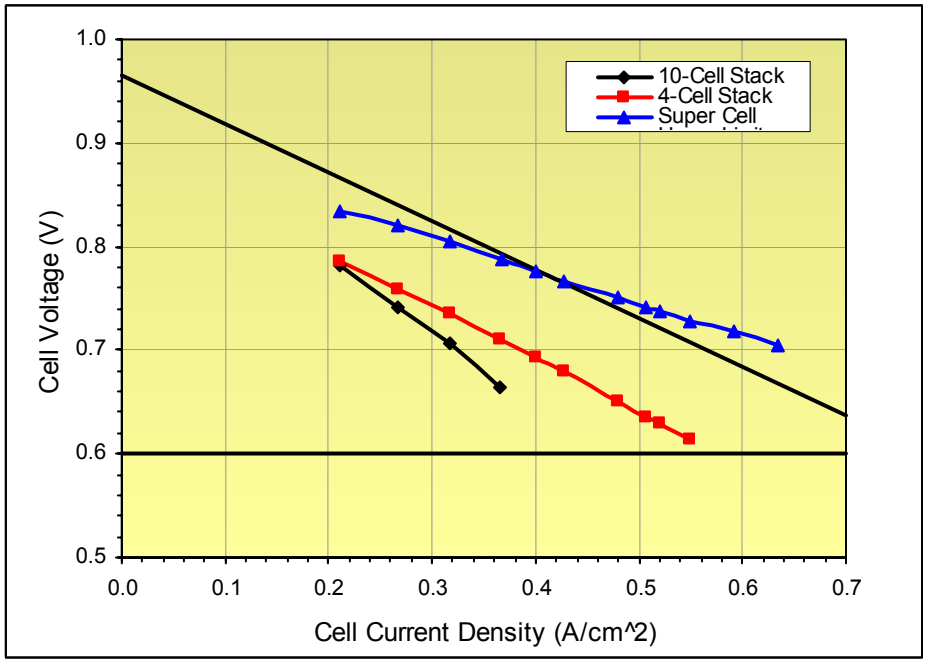

Figure 3.8 Representative stack and cell test results.

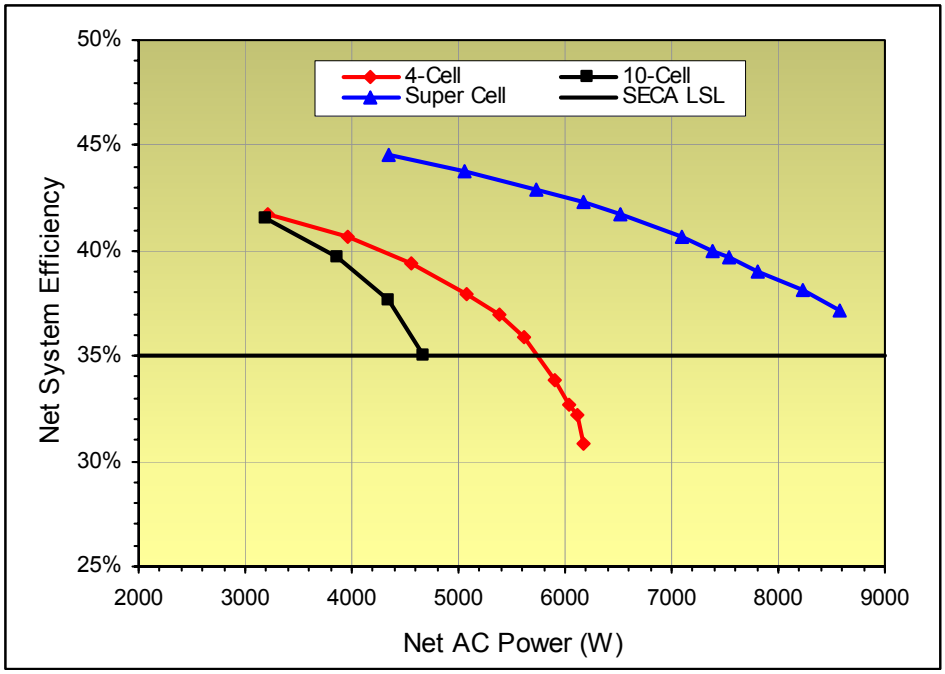

Figure 3.9 Projected system performance with 4x40 cell stack.

3.7 OPERABILITY ANALYSES

During the 6 months prior to prototype system testing, the system design and analysis task concentrated on refining the Aspen system performance model to include the "as-tested" performance results of the stack and other components within the system. In addition, a significant amount of time was spent examining various operating scenarios that may be encountered during the test phase and developing mitigation plans to address potential problem areas. The primary scenarios of interest included operation of the system at current densities greater than 0.6 A/cm^2, operation of the system at low fuel utilizations (i.e. < 80%), and operation of the system during a sudden switch to an open-circuit voltage (OCV) condition. In addition, the potential for carbon-deposition within the fuel processor was re-examined to affirm earlier conclusions regarding set-points for steam-to-carbon and oxygen-to-carbon ratios.

3.7.1 Potential for Carbon Deposition

A simple Aspen Plus simulation model was developed to help predict the potential for carbon deposition within the ATR fuel processor. The model (Figure 3.10) allows for the mixing and preheating of three component streams (fuel, steam, and air) prior to entering the ATR fuel processor. The streams leaving the mixer were assumed to be fully mixed. This is an important assumption to consider, since localized variations in steam-to-carbon ratios and oxygen-to-carbon ratios can lead to carbon deposition within the fuel processor. The heater element (labeled REFTEMP) was used to set the temperature of the gas mixture prior to entering the ATR fuel processor. The fuel processor was modeled as an adiabatic "equilibrium" reactor and did not take into account reactor kinetic effects. The inclusion of reactor kinetics into the analysis may lead to different results. For instance, an equilibrium calculation may show that the potential exists for carbon deposition; however, the kinetics of the reaction might preclude such an outcome due to insufficient reaction time for carbon deposition to occur. The assumption of equilibrium was therefore considered to be conservative assumption.

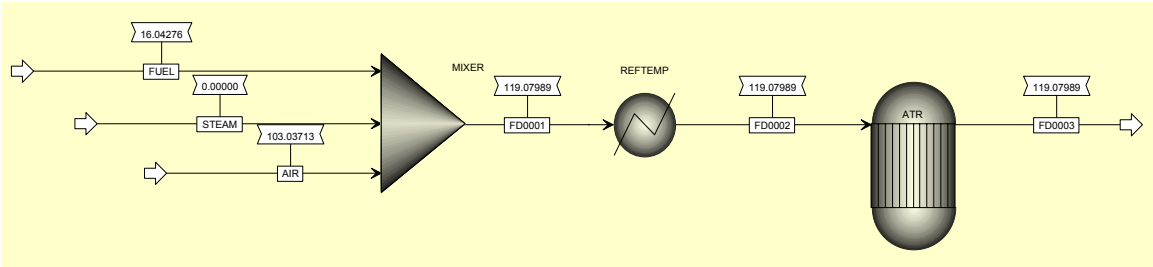

Figure 3.10 Aspen Plus simulation model.

A series of analysis runs were set up to determine the potential for carbon deposition as a function of fuel processor inlet stream temperature, steam-to-

carbon ratio, and oxygen-to-carbon ratio. Analyses were completed with fuel processor inlet temperatures of 150, 200, 250, 300, 350, and 400°C. For each of these fuel processor inlet temperature conditions, the steam-to-carbon ratio of the fuel gas stream was varied from 0 to 1.2, and the oxygen-to-carbon ratio was varied from 0.01 to 1.50. Figure 3.11 shows the equilibrium number of moles of carbon formed per mole of methane introduced into the system.

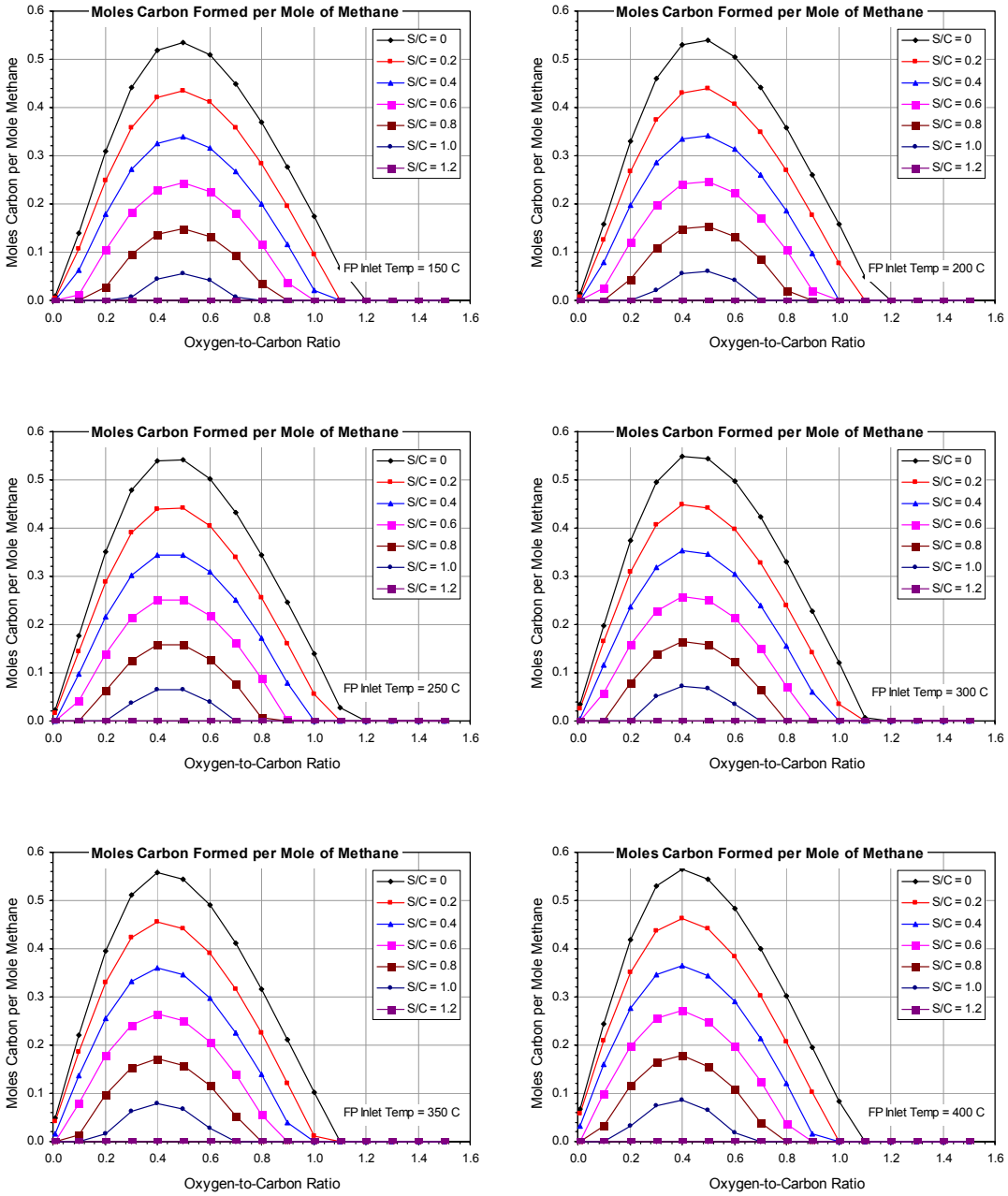

Figure 3.11 Carbon deposition potential.

Results from this analysis show that, for all values of oxygen-to-carbon (O/C) ratio between 0 and 1.5, carbon deposition should not be a concern if steam-to-carbon (S/C) ratios greater than 1.2 are maintained in the fuel gas mixture entering the ATR fuel processor (fully-mixed inlet stream). The analysis results were obtained over a range of fuel processor inlet steam temperatures varying from 150 to 400°C.

3.7.2 Operation at Current Densities Greater than 0.6 A/cm^2

The 2nd set of operability analyses were completed to determine the feasibility of operating the SECA PSD at current densities approaching 0.7 A/cm^2. System design specifications set an upper limit on current density of 0.6 A/cm^2. Pushing beyond 0.6 A/cm^2 was seen as one possible approach to increase net power of the system should the SOFC stacks show lower than expected performance. Concerns about operation beyond current density specification limits were expressed during the SECA Prototype System Risk Review.

For this set of analyses the current density was held constant at 0.7 A/cm^2 and the average cell voltage was varied from 0.55 V to 0.65 V. The range in average cell voltage was selected so as to bracket the expected performance of the SECA stacks. The expected stack performance at high current densities meant that it was necessary to extrapolate existing stack performance results attained at lower current densities.

With regards to system performance, the cathode airflow required to cool the stacks was generally seen as a limiting factor. The upper limit on cathode air flow was set based testing during the development of the cathode air blower. Various analyses were run with different assumptions on the allowable temperature increase through the cathode of the fuel cell to determine if all of the system and stack operating constraints could be met at the higher current densities.

In general, the analyses showed that under the right set of assumptions (high cell voltage, low fuel utilization, increased stack air temperature rise, etc.) it would be possible to theoretically operate at current densities of 0.7 A/cm^2. It was concluded at that time that, because of the number of assumptions used in the analysis, it would be extremely difficult to operate the system as built at current densities of 0.7 A/cm^2.

3.7.3 Operation at Lower Fuel Utilization

Analyses were also completed to determine operability concerns associated with operating the stacks at fuel utilizations lower than 80%. The analysis was completed using the Aspen Plus computer code. Stack performance data (S711 20-Cell Stack) was used to set the stack operating characteristics for the system. Since the stack performance data was provided over a limited range of current densities, the data was curve-fit and extrapolated

over the intended operating range of the SECA PSD system. Figure 3.12 shows the data provided and the resulting curve-fits extrapolated over a wider range of current densities.

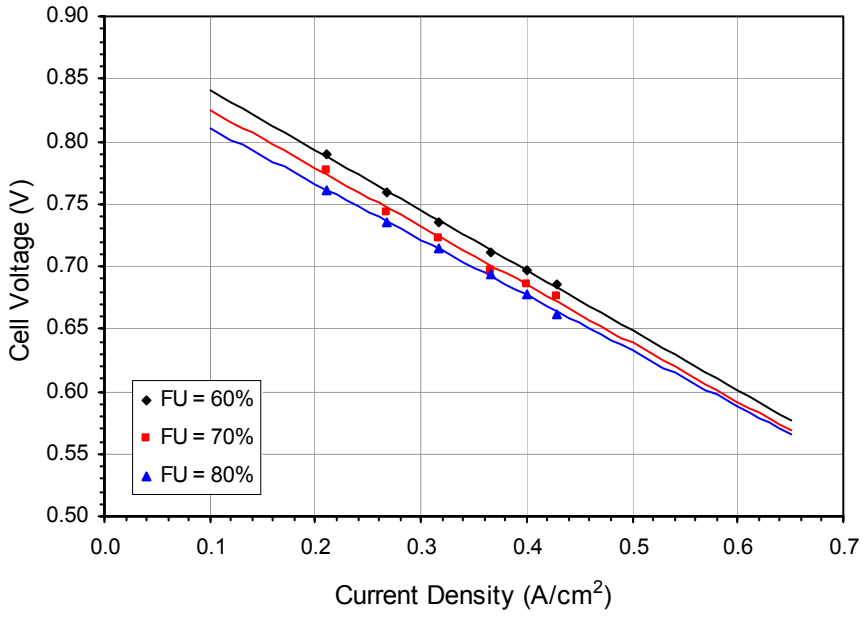

Figure 3.12 Stack performance data (S711 20-cell test data)

The stack model used in the analysis required the specification of cell voltage, current density, fuel utilization, and stack heat loss as inputs. The stack model used this information to perform a simple mass and energy balance, thereby determining the temperature of the streams leaving the stack as well as the temperature rise of the air stream across the stack.

A series of analyses were run assuming fuel utilizations within the stack of 80%, 70%, and 60%. The analyses were numerous and iterated to find solutions across the operating range of current densities that simultaneously satisfy constraints on the combustor inlet temperature, the cathode air blower flow, and the maximum temperature rise through the cathode.

Figure 3.13 and Figure 3.14 show the Net AC Power and Net System Efficiency for 60%, 70%, and 80% fuel utilization. The most significant observation is the reduction in net AC power due to operation at 60% fuel utilization within the stack. This result is extremely important to note, since it is counter to stack stand-alone testing experience where dropping fuel utilization within the stack can help maximize stack power output. Dropping fuel utilization within the stack from 80% to 70% shows a slight improvement in peak power. However, further decreases in fuel utilization result in decreases in net AC system power due to increased cooling air flow requirements and the increased power consumption of the cathode-air blower. Based on the results shown, the

peak power of the system was expected to be near 6.2 kW with a peak system efficiency of approximately 40%.

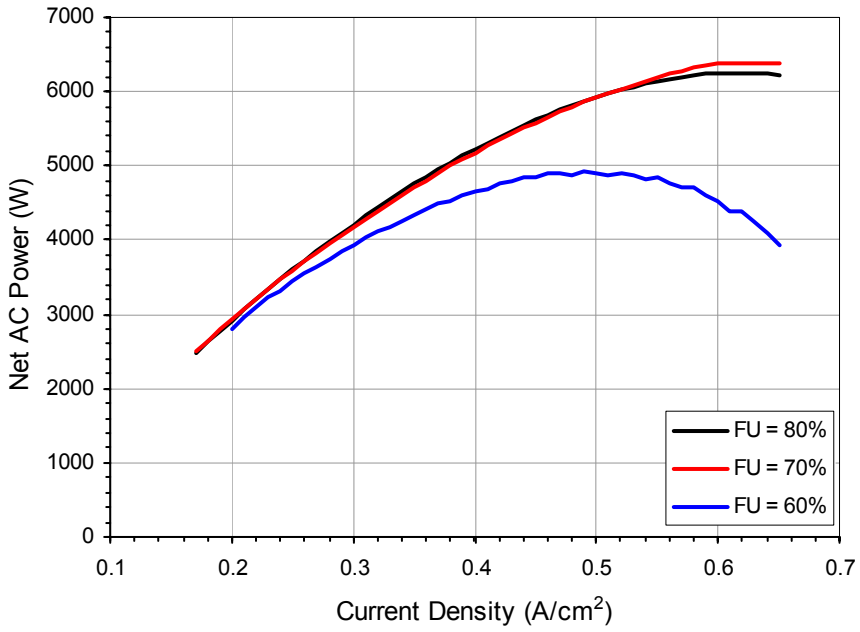

Figure 3.13 Net AC power – 2nd set of runs.

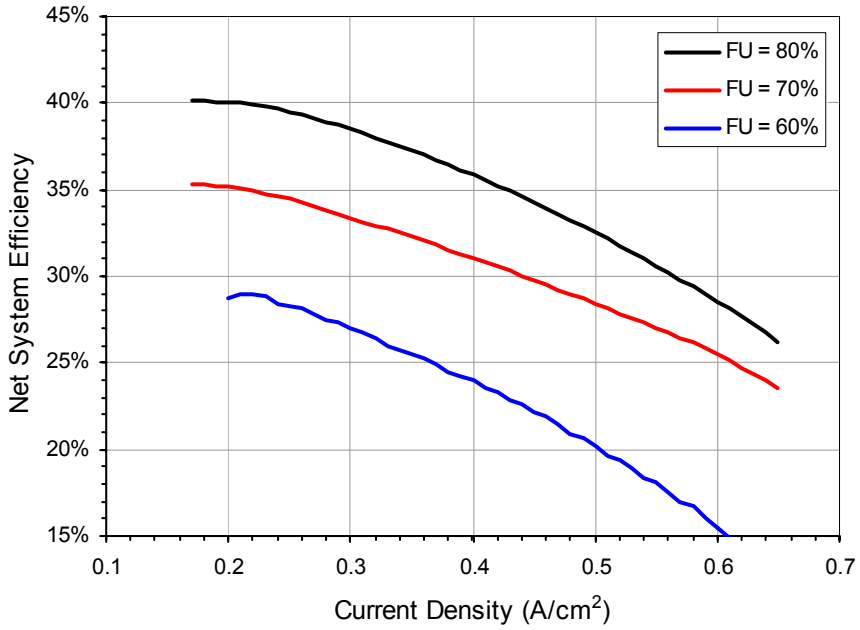

Figure 3.14 Net system efficiency – 2nd set of runs.

To alleviate concerns with high temperatures within the combustor, it was intended that excess capacity of the cathode-air compressor be used to provide additional cooling air to limit combustor temperatures. This strategy has significant limitations. First, the excess airflow capacity required, especially when running the stacks at 60% fuel utilization, is limited. For this stack operating condition, the analyses showed that sufficient excess cooling air can only be provided if the system is operated at low current densities. A second limitation is that the addition of too much cooling air results in the lowering of downstream temperatures, thereby affecting the ability of downstream components, most notably the steam generator, to perform their intended functions. Finally, operation at 60% fuel utilization within the stack will not increase the net AC power output of the system but will, in fact, reduce the net AC power produced. This is due to the additional cooling airflow requirements and subsequent power consumption required by the cathode-air blower.

3.7.4 Operation During OCV Condition

This final set of operability analyses describes the results of SECA PSD system performance calculations to quantify concerns associated with the stacks going into an Open Circuit Voltage condition during prototype system testing. When the SECA system operates at an OCV condition, no fuel consumption occurs in the stacks. As a result, all fuel is mixed with oxidant (air) and is burned in the combustor. Because of the high heat content of the fuel-air mixture, the potential exists for temperatures in the combustor that could exceed its temperature operating limits. Exceeding the temperature within the combustor could also damage components downstream of the combustor, such as the fuel processor air preheater and the cathode air preheater.

Several analyses were conducted with various strategies to mitigate combustor over-temperature should the system go to an unexpected OCV condition. These strategies were evaluated and the best strategy selected for implementation in the prototype system.

4 COST ESTIMATE

The overall system costs, including the stack, the fuel processor, the thermal management sub-system, the air, fuel and water delivery sub-systems, the controls and power electronics related devices, were assessed in this task. Component cost models as well as system cost models were developed. These models matured as the design evolved from conceptual to prototype design. The evolution of the modeled system cost is shown in Figure 4.1. The reduction in system cost is a combined result of design, manufacturing process improvement, and cost data improvements.

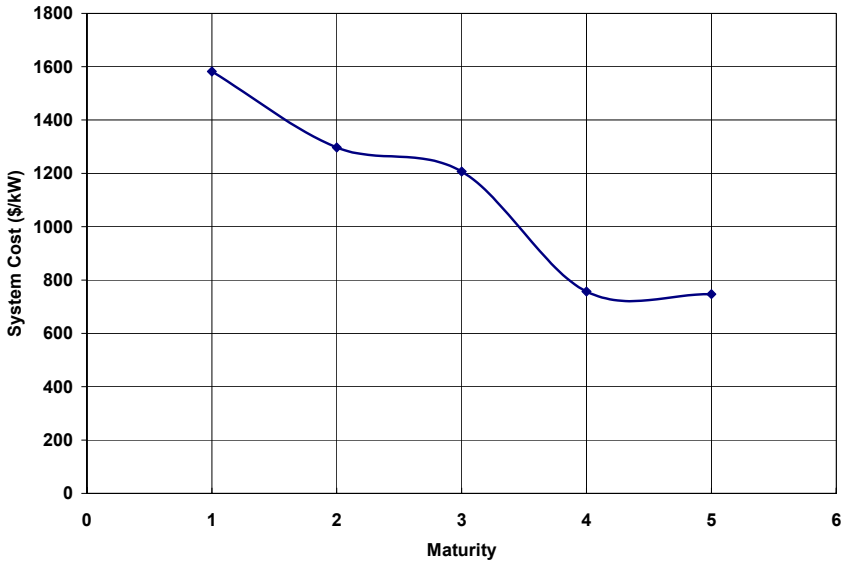

Figure 4.1. Evolution of system cost.

One of the major cost components in the system is the SOFC stack, which accounts for about 1/3 of the total system cost. The evolution of the modeled stack cost is shown in Figure 4.2. The stack design had several design concept iterations which are detailed later in Section 5. Steady improvements in manufacturing processes have also been made, as well as the materials cost was updated from low to high volume cost including the use of cost data provided by DOE.

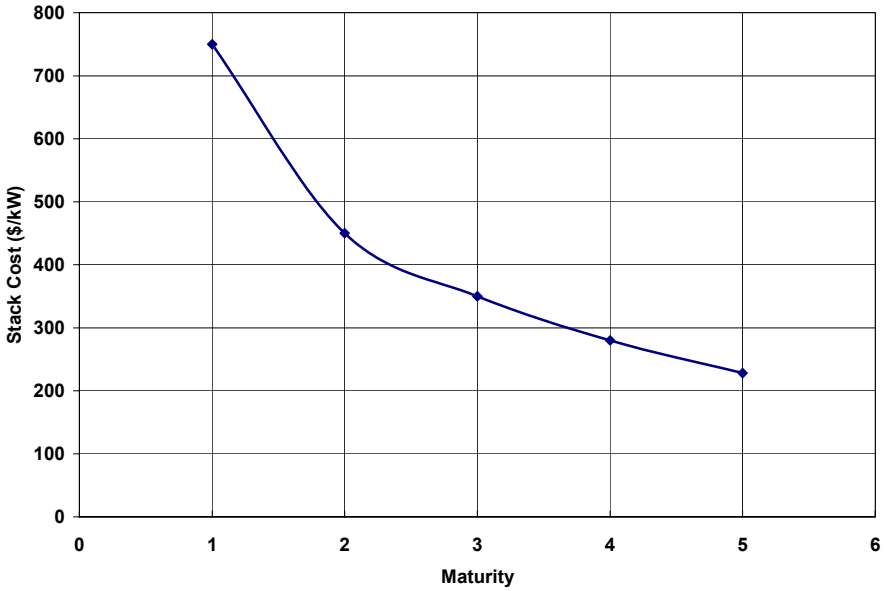

Figure 4.2. Evolution of stack cost.

The final high volume system cost that was based on the prototype design is delineated in the next few sections. The cost analysis has been audited and the auditor's recommendations are discussed.

4.1 HIGH VOLUME PROTOTYPE SYSTEM FOR PRODUCTION

For high volume production, it is assumed that the prototype is a mature system using mature manufacturing processes. The high volume system process flow diagram is shown in Figure 4.3. The system packaging and the component designs have been updated as appropriate, as well as testing and diagnostic devices used for research and development purposes have been removed. The key modifications of the prototype system for high volume production are discussed below.

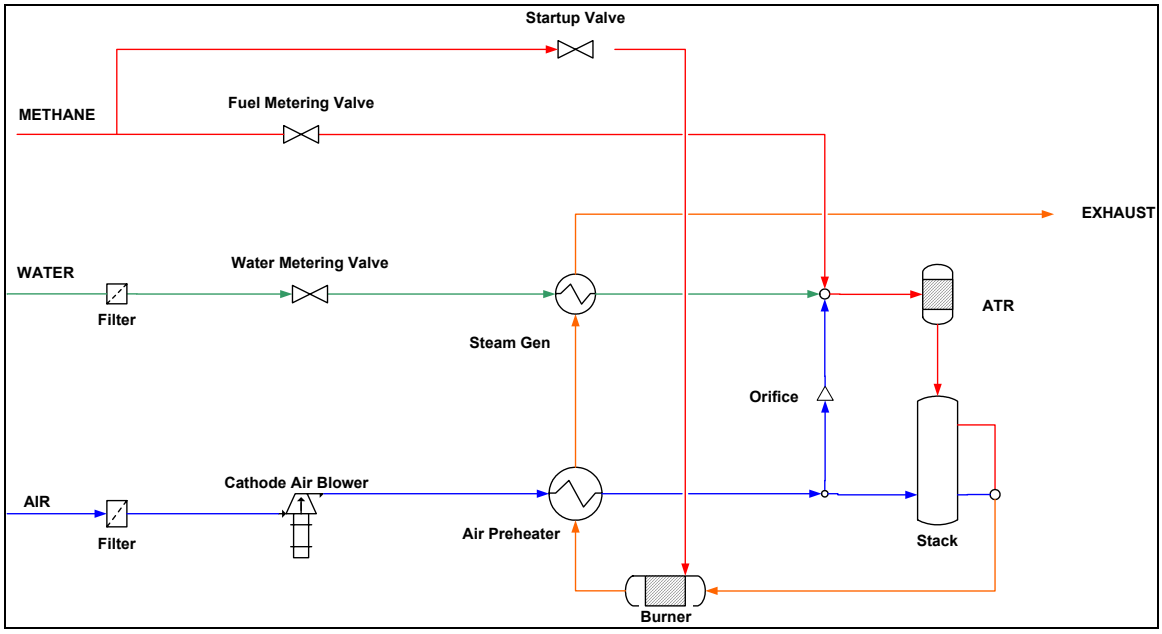

Figure 4.3. High volume system schematic

Air Preheater Bypass — The air preheater bypass line was removed. This bypass was used in the prototype to control the SOFC stack inlet air temperature. For a mature system, the inlet air temperature is fixed within an operating range and the bypass control is not necessary. The airflow rate varies only when the power level changes. As the power level decreases from the design point, the airflow rate decreases. At lower power levels, the stack is more efficient due to operation at lower current densities and thus less heat is to be removed. As a result, the stack temperature variation is lower with constant air utilization. Thus the inlet air temperature can be increased or decreased by increasing or decreasing the airflow rate with the compressor while still maintaining temperature variation limitations within the stack.

Fuel Processor Air Delivery — In the prototype, there is a dedicated fuel processor air delivery system that was removed for the high volume system. An air blower was used to control the airflow rate and a bypass line was used to control the temperature. It was demonstrated during the prototype testing that the bypass line for temperature control was not necessary. Aspen analysis confirmed that these components are not required. The fuel, water and airflow rates all increase or decrease proportionally depending on the power level. Thus the air to the fuel processor can be supplied with hot exhaust air from the air preheater with an orifice.

Startup Valve — In the prototype, a dedicated startup electrical heater is placed at the air preheater bypass line. For the high volume system, the tail gas burner will be utilized for startup heating. During startup, fuel from the fuel startup line and air from the airline are introduced to the burner. The hot exhaust air then heats up the inlet air recuperatively. The heated inlet air flows to the stack raising the stack temperature.

The high volume system bill of material (BOM) is derived from the prototype unit and is listed in Table 4-1.

Table 4-1 System components included in cost estimate.

Subsystem	Components
Stack	Four SOFC Stacks
Fuel Processor	ATR Pre-reformer
Air Delivery	Air Filter
	Air Compressor
	Fuel Processor Air Orifice
Fuel Delivery	Fuel Regulating Valve
	Fuel Startup Valve
Water Delivery	Water Filter
	Water Metering Valve
Thermal Management	Air Preheater
	Steam Generator
	Tailgas Burner
Electrical	AC Cable
	DC Harness
	Auxiliary Power Distribution Panel
	Key Switch Unit
	Low Voltage Power Supply
	Controller
	Cathode and Anode Inlet TC
	Voltage Monitoring
Packaging	System Enclosure
	Insulation
	Gas Flow Manifolds
	Stack Support
	Electrical Current Collection

4.2 COST ESTIMATE BASIS AND ASSUMPTIONS

The cost basis and key assumptions for the cost estimate generated in Phase I are summarized below:

- The system is a 5 to 10 kW stationary unit operating on natural gas. The cost is based on peak power and the peak power is determined by the prototype testing.
- The cost estimation was conducted on a system based on the Phase I prototype design projected for high volume production.
- The prototype system is designed with high-pressure natural gas and the system is designed to operate at ~2 psi.

- Water supply for the system is assumed to be available for fuel processing. The fuel processor is a heterogeneous ATR pre-reformer with supported catalyst.
- The SOFC stack is a half-sealed radial design with tape-calendared anode supported thin-electrolyte cells and stamped metal interconnect. The stack can process light hydrocarbon internally (internal reforming).
- All other components are available from suppliers and vendors including other GE business units.
- The production volume is assumed to be 50,000 units per year (250 MW/yr). The actual market that is addressable by a 5-kW SOFC modular system could be much higher. The lower production rate was selected to validate the DOE's estimates of the production volume required to meet cost objectives.
- DOE guidelines on certain material cost shown in Table 4-2 are used in this cost study.

Table 4-2 DOE guidelines on materials cost.

Material Costs ($/kg)	
Lanthanum Strontium Manganite	12
Yttria Stabalized Zirconia (>1um)	10
Yttria Stabalized Zirconia (<1um)	25
Lanthanum Strontium Ferrite	10
Lanthanum Strontium Cobaltite	36
Lanthanum Strontium $Cobalt_{0.2}$ $Ferrite_{0.8}$	25
Ni metal	8
Cr metal	16
Co metal	26
Stainless Steel	2.5
Ni/Cr Alloy	17
Rare Earth oxides	20

The cost estimate establishes a factory cost, which includes:

- Equipment and Plant Depreciation
- Tooling Amortization
- Equipment Maintenance
- Utilities
- Indirect Labor
- Cost of Capital

- Manufactured Materials
- Purchased Materials
- Fabrication Labor
- Assembly Labor
- Indirect Materials

The following costs are not included in the cost estimate:

- Research and Development
- Sales and Marketing
- General and Administration
- Warranty &Taxes

4.3 GENERAL APPROACH AND METHODOLOGIES

The general process for cost estimation of the high volume system involves the steps shown in Figure 4.4. Using this process, the estimation was divided into four major areas:

- SOFC stack and ATR fuel processor manufactured in plant. The stack and fuel processor are separated from other components and the cost is estimated separately because the design and manufacturing of the units are specific to the SOFC system developed in this program and are not available elsewhere.
- BOP procured from vendors. Cost of these components were estimated by vendors or estimated by a sourcing consultant which GE uses to support other product development, component manufacturing and cost reduction initiatives.
- High volume system packaging design. The prototype packaging design is optimized for the high volume system and its cost is estimated.
- System assembly in plant. A cost model was developed to estimate the assembly cost of the high volume system utilizing GE C&I (Consumer and Industrial) high volume manufacturing experience.

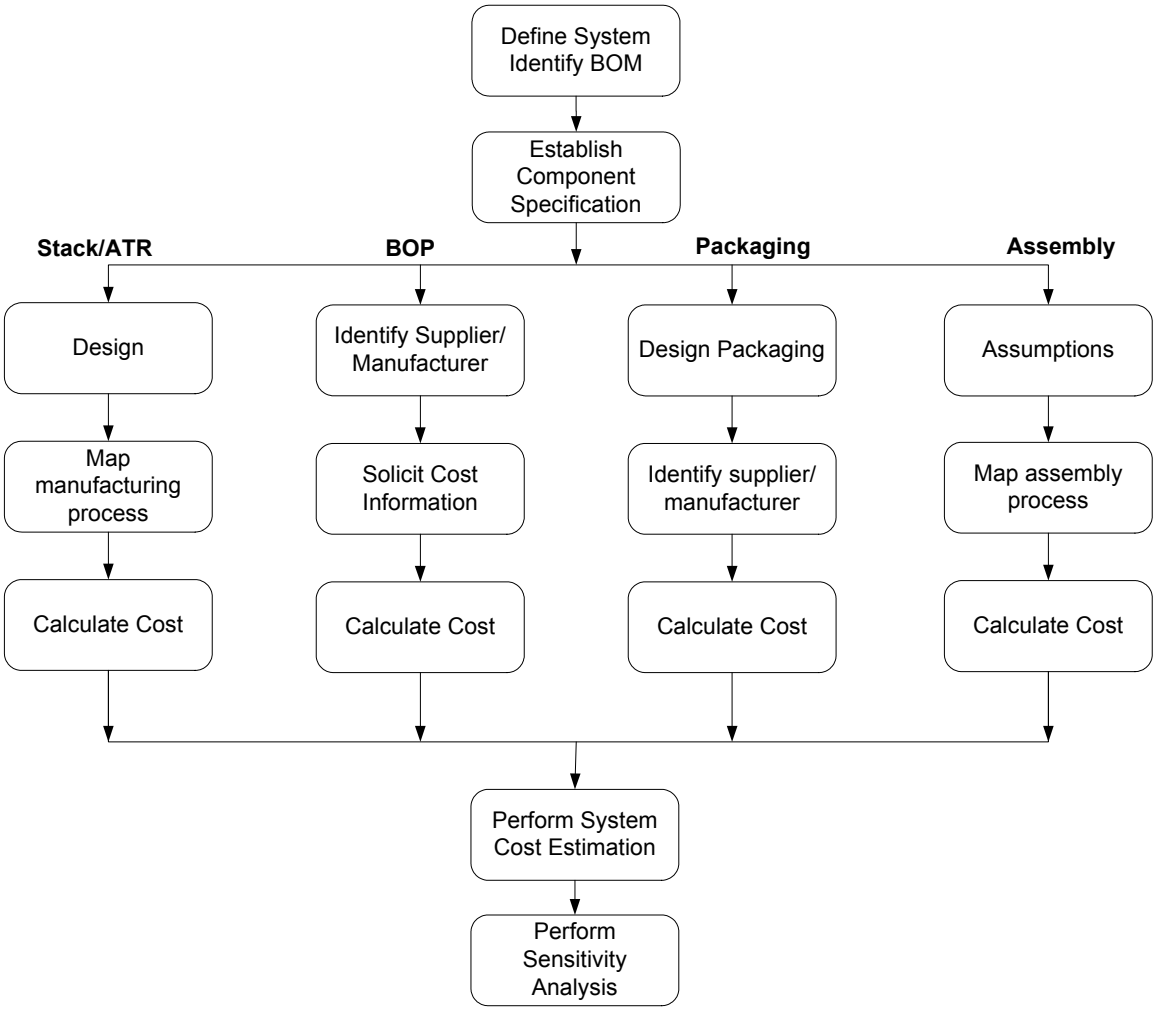

Figure 4.4. Process map for developing cost estimate.

4.4 COST ESTIMATE DETAILS

4.4.1 Stack

4.4.1.1 Prototype Stack Design Description

The target stack operating conditions were: 800 C, 80% fuel utilization and a power density of 0.3 W/cm^2 (0.7 V/cell at 0.428 A/cm^2). Based on cell/stack performance obtained, the prototype SOFC system is designed to consist of four 40 cell-stacks with a cell active area of 142 cm^2.

4.4.1.2 High Volume Stack Manufacturing

Several assumptions were made to make the prototype stack suitable for high volume manufacturing. The basis and main assumptions for SOFC stack manufacturing are:

Ceramic Cell Processing — Cells are made by tape calendaring and use screen printing to apply the cathode. First, anode, and electrolyte powders are separately mixed with organic binders, plasticizers, and pore formers (for electrodes) to form plastic masses that are rolled into tapes. Electrodes and electrolyte tapes of desired thickness ratio are then rolled together to form the cell tape, which is then cut to the desired size and sintered. The cathode powers are mixed with organic binders and solvents to create a thick film paste. This paste is then screen printed onto the electrolyte surface of the cell. The cell is then fired to partially sinter the cathode electrode. A schematic of the cell processing is shown in Figure 4.5. For the high volume processes a high level of automation is assumed. Also, the complete cell fabrication process is assumed to be of a continuous type with the appropriate equipment to support this type of fabrication, such as, powder feed hoppers, multiple roll sets in series and parallel, robotic part handling to move parts from one process line to another, and continuous furnaces for all firing steps.

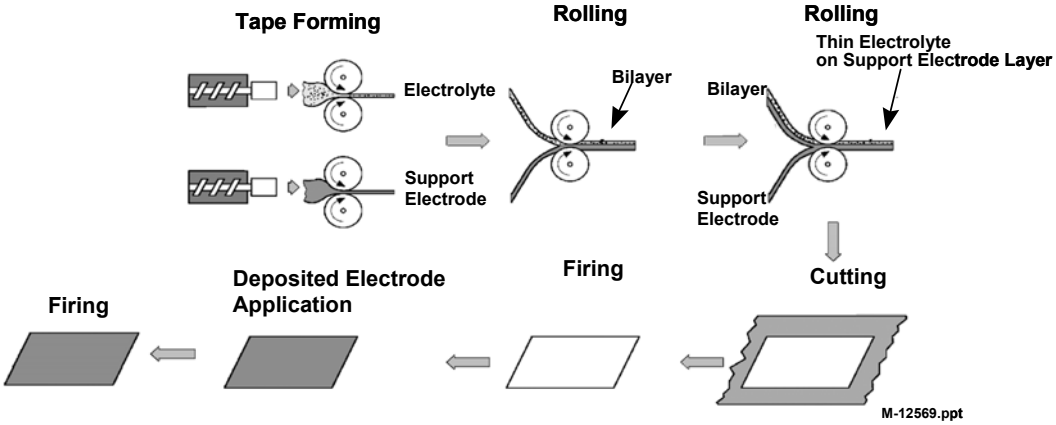

Figure 4.5. Cell processing schematic.

Interconnect Fabrication — The interconnect is fabricated by stamping thin metal sheets. The interconnect sheets are then brazed together to form the complete interconnect structure. The flow field depth is kept the same as that of the prototype design. Preliminary analysis has shown that forming interconnects with features of these depths are feasible with careful consideration to the geometry of the features. Future development and examination of the formability will be required to define the exact thickness of sheets required to meet the design requirements of the stack.

Stack Assembly — To assemble a stack, a base plate is used on which the cells and interconnects are stacked up. Cathode bond paste is applied to the contact surfaces of the interconnect and the cathode and manifold seals are placed on the pre-seal unit. These units are then stacked up to create the completed stack. Another base plate is used as the top plate over the stack of

cells and interconnects. A bolted compressive load was selected based on ease of assembly and transportation.

4.4.1.3 Stack Cost Model

The structure of the stack cost model is described in Figure 4.6. Different areas that make up the total stack cost, namely the labor, equipment, facility and materials costs are apparent on the right hand side of the diagram. The items listed on the left of the chart are the inputs of the model.

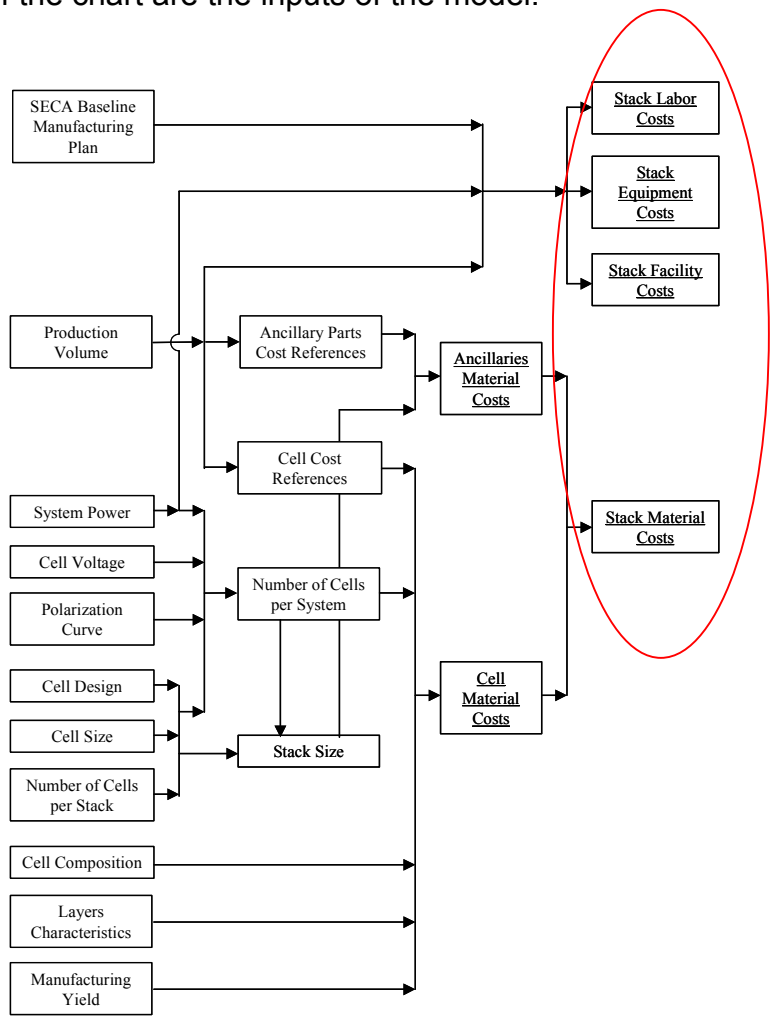

Figure 4.6. Stack cost model structure.

Figure 4.6 shows how the materials costs of the stack are calculated: knowing the system power target, the assumption of cell performance from system design flowdown and the operating point on this curve (voltage), allows the user to calculate the total electrochemical area needed for the system. Coupled with the stack and cell designs, this area is used to compute the overall dimension of the system, in terms of number of cells. In parallel, the cost of a cell is calculated knowing the cell composition and its physical characteristics

(thickness of the different ceramic layers, cell size) and the cost of each of its constituents (obtained from DOE guideline or as quotes from vendors). For high-volume production, the unit cell cost is coupled with a manufacturing yield assumption to generate the overall cell materials cost for a system. Similarly, the stack size computed earlier is used to generate the cost of the remaining items in the stack, by using the cost references for these ancillary parts from identified suppliers.

Other costs involved in the overall stack costs are calculated as shown in Figure 4.7. The manufacturing plan, when coupled with the intended production volume (50,000 units per year) and the system power, enables the user to determine the requirements for manufacturing processes, equipment and facility needs. With all the above information, labor, equipment and facility costs are then calculated.

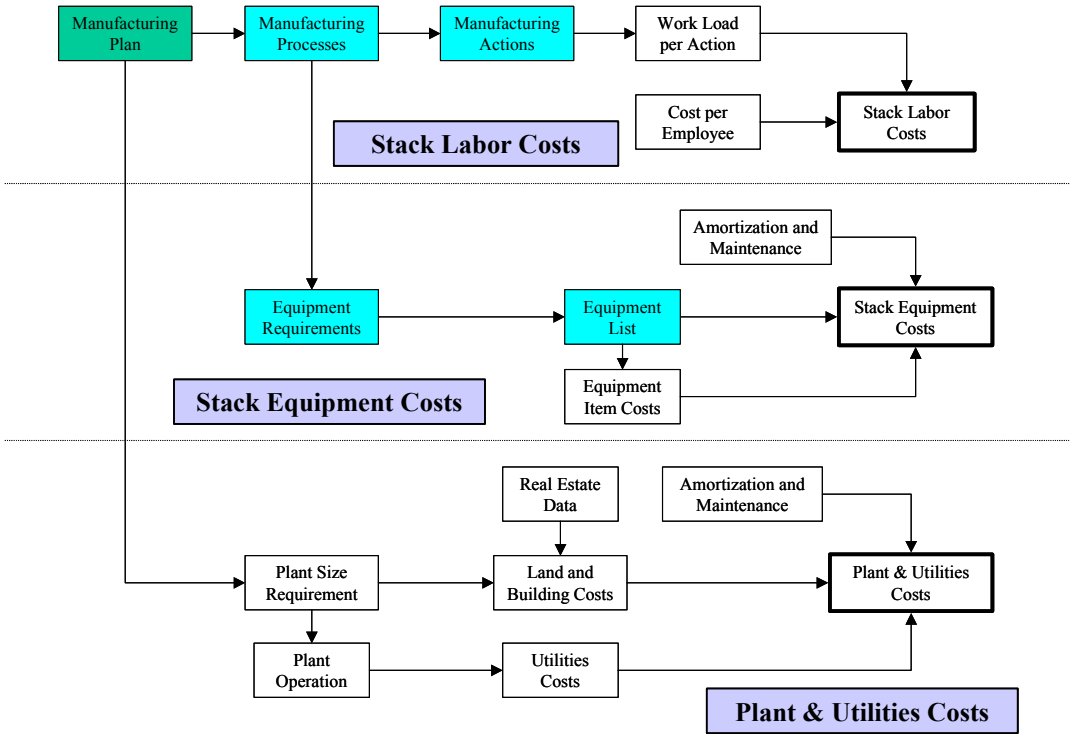

Figure 4.7. Labor, equipment and facility cost model structure.

4.4.1.4 Stack Cost Summary

A summary of the cost estimate for the SOFC stacks is given in Table 4-3 and the percent contribution of each category is presented in Figure 4.8. The estimated cost is $1,369 for the complete stack. As could be expected from a high volume process, the materials cost accounts for the majority of the cost with the interconnect being the largest contributor.

Table 4-3. Summary of Stack Costs

	$/system
Material	**$816**
Facility & Equipment	**$182**
Labor	**$279**
Operation & Maintenance	**$92**
Total	**$1,369**

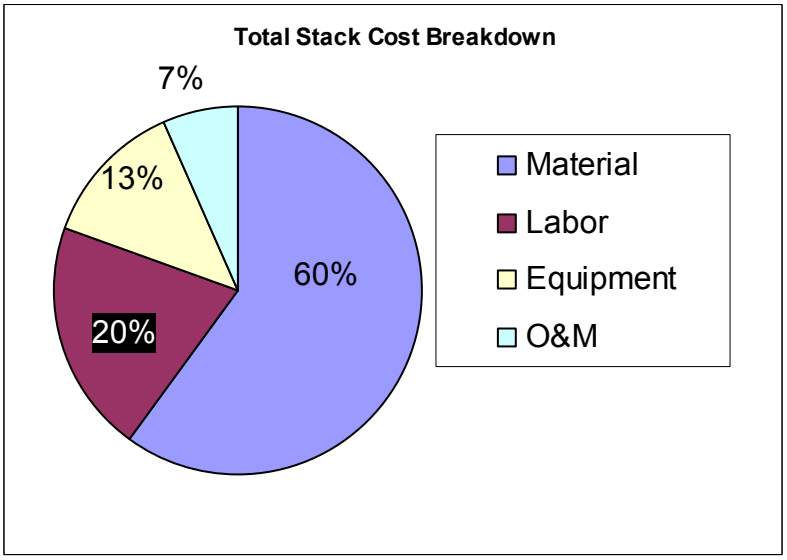

Figure 4.8. Percent contributions to total stack cost

4.4.2 Fuel Processor

4.4.2.1 Prototype ATR design description

A conceptual drawing of the fuel processor is provided in Figure 4.9 along with a picture of the prototype. The hardware is designed with a flange coupling that can be bolted to enable maintenance access to the catalyst. Thermocouples are placed both in front (TC1) and at the rear of (TC2) the catalyst to enable temperature measurements of the fuel and reformate, respectively, during fuel processor operation. For high volume production and systems integration, the TC's are removed. The flanges are also removed from the cost estimation since the unit would be welded to the stack fuel inlet manifold.

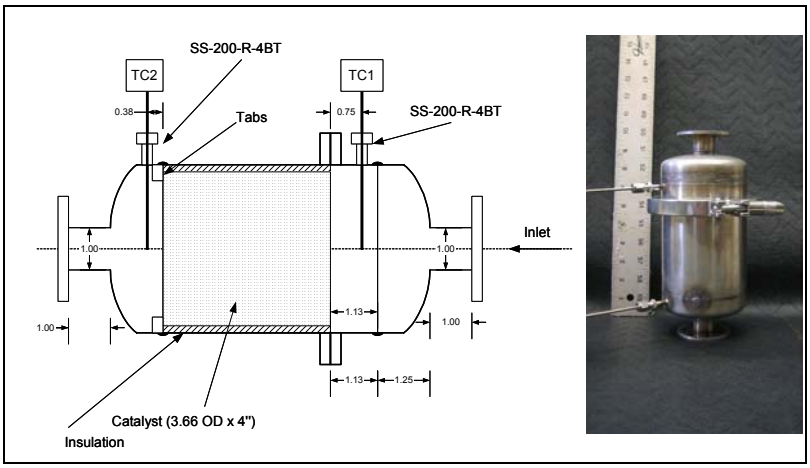

Figure 4.9. ATR fuel processor

4.4.2.2 ATR Cost Model

The cost model to fabricate 50,000 external fuel processor units was created from the prototype unit Bill Of Materials (BOM). A detailed breakdown of the material cost and processing cost for each piece was created. The cost to operate a small scale manufacturing facility annually was estimated as well. The framework of the model is shown in Figure 4.10.

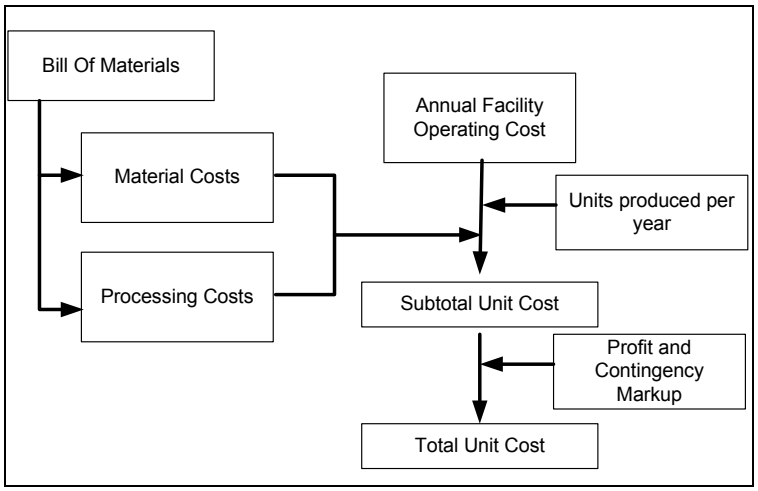

Figure 4.10. ATR cost model framework

Material and Processing Cost — The material and processing costs were derived directly from the prototype's BOM. The processing cost is about one quarter of the materials cost. The costs of the off-the-shelf components were obtained from vendors. The majority of the parts were either made from sheet metal or tube/rod. The dimensions of the raw sheet needed for each sheet metal part was listed and a manufactured scrap dimension, which refers to the scrap sheet metal produced as a direct result of the manufacturing process, was added. The part volume and weight was then calculated. Metal vendors were

contacted and provided costs per weight for the sheet metal and cost per foot for tube and rod used. The cost of the catalyst was estimated by the vendor, and is the major contributor of materials cost. The breakdown of the material cost analysis is shown in Figure 4.11.

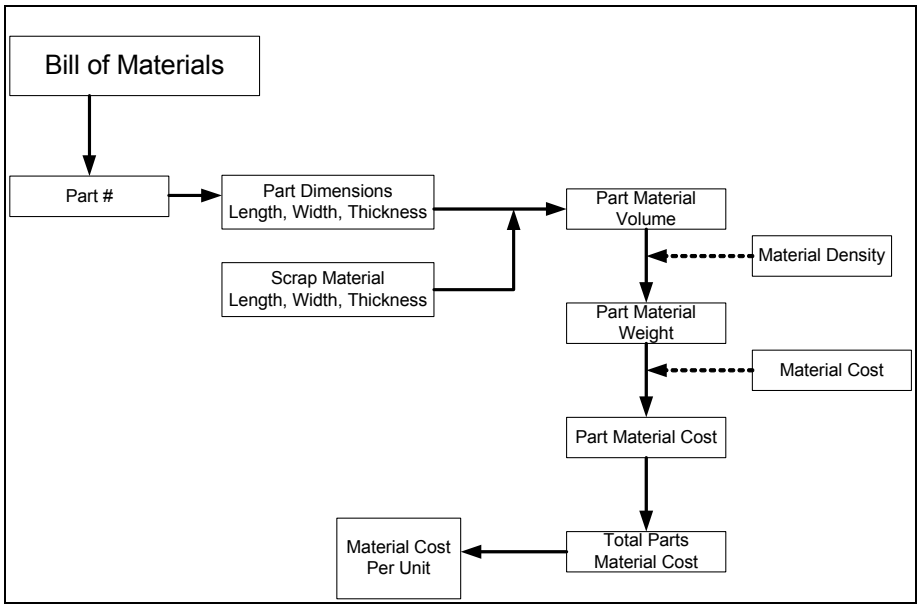

Figure 4.11. Material cost breakdown

Once the material cost for each part was determined, the manufacturing process cost portion was then estimated. The sheet metal parts were first sheared using a blanking die in a press machine to create the part blank. Some sheet metal parts were further processed using a piercing die in a press machine to produce internal holes and cutouts from the blank. A stamping process was used to form some parts. Finally, an assembly process to put all the parts together was performed. The time to perform each process per part was determined. The time was multiplied by a cost to perform each specific operation on a dollar per time basis obtained from manufacturing literature.[1]

The blanking, piercing, rolling, and assembly processes were given an operating time while the welding and machining processes were given a setup and operating time. The breakdown of the process cost analysis is shown in Figure 4.12.

[1] Geoffrey Boothroyd, Peter Dewhurst, Winston Knight; *Product Design for Manufacture and Assembly*; 1994 by Marcel Dekker, Inc.; **ISBN:** 0824785479

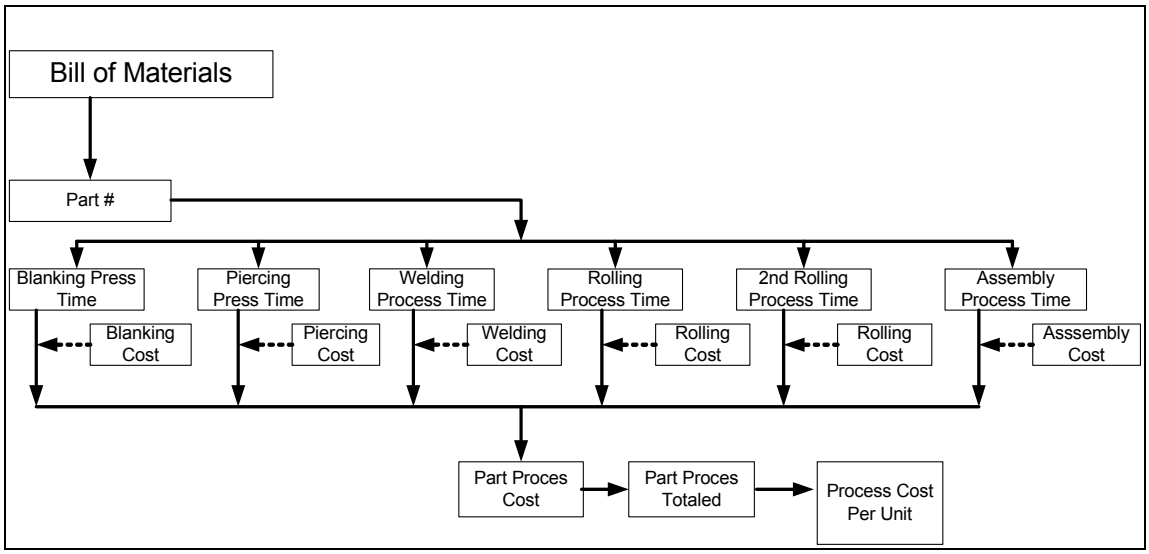

Figure 4.12. Process cost breakdown

4.4.2.3 ATR Cost Summary

The estimated cost is $120.6 per unit as shown in Table 4-4. The material cost accounts for the majority of the total cost. The breakdown of the materials cost is shown in Figure 4.13. The catalyst accounts for 52% of the total materials cost.

Table 4-4. Summary of fuel processor costs

Material Cost	$ 79
Processing Cost	$ 22
Operating Cost	$ 19
Total Unit Cost	$ 120.6

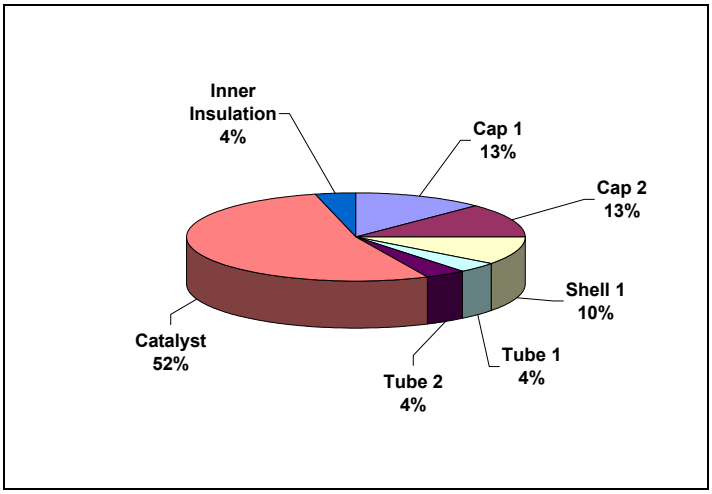

Figure 4.13. ATR materials cost breakdown.

4.4.3 Balance of Plant (BOP)

These components are well developed and can be purchased from vendors. Detailed manufacturing costs are provided for components developed specifically for this application, *e.g.* compressors and inverters by vendors. The sourcing consultant has estimated other component costs. Wherever possible, existing products that meet the component specification were used, and actual market pricing were obtained for high volume purchases. If no suitable product or pricing existed, or if the current manufacturers do not have the capacity to quote in sufficient volume, a broader market analysis was performed. In the situations where such an analysis was conducted, the facts, methods and assumptions were documented.[2]

4.4.3.1 Cathode Air Blower

The cathode air blower is used to provide air delivery to the system efficiently. A high-volume cost estimate for the blower was completed by the vendor. Table 4-5 summarizes the costs for this compressor. The motor and controller comprise the largest single contributor at 36% of the cost. The details of the estimation are documented.

Table 4-5. Summary of main air blower cost

Summary of Costs	Cost per Pump	Percent
Casting costs	$53.45	14%
Machining costs	$61.12	16%
Off the shelf component costs	$53.76	14%
Motor and controller costs	$137.27	36%
Assembly and quality test costs	$29.33	8%
Support and Management Costs	$8.99	2%
Scrap and rework costs	$33.49	9%
GRAND TOTAL	$377.42	

4.4.3.2 Cathode Air Preheater

The air preheater is used to heat the air to the stack operating temperature. The heat exchanger designed for this application employs a two-pass cross counter-flow configuration. The core of the heat exchanger weighs

[2] *SOFC Component Market Pricing Report*, Report to GE HPGS, 5/12/2005

about 17 lbs. The material cost of the core is estimated to be about $130 with an Inconel cost of $17/kg.

The sourcing vendor performed a cost estimate for the unit. They were unable to identify any high volume manufactured heat exchangers that operate with the above specification. Thus a standard copper tube-fin Lytron product (6310G3BD) that is currently mass produced was quoted to establish a pricing baseline ($60 made of copper). The baseline price was then adjusted to accommodate the changes to materials and manufacturing that would be necessary to meet the more rigorous requirements of the fuel cell application. Price ratios for raw materials were obtained from the London Metals Exchange, and additional labor estimates were obtained from heat exchanger design and manufacturing experts. The price ratio of Inconel to copper is 9.43/1.52. It is estimated that two hours additional labor per unit were needed for specialty metal welding instead of brazing. Thus the estimated unit cost is $402.

4.4.3.3 Steam Generator

The steam generator supplies steam to the fuel processor. The cost estimate methodology used is similar to that of the air preheater. The same Lytron heat exchanger quoted above was used to establish a baseline. The baseline price was then adjusted to accommodate the changes to materials and manufacturing that would be necessary to meet the more rigorous requirements of the fuel cell application. The price ratio of 316L to copper is 1.89/1.52. It was estimated that one hour of additional labor per item was required for welding instead of brazing. Thus the estimated unit cost totals $89.4.

4.4.3.4 Fuel Metering Valve

The sourcing vendor performed the cost estimate for this unit and Burket was identified as the supplier. The quoted cost is $120 for 50,000 units/year.

4.4.3.5 Filters

Filtration requirements for the SOFC system are in-line with standard industry requirements. A variety of air and water filters are readily available in the marketplace, so the main barrier to accurate cost estimation is the identification of suitable representative items from among the many choices. All the filtration manufacturers that were contacted expressed a willingness to develop custom filter products to meet the needs of the SOFC system. This would likely reduce per-item costs further and would simplify inclusion of the filters into the overall SOFC system assembly.

Pall, a global filter manufacturer, was identified as the manufacturer for the water filter. The quoted unit price is $45 for 50,000 units including housing and filter assembly. Airguard was identified as the manufacturer for the air filter. The estimated cost is $10.50 for 50,000 units.

4.4.3.6 Thermocouples

There are two thermocouples in the system: one measuring the anode fuel inlet temperature and one measuring the cathode inlet temperature. These thermocouples are made of two-foot long 1/8th inch thick Inconel thermocouple wire. The cost of each wire is $5 based on catalog pricing.

4.4.3.7 Electrical System

The electrical system includes electrical wiring, power conversion and control devices. For AC power, an inverter is used to convert the fuel cell DC into AC. The input to the inverter is 88-153 Vdc with 80 Amp current. The output is single phase 120/240 Vac. The target efficiency is 95%. The control system is used to maintain stack and system operating conditions including reactant flow rates and stack operating temperatures and to control the startup and shutdown sequences.

The inverter cost is $445, the highest cost item. The details are shown below. The next highest cost item is the controller at $110. The controller cost was estimated based on mature controller technologies, such as microturbine generator controllers, and car ABS controllers. The total estimated cost is $673. Excluding the inverter, the cost is $228.

The inverter cost was estimated by the inverter vendor who fabricated the inverter for the prototype unit. The cost is estimated to be $445/unit at a production volume of 50,000 units per year. Table 4-6 shows the cost breakdowns.

Table 4-6. Inverter cost breakdown

Unit Cost	**$**	**305**
G&A	**$**	**91**
Profit	**$**	**40**
Warranty Dollars	**$**	**9**
Total Price	**$**	**445**

4.4.4 System Packaging

The component with the biggest impact in the system package design is the stack enclosure; the remaining balance-of-plant components are positioned to feed and receive process connections from it. The Phase I prototype has been designed to have sufficient room for ease of installation and removal of the components. It was also designed to allow room for component data gathering and diagnostics. Furthermore, the system was designed to have the balance of plant separated from the stack enclosure for ease of component replacements. Thus there are opportunities to integrate and optimize the system packaging and dramatically reduce system cost.

An integrated packaging design was developed for high volume production and is shown in Figure 4.14. The top is a hot section containing the stacks. The stack weight is transmitted to the base of the system with metal

rods. The middle section includes the thermal management system with the temperature gradually decreasing from top to bottom. In this section, the cold reactants flow upward while being heated by the hot exhaust gas flowing downwards. The bottom section is a cold section that includes the electrical components, blowers, and control valves. The flow distribution manifolds and other system components are integrated as well.

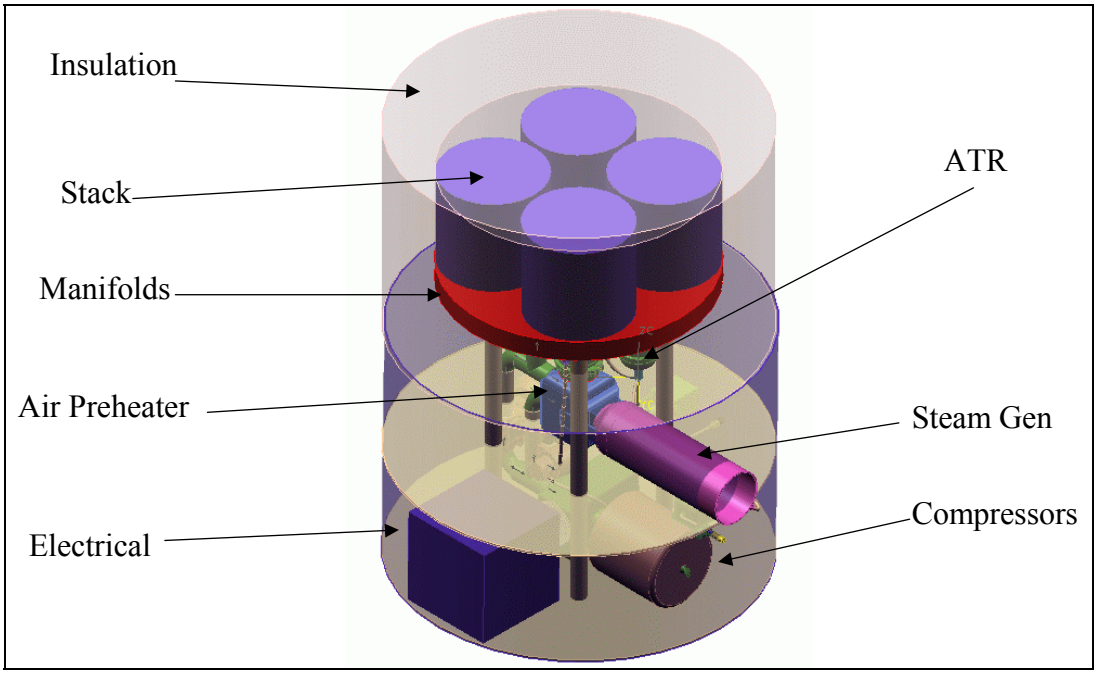

Figure 4.14. Product packaging design.

The cost of the system packaging is $664 per unit which includes the stack gas distribution manifold, insulation, pressure boundary, stack support structure, and current collection. The insulation and the metal pressure boundary constitute the majority of the cost. These costs decrease as the size of the stack decreases. The stack manifold is also expensive and this component would be eliminated if one stack with larger active area cells were used. A cost estimation with a larger active area stack is discussed in later sections.

4.4.5 System Assembly

A bottoms-up approach was taken to estimate the assembly cost. The prototype system was reviewed and assembly processes were identified. Sizes of the workstation, equipment and labor needs were identified for each process. The cost for each of these items was then estimated. The final plant is a 110,000 ft^2 building situated on 10 acres of land. The total cost of the facility including the land, buildings and equipment is about fifteen million dollars. The site is operated with a crew of 120 people. The details behind the system assembly cost will be discussed in the following sub-sections.

4.4.5.1 Assumptions

The system assembly assumed that all components, including the SOFC stacks, have been pre-manufactured. It is assumed that the facility is sized for 50,000 units, with no spare capacity. The facility will be a greenfield development located in the southeast of the U.S. A 7-day workweek with two 12-hour shifts was assumed. Four crews rotate on a 4 days on 3 days off and 3 days on 4 days off schedule. A productivity of 20 hours out of 24 hours was also assumed. This is equivalent to 146 units per day, 73 units/shift, 7.3 units/hr, and 8.2 minutes per cycle. The cycle time is used to determine the labor and equipment needs.

4.4.5.2 Workstation

The workstation size was determined based on the size of the unit. For this analysis, the system is assumed to be 4 x 8 x 6.5 ft, the size of the prototype unit. A workstation of 25 x 25 ft was determined to be appropriate.

4.4.5.3 Assembly Processes

The system assembly is divided into three subassembly lines, the base assembly, the table assembly, and the final assembly. The base assembly includes the base plate, the electrical components, and the exhaust ducts. The table assembly includes the components between the SOFC stack and the rest of the BOP. This includes the table that supports the stack, the stack manifold that rests on top of the plate, the delivery components that hangs on the table below. The final assembly includes merging of the base assembly and table assembly, completing the stack assembly, and the final wiring, and packaging for delivery.

Base Assembly — A process map of the base assembly process is shown in Figure 4.15. The first step includes the assembly of the base plate (the H frame) which supports the system weight, the assembly of the control boxes, and the assembly of the screen that separates the electrical from the rest of the system. Next in step two, the electrical harness connections, and the air and fuel control piping are assembled. In step three, the exhaust piping is mounted to the base plate. The weight, dimensions and the number of joining bolts are specified in the figure to aid the determining of labor and equipments needs to be explained in later sections.

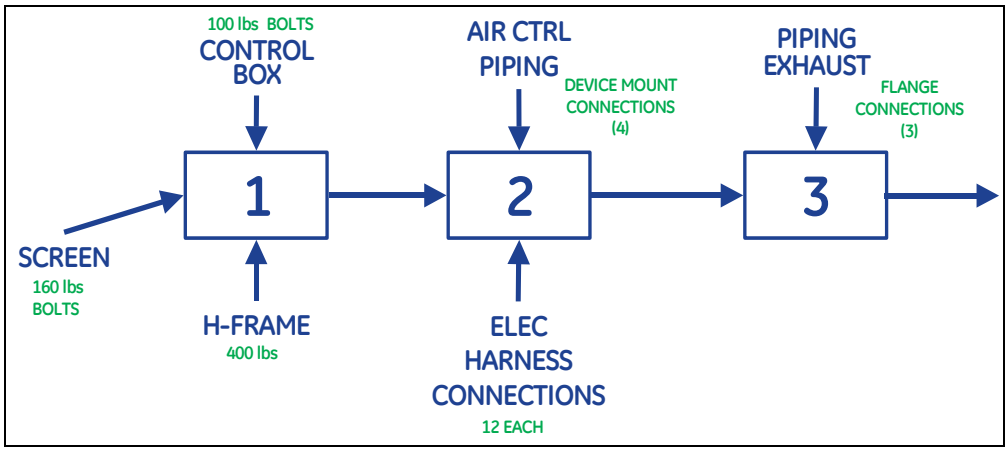

Figure 4.15. Base assembly process.

Table Assembly —The table assembly process is shown in Figure 4.16. In the first step, the base plate of the stack manifold enclosure is assembled to the table ring forming the base for other components to be joined to the assembly. Next the table is rotated 180° after the stack manifold box is attached to the table. The rotation makes the assembly of the rest of the BOP easier. In step two, the exhaust burner, the fuel processor, and the air preheater are attached to the table. After the air piping and the fuel piping are assembled to the table legs separately, the legs are attached to the table. The air bypass valve is also installed to the table.

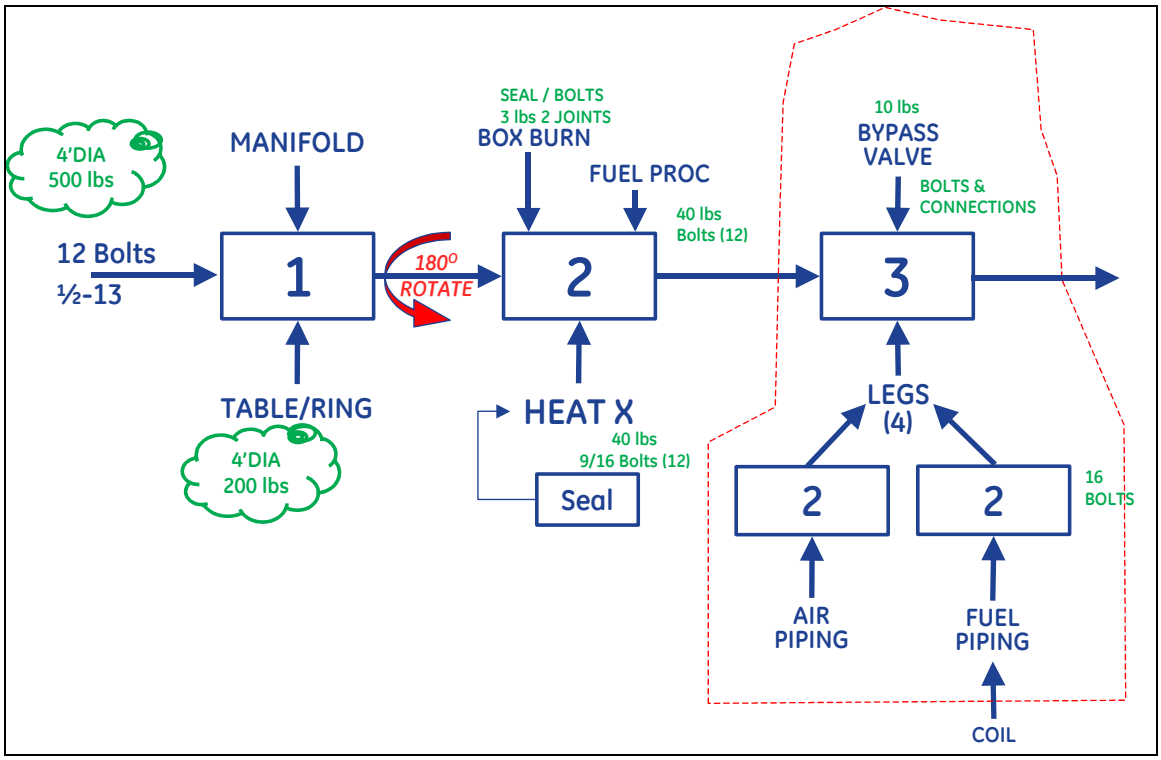

Figure 4.16. Table assembly process.

Final Assembly — The final assembly process is shown in Figure 4.17. The base assembly and the table assembly lines are merged, and the table assembly is rotated 180° and then attached to the base assembly. Next, the electrical and mechanical connections to the table are assembled, and the stack base is mounted to the box manifold. At this point, the fit test (t1) commences. The electrical continuity and mechanical leak tests are performed and any defects are repaired. After t1, the power rods are assembled followed by the installation of the insulation tube placed in the middle of the stacks. The stacks are then lowered to the stack base to complete the stack assembly process. In step 6, electrical connections are made to the stacks including current and voltage monitoring connections and then test (t2) is conducted. With stacks assembled and wires connected, the stack enclosure hat is then lowered and sealed. At this point, the final functional test begins. After testing, the final system enclosure is assembled and ready for final packaging. The assembly process is completed at step 9, packaging for delivery.

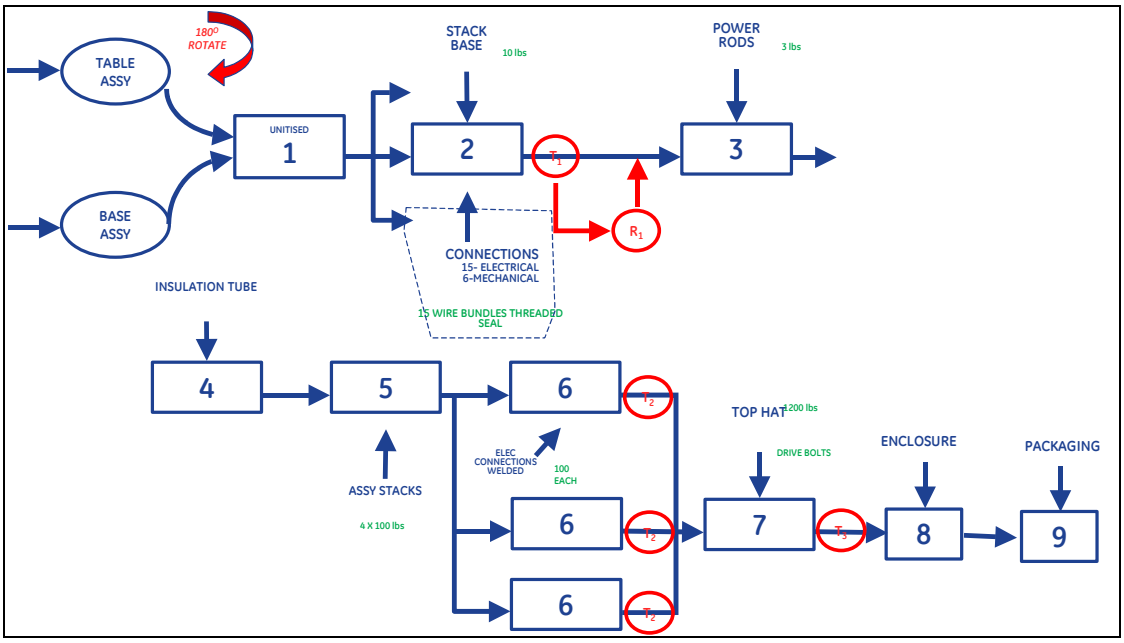

Figure 4.17. Final assembly process.

4.4.5.4 Conveyance Methods

For the table assembly, the conveyor system includes cars on powered rail system. Each cart is self-contained with electrical drive and the ability to rotate the table while on the cart, which would be operator-controlled. There is a return loop to the beginning making the system continuous.

The base and the final assembly conveyor systems are the same. The bases would be designed to accept dollies or wheels on a gauge matching

tracks, which are embedded in the floor. Conveyance of the base assembly is done through a drag chain system, also embedded in the floor. The drag chain mechanism would be engaged and disengaged from the bases by the operator through raising and lowering the “hitch” which couples with pins on the drag chain.

4.4.5.5 Plant Layout

A schematic of the assembly layout is shown in Figure 4.18. The assembly process starts from the left and the finished product ships out from the right side of the building. Incoming material flows into the processes from both sides of the assembly building. The table assembly line merges with the base assembly line to form the final assembly line. The final testing area is large due to the long testing time assumed, 5 hours. The numbers in the picture are the process step numbers shown in the previous sections. Each process is to take about 8.2 minutes. If a number is repeated there are two scenarios; if the numbers are repeated vertically then there are two units being assembled simultaneously (as in the final assembly line), if the numbers are repeated horizontally a single unit passes through a work cell that is twice as long a the standard cell (as shown in step 2 of the table assembly).

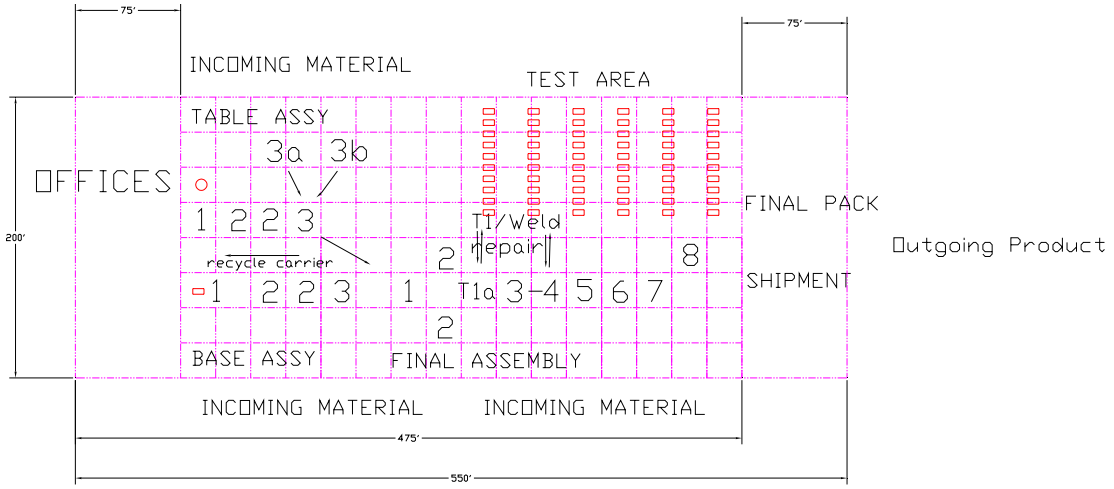

Figure 4.18. SECA system assembly plant layout.

4.4.5.6 Plant Cost

The facility cost is determined based on the plant layout shown in Figure 4.18. The workstation, the building, and land cost are summarized in Table 4-7. The facility is located in the southeast of the U.S and the total cost is $14,050,000.

Table 4-7. Facility cost (costs are in unit of thousand dollars).

	Cost each	Qty Req.	Total Cost
Bldg 110M sq. ft	0.125	110,000	13750
Land 10 acres	15	10	150
Workstation costs	7.5	20	150
Total			14,050

For each subassembly, the assembly method and equipment required were determined. The labor requirements were identified as well. These costs are summarized in Table 4-8. The total equipment cost is estimated to be $1,355,000. The plant requires 30 operators per shift. Since there are four shifts, a total of 120 operators are required in the plant.

Table 4-8. Summary of equipment and labor needs.

	Equipment Cost	# of heads/shift
Base Assembly	394	4
Table Assembly	425	6
Final Assembly	537	20
Total	1,355	30

4.4.5.7 Unit Assembly Cost

The unit assembly cost is obtained once the annual cost of the facility is determined by considering the appropriate amortization schedule. The schedule is the same as that used in the stack cost model, 20 years for the equipment and the facility. The estimated labor cost is $124.2/unit. The equipment and facility costs are estimated to be $1.4 and $7/unit, respectively. The high labor cost reflects the large number of steps required for system assembly. The total system assembly cost is $133/unit.

4.5 SYSTEM COST ANALYSIS WITH A LARGER ACTIVE AREA STACK

The Phase I SECA stacks are made of cells with active area of 142 cm^2. With cell active area four times larger than that of the prototype, only one stack with forty cells is required for the SECA system. Assuming the total active area remains the same, the manufacturing cost will decrease as the number of pieces decreases. Also as the cell area increases, the cell area to the total plan-form ratio also increases. Thus, the interconnect materials cost also decreases. The cost of the end plates and the cost of the compression system are also reduced. The cost of the larger area stack was estimated using the cost model described previously and is estimated to be $960, compared with $1369 for the prototype stacks.

With one stack, the system packaging cost can also be reduced. To maintain the same amount of heat loss as that of the prototype, the insulation

required to maintain the same heat loss is reduced. Thus, the stack enclosure diameter with the single stack is significantly reduced. Additionally, using one single stack, the gas distribution manifold is no longer necessary. A packaging design for the one-stack system is shown in Figure 4.19. The design is the same as that of the four-stack system except that the four-stack enclosure is replaced by the one-stack enclosure.

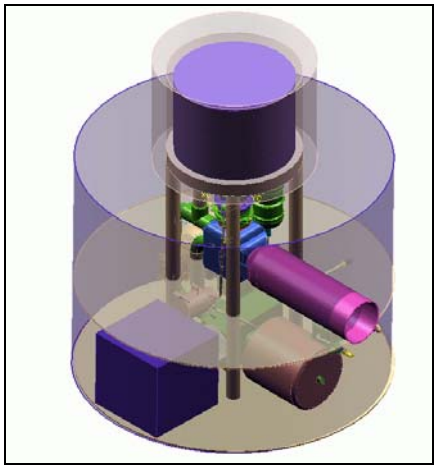

Figure 4.19. One-stack system packaging design.

As a result of smaller packaging, the pressure boundary and the insulation costs are decreased. Compared with the four-stack system, the packaging cost decreased by $396. Thus, the total savings with the one-stack system is $713. The system cost with the one-stack system is summarized in Table 4-9. The one stack system is shown to have the potential of reaching the SECA phase II cost target of $600/kW.

Table 4-9. System cost of the one-stack system.

Stack	$960
Fuel Processor	$121
Air Delivery	$394
Fuel Delivery	$221
Water Delivery	$239
Thermal Management	$531
Electrical	$238
Packaging	$211
Assembly	$133
Total	$3,049
$/kW, based on 5.4 kW	$565

4.6 SYSTEM COST SUMMARY AND SENSITIVITY ANALYSIS

4.6.1 System Cost Summary

The total unit cost for the system is $3,910 which results in $724/kW with the 5.4 kW demonstrated in the prototype system test. The system cost breakdown is given in Figure 4.20. The SOFC contributes more than 1/3 of the total cost. The fuel processor contributes 3% of the total cost. The thermal management system, which heats up the reactants and recovers heat from the exhaust, contributes 14% of the total cost. The packaging cost which includes thermal insulation is estimated to be 17%. The fuel, water, and the air delivery systems contribute 6%, 6%, and 10%, respectively.

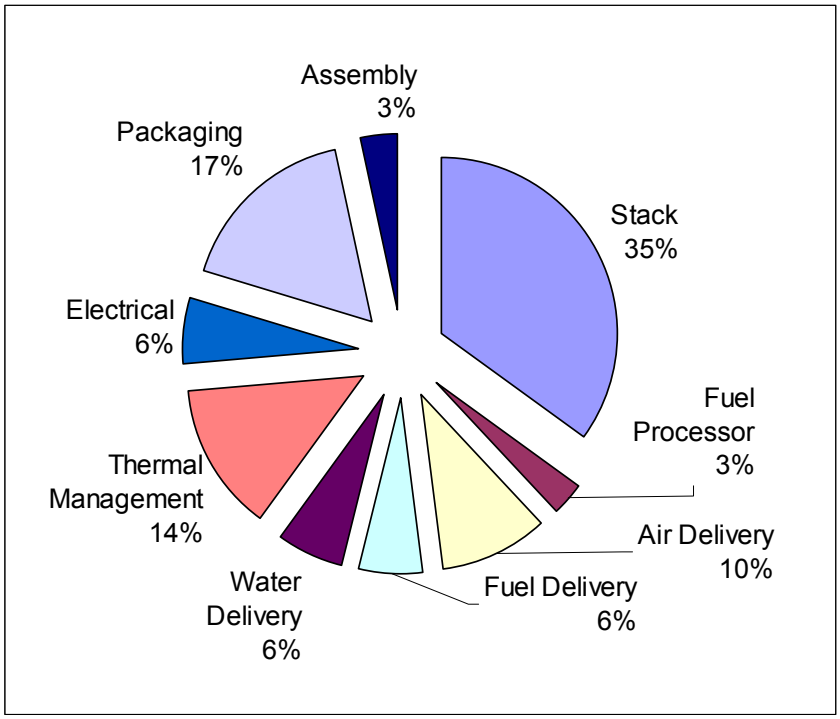

Figure 4.20. Cost break down of SECA SOFC system.

4.6.2 Sensitivity Analysis

The cost implications of assumptions are explored in more detail here and alternatives to the current design and cost implications are studied. The range of uncertainties in the design and manufacturing variables are delineated. A Monte Carlo simulation is performed, and the confidence interval of a +/-25% variation is determined. Component and subsystem cost variations were explored in detail and Monte Carlo simulations run to assess the sensitivity of the projected system cost. Fairly large standard deviations are used in the analysis. As more units are demonstrated and the technology becomes more mature, these variations would be reduced.

A sensitivity chart is shown in Figure 4.21. The system cost is most sensitive to the cost of the stack. The stack contributes 35% of the total system cost and is a strong function of stack design. System design that minimizes the airflow rate lowers the cost of the next cost sensitive components, the thermal management system. The systems cost is also sensitive to the packaging cost, and the packaging cost is sensitive to the stack design. Thus, system cost is most sensitive to the stack design which presents the greatest opportunity to drive down system cost in Phase II of the SECA program.

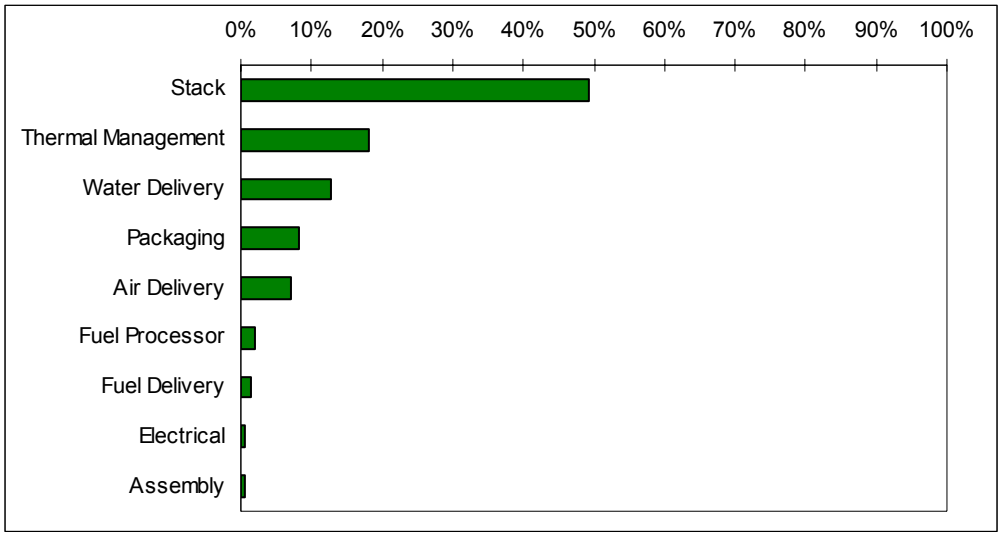

Figure 4.21. SECA class systems cost sensitivity chart.

A frequency chart is shown in Figure 4.22 which shows the overall variation in per unit system cost. The confidence internal with a +/-25% variation from the mean is determined to be 83%. The system cost is shown to be between $2917 and $4863.

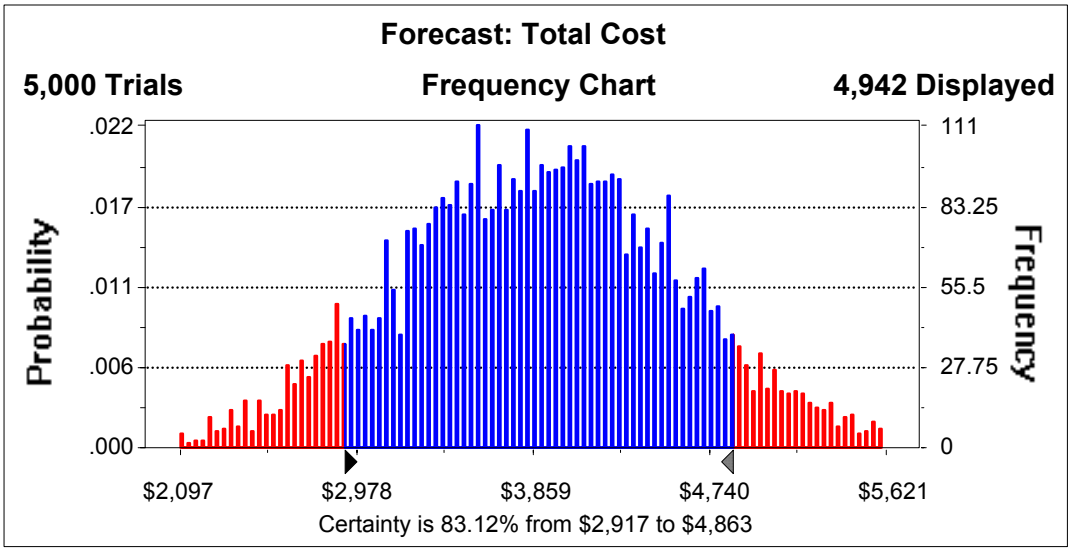

Figure 4.22. System cost Monte Carlo analysis results.

4.7 IMPACT OF DEGRADATION ON SYSTEM COST

The SECA Phase I system has a cost of $724/kW when manufactured at 50,000 units per year. During testing, the prototype demonstrated a peak power of 5.4 kW, which established the power rating. However, the fuel cell could degrade at a rate of 0.2% per 1,000 hours. This section discusses the impact of degradation on cost for a period of 40,000 hours of operation.

To achieve 5.4 kW peak power at the end of 40,000 hours of operation, the active area in the prototype stacks would need to increase by about 8%. The prototype consists of four 40-cell stacks. Thus, twelve more cells would be needed to accommodate power degradation as shown in Equation 4.3. Each stack will increase by three cells. Hence, the total stack cost increases from $1369 to $1482 as shown in Table 4-10. With the addition of three cells, the stack height increases by 2 cm leading to a packaging cost increase of $6.41 for additional insulation and metal. The balance of the system components remains the same since each component would be operated at a lower capacity level until near the end of 40,000 hours. Consequently, the system cost increases from $3910 to $4029. With a 5.4 kW peak power, the system cost is $746/kW at the end of 40,000 hours of operation.

$$number\ of\ additional\ cells = 4 \times 40 \times 8\% \approx 12 \qquad (4.3)$$

Table 4-10. Stack cost with 172 cells.

	$/system
Material	**$896**
Facility & Equipment	**$194**
Labor	**$301**
Operation & Maintenance	**$92**
Total	**$1,482**

5 STACK DEVELOPMENT

The objective of the SECA Phase I stack development effort was to develop a stack or set of stacks that were capable of meeting a set of performance and cost requirements and would interface and function with the remainder of the prototype system. The final stack targets which were flowed down from the system design effort are outlined in Table 5-1. Note that for simplicity, the performance target is identified as a single operating point, while in reality the stacks were required to operate over an operating window defined by the requirements of system operation.

Table 5-1. Final SECA stack requirements

Requirement	Units	Target	Comments
Number of stacks	#	4	System designed to accommodate 4 stacks, flow parallel, electrically in series
Number of cells	Cells/stack	40	
Gross Power	W/stack	1704	
Power Density	W/cm^2	0.300	All these to be met simultaneously
Cell Voltage	V/cell	0.70	
Fuel Utilization		80%	
Steady-State Degradation	%/500h	1	Half of allowable system degradation allocated to stack
Cycling Degradation	%/10 cycles	1	Half of allowable system degradation allocated to stack
Air-Side Pressure Drop	psi	0.5	
Projected Cost	$/kW	200	$200/kW target for stack

Meeting the stack targets required development in the following areas:

- *Stack Design* - It was determined during the program that GE's pre-existing stack designs were not adequate for meeting the SECA targets, particularly the fuel utilization and pressure drop requirements. Two design iterations over the course of the program led to the final stack design used in the prototype system.

- *Cell Development* - At the beginning of the program, GE's cell technology was not capable of consistent, stable operation at high fuel utilization. Power density also needed to be improved significantly to meet the SECA Phase I requirements. Improvements in cell architecture were made that bridged these gaps.
- *Stack Materials* - Stack performance is dependent not only on the cells, but also on having appropriate interconnect, seal and bonding materials. Development work was conducted on all of these materials, aimed at validating existing materials as well as identifying improved ones.

Details of the work in these three areas are given in the discussion that follows.

5.1 STACK DESIGN DEVELOPMENT

During the course of the program, three major stack design iterations were undertaken to address inadequacies of previous designs and lead to stacks that could meet all the requirements. At the beginning of the program, two stack designs were under consideration (and were described in the proposal), but both had serious shortcomings and neither was sufficiently mature to downselect. The first of these, the sealless radial design, was a center-fed, externally manifolded design which relied on small diameter tubes to feed reactants into the individual cells. These tubes created an unacceptably high pressure drop through the stack. In addition, scale-up to stacks with large numbers of cells presented a challenge, as the manifold system was not very tolerant to dimensional variation or changes that would occur during startup. Finally, the thermal management of sealless stacks was not well understood and the inability to control edge combustion represented a major concern.

The alternative design, called the unitized design, also had significant perceived disadvantages. This design was a square design with straight-through reactant flows. The design had flow distribution and pressure-drop concerns as well as sealing problems, and it had not been satisfactorily demonstrated at any significant size.

After the initial assessment of existing designs, a new design effort was kicked off with a series of brainstorming sessions to develop alternative concepts. From these concepts, two designs were selected for further evaluation. These designs are outlined below.

5.1.1 Square Half-Sealed Design

The square half-sealed design is based on a square cell with fuel inlet and outlet manifolds. Figure 5.1 shows the square cell module design. The cell module consists of cell, anode picture frame, stamped anode flow field sheet, cathode flow fin, and two composite manifold spacers. The cell, the anode picture frame, and the anode stamped flow sheet forms the anode flow field, which could be serpentine or "straight-through". The cathode flow field is formed

by cell, cathode air fin, and anode stamped flow field sheet. Both fuel and air flow from one side to the opposite side of the stack. The fuel comes in from the main fuel inlet manifold, flows through the anode flow field, and exits to the main fuel outlet manifold. The air flows straight through the cathode flow field from one side to the other of the cell module.

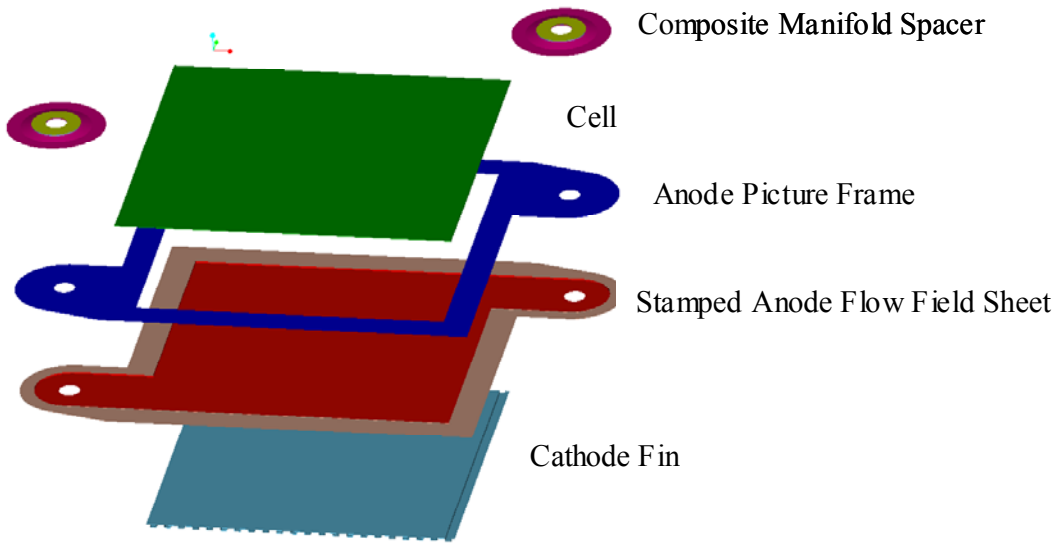

Figure 5.1. Cell module design of square half-sealed stack design

Beside the two manifold seals, the cell seal is at the periphery of the cell. Three of the four sides of the cell seal may leak directly to the cathode flow field, across the flow fields. Also, the seal at the fuel inlet and the portion of the two side seals are at the upstream of the fuel flow, which is at high fuel content. The seal requirement for the cell seal is high to prevent hot spots in the flow fields.

5.1.2 Circular Half-Sealed Design

The circular half-sealed design is based on the circular cell. The cell module includes the cell, anode flow field sheet, manifold flat sheet, manifold sheet, cathode flow sheet, and three composite manifold spacers. Both fuel and air flow from the manifolds at the cell periphery to the center of the cell module and then flow outward over the anode and cathode flow fields from the center to the periphery respectively.

The advantage of the circular design is that the cell seal is at the downstream of the fuel flow. Any leakage from the cell goes out of the stack module to the air outlet manifold formed by the insulation around the stack and is consumed by the large stack air flow. The temperature rise caused by the leakage will be minimum.

The stack module, shown in Figure 5.2 is about 12” high, 11.5” wide, and 9.5 deep. The fuel and air are distributed to each cell module through inlet manifolds. The spent fuel is collected by the spent fuel manifold, while the spent air is collected by the manifold formed by insulation.

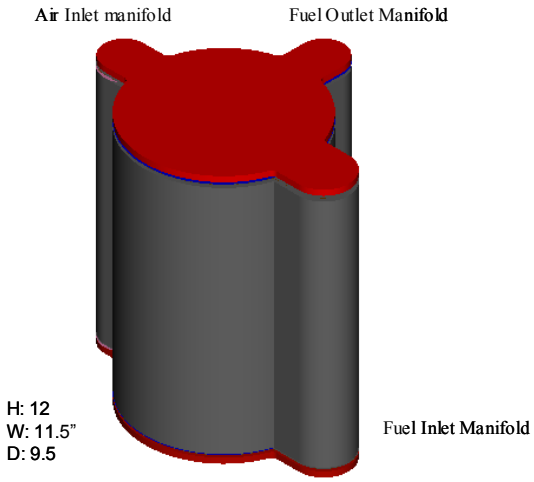

Figure 5.2. Stack module of circular half-sealed stack design

5.1.3 Analysis of Baseline Designs

5.1.3.1 Flow Analysis

Computational fluid dynamics (CFD) analyses were conducted to understand and optimize the flow uniformity in all basic flow fields for the stack concepts. CFD analysis was conducted for the four basic flowfields:

- Serpentine flow
- Straight-Through flow
- Spiral flow
- Radial flow

The CFD results show that for all these four flow fields, reasonable cell-level uniform flow can be achieved.

5.1.3.2 Thermal Analysis

Thermal and flow analysis of half sealed square and circular stack design were conducted. Three dimensional CFD models for single cell stacks were built for each geometry to conduct the analysis.

Models were used to compare the effect of different heat generation assumptions on the cell temperature profile. A linear profile was based on the

assumption that heat generation decreases by a factor from the center to the perimeter of a cell. Another profile was based on uniform heat generation. These two profiles were found to bound the published data as well as in-house electrochemical model based data. A user defined function (UDF) was generated to apply the profiles to the circular geometry within the CFD models.

Figure 5.3 shows the comparison of different geometries. Temperature drop across the seal is significantly higher for a square cell than a circular cell. Temperature drop across the cell is less for linearly decreasing (LD) heat generation than that for uniform heat generation. This indicates that uniform heat generation assumption is the worst-case scenario. Temperature contours were obtained for the circular cell with manifold using uniform heat generation. Temperature drop across the cell was found to be significantly less than that for a cell without the manifold.

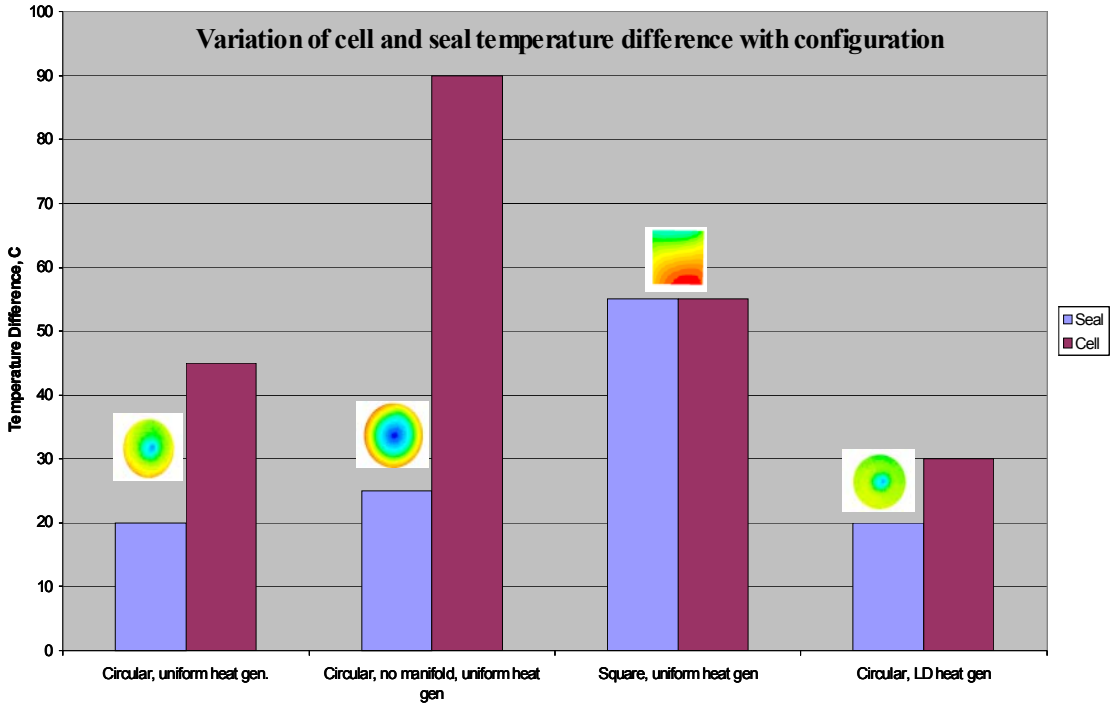

Figure 5.3. Comparison of different geometries

5.1.4 Initial Down-Selection

After the selected designs were developed and analyzed more fully, a down-selection was held, at which the circular half-sealed design was chosen as the baseline SECA stack concept.

5.1.5 Test Vehicle Design

The SECA stacks are designed to be fabricable from thin stamped interconnect sheets, joined by brazing, welding or similar operation. Because the initial startup cost of stamping interconnect sheets is high (because of the dies required) and the expectation that multiple interconnect design iterations will be required to achieve the optimum configuration, the decision was made early in the program to simulate stamped interconnects using thicker sheets which would be cut and brazed to form the final interconnect.

Testing of several stacks with this design was performed. One 5-cell, one 6-cell, and two 10-cell stacks were tested with achievement of 75% fuel utilization and maximum power of 0.5 kW. Following the completion of the testing, a risk review was conducted on this stack design. The review identified several major risks:

- Manifold seal leakage
- Cell seal leakage
- Cost of interconnect
- Cell shorting
- Manifold shorting
- Cell cracking
- Tolerance stack-up for interconnect

To address the above risks, a brainstorming session was held to develop additional ideas/concepts. Three key modifications to the design came out of this session.

- *Quality Control* – Additional steps were added to the stack build process to enable screening out of bad cells and interconnects before they are used in the stack.
- *Improved Manifold* – An improved manifold design was developed which significantly improved sealing while decreasing stack cost.
- *Reduce the Metal Layers in the Interconnect* - The result was reduced cost and labor to make interconnects and assemble stacks.

5.1.6 Concept Design of 6kW Stack

The 6 kW stack assembly has 4 stack modules of 1.6 kW, which are configured electrically in series and plumbed together in parallel manner for flow distribution.

5.1.7 Analysis and Testing of Final Design

The stacks that were used in the SECA prototype system were made using the second iteration of design described above. Significant mechanical, flow and thermal analyses were required to optimize the stack design. These analyses will be summarized here. Ideally, the stack design will simultaneously optimize a number of parameters:

- Minimum leakage through seals;
- Minimum pressure drop through the interconnect to reduce the system air blower power parasite;
- Minimum thermal gradients on the cell;
- Maximum flow uniformity within the cell.

However, as will be seen, many of these requirements conflict with each other, and analyses were required to find the optimal trade-offs.

5.1.7.1 Flow Analysis

Flow analysis was performed to determine the overall air-side pressure drop through the stack. At the SECA design point, the air pressure drop requirement from the system was 0.5 psi. This number was flowed up to the system design team and deemed acceptable. Pressure drop data on full-size stacks at operating conditions could not be directly determined from the prototype system test. However, on subscale stacks, the pressure drop has consistently been at or below 0.5 psi at the design point.

5.1.7.2 Thermal Analysis

One goal of the stack design is to minimize thermal gradients on the cell and maximum temperature of the interconnect metal. Meanwhile, increasing allowable air ΔT through the system gives a significant boost to system efficiency. With the new design, the air ΔT is expected to be significantly higher than the cell ΔT. Analysis was done to quantify this difference. Also, the cell temperature is everywhere higher than the air temperature, and the inlet air temperature is quite low, which means that the temperature requirements on the system air preheater materials are reduced.

5.2 STACK MANUFACTURING AND TESTING

5.2.1 Interconnects

The interconnects are fabricated using multiple layers which are water-jet cut and then laminated together to represent the flowfield. As discussed previously, this manufacturing method allows for design flexibility without requiring up front investment in tooling for stamping of interconnects.

Every part that is received is leak-checked to make sure there are no leak paths through the braze. Also, the surface of each part is profiled to make sure it meets flatness and parallelism specs.

5.2.2 Quality Control

Interconnect and ceramic parts are subjected to a large number of quality control processes. In order to be used in a stack, parts must be:

- *Crack-free* - if the cell is chipped or cracked, the part is discarded or recycled
- *Leak-tight* – interconnects leakage must be within specification
- *Highly resistive* - resistance through the cell is measured and must fall within the specification
- *Unblocked* - pressure drop is measured from the anode inlet to outlet manifolds, and parts with excessively high pressure drop are discarded or recycled

All of the above data is collected and captured in a stack part database, which is used to manage all parts. This has proven to be tremendously important, because stack performance data can now be correlated with QC data, leading to refined specification limits and acceptance criteria. Using the parts data-base for stack post-mortem investigation has led to specification revision and better stack reliability.

Before they are released for use in stacks, each individual fuel cell is subjected to a load test to ensure it has sufficient fracture resistance to survive stackup. Depending on the use planned for the cell, the load at which it is proof-tested varies. This test has been fairly effective at reducing in situ fractures, but by no means perfect.

5.2.3 Stack Assembly

A fully-assembled stack, pre-firing, is shown in Figure 5.4. Stacks are assembled in a fixture inside a test stand. The fixture used for the system prototype stacks can be used to move an assembled and/or tested stack in and out of a test stand. This fixture is shown in Figure 5.5 below. All stacks, including those intended for use in the SECA prototype system, are initially fired and tested in a test stand. For the system prototype stacks, this serves as a qualification process. The stacks must operate stably at a defined set of operating conditions in order to be considered for use in the system. Stack performance at each operating point is also a consideration, obviously, but stability is paramount.

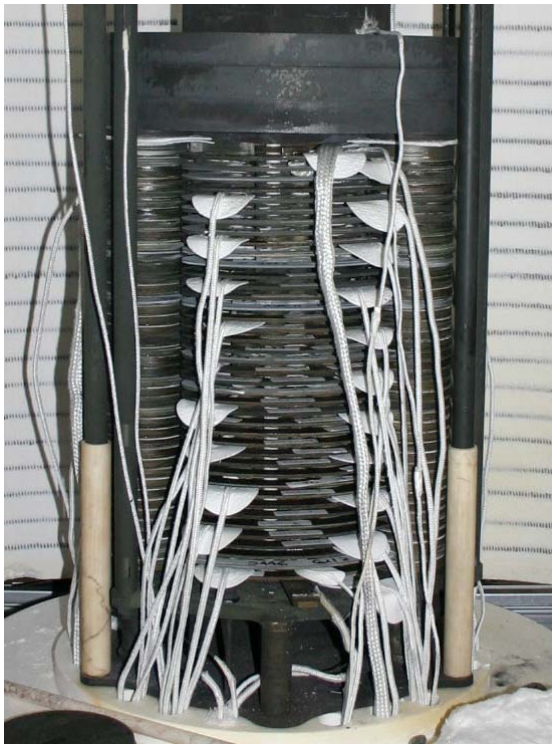

Figure 5.4. S583, a 40-cell stack, fully assembled before firing.

Figure 5.5. The fixture for building SECA system stacks. Here, it is installed into a test stand furnace.

Many stacks of various sizes were built and tested during the program. Only the 20-cell Gen 1 stacks and the 40-cell Gen 2 stacks that were incorporated into the SECA prototype system will be discussed here.

5.2.4 Gen 1 System Stacks S660, S711, S720, S732, S745

The first generation of the SECA prototype system used 4 20-cell stacks. Five stacks were built to meet this supply and include a spare if any issues were to arise with one of the four selected stacks. In the end, all 5 stacks were used in the various Gen 1 system tests. All 5 stacks were built using the standard stack assembly process, and tested according to a controlled test plan (the plan did evolve slightly from test to test).

Overall, all 5 stacks performed very well. Three stacks were run through the entire operation range called out in the test plan without any signs of instability. Stack 1 (S660) was not run at high fuel utilization (U_f) and low current in ATR fuel, because of a control problem with the test stand water supply, but it ran stably over all tested conditions. In stack 4, a single cell (cell #13) was unstable at 80% U_f and currents above 38A. For this reason, stack 4 served as the backup stack, although it was eventually used in later testing.

Performance of the 5 stacks is shown in Figure 5.6 to Figure 5.10. The first three plots show polarization curves at 60% and 80% U_f in simulated ATR fuel. The next plot compares the cell-to-cell voltage distribution of the stacks at a constant operating condition (60% U_f, ATR, 60.8A). The final plot compares performance of stack 5 (S745) at 17% and 25% U_{air}. Some notable results:

- Stack reproducibility was very good. At all operating conditions, the power of each stack was within 5% of the mean power for that condition. Cell-to-cell variation within a stack was quite wide (Figure 5.9), but this degree of variation was not observed at the stack level.
- The target for stack performance in SECA Phase I was 0.300 W/cm^2 at 0.7 V/cell (equivalent to 0.428 A/cm^2) at 80% U_f in ATR reformate. These system stacks fall just short of this performance. At 0.428 A/cm^2 and 80% Uf in simulated ATR fuel, the average cell reached 0.288 W/cm^2, or 96% of the target power density. The best stack, S720, reached 0.294 W/cm2 (with S745 just behind at 0.293), or 98% of the target. Even so, the performance demonstrated in these stacks, particularly at low current density, should be more than adequate to exceed the 35% system efficiency target, according to system models.
- End effects were clearly observed in these stacks, both in temperature and performance. The 2-3 cells at the top and bottom of the stack were generally 30-40°C cooler than the other cells, and correspondingly lower performance was generally (but not always) seen in the stacks. Obviously, cell-to-cell performance uniformity is a significant area of opportunity for improvement in the next phases of SECA.

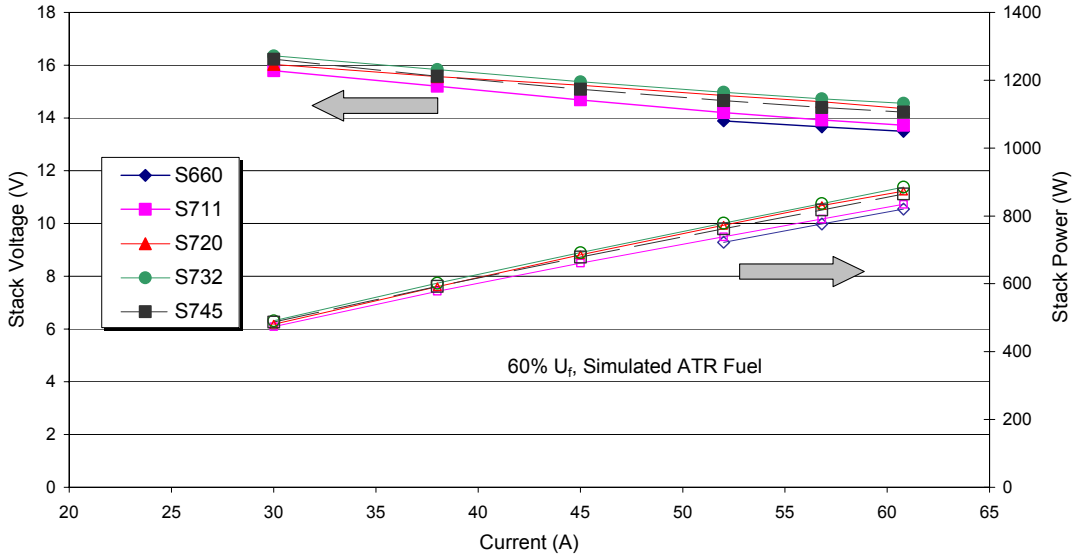

Figure 5.6. Full-stack polarization curves of the five Gen 1 system stacks at 60% U_f in simulated ATR fuel.

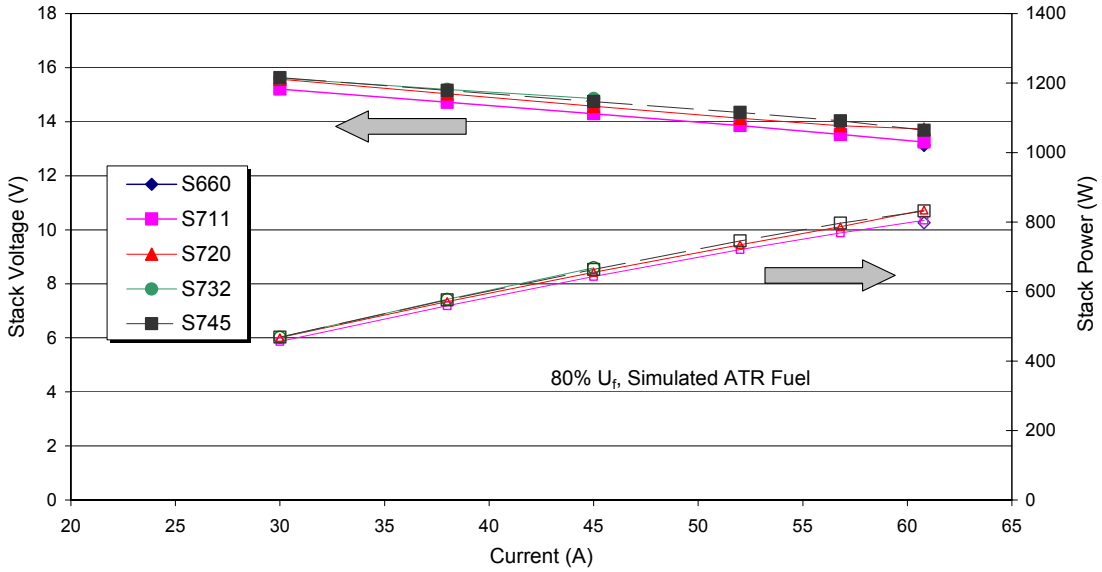

Figure 5.7. Full-stack polarization curves of the five Gen 1 system stacks at 80% U_f in simulated ATR fuel.

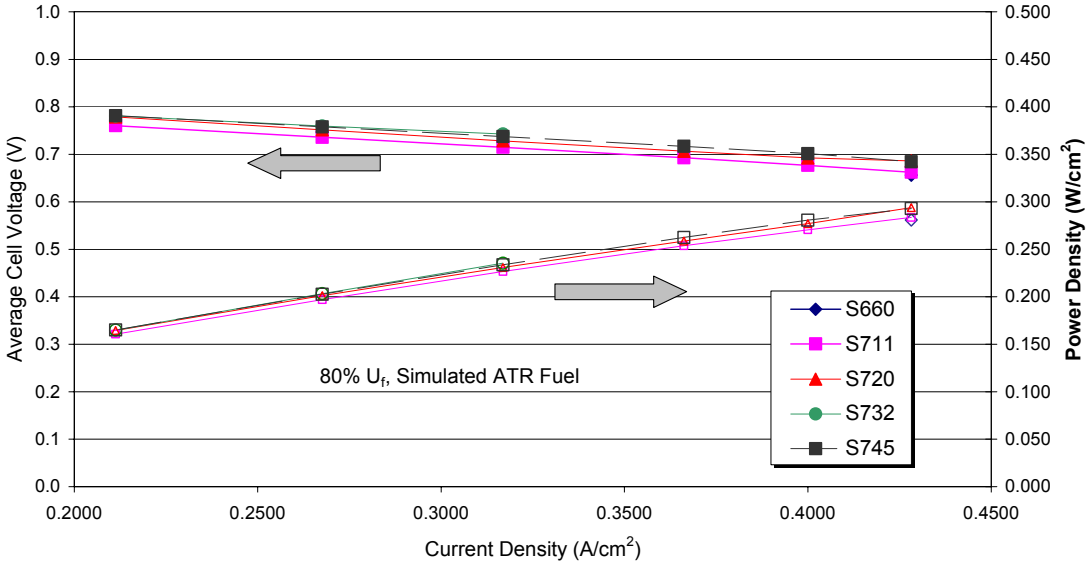

Figure 5.8. Normalized polarization curves of the five Gen 1 system stacks at 80% U_f in simulated ATR fuel.

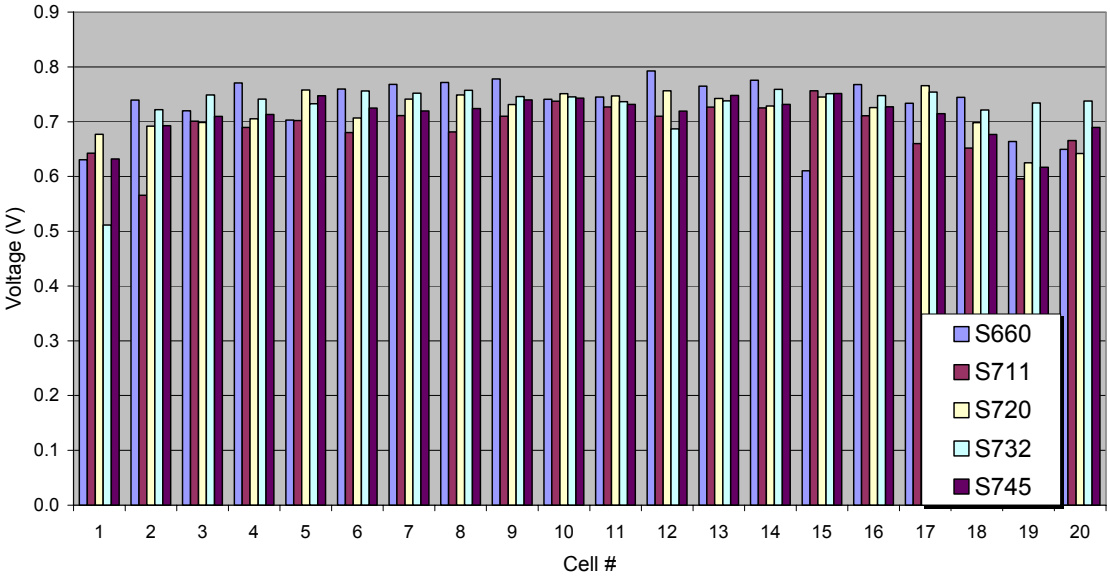

Figure 5.9. Cell-to-cell voltage distributions of the five Gen 1 system stacks at 0.428 A/cm^2 and 60% U_f in simulated ATR fuel.

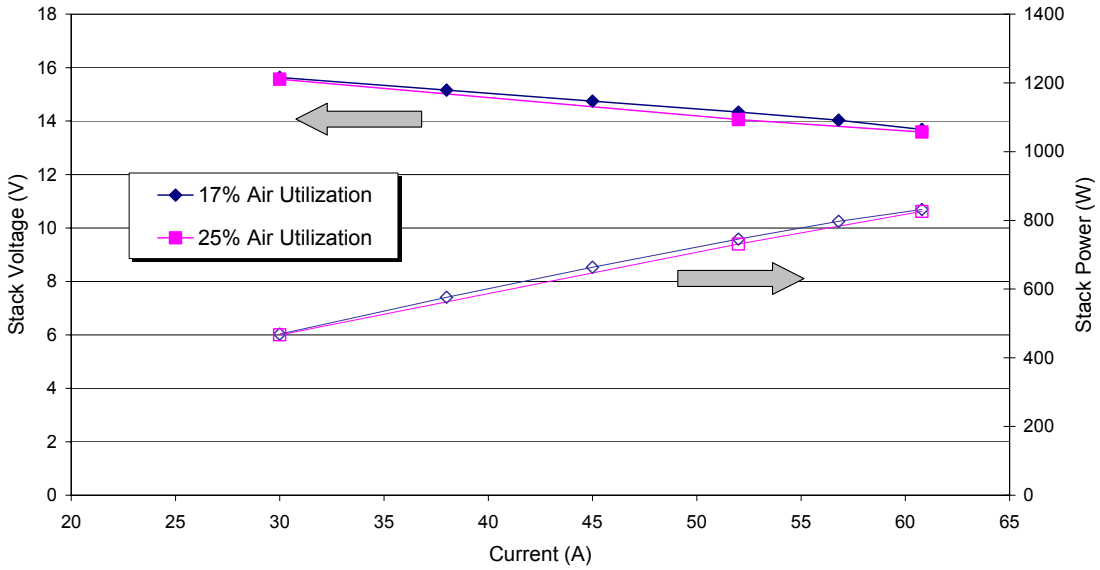

Figure 5.10. Polarization curves of S745, system stack #5, at different air utilizations. The curves were taken in simulated ATR fuel at 80% fuel utilization.

5.2.5 Gen 2 System Stacks S816, S861, S875, S885, S895, S922

Six 40-cell stacks were built in advance of the Gen 2 SECA prototype system test. All 6 stacks were built using the standard stack assembly process, and tested according to the test plan. The second stack, S861, did not reach the point of testing because the top of the stack shorted against the test fixture during the heatup. The resulting uncontrolled current flow through the entire stack damaged the stack significantly and it could not recover. The fifth stack, S895, showed poor performance stability at 80% fuel utilization, and was thus chosen as the back-up stack for the system test. Performance data of the four stacks that were used in the system are summarized in Figure 5.11 to Figure 5.14.

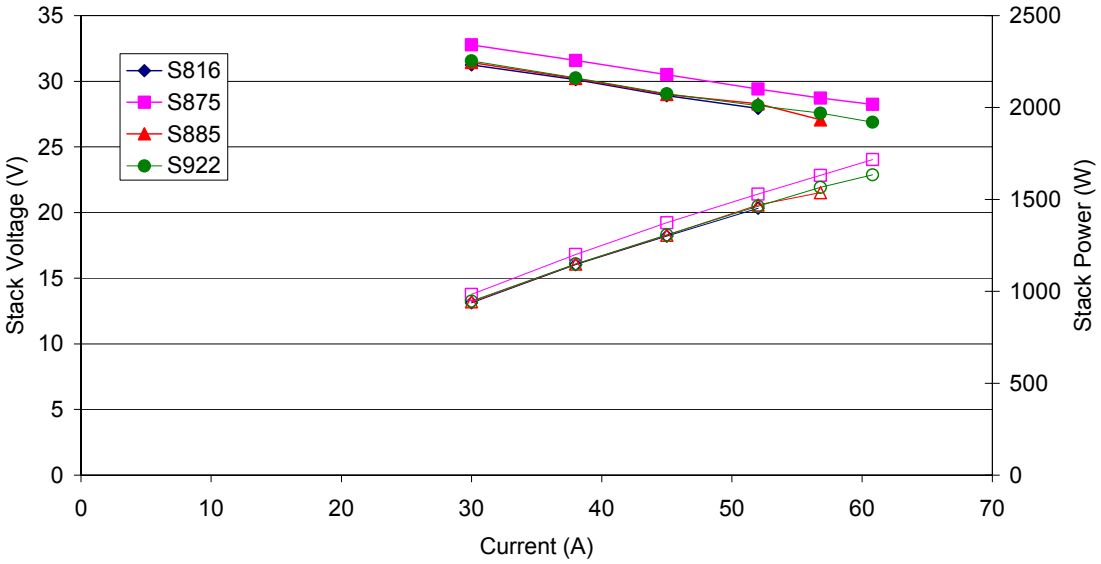

Figure 5.11. Full-stack polarization curves of the four Gen 2 system stacks at 60% U_f in simulated ATR fuel.

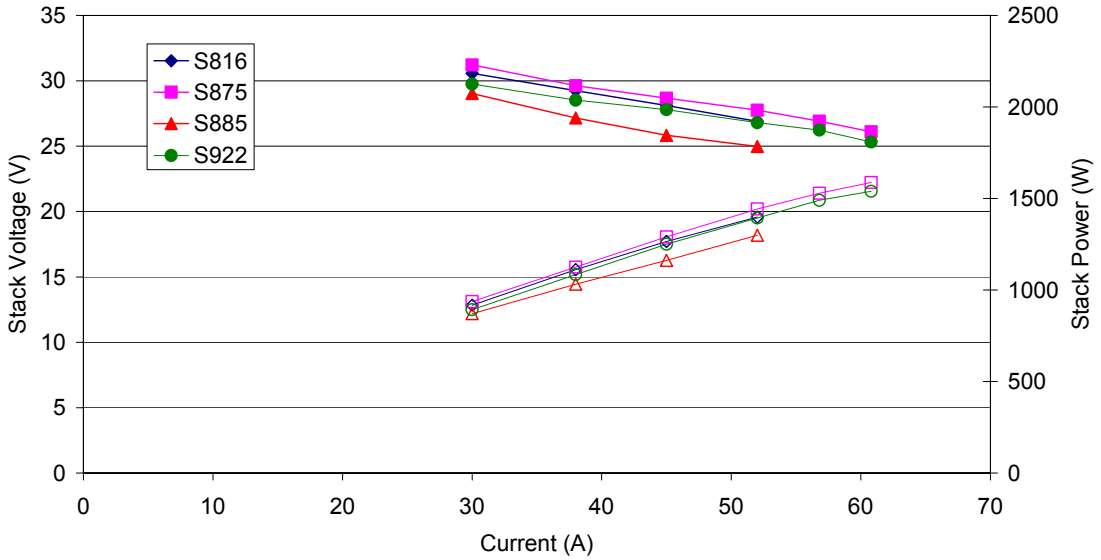

Figure 5.12. Full-stack polarization curves of the four Gen 2 system stacks at 80% U_f in simulated ATR fuel.

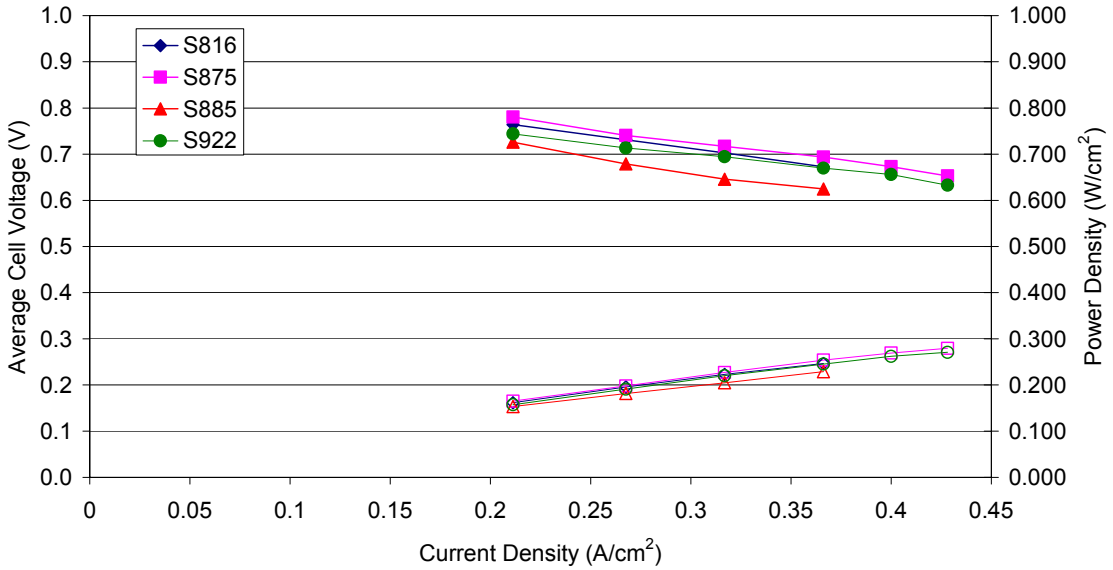

Figure 5.13. Normalized polarization curves of the four Gen 2 system stacks at 80% U_f in simulated ATR fuel

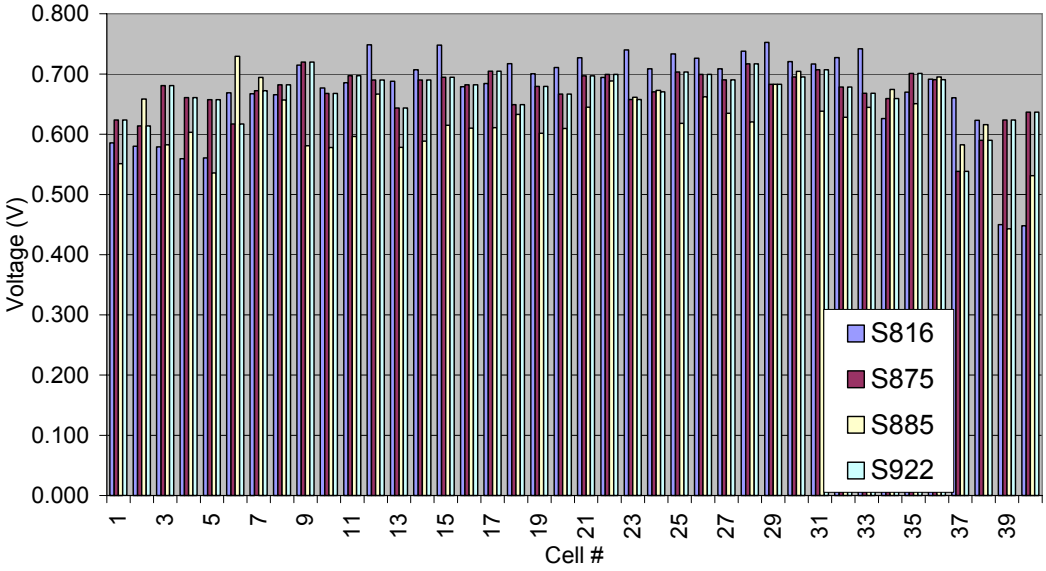

Figure 5.14. Cell-to-cell voltage distributions of the Gen 2 system stacks at 0.366 A/cm^2 and 80% U_f in simulated ATR fuel.

The Gen 2 stack results were, in general, similar to but slightly worse than the Gen 1 stack results. Notable results.

- Stack reproducibility was still good. At all operating conditions, the power of each stack was within 10% of the mean power for that condition. Again, cell-to-cell variation within a stack was wide but washed out in the stack-level results.

- The Gen 2 system stacks missed the target performance by more than the Gen 1 stacks. At 0.428 A/cm^2 and 80% Uf in simulated ATR fuel, the average cell reached 0.279 W/cm^2, or 93% of the target power density. However, this is skewed by the fact that two stacks were not tested at this power density in the test stand because of constraints on minimum cell voltage (these constraints have since been lifted, as stable operation at voltages has consistently been demonstrated). Once again, however, performance was good enough to achieve greater than 35% efficiency in the system test.
- End effects were more dramatic in these stacks. The top 2-3 cells tended to have much lower temperature (50+°C) than the other cells and significantly lower performance beyond what would be expected by the temperature difference. This is the reason for the reduced overall stack performance, as performance of cells in the middle of the stacks was very similar to that observed in the Gen 1 stacks.

5.3 CELL DEVELOPMENT

At the beginning of the program, a gap analysis was conducted comparing cell performance to the preliminary performance targets. At that time, the performance target for the stack was 0.300 mW/cm^2 at 0.75V/cell with 80% fuel utilization in ATR reformate. The performance gap, shown in Figure 5.15, was large. The actual performance capability at that time was estimated as 35-75 mW/cm^2 at the appropriate operating conditions. Over the course of the program, the target was adjusted to 0.70V, but this makes little difference in the size of the initial gap, as performance at that time was only 70-140 mW/cm^2 in multi-cell stacks.

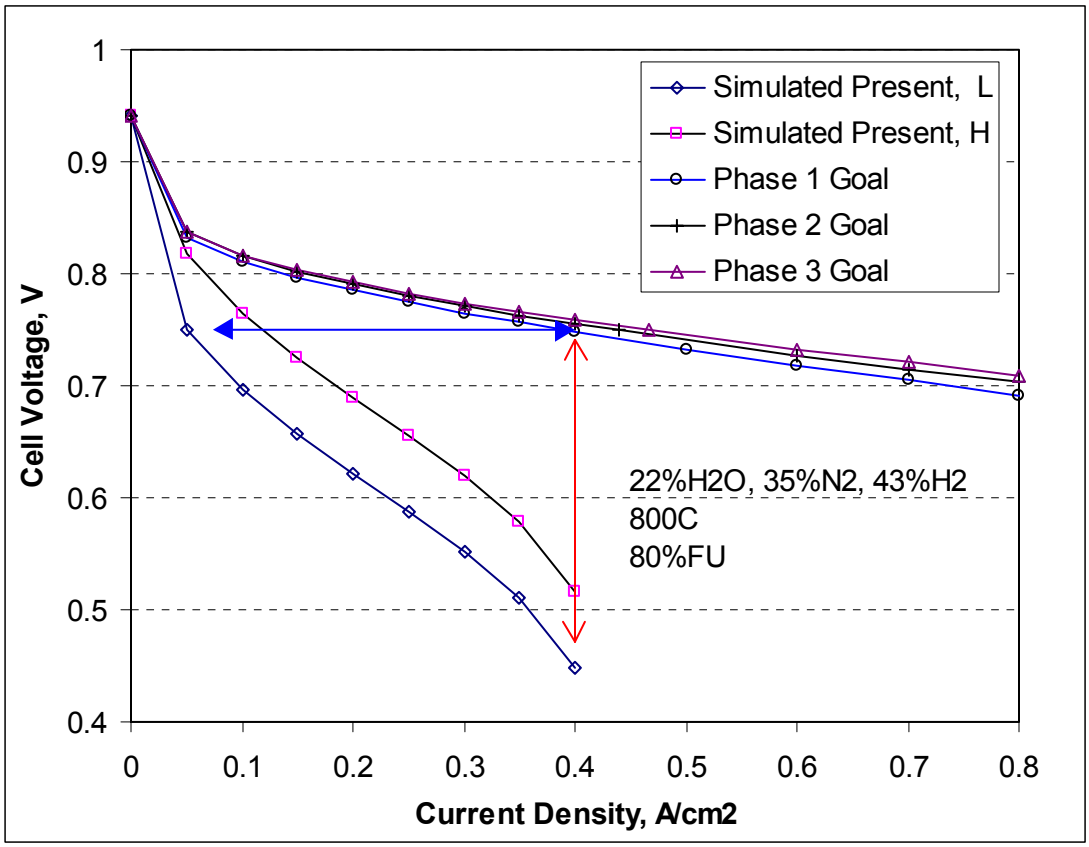

Figure 5.15. Performance gap between target and estimated performance at program start.

A great many studies and experiments were conducted to evaluate and improve cell performance during SECA Phase I. A number of modifications resulted in modest cell performance improvement, but were not incorporated into the final SECA cell design. There were two key improvements which led to achieving the required performance in the cells. These will be summarized here.

5.3.1 Sealed Module and Stack Design

In the early stages of the program, most testing was performed using sealless radial single-cell modules. Performance of these modules was quite good at low fuel utilization, but dropped dramatically as fuel utilization exceeded ~60%. When the half-sealed stack design was developed and test vehicles produced, the difference in performance was immediately clear. The first two tests using square half-sealed test vehicles achieved stable performance at 90+% fuel utilization with much smaller performance losses than previously observed. At 90% fuel utilization and 0.7V (in dilute hydrogen fuel), performance was ~0.230 W/cm^2. See Figure 5.16 for data from these vehicles, which used baseline cells. Thus, the baseline cells available at the beginning of the program had a significantly higher performance entitlement than was observed with the

test vehicles available at the time, and by using sealed modules and stacks, the performance gap was dramatically reduced.

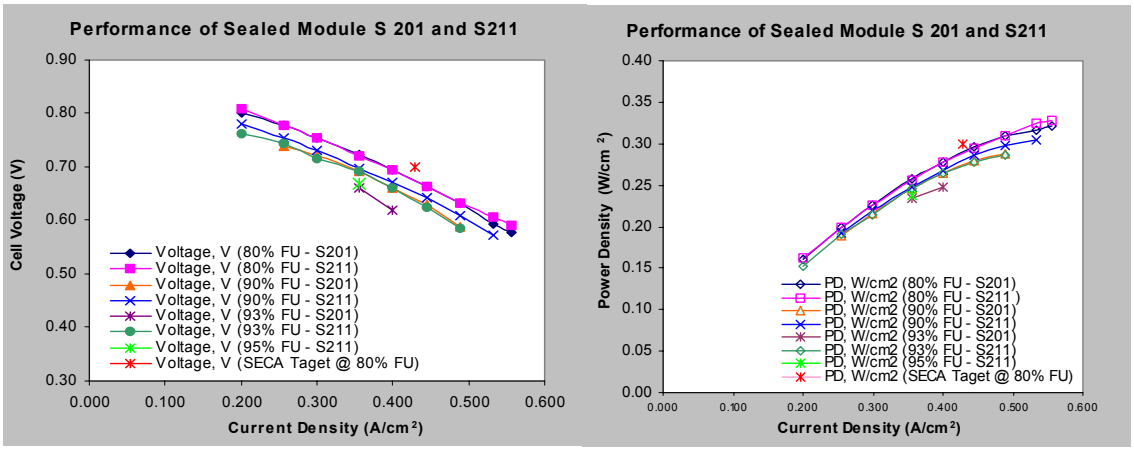

Figure 5.16. Polarization curves of square half-sealed test modules S201 and S211.

5.3.2 Anode Improvement

An improved electrolyte-anode bilayer architecture was identified which produced significant performance improvements. The improved cells use an anode labeled Anode C', and differ from baseline cells primarily in microstructure while using the same basic material set.

In performance testing, the Anode C' has led to improved performance at all fuel utilization levels, but particularly dramatic performance improvements at high utilizations. See Figure 5.17 for a comparison of performance of two full-size cell modules containing (16 cm diameter) Anode C' cells to one of the best-performing baseline cells. The data shown was taken at 88% fuel utilization, and the improvement is quite dramatic. At the SECA design point current density (0.428 A/cm^2), both cells produce more than 20% greater power than the baseline cell in dilute hydrogen, and both exceed the SECA target voltage of 0.7 V by more than 4%. These results were obtained with dilute hydrogen fuel; testing of these cells on ATR fuel showed similarly high performance. The effect of the improved anode at high utilization is also dramatic, and can be seen in Figure 5.18. In this plot, the total module ASR is calculated as a function of fuel utilization. As can be seen, the ASR of cell S417 (Anode C' cell) is at all points significantly lower than cell S229 (baseline cell), and further that there is no significant increase in ASR as utilization increases, even to 95%. By comparison, a significant mass transport limitation can be observed in the baseline cell at utilizations above 80%.

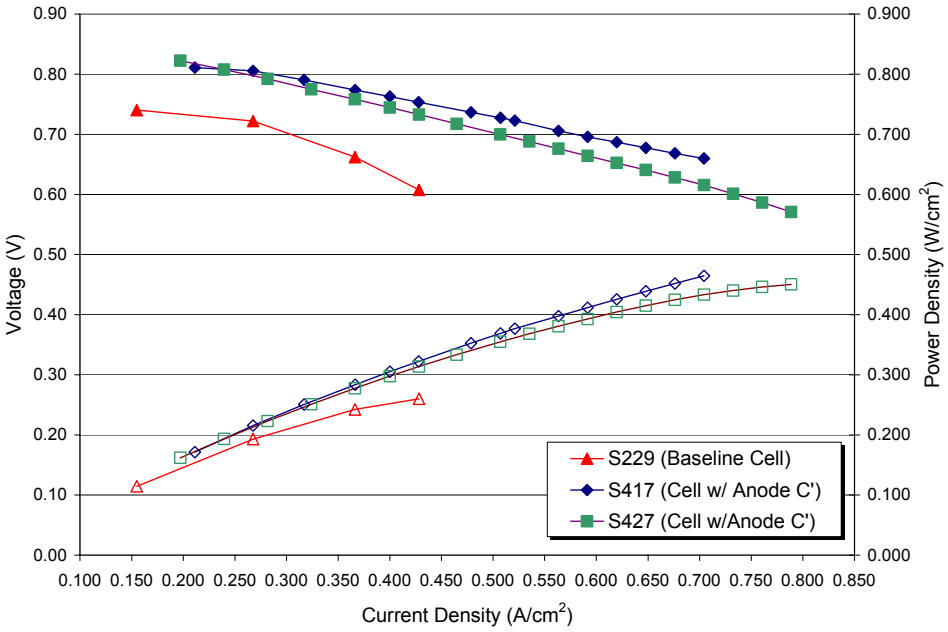

Figure 5.17. Performance of cells containing Anode C' (S417 and S427) compared to baseline cell performance (S229). All tests were on 16 cm diameter cells using half-sealed modules of the Turtle stack design.

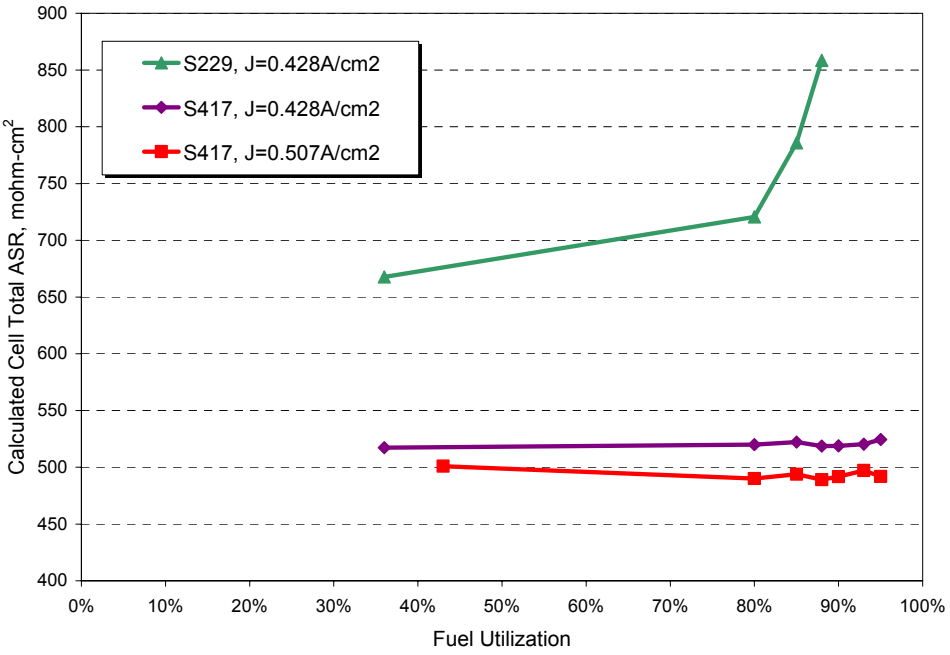

Figure 5.18. Area specific resistance (ASR) of baseline cell module S229 and improved cell module S417, showing the robustness of Anode C' cell performance to fuel utilization.

Degradation testing was performed on cells containing Anode C'. The tests compare quite favorably with the baseline range that has been established during several 1000-3000 hour tests. The results indicate that the new anode architecture has no detrimental effect on the degradation rate.

The overall result of these improvements was that the gap in performance at the module level was closed, and in fact, final performance exceeded the target by ~15%. This performance improvement at the module level did not translate perfectly to stacks – the performance knockdown with stacking is ~20% and needs to be addressed through further improvement in Phase II of SECA.

5.4 STACK MATERIALS DEVELOPMENT

Aside from the cell, the other key components of the stack include the seals and the interconnect (particularly as it relates to degradation). Each of these was addressed to some extent during the course of this program.. In this report, key results and the materials used in the final stacks will be discussed.

5.4.1 Seals

5.4.1.1 Cell Seals

At the beginning of this program, most testing was being performed with sealless modules. As discussed in Section 5.3.1, a distinct performance advantage was observed upon transitioning to a sealed module. The primary seal used throughout the program was a seal developed prior to the start of the program, a glass-ceramic referred to as NS-7. A great deal of evaluation of this sealant was performed and the conclusion was reached that NS-7 was adequate for use as a cell seal, but was not optimal by itself for manifold sealing. Details on the tests on NS-7 can be found in the semi-annual reports.

5.4.1.2 Manifold Seals

In the current stack design, the manifold seals are more critical than the cell seals from a leakage perspective. However, the manifold seals can also be subjected to higher loading than the cell seals. As a result, compressive seals were evaluated and adopted for use on the manifolds.

5.4.2 Interconnect Metal

The baseline interconnect metal it did not change over the course of the program. The stacks used in the final system demonstration used this baseline metal in the interconnects. A number of approaches aimed at identifying

improved interconnect materials were pursued, but a significantly better solution was not clearly identified. Some of the notable activities are discussed here.

5.4.2.1 GE-Developed Alloys

As part of GE's internal SOFC development program, a number of potential interconnect alloys were developed, fabricated and evaluated for oxidation growth and conductivity, Cr volatility and cost. Three of these, GE-7, GE-8 and GE-13, were initially down-selected for further study. ASR data of the oxidized metals showed promise and it was believed that these alloys had the potential to improve on the baseline metal performance.

Down-selection to a single material, GE-13, was made based on performance results and stability of the oxide. A slightly modified version of this alloy, GE-13L, was fabricated for potential use in SECA stacks. Unfortunately, fuel cell tests with GE-13L did not indicate the degradation benefit expected based on the oxidatiion data. As these tests occurred very close to the time that the materials had to be locked down for the final SECA stack builds, the decision was made not to use GE-13L in those stacks. The GE alloys need further evaluation as we move forward in the program.

5.4.2.2 Coatings

Evaluation of coatings were begun during Phase I. Material was obtained and brush-coated on the cathode flowfield. A cell module was then assembled and tested. Initial performance was good, with very low ohmic resistance, as measured by impedance spectroscopy (~130 $m\Omega$-cm^2 vs. a typical value of ~280 $m\Omega$-cm^2). Over 150 hours of testing, no degradation was observed. Unfortunately, a facilities outage prematurely aborted the test. Again, these tests were too late to commit to this coating for the stack builds for the demonstration test. Evaluation of coatings is ongoing now as part of SECA Phase II..

6 FUEL PROCESSING

This section of the Phase I SECA final report traces activities related to the development of processes, materials, and hardware used for fuel processing in the SECA system. Work was performed in this area throughout the Phase I and encompassed a variety of fuel processing-related activities which included:

- Design and fabrication of test hardware for the evaluation of fuel processing materials
- Evaluation of catalyst materials for potential use in the SECA fuel processor
- Design, modeling, fabrication, and testing of fuel processor hardware
- Long-term studies of the SECA fuel processor

- Operation and evaluation of the performance of the SECA fuel processor integrated with an SOFC stack
- Studies pertaining to internal reformation.

Each of these activities is described in greater detail in the forthcoming sections below.

6.1 FUEL PROCESSING TEST HARDWARE

Fuel processing activities planned for the initial portion of Phase I included the testing and evaluation of numerous catalyst materials for potential use in the fuel processing hardware. It was apparent in the early stages of the program that test hardware designed specifically for and dedicated to fuel processor and fuel processing catalyst evaluation would be needed. Two test stands were developed to provide flexibility and automation while permitting safe and unattended 24 hour testing. A photograph of this test facility and the data acquisition station are provided in Figure 6.1 and Figure 6.2, respectively. These stands were utilized throughout SECA Phase I for material and hardware testing and promises to be of significant value for subsequent phases of the program.

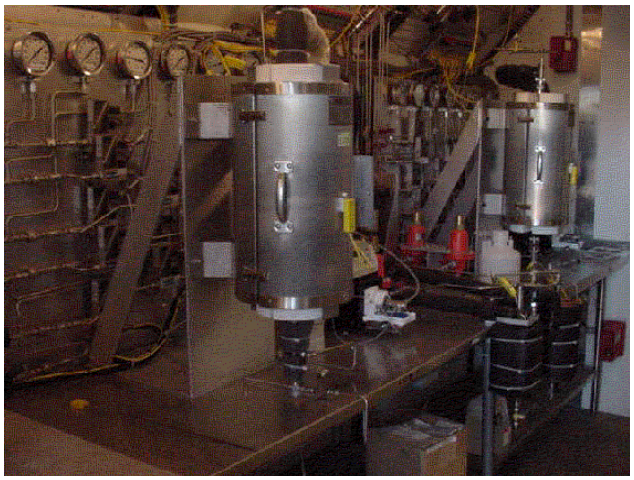

Figure 6.1 Fuel processing test facility at HPGS.

Figure 6.2 Data acquisition console for the fuel processing test station.

6.2 FUEL PROCESSING CATALYST DEVELOPMENT AND EVALUATION

The aggressive efficiency requirements of the SECA program coupled with the need for fuel flexibility mandated the selection of an autothermal reformer (ATR) fuel processing approach. However, what was not clear was the precise method of ATR implementation. Two candidate implementation methodologies for the ATR that were considered are illustrated in Figure 6.3.

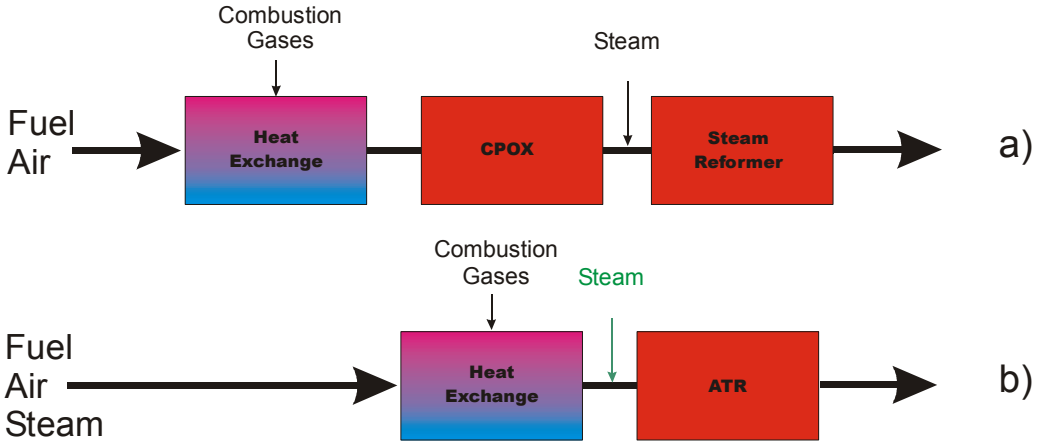

Figure 6.3 Possible means of ATR Implementation. The method illustrated in a) makes use of both CPOX and SR catalysts while b) employs commercial ATR catalytic materials.

In the first method shown, commercial catalytic partial oxidation (CPOX) and steam reforming (SR) catalysts are arranged serially in a reactor to achieve ATR fuel processing. This approach, while somewhat cumbersome to control and potentially more expensive, offers the ability to optimize performance and potentially achieve high efficiency within the reformation step. In the second

method shown, a single bifunctional catalyst is utilized and steam is provided in a manner to minimize system cost and complexity. This latter methodology has the added advantage that a number of commercial companies are actively involved in the development and understanding of catalytic materials to function in this application approach.

To evaluate these two potential means of ATR operation, a two-pronged research and development strategy was undertaken that built upon previous experience within GE in fuel processing. The first approach exploited previous developmental experience within GE in the area of highly active, supported CPOX catalyst materials. The goal of this effort was to develop an inexpensive and highly active CPOX catalyst to incorporate with either a commercially available or an internally developed SR material. The second approach involved evaluation of readily available commercial catalyst materials.

6.2.1 Internal CPOX and SR Catalyst Evaluation

Two candidates were downselected for the CPOX and SR catalysts based upon previous experience and were evaluated to provide a better understanding of material performance and operational limitations.

In the first test, a monolith-supported precious metal catalyst was tested. This material, a made-in-house, rhodium-based catalyst supported on alumina monolith, had been used previously with success at GE as a CPOX catalyst. In these tests, the supported catalyst was evaluated for its ability to function both in CPOX and SR modes (i.e., steam was added to the test stream). As part of the evaluation, a number of factors were considered to determine their response on the key fuel processor performance requirements. These factors included the following, evaluated over the range of conditions listed:

- Flow velocity: 1 to 4 ft/sec
- Oxygen-to-carbon ratio (O/C): 0.72 to 1.17
- Steam-to-carbon ratio (S/C): 0 to 3
- Inlet catalyst temperature: 500 to 800°C (as measured 1/8” from catalyst surface)
- Catalyst load (i.e., rhodium load): 6 to 12% by weight
- Catalyst bed length: 0.75 to 1.50 inches

To further determine the effects of the variables, a Design of Experiment (DOE) approach was utilized. In addition, the DOE tools allowed the critical factors affecting CPOX catalyst performance to be identified, along with any interactions that might have occurred among these factors. The DOE process involved the selection of factors affecting responses, the development of an analysis case matrix, testing of the cases to determine the response values,

analysis of the DOE responses, and the selection of factor settings necessary to optimize system performance.

The responses selected for this DOE were derived from the fuel processor design requirements, and included the following:

- Hydrogen content (molar percent, dry)
- Total hydrogen and carbon monoxide content (molar percent, dry)
- Methane content (molar percent, dry)
- Conversion efficiency (defined as the total hydrogen product flow divided by the methane flow, divided by the catalyst volume, divided by the catalyst weight).

After conducting the 16 CPOX catalyst test cases, the flow velocity, the oxygen- to-carbon ratio, the steam-to-carbon ratio, the inlet temperature, the catalyst load, and the bed length factors were analyzed for statistical significance. This was performed for the hydrogen content, total hydrogen and carbon monoxide content, methane content, and conversion efficiency responses using normal and Pareto charts of the factor effects. In addition, transfer functions relating the values of the factors to the responses were also determined, and allowed for optimization of CPOX catalyst configuration. Based on the results, the flow velocity, the oxygen-to-carbon ratio, the inlet catalyst temperature, the catalyst metal loading, and the catalyst bed length were all found to be statistically significant with respect to the performance requirements. The steam-to-carbon ratio was determined not to be statistically significant with respect to its effects.

Models were developed to predict the hydrogen product content, the total hydrogen and carbon monoxide product content, the methane product content, and the hydrogen conversion efficiency. These models were then used to optimize the design conditions for a CPOX catalyst for the SECA program application. The results of this optimization indicated that the most optimum CPOX reactor configuration would be one with the minimum metal loading and minimum bed length.

One significant observation during these evaluations was that the CPOX catalyst would only light off at inlet temperatures above 450°C. As a result, only temperatures above 500°C were evaluated.

In the second test, a commercially available steam reforming catalyst was examined. This catalyst was obtained in the form of alumina-supported pellets and was tested in a plug flow reactor geometry. A DOE strategy guided both experiment selection and data analysis to determine the primary operational variables that affected catalyst performance. In a manner similar to that used in the previously described DOE, gas composition was monitored using gas chromatography to provide a direct measure of conversion efficiency.

From these tests, the performance model determined that temperature, gas space velocity, and the steam-to-carbon ratio were the most significant factors that affected effluent gas composition and the level of methane conversion. Pressure was not found to be a significant factor in these experiments, implying the absence of an effect or the use of a too narrow range in pressures tested.

6.2.2 Commercial ATR Catalyst Evaluation

In order to verify the performance of the catalyst and to obtain experimental data for the model development, a number of lab-scale catalyst tests were performed on candidate catalyst materials. The testing was conducted with four main objectives in mind. The first was to confirm whether the catalyst could operate at the relatively low 300°C inlet gas temperature required by the current prototype system design. If the catalyst could perform under these conditions, then an integrated heat exchanger would not be required and the fuel processor design would become much simpler. The second objective was to determine the catalyst capacity. This would determine the amount of catalyst required to reach the target reformate flow. The third objective was to characterize the sensitivity of the performance of the catalyst to changes in O/C and S/C ratios and to obtain experimental data for the development of a kinetic model. The final objective was to run a 100-hour steady state test to determine if there were any short-term degradation issues for a catalyst at the requisite operating conditions.

Four critical hardware design variables were identified. Three of them are identical to those described previously – gas hourly space velocity (GHSV), S/C ratio and O/C ratio. The fourth was catalyst inlet temperature, which was defined to be the temperature of the process gases (methane, air, steam) delivered to the catalyst monolith. A test matrix to fully map the performance of the catalyst was created according to catalyst manufacturer's recommendations and unit requirements. The operating ranges for the design variables were used to define the test matrix for the catalyst materials.

Samples were evaluated in the bench scale reactor pictured in Figure 6.4. The reactor was made of 1" pipe mounted inside of a 3-zone electric furnace (see the figure). The process gases were monitored by mass flow meters. A small accumulation tank was used to prevent pulsation in the steam flow. A thermocouple placed ½'' in front of the catalyst monitored the inlet gas temperature, while the furnace was used to maintain the catalyst at a constant temperature. A gas chromatograph measured the reformate composition and independent infrared monitors for carbon monoxide (CO), carbon dioxide (CO_2), and methane (CH_4) were used to confirm the gas chromatographic results.

Figure 6.4 The bench-scale catalyst reactor and furnace.

Specific hydrogen production and methane conversion performance targets for the catalyst are the result of calculations based upon the needs of the prototype system design at that time. Reformate targets were established base on equilibrium predictions and the conceptual system design. Figure 6.5 illustrates the hydrogen and methane percentages in the reformate gas stream at different S/C values for one test catalyst. Each S/C range was operated at three inlet temperatures with a constant O/C of 0.76. The results show that in order to achieve 65% fuel conversion and 39 vol% (dry) H_2, it is necessary to operate at a S/C between 1 to 1.2 with a catalyst inlet temperature of 500-540°C at a GHSV of 10,000 hr^{-1}. The test followed the trends predicted by the catalyst manufacturer. The fuel conversion increased as S/C increased.

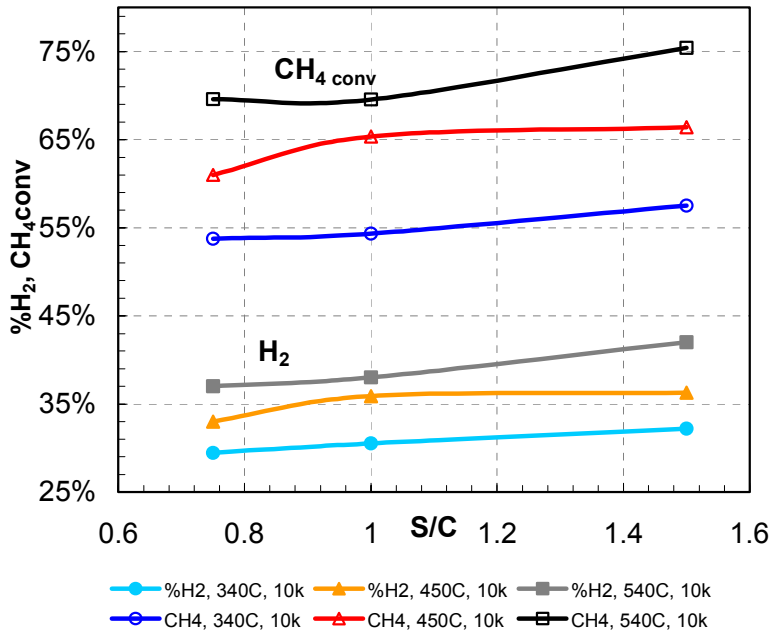

Figure 6.5 Hydrogen production and methane conversion levels for candidate catalyst material as a function of steam-to-carbon ratio with a constant O/C ratio of 0.76.

Figure 6.6 shows the hydrogen percentage and methane fuel conversion versus the O/C ratio at different catalyst inlet temperatures. For this set of experiments, the S/C ratio is held constant at 1. As these data indicate, the catalyst must be operated at an O/C of 0.76, a GHSV of 10,000 hr^{-1} and a T_{inlet} of 500°C in order to achieve the required hydrogen and fuel conversion levels. The figure also shows that as the O/C was increased, fuel conversion increased, but the hydrogen concentration in reformate remained constant. This implies that the steam reformation reaction was limited by low steam concentration, while the oxygen addition led to complete oxidation of additional amounts of methane.

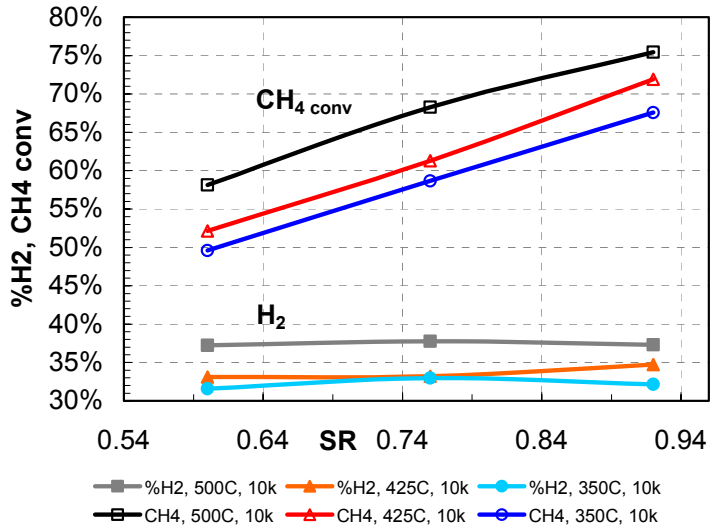

Figure 6.6 Hydrogen production and methane conversion levels for candidate catalyst material as a function of oxygen-to-carbon ratio with a constant S/C ratio of 1.0.

Figure 6.7 shows the concentration of hydrogen in reformate and the fuel conversion versus catalyst inlet temperature at different levels of GHSV and S/C with the O/C ratio set to 0.76. To reach the target hydrogen and fuel conversion levels, it is necessary to have an inlet temperature of greater than 500°C with a S/C of at least 1. With the increase of inlet gas temperature, hydrogen concentration as well as fuel conversion increased.

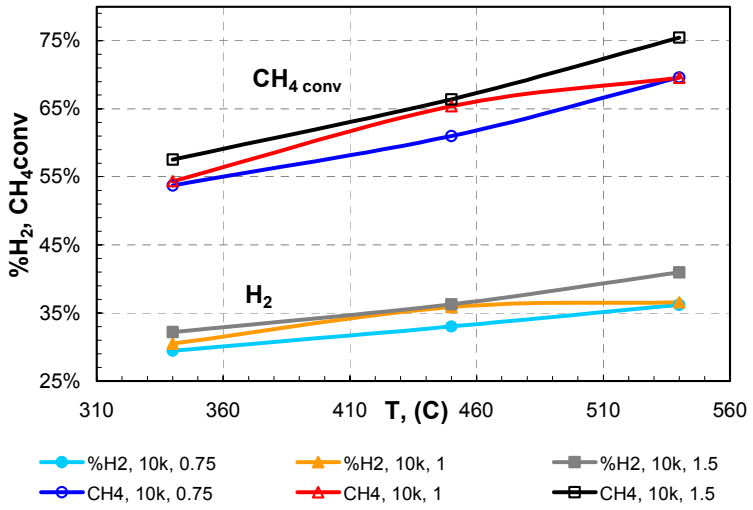

Figure 6.7 Hydrogen production and methane conversion levels for candidate catalyst material as a function of inlet gas temperature with a constant O/C ratio of 0.76.

Once the effect of design variables on the performance requirements was established, the catalyst was operated at a single point for 100 hours to determine if there were any short-term degradation effects at the target operating point. The S/C ratio was set to 1, the O/C was set to 0.76, the GHSV was set to 10,500 hr^{-1}, and the catalyst inlet temperature was held at 500°C. The results of the endurance test are shown in Figure 6.8. An inspection of the level of hydrogen produced during this time indicates that no severe degradation of the performance occurred over the duration of the test.

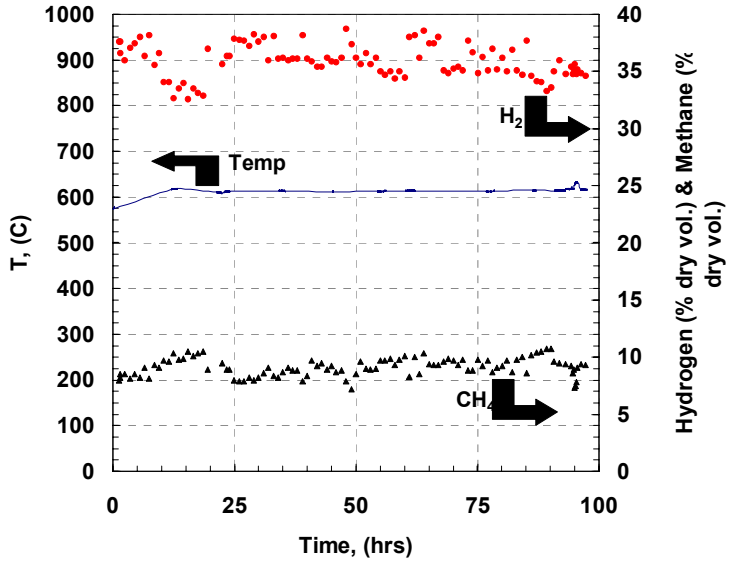

Figure 6.8 Short-term endurance study of targeted ATR catalyst.

One very interesting result of the test is indicated in the hydrogen production level between 10 and 20 hours in Figure 6.8. During this time of unattended operation, the water/steam supply decreased such that the incident S/C ratio decreased from 1 to 0.8. This event occurred again between 50 and 60 hours. As shown by the data in the figure, the decrease in S/C caused an immediate decrease in hydrogen concentration that was recovered once the S/C ratio was restored to 1. Significantly, this result indicates that the catalyst can withstand relatively low levels of S/C without coking for short periods. After the 100 hour test, the catalyst was removed and inspected for carbon formation. No carbon was found either on the catalyst or within the reactor piping.

Overall, the bench scale catalyst testing demonstrated that the candidate commercial ATR catalyst would meet all of the performance requirements of the prototype system except for the requisite inlet fuel temperature. The tests demonstrated that a fuel mixture having minimum inlet temperature of approximately 500°C would be required to yield reformate of the desired composition. This fact, coupled with the knowledge that the current SECA

system configuration supplied fuel at only 300°C, indicated that a heat exchanger would be necessary somewhere in the hardware design to ensure that the gas would have the necessary heat content to sustain reaction over the catalyst surface.

Based upon the encouraging results of the commercial ATR catalyst, all internal fuel processor catalyst development activities within GE were halted at this point in the SECA Phase I program. Further, the catalyst test results indicated that it was now appropriate to begin design activities for the fuel processor hardware.

6.3 FUEL PROCESSOR HARDWARE DESIGN, DEVELOPMENT AND TESTING

Based on the bench scale results, the primary design challenge in developing the external fuel processor was dealing with the required inlet temperature for the catalyst. To meet this challenge a heat exchanger was incorporated into the original design of the reformer. While this unit was found to achieve all technical components requirements such as reformate composition, S/C, O/C, etc., it was found that the addition of the heat exchanger led to a fuel processor design that was too expensive (projected fuel processor costs exceeded the component cost allotment) and that constrained significantly the packaging of the overall SECA system hardware.

However, based upon an experimental observation made during the testing of the prototype of the fuel processor and subsequent follow-on testing, it was learned that the process gas preheating step was unnecessary for successful unit operation. As a result, the fuel reformer was redesigned and a second prototype was constructed and evaluated that did not have the resident heat exchanger. Similar to the first design, Prototype 2 met or exceeded all technical performance requirements, and met hardware cost targets.

A description of the fuel processor hardware development during Phase I of the SECA effort is provided in the following sections of this report.

6.3.1 Prototype 1

6.3.1.1 Fuel Processor Conceptual Design and Modeling

A successful fuel processor design is one that can utilize system inputs and provide the requisite outputs that enable the overall SECA system to function at the desired operating point and at the desired level of efficiency. Based upon system calculations, a set of component input and output specifications was derived for the fuel processor, and these specifications were used to drive the primary design of the unit.

One of the most demanding of the requirements of the fuel processor and one that has a significant impact on hardware design is the ~ 300°C inlet gas

temperature requirement. If the catalyst can operate at feed temperatures of 300°C, a simple, one-pass catalyst bed can be used, as shown in Figure 6.9. In this configuration, the feed gas can be fed directly to the ATR catalyst and the product gas from the ATR catalyst can proceed directly to the SOFC stack. However, as indicated in the previous section, lab-scale catalyst experiments demonstrated a minimum inlet gas temperature of 500°C to be necessary for the reformation reactions to occur. If the catalyst requires feed gas temperatures higher than 300°C, a heat exchanger must be integrated with the ATR reactor (as shown in the figure below) to raise the temperature of the inlet gas to a level consistent with catalyst operation. The preheated gas is then fed to the ATR catalyst.

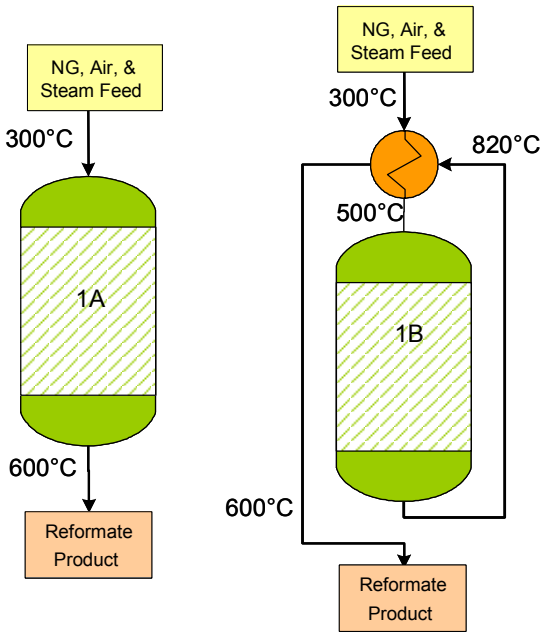

Figure 6.9 Single pass reactor (1A above) design versus an integrated ATR/heat exchanger design (1B).

Once the requirements were fully defined, design variables that affect the requirements were identified and a model of the fuel processor was created. The model facilitated a number of important design operations including: 1) the engineering analysis for the detailed design of the fuel processor; 2) the analysis of the effects of design variables on requirements, and; 3) the creation of a detailed process operations map. Primary design variables implemented by the model are GHSV, O/C, S/C, and the inlet gas temperature into the processor. Primary requirements described by the model are methane slip in the output reformate stream, product gas temperature from the fuel processor, and the maximum temperature of the ATR catalyst. The model was developed using MATLAB software. The ATR model did not account for coking processes or other mechanisms of catalyst deactivation.

Figure 6.10 illustrates the use of modeling in predicting the influence of design variables on the methane slip level in the output reformate stream. In the top portion of the figure, the effects of S/C and gas space velocity on methane level are shown; the bottom portion of Figure 6.10 illustrates the effect of inlet temperature and O/C on methane slip. The fuel conversion requirement is 9 vol% (dry) of unreacted methane in the reformate stream. As indicated in the figure, GHSV variations have minimal impact on the methane slip. Varying S/C from 0.6 to 1.4 also has a minor impact on methane slip, and shows only a change of 9.5 vol% to 6.5 vol% (dry) in methane slip. However, the data show that O/C and inlet gas temperature strongly affect the level of methane slip. Varying the inlet temperature from 220°C to 380°C and the O/C from 0.6 to 0.92 led to a change in the methane slip level from 4 vol% to 16 vol% (dry).

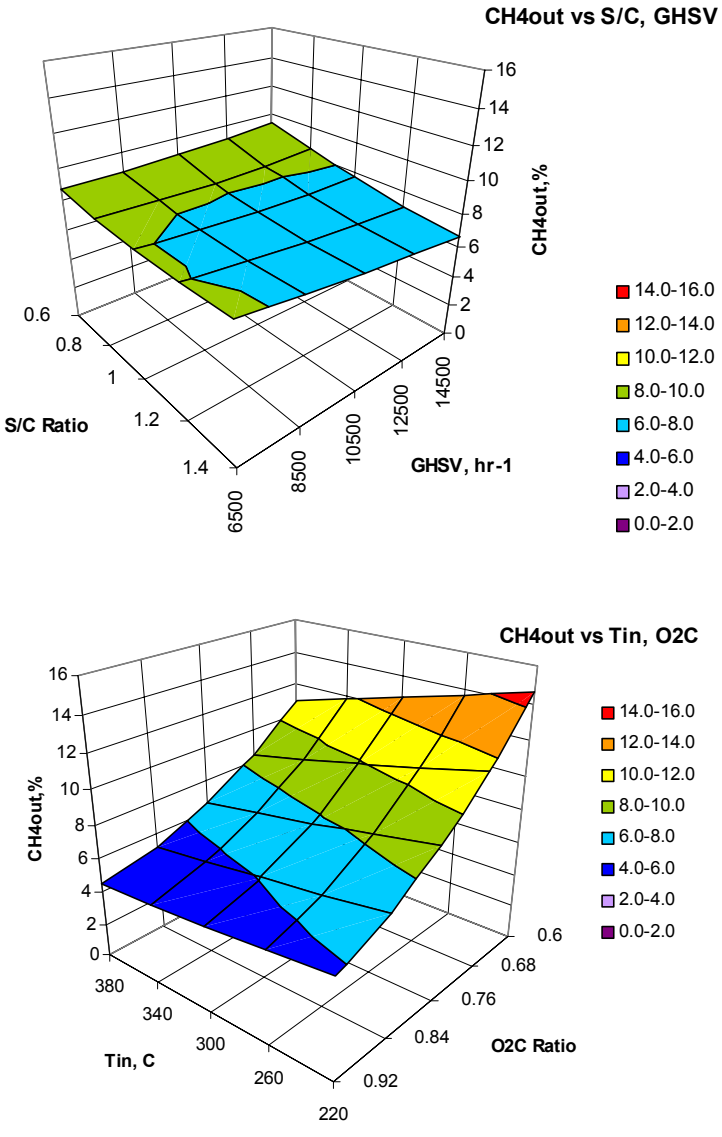

Figure 6.10 Methane slip as a function of various design variables.

Figure 6.11 shows the influence of the design variables on the outlet temperature of the gas. The target for outlet gas temperature is 600°C. As was the case for methane slip, space velocity and S/C were found to have a minimal effect and vary the outlet gas temperature from 530°C to 650°C. On the other hand, O/C and inlet temperature variations generate larger effects and lead to a variance in outlet gas temperature from 500°C to 700°C. The most significant effect is observed when both inlet temperature and O/C are increased.

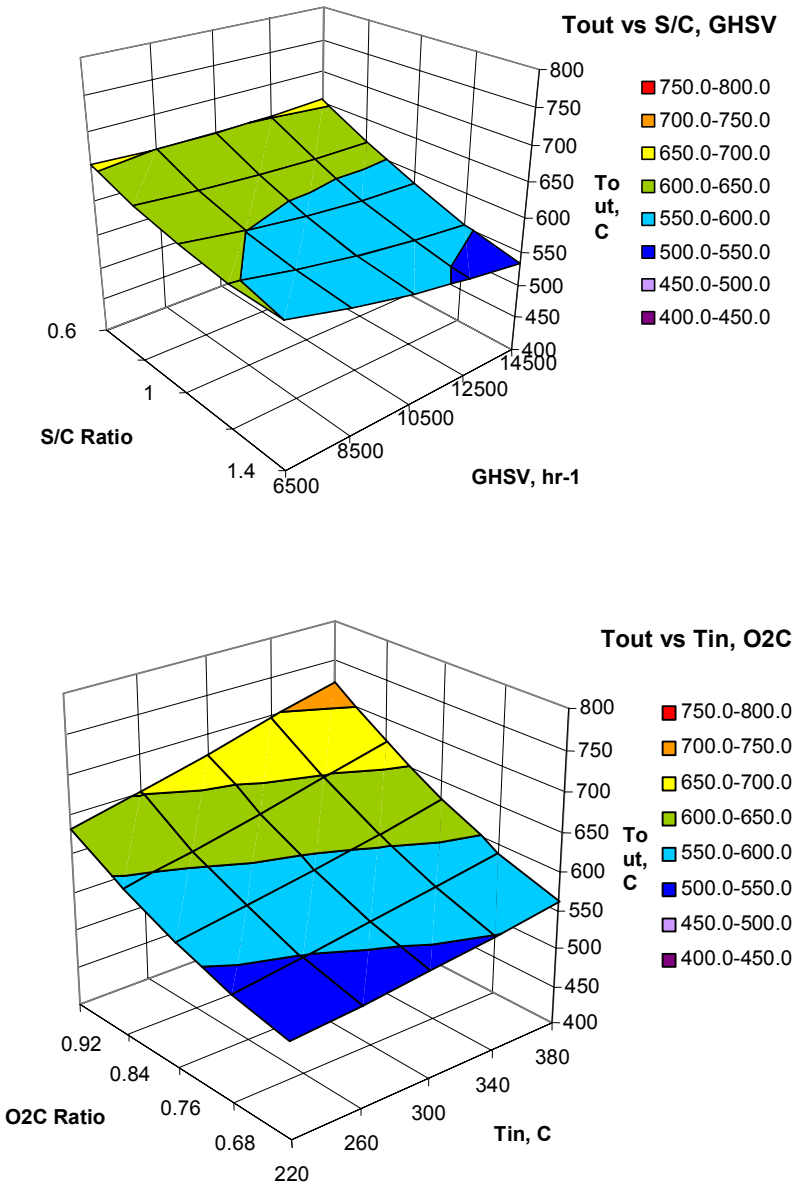

Figure 6.11 Outlet gas temperature as a function of design variables.

The ATR process consists of partial and complete oxidation reactions of methane, which are fast and strongly exothermic, and steam reforming reactions involving methane, which are slow and endothermic. The fast oxidation reactions produce a temperature spike inside the catalyst that is significantly higher than the exit gas temperature. In a standard ATR system (e.g., a system for PEM fuel cells), the S/C ratio is typically in the range of 2 to 3. This high level of steam in the process gas helps to reduce the internal catalyst temperature so that a higher range of O/C and inlet gas temperatures can be used without fear of catalyst damage due to locally high surface temperature. Due to the very low S/C requirement for the SECA SOFC system (a result of the high target system efficiency), the inlet gas temperature and O/C must be monitored closely to avoid damaging the catalyst. Discussions of catalyst operation with the manufacturer have revealed that a maximum temperature should not be exceeded without risk to the catalyst structure. Based upon these discussions and the 8 month catalyst lifetime target, a maximum catalyst temperature limit was established.

The fuel processor model was used to determine how the design variables affected the maximum catalyst temperature, and the results are shown in Figure 6.12. The data from the model show that an increase of O/C and inlet temperature lead to significant increase in the catalyst temperature as one might anticipate. Decrease of S/C has a strong negative effect. Increasing the S/C ratio increases the steam reforming reaction, which, in turn, consumes heat and decreases the maximum temperature inside the ATR monolith. Significantly, the model identified regions (shown in yellow and orange in Figure 6.12) where the system should not be operated in order to preserve catalyst activity and meet the lifetime requirements.

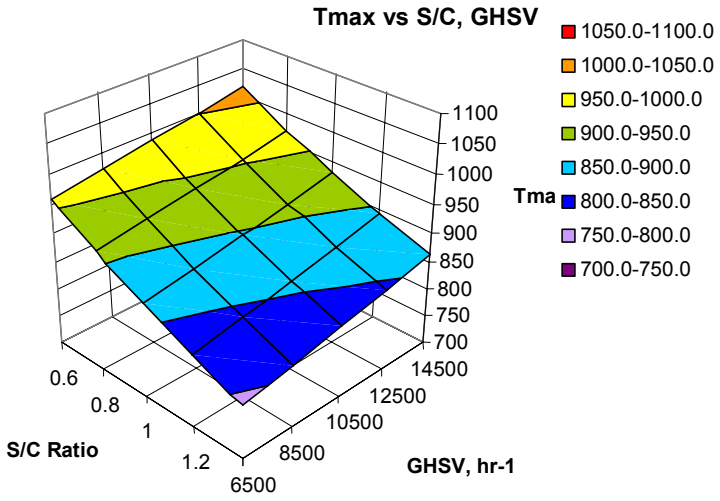

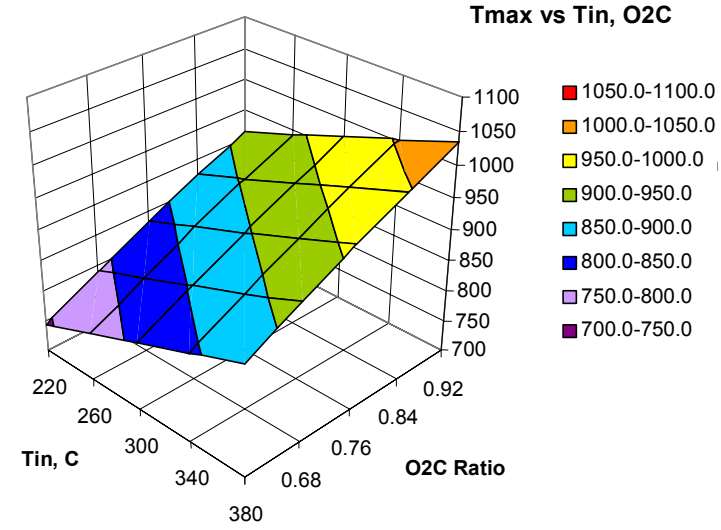

Figure 6.12 Maximum catalyst temperature as a function of design variables.

6.3.1.2 Hardware Design

Based upon the results of the catalyst testing and the information obtained from the modeling studies, a design for the external fuel processor was developed. Figure 6.13 shows an external view of the fuel processor and the processor in cross section. The feed process gas at 300°C is fed to the fuel processor utilizing a 1'' tube. The feed process gas is heated in an annular heat exchanger, where it captures heat from the reformate gas (the feed process gas

is shown as light blue in Figure 6.13). The gases enter the lower cap, turn, and flow upward through the ATR catalyst. The net reforming reaction is exothermic, and the reformate gas leaves the ATR catalyst bed at an elevated temperature. The reformate gas flows upward through an annulus transferring heat to the feed process gas. The reformate gas exits the top of the fuel processor through a 1'' tube at 600°C and flows to the fuel cell.

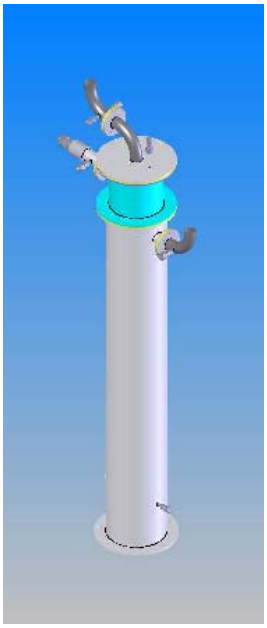

Figure 6.13 External views of the fuel processor.

To enable start-up times of less than 15 minutes, an integrated burner was built into the bottom of the fuel processor. The heat from the burner flue gases is transferred to the catalyst. The burner flue gas exits through a 1'' tube at the top of the unit. One of the advantages of this type of burner design is that there is no direct burner flue gas contact with the reformate gas side of the fuel processor. The design ensures that the reformate side of the fuel processor is never exposed to or cycled between an oxidizing and reducing environment, which would potentially cause serious material corrosion issues. It also ensures that oxygen from the burner is not passed on to the fuel cell where it may damage the anode.

Additional requirements of note during the design process included unit pressure drop, the required heat exchanger length, radiative heat loss from the unit, and the surface temperature of the fuel processor. The required heat exchanger length for differing reformate loads was calculated, and the results are shown in Figure 6.14. The nominal capacity load is 6.5 kg/hr reformate, which results in a theoretical heat exchanger length requirement of 0.34 meters. This length was extended to 0.38 meters to ensure even gas distribution and greater effectiveness. A 25% increase of heat exchanger length was further added as a safety factor, which yielded a final length of 0.58 meters.

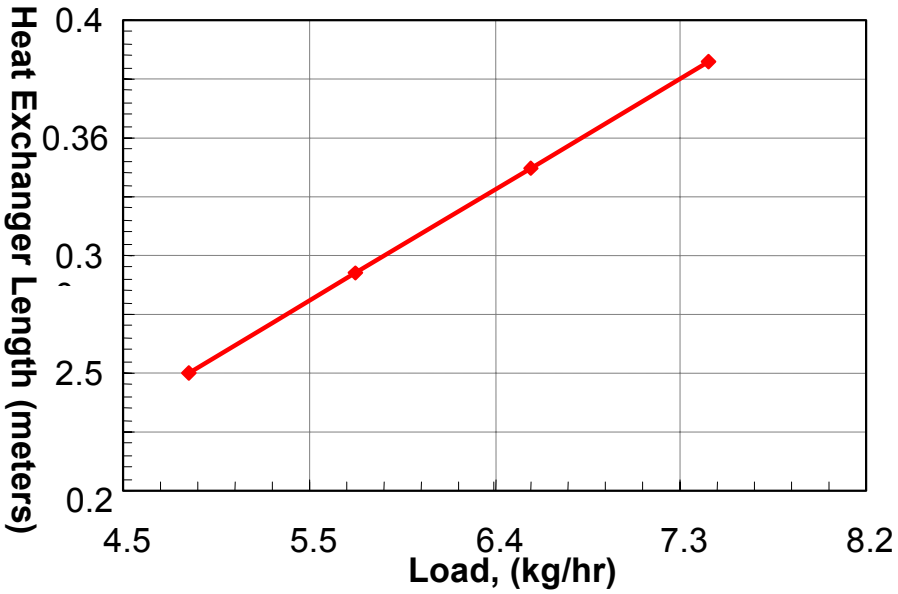

Figure 6.14 Heat exchanger length versus system load.

Figure 6.15a contains a photograph of the completed unit and shows the fully assembled reactor while Figure 6.15b on the right shows the disassembled reformer hardware and its two primary components.

a) b)

Figure 6.15 Photographs of the External Fuel Processing Hardware. a) Complete assembled unit, b) Disassembled unit showing the two primary components.

Thermocouples were installed in the process gas inlet tubing, at the exit of the catalyst, in the reformate gas exit tubing, and above the startup burner. Due to the reactor configuration, it was not practical to place a thermocouple at the entrance of the catalyst. A pressure transducer was installed in the process gas inlet tubing to monitor system pressure, and an orifice restriction was place in the exit gas tubing to simulate backpressure from the SOFC during testing. The pressure drop across the reactor was measured from the inlet tubing to the exit tubing.

The piping and instrument layout of the fuel processor test stand is shown in Figure 6.16. The test stand meters all flows to the reactor using mass flow meters and control valves. The sulfur-containing compounds in the natural gas used for the performance mapping were removed using a low temperature desulfurization reactor filled with activated carbon catalyst upstream of the ATR reactor. The process gases (natural gas, air, and deionized water) are mixed and heated in a 10 kW electric furnace to the desired inlet temperature prior to entry into the fuel processor. The gases flow into the fuel processor and out to a flare following reformation through insulated metal flex lines.

The data acquisition modules and the safety system were installed in an electrical box on the test stand. Reformate gas samples from the exit tubing were drawn through a chiller to remove any water and then fed to a gas chromatograph (GC) for compositional analysis. The reactor is shown installed on the test stand in Figure 6.17.

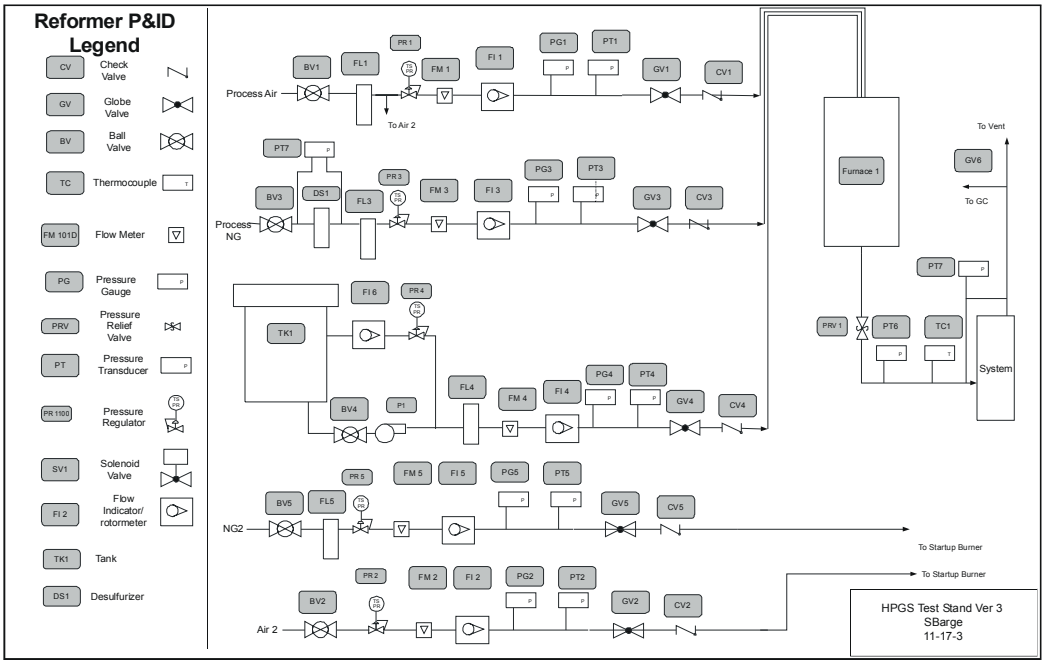

Figure 6.16 Fuel Processor Test Station Piping and Instrument Diagram.

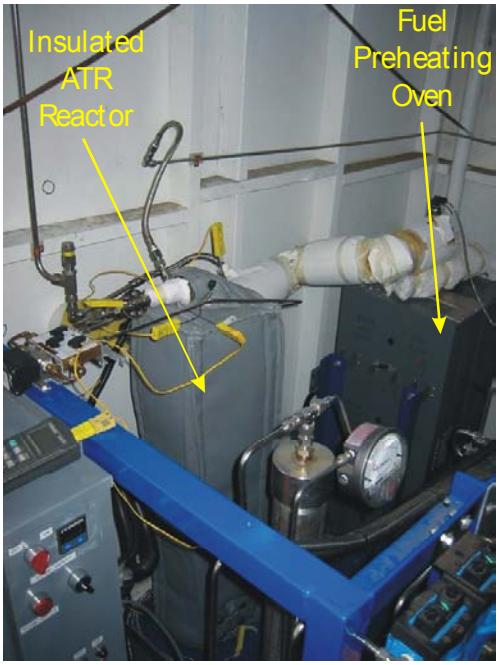

Figure 6.17 ATR prototype mounted in the test station.

During the initial test period, the ATR prototype was operated for 42 hours with 9 start/stop cycles. Eight tests were performed using pipeline natural gas and one was performed using commercial grade propane. The major operational parameters varied during testing were oxygen-to-carbon ratio (O/C), steam-to-carbon ratio (S/C), process gas inlet temperature, and the reformate mass flow rate (kg/hr).

The fuel processor met or exceeded most of the performance targets at the inlet specifications. The reactor demonstrated its ability to reform an alternative fuel (propane) for six continuous hours with no apparent loss of conversion efficiency. A comparison of targets versus test results for 6.5 kg/hr reformate mass flow using natural gas is shown in Table 6.1. The reactor only failed to meet the gas exit temperature requirement.

Table 6.1 Specifications, targets and results for the external fuel processor tests.

	Hydrogen (% vol. dry)	Methane Slip (% vol. dry)	Exit Temperature (deg °C)	Pressure Drop (Pa)	S/C	Inlet Temperature (deg °C)	O/C
Target	39	7	600	2070	1	300	0.76
Results	41	7	370	600	1	300	0.76

Testing Using Propane - One of the key milestones for the fuel processing portion of Phase I SECA was unit operation using an "alternative" fuel to demonstrate fuel flexibility of the hardware. Propane was selected for this demonstration due to its widespread availability and the fact that it is the fuel of choice for many remote applications. Sulfur compounds contained in the propane were removed prior to introduction into the fuel processor using a low temperature desulfurizer fabricated in GE. The reformer reactor was heated prior to fuel introduction using the startup burner (Figure 6.18). The process gases were preheated to 200-300°C by the electric furnace on the fuel processor test station (Figure 6.17) and fed to the reactor for 6 hours (Figure 6.18). The reformer operated with an O/C of 0.84, a S/C of 2.7, and a propane flow rate of 5 liters per minute. Flow and S/C conditions were selected to mimic a 5 kW flow rate equivalent and to protect the unit from carbon formation, respectively. The fuel processor output while operating on propane is provided in Figure 6.19 and was typically 45% H_2, 15% CO_2, 10% CO, and 8% CH_4 on a dry basis.

The reformate composition results of the propane test corresponded very closely with the equilibrium model predictions as shown in Figure 6.20. It should be noted that the only hydrocarbon monitored during this test was methane, so other carbon-containing species could have been present in the reformate.

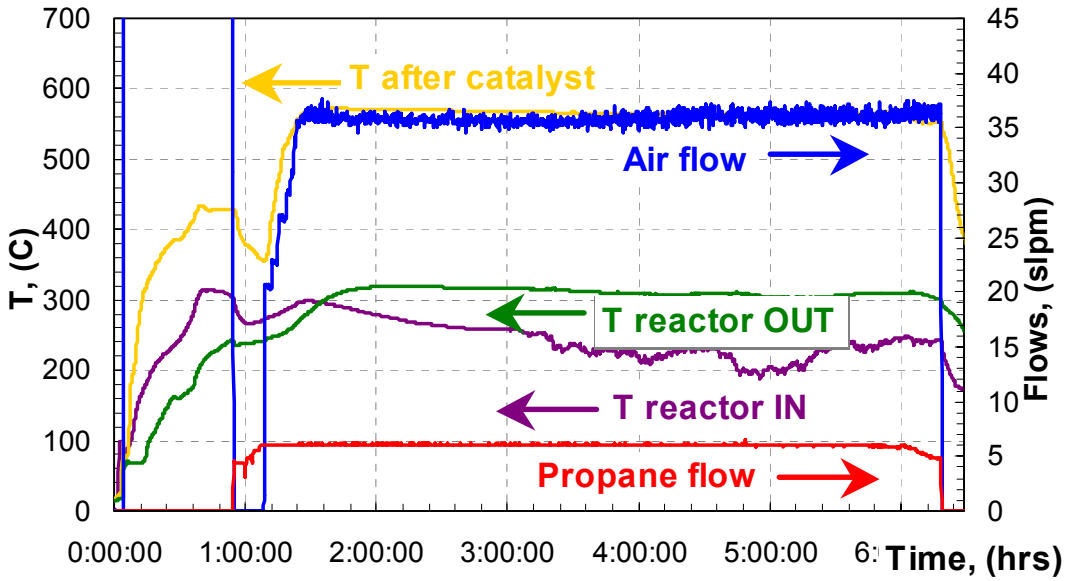

Figure 6.18 Process gas flows and temperatures for fuel processor test using propane.

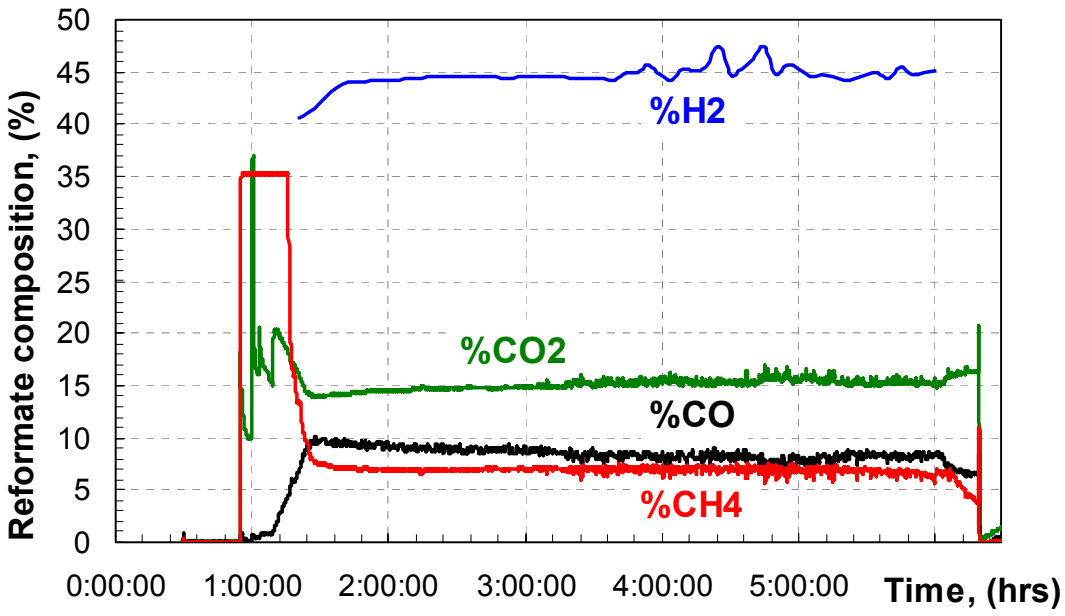

Figure 6.19 Reformate composition for fuel processing test using propane.

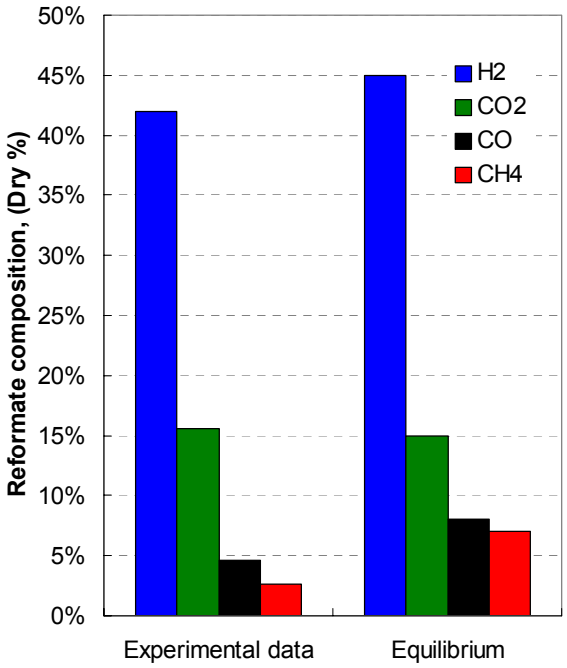

Figure 6.20 Experimental and results predicted from equilibrium for the propane test.

Testing Using Methane - Methane is the primary fuel of the SECA system, so a number of tests were conducted on the external fuel processor using methane. As before in the propane testing, methane was obtained from a readily available commercial source, which was line natural gas. Similarly, sulfur-

containing compounds were removed prior to fuel introduction into the processor using a desulfurizer.

Output reformate composition and temperature targets for the unit were provided from system analysis for ATR unit operation using methane.

Key to the successful operation and control of the fuel processing unit is a thorough understanding of the unit's behavior under a variety of operating conditions. Accordingly, an array of tests was performed by varying inlet operating parameters to determine the corresponding effect on reformer output.

Initially, O/C was varied using an inlet temperature of 300°C and a S/C of 2. The results are shown in Figure 6.21. As is readily apparent in the figure, O/C had a significant effect on methane conversion. By varying the O/C, it was possible to vary the methane slip in the reformate steam from 10 vol% dry to 2 vol% dry. At the same time, the hydrogen concentration only changed from 41 vol% to 43 vol% dry. As anticipated, an increase in the O/C led to an increase in the reformate gas exit temperature; an increase in O/C from 0.66 to 0.98 raised the temperature of the reformate from 315°C to 350°C. As more oxygen is fed to the exothermic partial oxidation reaction, more heat is liberated at the expense of the level of methane that escapes the combustion process. Figure 6.21 also shows that the results of the test using methane were very consistent with the equilibrium model predictions. Points in the figure correspond to calculated equilibrium levels of methane and hydrogen and almost all correspond directly with experimentally determined levels.

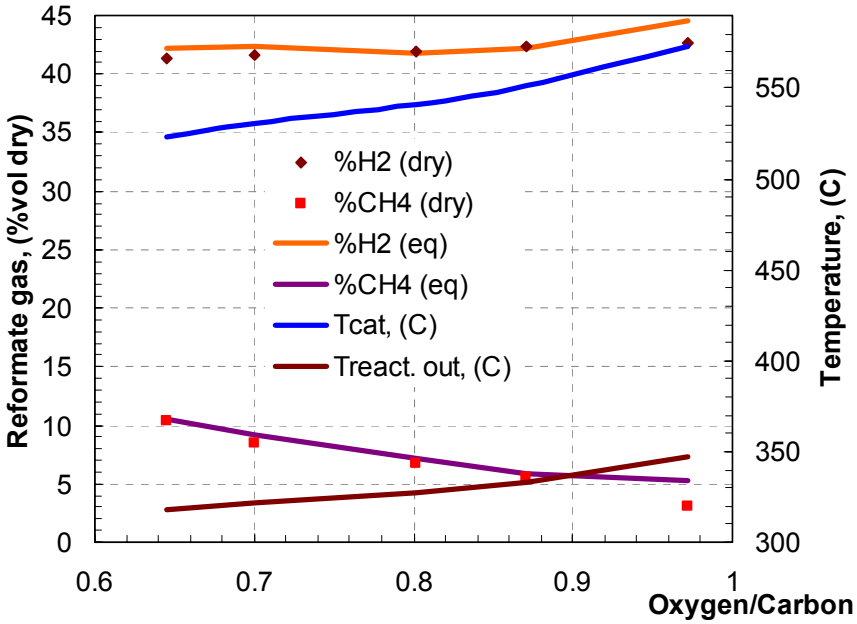

Figure 6.21 Reformate Gas Concentration and Exit Temperature as a Function of Oxygen-to-Carbon Ratio. The S/C and gas inlet temperature were held constant at 2 and 300°C, respectively.

In a second set of experiments, both O/C and S/C were fixed while the process gas inlet temperature was varied from 300°C to 385°C to determine the effect on reformate gas concentration and gas temperatures. The results of these experiments are shown in Figure 6.22. The increase in fuel inlet gas temperature had little effect on the reformate gas methane and hydrogen concentrations. Hydrogen varied by less than 1.5 vol% dry, while the methane varied by less than 1 vol% dry. The catalyst exit temperature remained almost constant and the reformer exit temperature increased only from 320°C to 350°C.

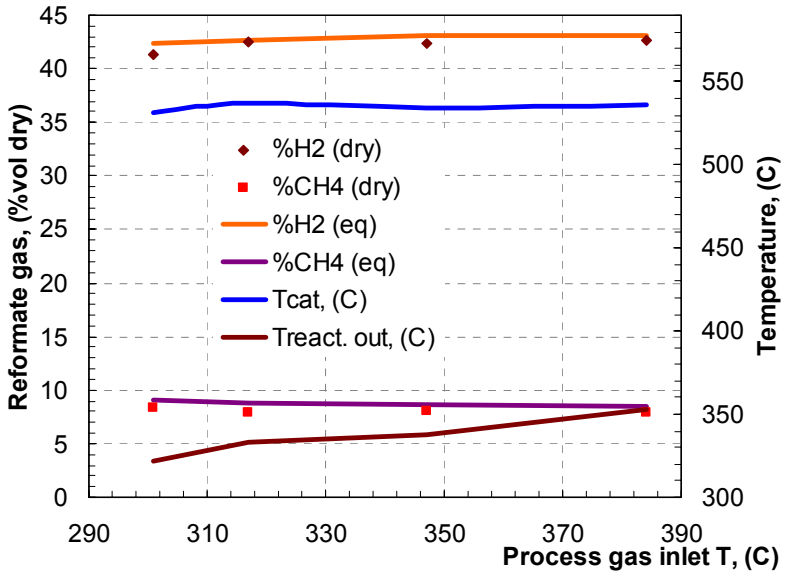

Figure 6.22 Reformate gas composition and exit temperature as a function of inlet process gas temperature. For this series of experiments, the S/C and O/C were held constant at 2 and 0.70, respectively

.

In yet another set of characterization experiments, O/C was fixed at 0.70 and the process gas inlet temperature was held constant at 280°C while the S/C was varied from 1 to 2. The results from these experiments are shown in Figure 6.23. The data in the figure indicate that the S/C ratio had little or no significant effect on either the hydrogen or methane concentration in the reformate stream. Over the range of S/C's tested, the hydrogen concentration was relatively constant at 42 vol% dry and the methane was approximately 5 vol% dry. On the other hand, the S/C did have a slight yet noticeable effect on CO and CO_2 levels. In the S/C range from 2 to 1.4, the CO level remained constant at 9% vol. dry and the CO_2 remained constant at 10.5% vol. dry. Below a S/C of 1.4, the CO level began to increase and the CO_2 level began to decrease with decreases in the S/C. At an S/C of 1 the CO level was 10.5 vol% dry and the CO_2 was at 9 vol% dry. These results are consistent with the equilibrium shifts in the water gas shift reaction and are consistent with those predicted by equilibrium models.

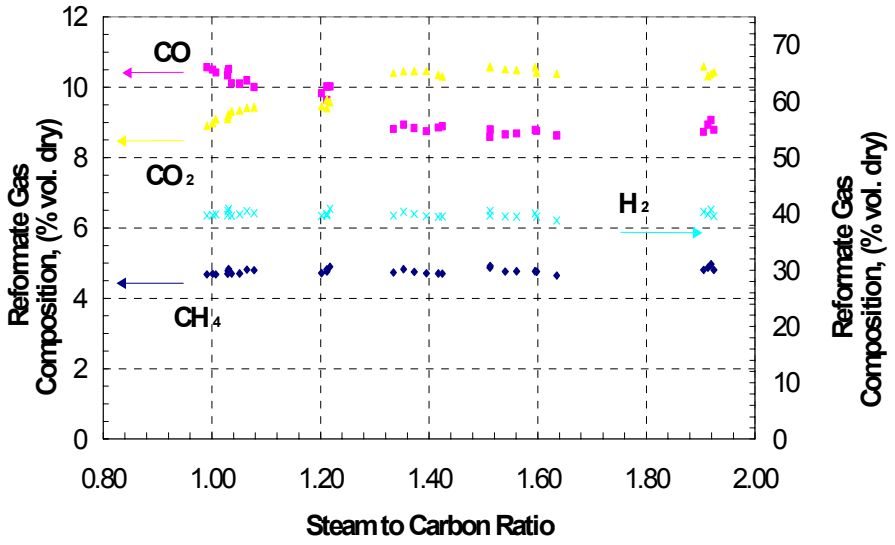

Figure 6.23 Reformate gas composition as a function of steam-to-carbon ratio. For this set of experiments, the O/C and the inlet gas temperature were fixed at 0.70 and 280°C, respectively.

The external fuel processor performance was also evaluated at various throughput rates to simulate operation at different system load levels. Here, the reactor was provided with methane to yield a reformate flow at three distinct loads: 2.5, 6.5 and 10 kg/hr. These tests were performed with an S/C of 1 and a process gas inlet temperature of 300°C. The O/C was varied between 0.76 and 0.80 during these tests in order to maintain a constant level of methane slip. The results are shown in Figure 6.24. As the data in the figure would tend to indicate, the reactor performed well over the operating range. Hydrogen and methane slip levels varied by less than 1 vol% dry and the exit temperature increased from 340°C at the low load to 400°C at the high load.

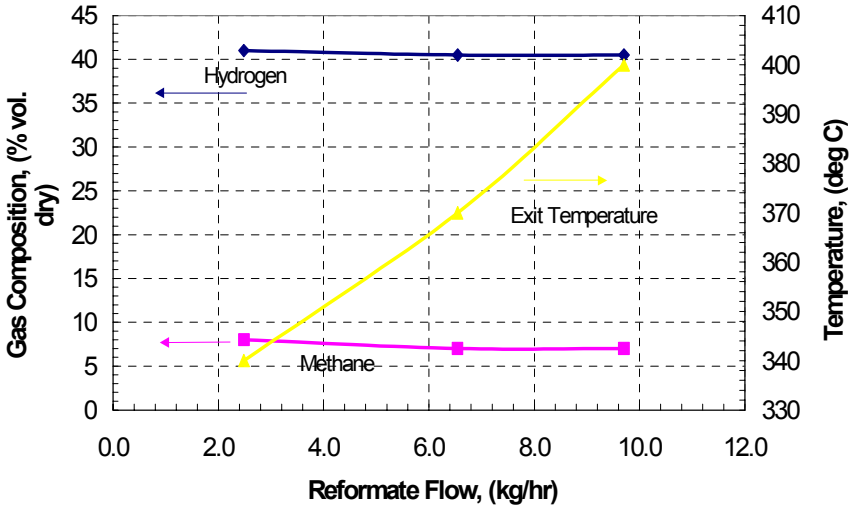

Figure 6.24 Fuel processor performance as a function of reformate load. For these experiments, the S/C and the inlet process gas were fixed at 1 and 300°C, respectively. The O/C was adjusted to maintain a constant methane slip level of approximately 7%.

During testing, one major performance target that was not met was the reformate gas exit temperature. Consistently, exiting reformate gas temperatures fell below those predicted by unit performance models that were successfully predicting other performance parameters such as exiting reformate composition. As an example, for steady state fuel processor operation with a S/C of 1, an O/C of 0.61, and a process gas inlet temperature of 300°C, the measured reformate gas exit temperature was 400°C while the kinetic model predicted an exit temperature of 600°C.

To locate the source of the discrepancy, a separate series of tests was performed to identify and potentially repair areas of excessive heat loss on the reformer. Here, air without fuel was preheated to a known temperature and was forced through the system. Ideally, with the use of air alone, the exit temperature of the gas should match precisely that of the inlet as no chemical reaction can occur. The inherent level of heat loss in the unit can then be estimated from the difference in the gas temperature entering the fuel processor and the gas temperature exiting the fuel processor. The results of these experiments for various insulation and space velocity conditions are presented in Figure 6.25.

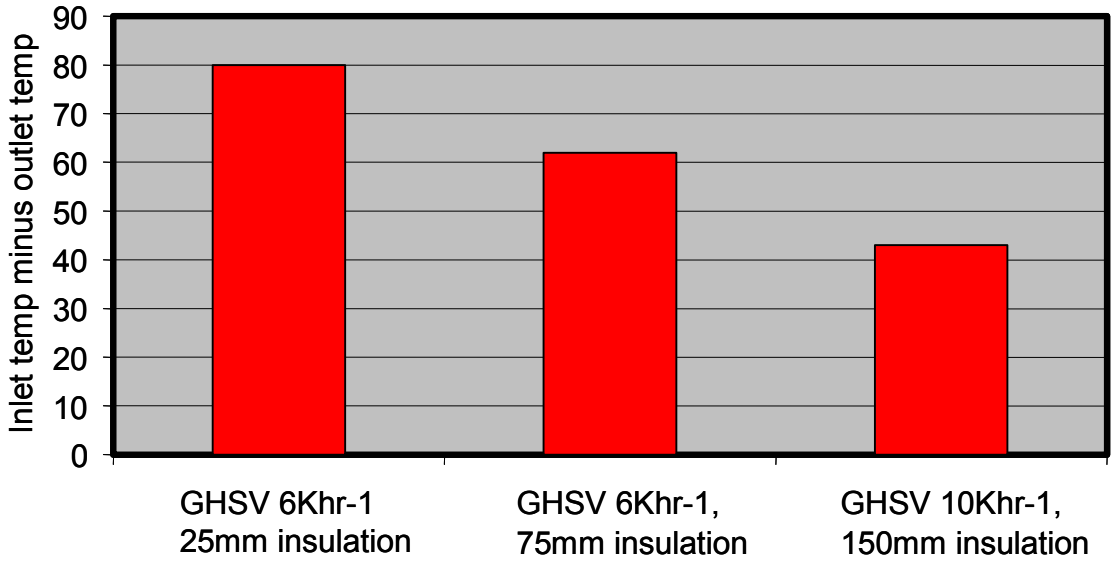

Figure 6.25 Difference in Temperature Between the Gas Inlet and Gas Outlet for the Fuel Processor under Various Test Conditions.

As shown in Figure 6.25 with the 25 mm thick commercial insulation, the difference in the inlet and outlet air temperatures was ~ 80°C. Insulation around the reactor was then increased to 75 mm by combining Silglass with commercial

grade fiberglass and the unit was then operated at two air flows. The data show that the additional 50 mm of insulation reduced the temperature difference by 25%. Operation of the reactor under a higher air flow rate reduced the difference between the inlet and outlet temperature by an additional 25%.

The data from the fuel processor heat loss tests were combined with the heat loss model based on the experimentally measured insulation temperatures and the results are shown in Figure 6.26. The surface temperature calculations and model energy balance calculations both confirmed that at 6.5 kg/hr reformate flow, 75 mm of insulation would reduce the heat losses from 750 Watts to less than 125 Watts and increasing the insulation further to 150 mm would have a minor effect on further reducing heat losses.

Despite the significant reduction in unit heat losses achieved with the increased insulation levels, the reformer still did not yield a reformate with an exit gas temperature of 600°C as predicted by the performance model and as needed in the system configuration. In the kinetic model, there are two primary reactions assumed to occur within the catalyst: the catalytic partial oxidation reaction (CPOX) and the steam methane reforming reaction (SR). The exothermic CPOX reaction occurs very quickly, and the one dimensional model has predicted that the reaction is completed within the first 10 mm of the catalyst. The SR reaction is a much slower, endothermic reaction. With the added insulation it was necessary to reduce the O/C ratio in order to obtain the desired 7 vol% dry methane slip. It was predicted in the kinetic model that the steam methane reforming reaction would not reach equilibrium and that the methane slip would be higher than the equilibrium slip. Significantly, the test results showed that the ATR catalyst behaved in the fuel processor apparatus as an equilibrium catalyst. Methane that was predicted to pass unreacted through the SMR section actually did react and generated more hydrogen, less methane slip and absorbed heat. According to the equilibrium model, the catalyst exit temperature is required to be 590°C to achieve 7 vol% dry methane slip instead of the originally predicted 800°C based on the kinetic model (see Figure 6.27). It was not possible to operate the reformer at higher O/C ratios to increase the exit temperature because the increased heat generated by the CPOX reaction would increase catalyst temperature, perhaps excessively, and decrease methane slip as shown in Figure 6.27 as the catalyst is operating under equilibrium conditions.

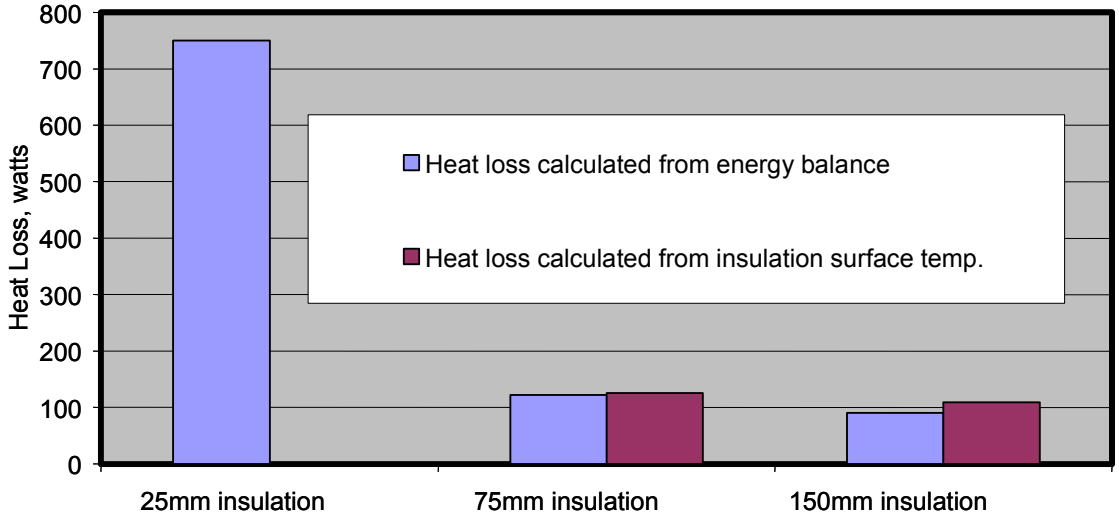

Figure 6.26 Reformer heat loss as a function of insulation thickness.

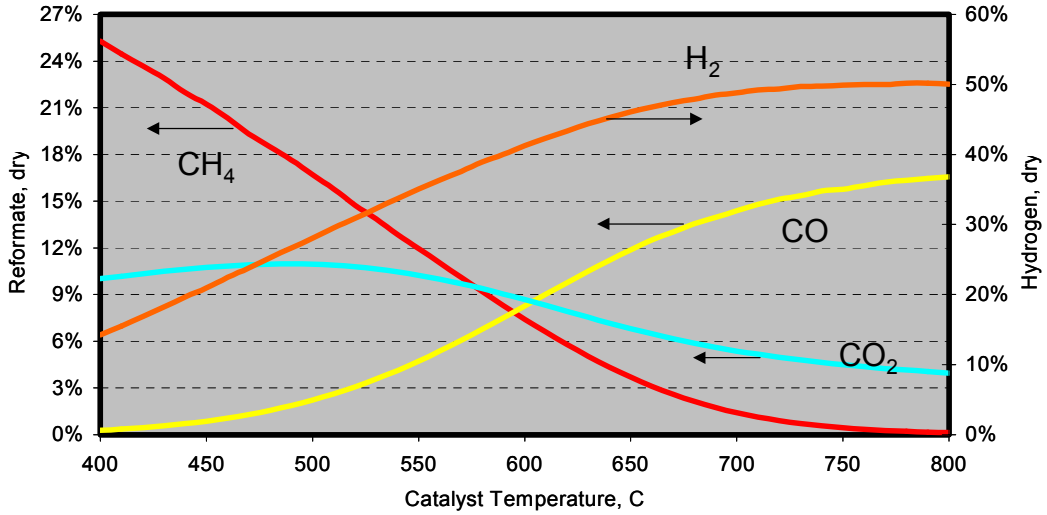

Figure 6.27 Reformation equilibrium composition as a function of catalyst temperature. For these calculations, the S/C and O/C were assumed to be 1 and 0.76, respectively.

6.3.2 Prototype 2

At this point in the development of the fuel processor, a prototype unit with a resident heat exchanger had been fabricated and tested extensively for performance over a range of operational parameters anticipated for the SECA system. The results of these tests demonstrated that the unit would meet all of the operational requirements necessary for the SECA system despite a relatively high level of heat loss. A second series of tests was undertaken to better understand the thermal characteristics of the fuel processor hardware, and during these experiments it was observed that methane reformation was

occurring over the ATR catalyst at fuel gas inlet temperatures substantially less than those recommended by the catalyst makers. This result was highly significant in that it showed that the heat exchanger located at the front end of the reformer was no longer necessary and that the size and complexity of the fuel processing unit could be reduced substantially. Based upon these observations, the fuel processor was redesigned and made much smaller. In this section, the new fuel processor design and its evaluation is discussed.

6.3.2.1 Design and Hardware

The goal of the design was to simplify the fuel processor design to aid in system cost and reduce the complexity of integrating the unit into the prototype system. Hardware complexity is greatly reduced from that of the initial version of the hardware, which included a shell-in-tube heat exchange section that preheated the fuel gas prior to its contact with the active catalyst surface. In the new fuel processor design, the fuel mixture is introduced directly into the active catalyst area without gas preheat. The hardware was designed with a flange coupling that permitted either bolting, to enable maintenance access to the catalyst (at a cost of potential fuel leakage), or welding, to prevent fuel leakage and efficiency losses. Thermocouples were placed both in front (TC1) and at the rear of (TC2) the catalyst to enable temperature measurements of the fuel and reformate, respectively, during fuel processor operation. Because of the critical need to monitor the exit gas temperature, triple redundancy was provided for TC2. The diameter of the hardware was such that it accommodated a catalyst diameter that is readily available commercially. The fabrication material for the fuel processor unit, like its predecessor, was Inconel. This choice was made in order to ensure that the hardware could withstand the high temperature of the reformation process and to extend the overall lifetime of the unit.

The impact of the redesign effort on the size of the fuel processing unit is illustrated clearly in Figure 6.28. In this figure, photographs of both the old and new fuel processing hardware are provided along with appropriate size references. Particularly noteworthy is the photo on the right of Figure 6.28, which provides a direct comparison of the volume of the two processors. The need for fuel gas preheating and the heat exchanger increases substantially the overall length of the processor as sufficient heat transfer surface area is required to accommodate the higher fuel flow rates when the SECA unit is operating at maximum power.

Figure 6.28 Photographs of the Fuel Processor Hardware. The photo on the left shows the redesigned fuel processor while the photo on the right shows both the old and new processors together.

The smaller fuel processor design has a significant impact on the overall packaging of the SECA system. Shown in Figure 6.29 are conceptual drawings for both fuel processor designs and the impact of the design on overall system layout. With the larger fuel processor package and the need for its vertical alignment, it becomes difficult and cumbersome to position the fuel processor near the stack enclosure. The overall height of the system must be increased to accommodate the processor thereby increasing further the potential for system heat loss. On the other hand, the reduced size and flexibility of the new fuel processor design enables the positioning the reformer in proximity to the SOFC stacks. In this way, overall system size and potential heat losses are minimized. With the smaller design package, the unit could be placed conceivably within the stack enclosure to further increase the efficiency of the fuel processing step and the system, though the current SECA system design has the fuel processor located just beneath the enclosure. A further appreciation of the size reduction afforded by the new design is provided in the figure as well; the fuel processing units shown are drawn to the same relative scale in the figure.

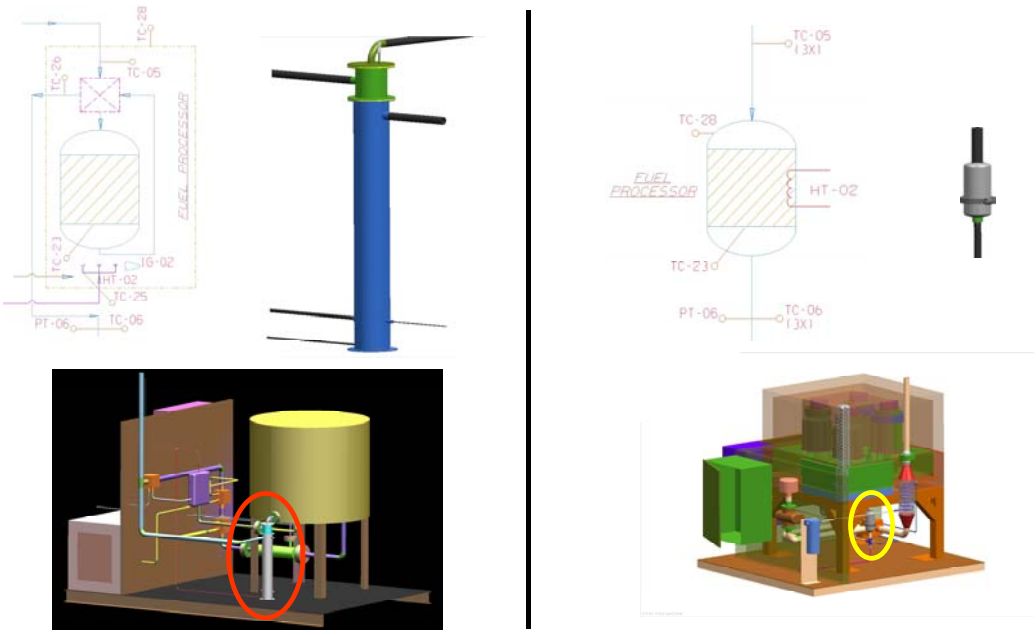

a) b)

Figure 6.29 The system packaging benefit of the new fuel processor design. Shown in a) and b) are the design packages for the old and new processor designs, respectively.

6.3.2.2 Performance Testing

A face centered, central composite Design of Experiments (DoE) test protocol was used to evaluate the performance of the new fuel processor. Key control variables in the DoE used for the evaluation were the oxygen-to-carbon ratio (O/C), the inlet gas temperature, and the fuel flow. The overall test protocol is depicted in Figure 6.30 and encompassed ranges in the control variables that are anticipated in routine SECA system operation. Key performance variables measured include the level of methane slip from the processor, the level of hydrogen in the reformate, and the temperature of the reformate. With the performance data in hand from these tests, it would be possible to predict steady state fuel processor performance for off design point operation.

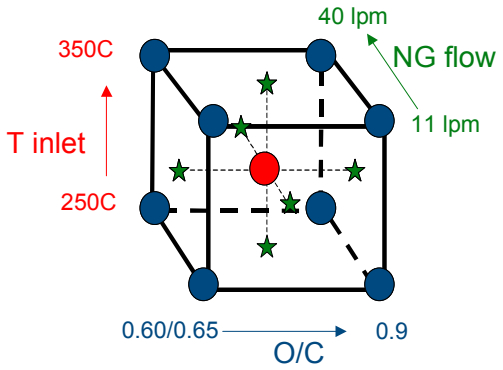

Figure 6.30 Design of experiment protocol used for the fuel processor evaluation.

The maximum fuel flow (natural gas) that could be tested was limited by flow restrictions in the test station; the current estimation of the maximum fuel flow that can be processed by the fuel processor is roughly 75 to 80 L/min. Another important point to be mentioned is that this testing made use of commercial natural gas as the primary fuel; a desulfurization unit removed sulfur-containing odorants from the natural gas prior to its entry into the fuel processor. Thus, this testing represented a more realistic and demanding evaluation of the fuel processor performance as compared to the bottled methane fuel used for SECA prototype system.

Over 20 separate tests were performed as part of this DoE, five of which were replicates, which served to evaluate reproducibility of the unit and the test approach. Data representative of those collected for this set of experiments are presented in Figure 6.31. Here, results are shown for the fuel processor operating with variable inputs consistent with the nominal SECA operation point. These data showed that the processor could indeed meet all of the targets set forth by the system design. Particularly noteworthy was the stable operation achieved when using a fuel stream heated to only 300°C.

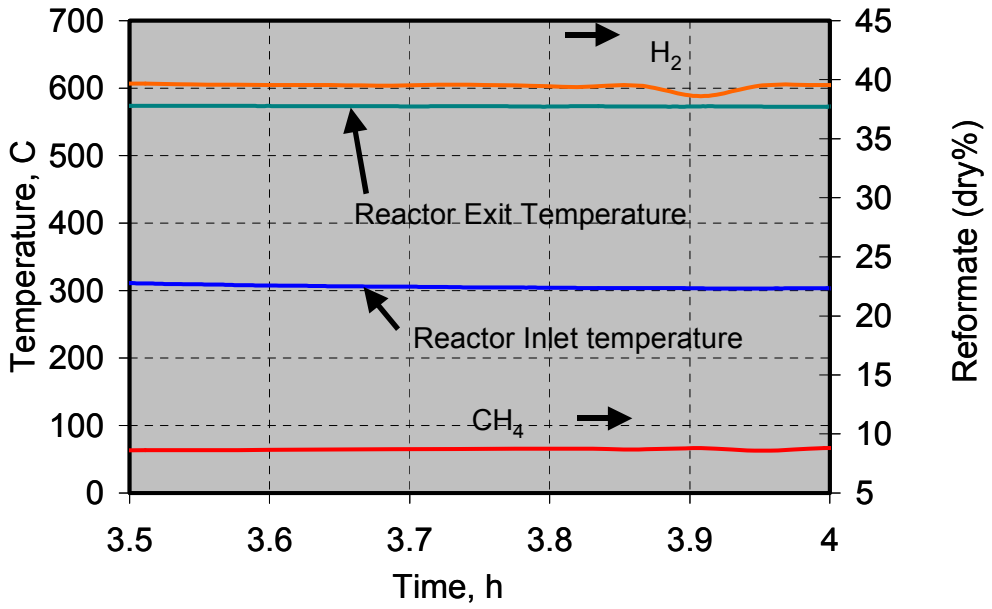

Figure 6.31 Fuel processor performance at the nominal SECA operating point.

Another advantage of the smaller fuel processor package not reflected explicitly in the data of Figure 6.31, but measured during the experiment pertains to pressure drop. As might be anticipated, overall SECA system efficiency increased when the pressure drop within its components was minimized. Because of the straight fuel path that is inherent to the new processor design and the characteristically low pressure drop associated with monolith-supported catalysts, the new fuel processor possesses an extremely low pressure drop.

Shown in Figure 6.32 is the calculated reformate composition based upon the assumption of equilibrium for the reformation reactions. The figure provides calculated data for two temperatures, 594°C (the temperature calculated for the outlet reformate based upon the current fuel processor model) and 570°C. From these data, it is readily apparent that the reformate composition corresponds almost exactly with that calculated for 570°C and not the higher temperature. Thus, from the reformate composition data, it appears that the temperature of the reformate exiting the catalyst is 570°C versus the target of 600°C established from system models. This result is not unexpected as small, as yet unaccountable heat losses are likely occurring within the fuel processor test station that would reduce the reformate temperature by ~ 20°C. Furthermore, the small temperature differential indicated that the level of thermal insulation for the fuel processor indeed protected it from excessive heat loss.

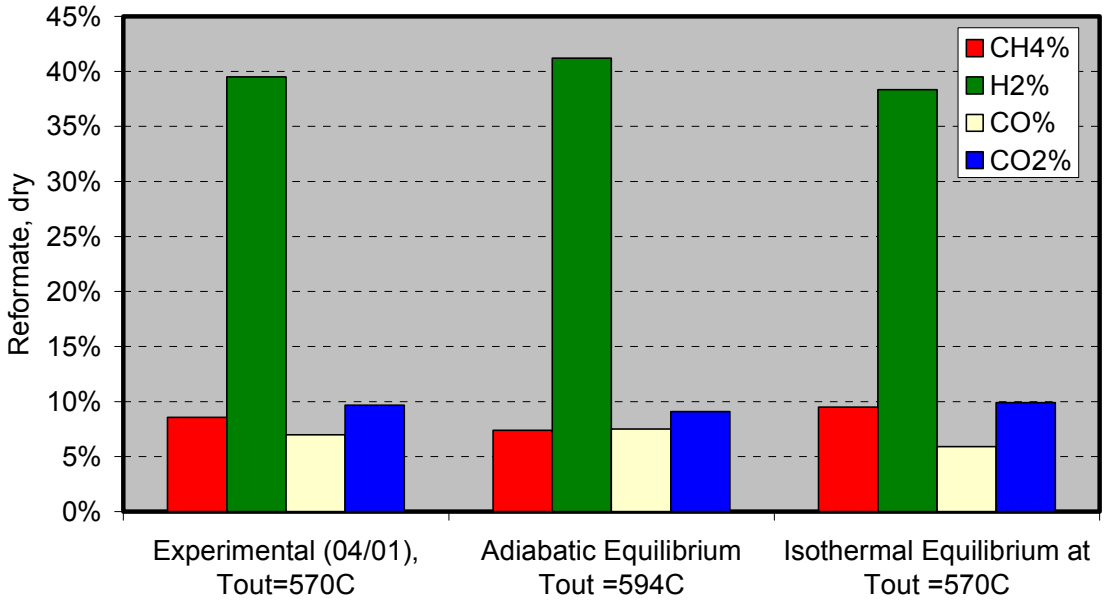

Figure 6.32 Equilibrium-calculated reformate composition versus measured reformate for the data shown in Figure 6.31.

The high level of agreement between the calculated and the experimentally measured concentrations for the reformate constituents validated the assumption of equilibrium control for the reaction. For this experiment, the calculated space velocity was approximately 10,000 hr^{-1}, which is well below the level reported by the catalyst manufacturer as being at the threshold for equilibrium control. This confirmation of equilibrium control is extremely valuable in that it reduces uncertainties associated with system models of the fuel processor.

In another experiment, the fuel flow was increased by 50% to 45 L/min and the same measurements and calculations were repeated. The results of this experiment are presented in Figure 6.33. Here, with the increased fuel flow (gas hourly space velocity ~ 15,000 hr^{-1}), larger discrepancies began to emerge between the experimental and calculated reformate exit temperatures (calculations assume knowledge of the thermal profile of the hardware obtained from earlier heat loss measurements) assuming an equilibrium controlled reaction. These discrepancies are most likely due to the gradual loss of equilibrium control of the reactions occurring over the catalyst. Of these reactions, the steam reformation portion of the reaction is the slowest kinetically and undoubtedly drove the disagreement between experiment and model.

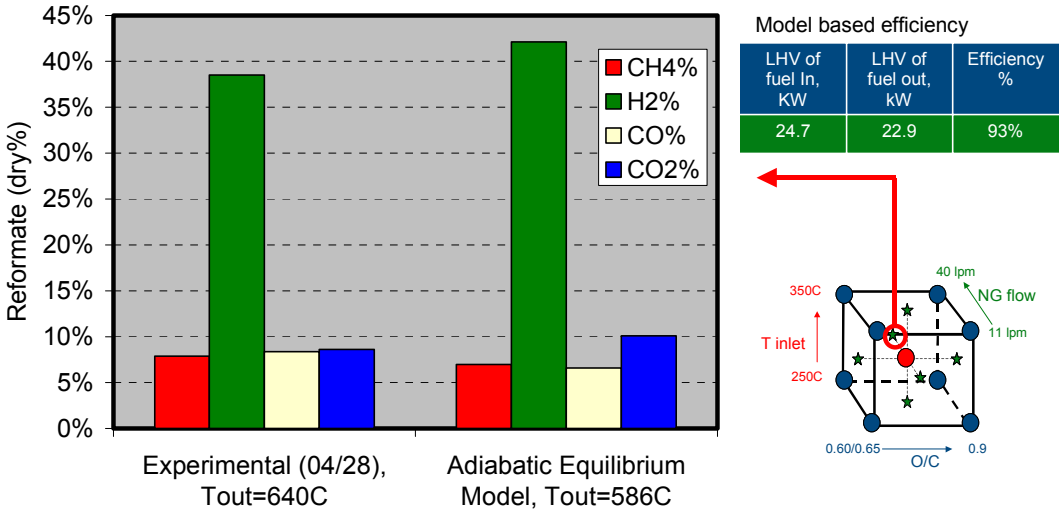

Figure 6.33 Calculated and experimental reformate composition for higher fuel gas flow. Operating parameters for this test included: O/C = 0.76, natural gas flow = 45 L/min, S/C = 1.2, inlet fuel temperature = 300°C.

A calculation for the overall thermal efficiency of the fuel processor was also performed for the data presented in Figure 6.33; the input data and the results are shown in the upper right hand corner of the figure. Based upon knowledge of the heat contents of the fuel provided to the processor and the gas compositions exiting the unit, an efficiency of 93% was determined.

As mentioned previously, one of the surprising results of this work in fuel processing was the discovery that lower inlet fuel temperatures could be used with little or no loss of fuel reformation capability. In the DoE, a lower inlet fuel temperature of 250°C was evaluated; these data are shown for the high flow rate case in Figure 6.34 in an experiment that was run for approximately 3 hours. The corresponding equilibrium and thermal efficiency calculations for this experiment are provided in Figure 6.35. The data shown in Figure 6.34 demonstrate that the target outlet gas temperature of 600°C can be met with little difficulty despite the low inlet fuel temperature. With the lower temperature for the incoming gas stream, however, additional heat transmitted to the reformate stream must be generated from the combustion of the methane fuel during the partial oxidation reaction over the ATR catalyst. As a result, more oxygen is needed (higher oxygen-to-carbon ratios), lower methane slip levels are observed as more methane is consumed in the fuel processor, and the overall thermal efficiency of the unit is reduced. The latter anticipated result is confirmed in the thermal efficiency calculation, which is included in Figure 6.35.

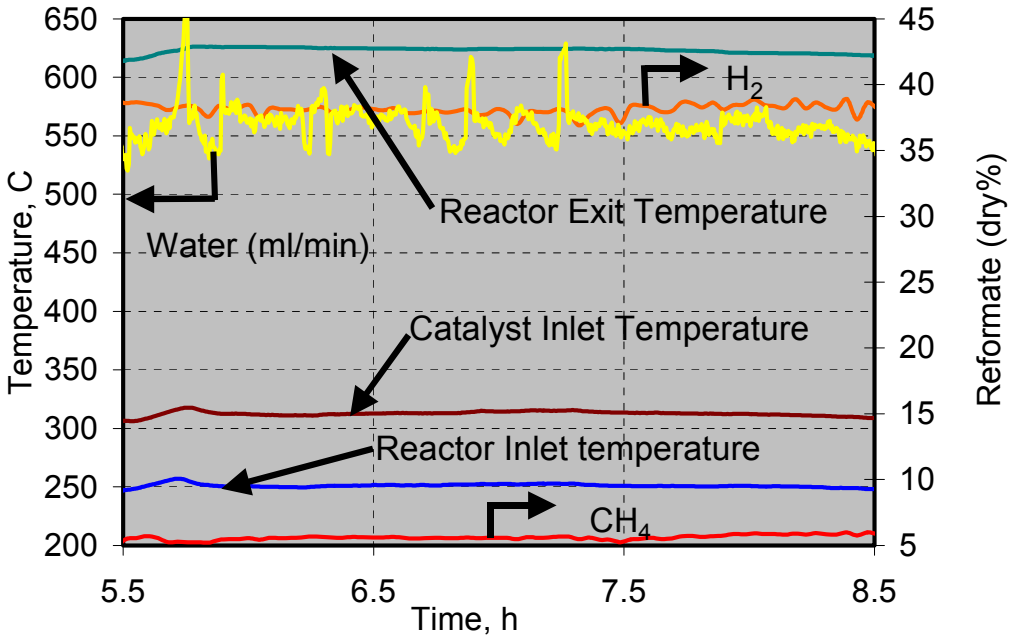

Figure 6.34 Fuel processor performance at elevated gas flow and low inlet gas temperature. Operating parameters for this test included: O/C = 0.88, natural gas flow = 45 L/min, S/C = 1.0, inlet fuel temperature = 250°C. Fluctuations in the water delivery system lead to fluctuations in hydrogen output via the steam reformation reaction.

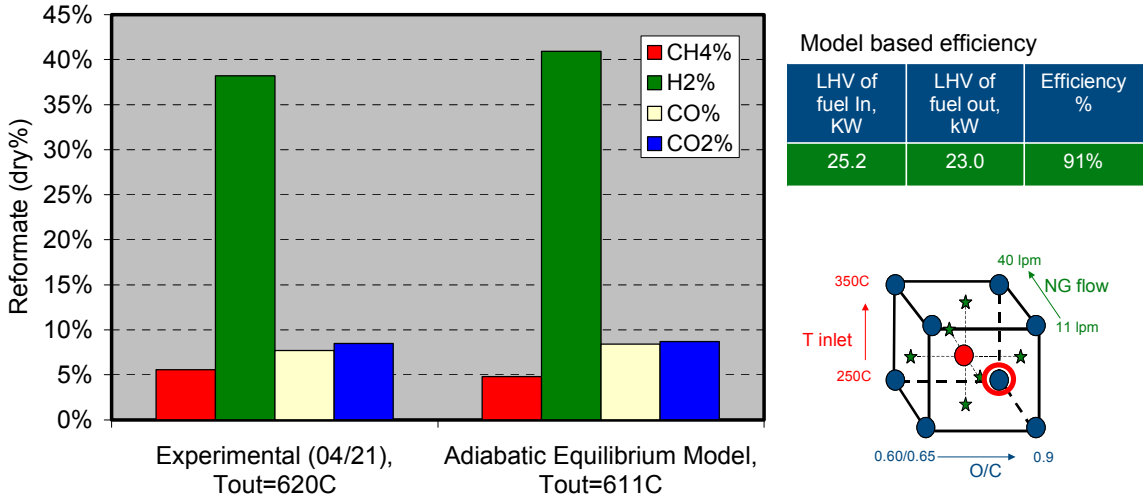

Figure 6.35 Calculated and experimental reformate composition for higher fuel gas flow with lower temperature fuel. Operating parameters for this test included: O/C = 0.88, natural gas flow = 45 L/min, S/C = 1.0, inlet fuel temperature = 250°C.

Following the completion of the DoE, attempts were made to collect data to determine the long-term stability of the fuel processor. These attempts were

somewhat unsuccessful due not to the fuel processor itself, but to instabilities in the water delivery subsystem of the test station. These instabilities are somewhat evident in the water delivery trace provided in Figure 6.34 and precluded the collection of long-term data of acceptable quality.

Data indicative of the short-term stability of the fuel processor are presented below in Figure 6.36. These data were collected over a period of approximately 6 hours and demonstrated a high level of reproducibility and consistency in operation. This level of stability was observed repeatedly throughout the DoE and indicates the capability of the fuel processor to provide fuel for the SOFC stacks in a consistent manner. It is also noteworthy that the catalyst evaluated here had seen over 30 start/stop cycles and over 500 hours of cumulative operation prior to this test.

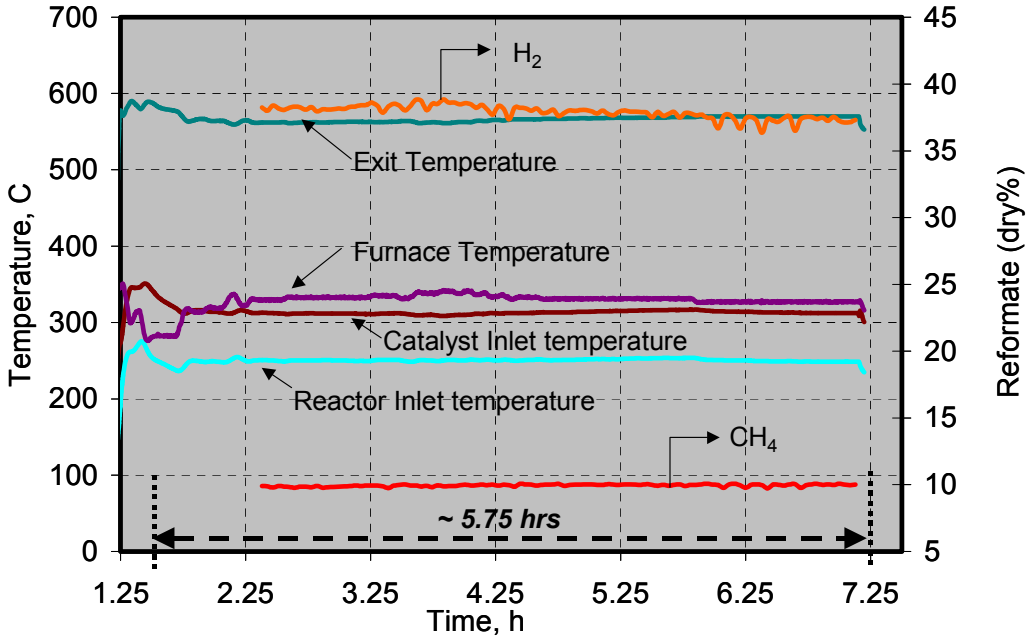

Figure 6.36 Short-term stability of the fuel processor. Short-term fluctuations observed in the plot for hydrogen composition were due to instabilities in the water delivery system.

At this point, testing of Prototype 2 was halted and a post mortem examination of the unit was performed. Inspection of the catalyst after the testing showed some discoloration at the center of the catalyst which was hypothesized to be due to either poor flow distribution or poor mixing prior to entering the catalyst. An analysis was then conducted of the feed stream distribution over the catalyst bed inside the fuel processor to assess flow uniformity. Simplified modeling of the flow distribution showed that the feed mixture distribution could be improved by installing a simple baffle plate upstream of the catalyst bed. Based upon the flow analysis, a baffle plate positioned inside the fuel processor

hardware directs the feed mixture stream to disperse over wider area and improves feed stream mixture and distribution.

6.3.3 Long-Term Fuel Processor Evaluation

The fuel processor testing demonstrated that the Prototype 2 design could meet all of the operational and cost requirements of the SECA system. However, long-term testing of the fuel processor was needed to both validate the long-term stability of the catalyst and to understand any degradation that might be seen so that the operation of the prototype system could be modified to accommodate any diminished reformer performance. Additionally, more detailed performance mapping over a wide range of operating conditions was planned to support the prototype system operation. The goal of this testing was to operate the fuel processor stably at system level flows for greater than 1500 hours.

The fuel processor test stand was modified to accommodate this long-term stability test by the addition of many features for increased system reliability and safety. Figure 6.37 shows the process and instrumentation diagram (P&ID) of the upgraded test stand. Both methane and air flow were controlled by mass flow controllers in the test stand. For increased system reliability, methane and air flow could also be controlled by bypassing the mass flow controllers and manually controlling flow using needle valves and a calibrated rotameter. De-ionized liquid water delivery was controlled through a metering pump. Air entered the pre-heating line inside the pre-heating furnace and carried de-ionized water for accelerated and stable steam generation. Methane flow was designed to bypass the pre-heating furnace to avoid any unwanted carbon deposition in pre-heating line. The preheated air-steam mixture was mixed with cold methane outside the pre-heating furnace and this methane-air-steam mixture flowed through the catalyst bed inside the external fuel processor hardware. Insulation was applied on the feed line between pre-heating furnace and external fuel processor hardware to minimize heat loss.

The external fuel processor hardware was installed vertically and was instrumented with multiple thermocouples and pressure transducers. Thermocouples were inserted at multiple locations inside the catalyst bed to clearly understand temperature distribution along its length and validate the fuel processor modeling work. Once the fuel processor reformate stream left the fuel processor hardware, it entered a coiled heat exchanger for liquid water condensation. Gas chromatography (Agilent 3000 Micro-GC) provided the compositional analysis of both the feed and reformate streams. Figure 6.38 shows pictures of the upgraded fuel processor test stand with the fuel processor housing installed.

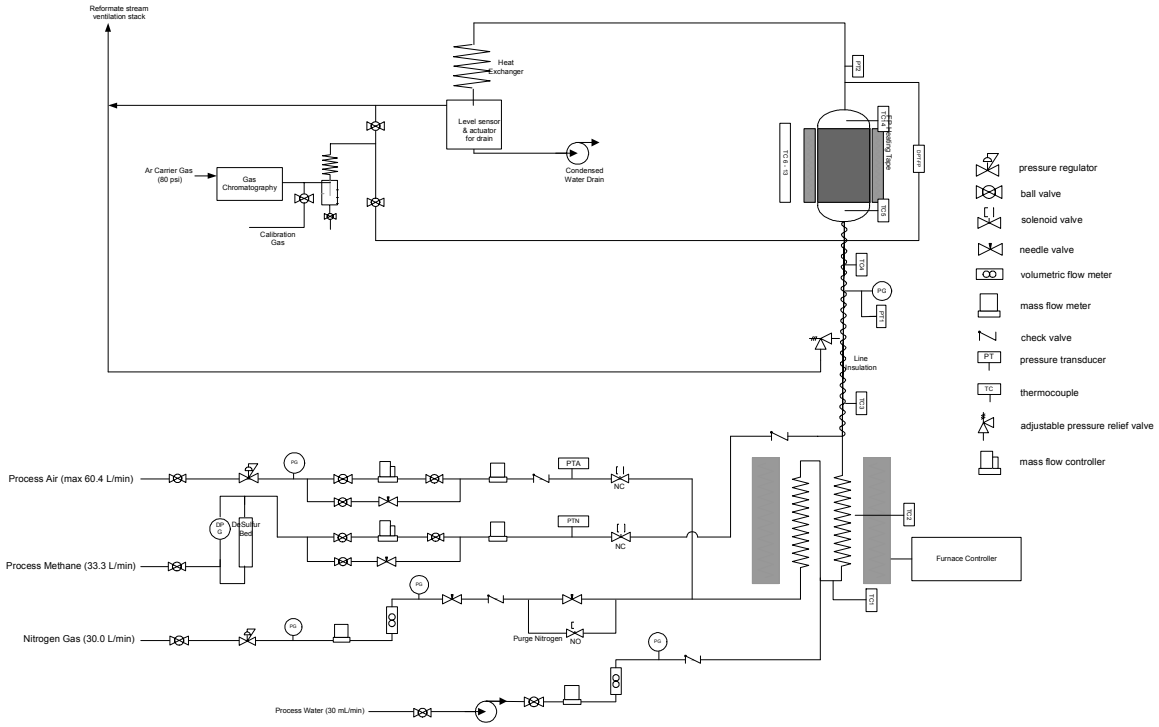

Figure 6.37 Process and instrumentation diagram of external fuel processor test stand.

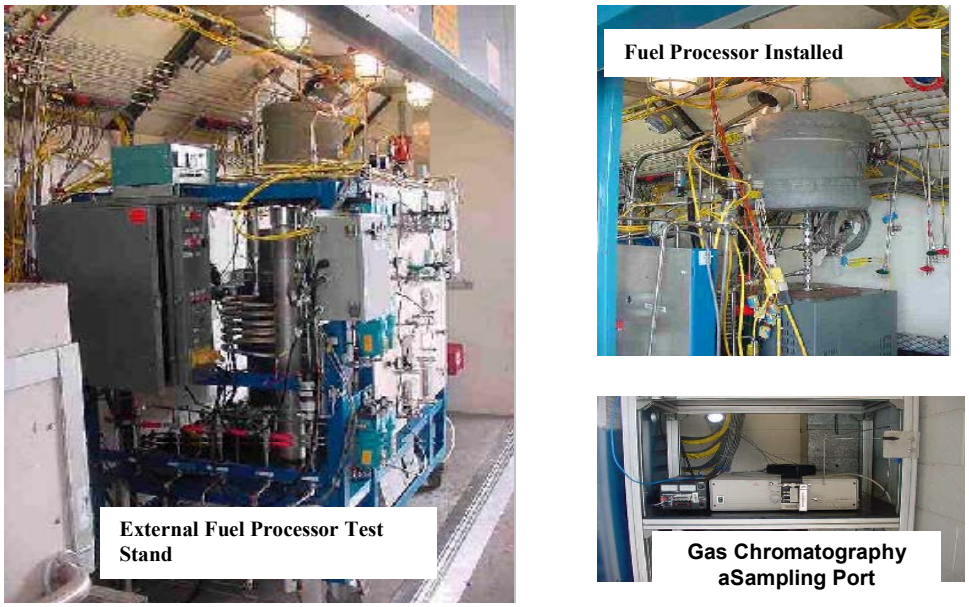

Figure 6.38 The external fuel processor test stand.

The SECA fuel processor was tested for 1373 hours using fixed operational conditions similar to those anticipated in the SECA system. During this time, a number of unscheduled interruptions occurred (three CH_4 mass flow

controller failures and one liquid water flow meter failure). Throughout this test, critical performance data (reformate composition, outlet temperature and pressure drop) were monitored for any changes in fuel processor performance. As shown in Figure 6.39, stable CH_4 conversion and H_2 composition were measured over the test period. The fuel processor outlet temperature remained stable at 550°C. All these observations indicated that the fuel processor was performing stably and did not indicate any sign of failure or degradation.

One thing to note is that there was a gradual shift in the liquid water flow after 900 hours and this problem led to a reduced S/C ratio in the feed stream. From Figure 6.39, the CO content in the reformate stream rose and the CO_2 content dropped gradually in a manner consistent with the water gas shift reaction.

The fuel processor temperature after 900 hours of operation is shown in Figure 6.40. As shown in the figure, while the fuel processor inlet temperature remained constant at 300°C, the catalyst front, the catalyst halfway point and the fuel processor outlet temperatures were found to rise gradually. The observation of the reformate composition change in Figure 6.39 along with gradual catalyst bed temperature rise observed in Figure 6.40 is consistent with the gradual shift in the liquid water flow. An independent check of liquid water meter after the completion of the long-term test confirmed that the actual water flow rate was considerably lower than the water flow reading by the water meter.

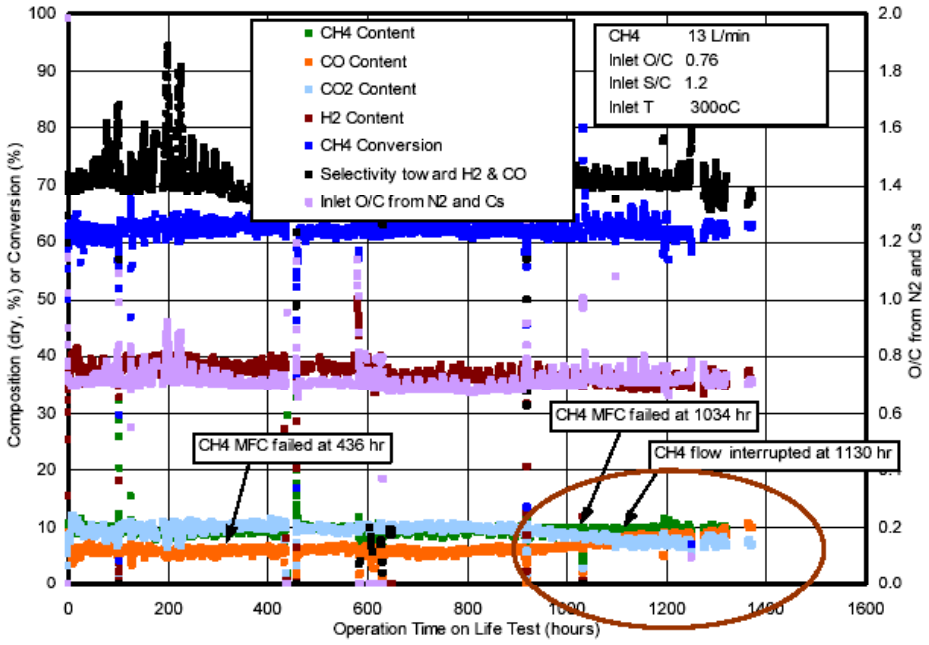

Figure 6.39 Long-term testing of the SECA fuel processor.

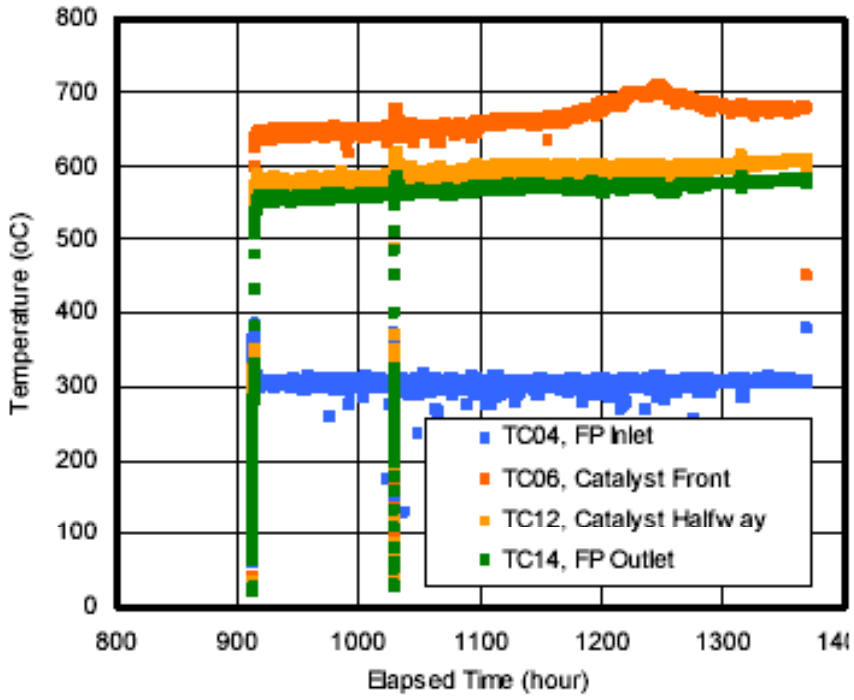

Figure 6.40 Fuel processor temperatures measured during long-term testing.

The performance of the fuel processor was assessed throughout the long-term test at a number of different operational conditions. As an example, the performance of the unit was checked using a low and a high methane flow rate of 13 L/min and 52 L/min, which corresponds to turn-down ratio of 4. An inlet S/C ratio of 1.0 and 1.2 and an inlet O/C ratio of 0.72, 0.76 and 0.8 were also employed, respectively, for performance mapping.

The performance mapping of the fuel processor is summarized in Table 6.2. It should be noted that the fuel processor inlet temperature was maintained at its setting temperature of 330°C with a methane flow of 13 L/min. However, preheating of the methane feed mixture of 52 L/min could not be achieved properly as the fuel processor inlet temperature could only reach 250°C at the high flow condition.

As in the catalyst evaluation studies, methane conversion across the fuel processor was found to be quite sensitive to changes in the inlet O/C. As shown in Figure 6.41, an increase in the inlet O/C from 0.72 to 0.80 raised the methane conversion from 60 – 62% to 66 – 68% for a methane flow of 13 L/min and from 64% to 70% for a methane flow of 52 L/min. Methane conversion is seen to be higher at the higher flow of 52 L/min by approximately 2 – 4% as compared to the low flow condition of 13 L/min, due primarily to a decreased percentage of heat loss to the environment at the increased methane flow.

Table 6.2 Performance mapping summary of SECA fuel processor

Test Step	Sub-step	CH4 L/min	O/C	S/C	CH4 Slip (%, dry)	CH4 Conversion (%)	Inlet oC	Outlet oC
2	1	13	0.76	1.2	9	64.5	333	563
	2	13	0.76	1	9.4	62.9	330	570
	3	13	0.8	1.2	8	67.8	331	571
	4	13	0.8	1	8.3	66	330	575
	5	13	0.72	1.2	10.1	62.1	333	557
	6	13	0.72	1	10.3	60.4	330	562

Test Step	Sub-step	CH4 L/min	O/C	S/C	CH4 Slip (%, dry)	CH4 Conversion (%)	Inlet oC	Outlet oC
3	1	52	0.76	1.2	7.8	66.8	248	575
	2	52	0.76	1	7.8	66.6	238	575
	3	52	0.8	1.2	6.7	70.1	245	585
	4	52	0.8	1	6.7	70.1	244	586
	5	52	0.72	1.2	8.5	64	237	563
	6	52	0.72	1	8.5	64.3	244	568

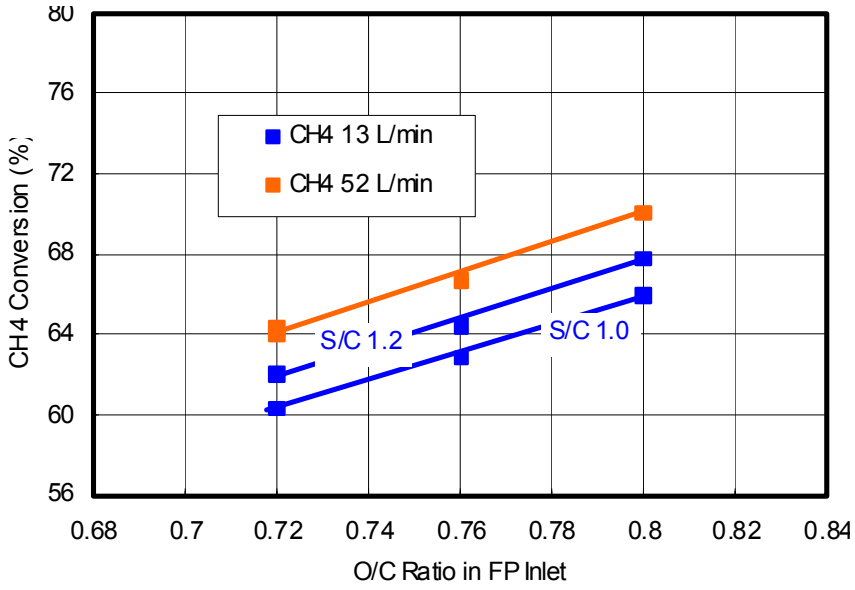

Figure 6.41 Methane conversion measured with inlet O/C ratio.

Fuel processor performance measured during the long-term test (methane flow of 13 L/min, O/C = 0.76, S/C = 1.2, inlet preheating at 300°C) was compared with that using the assumption of “adiabatic” thermodynamic equilibrium, which was predicted using the ASPEN modeling package. The experimentally measured reformate composition and fuel processor outlet temperatures are shown in Table 6.3 and compared with thermodynamic equilibrium values (under the assumption of “zero” heat loss). It should be noted that the wet reformate

composition shown in the table was determined from dry reformate composition using elemental balance equations.

Table 6.3 Reformate composition measured and predicted.

	Experimental	Equilibrium
Reformate Composition (%)		
H2	33	34.8
H2O	17.7	16.9
CO	4.8	5.9
CO2	8.2	8
CH4	7.7	5.9
N2	28.6	28.4
FP Outlet Temp (oC)	552	582

With the reformate stream composition and fuel processor outlet temperatures shown above, the heat loss from the fuel processor to the environment was calculated to be approximately 150 Watts. This heat loss was calculated based upon the measurement of reformate composition from the operating processor and the composition anticipated assuming thermal equilibrium and zero heat loss. The 150 Watt heat loss from fuel processor is estimated to be 1.9% of the thermal input by 13 L/min of the methane flow into the fuel processor.

6.4 INTEGRATED FUEL PROCESSOR-SOFC STACK TESTING

With the completion of the ATR fuel processor design and the subsequent hardware evaluation, efforts were begun to integrate and test the reformer with an SOFC stack. In the laboratory, fuel cell modules (both single-cell and multi-cell stacks) had been evaluated successfully using both dilute hydrogen streams and pre-mixed “simulated” reformate streams. Previous experience on other SOFC programs has demonstrated the integrated operation of a fuel processor and an SOFC stack to be non-trivial. Carbon formation and the inability to accommodate transients in fuel or steam feeds can be an extremely serious issue for these devices, and a clear understanding of how the reformer and the SOFC stack respond to system perturbations was paramount to the successful operation of the SECA system.

This integration task also provided information on SOFC operation using a “real” reformate stream generated by the fuel processor using a methane, steam, and air fuel stream. The performance of the fuel cell stack running on the reformate stream was measured and compared with the fuel cell stack performance obtained with a diluted hydrogen stream to determine and understand issues related to fuel cells running on “real” reformate fuel. Also, the operation points of the fuel processor (feed steam-to-carbon ratio, oxygen-to-

carbon ratio and pre-heating temperature) were varied over pre-determined ranges and the resultant reformate gas compositions and fuel cell stack performance changes were monitored. Of particular interest here were potential interactions between the hardware that might impact SOFC performance.

A schematic of the integrated test system is shown in Figure 6.42. Process gases (methane, hydrogen and air) were mixed and humidified prior to introduction into the fuel processor. The steam-air (and other gases) mixture flowed down a heated gas line and was mixed further with fuel gas (methane). A bypass leg was added so that the SOFC could be operated independently from the external fuel processor to establish the fuel cell's baseline capability on dilute hydrogen. The use of this bypass fuel line was aimed at understanding if there were any issues related to fuel processing hardware materials on SOFC stack performance.

The fuel processor was instrumented for temperature measurements at multiple locations both in and around the unit to provide information related to thermal management. A temperature controller was used to control the heat supply into the fuel processor so that the temperature of the exiting reformate stream could be raised to any level to evaluate equilibrium conditions at any given target temperature.

The performance of the external fuel processor was measured by analyzing the composition of the reformate stream using gas chromatography. The gas chromatography analysis was also used to double-check the composition of the fuel processor feed mixture. The differential pressure through the anode flowfield and cathode flowfield were measured, respectively, and a pressure relief valve was installed to prevent any accidental pressure build-up in the system.

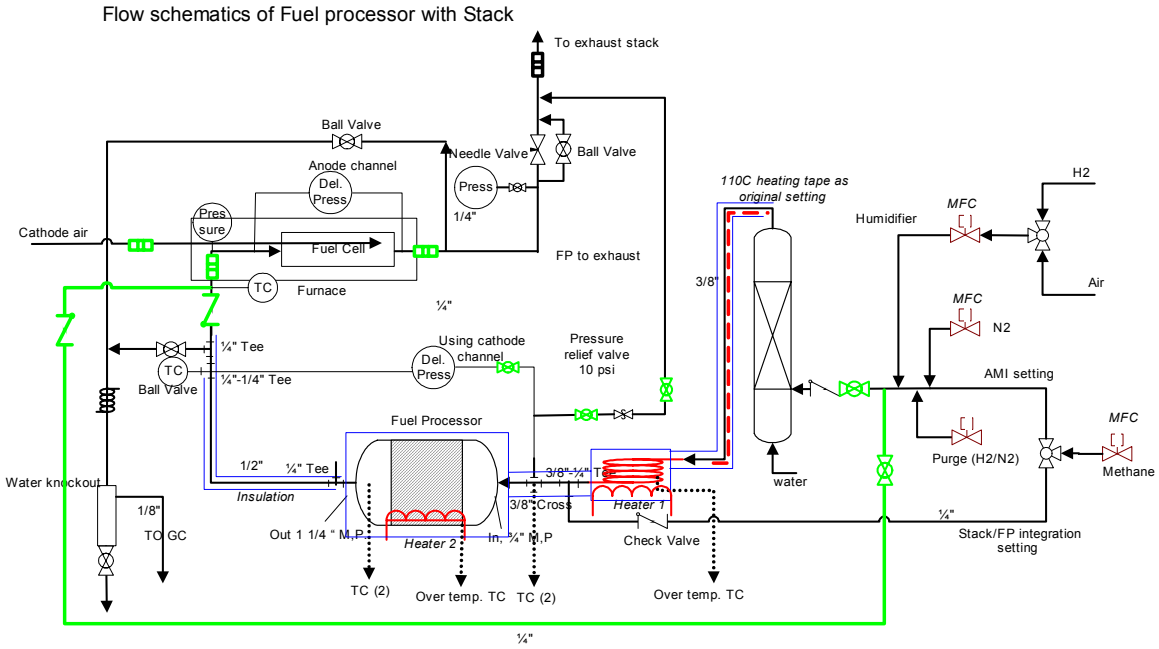

Figure 6.42 Schematic of eternal fuel processor – SOFC stack integrated test.

A series of 12 test was conducted with stacks ranging in size from one to five cells. Single-cell tests had been successful previously in achieving the expected performance on ATR fuel. However, through the majority of stack testing, the performance of multi-cell stacks was found to be below expectations until the final test (S782) in the series. A root cause analysis (RCA) performed on the problem revealed a problem that originating from the test station and related to the manner in which stacks were initially started.

The stack in Test S782 was successfully tested in another test stand on dry hydrogen prior to being moved to the integrated fuel processor test stand. The comparison of dry hydrogen performance can be seen in Figure 6.43. The overall drop in voltage performance for the stack was consistent with the performance drop seen with the first thermal cycle of other multi-cell stacks. After dry hydrogen testing, the SOFC stack was then successfully tested on ATR reformate from the fuel processor for a time in excess of 400 hours.

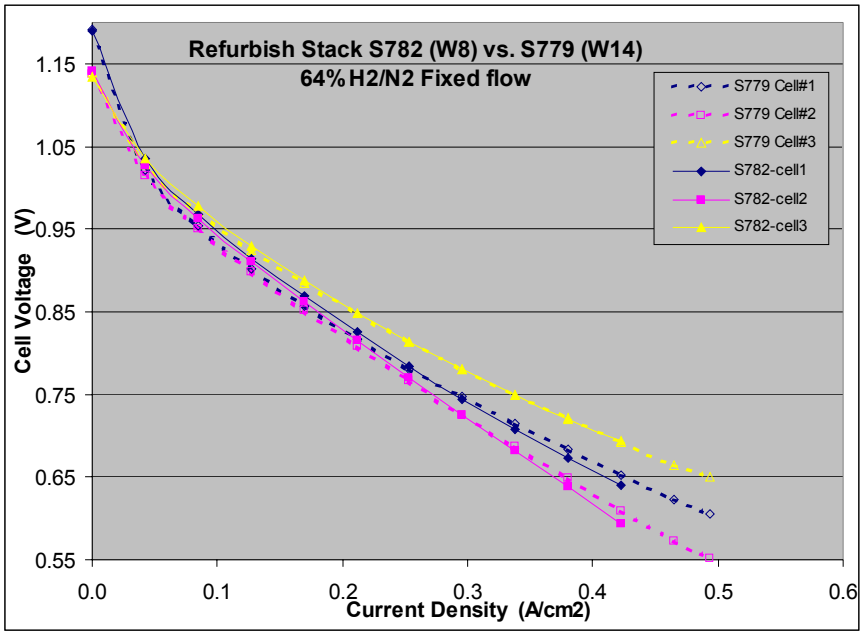

Figure 6.43 Performance comparison for stack S782 with previous tests.

Therefore, Test S782 built upon previous successful single-cell tests showing that there was no fundamental issue in operating the SOFC stack with the prototype system's ATR fuel processor. With the completion of this test, it was clear that the redesigned ATR fuel processor was ready for incorporation and use in the SECA power generation system.

6.5 INTERNAL REFORMATION

The ability to harness and utilize excess waste heat from the SOFC stack is one of the key requirements of a high efficiency SOFC power generation system. Relocation of the reformation process (the endothermic steam reformation process) from an external fuel processing unit to within the intimate boundary of the SOFC stack is one method by which the excess heat of the SOFC can be exploited directly, thereby reducing the need for excess air flow and increasing the overall efficiency of the SOFC system. Thus, the development of materials, approaches, and technologies that enhance and support internal reformation are highly desirable and, indeed, are necessary for a commercially viable SOFC system.

There are a number of different methods for carrying out internal reformation. One of the most straightforward and deceivingly simple is to carry out the reformation reaction directly upon the anode of the SOFC. This is possible since the primary component of the anode is nickel, and nickel is a highly efficient and relatively inexpensive catalyst for steam reformation.

Within Phase I of SECA, various aspects of on-anode steam reformation were examined using detailed chemical and thermal modeling as well as a

variety of experimental approaches and apparatus. Experiments pertaining to the kinetics of the reaction were performed with the goal of understanding the magnitude and nature of the rate constant to be used in detailed fuel cell models. Tests that measured directly the efficiency of methane conversion over an actual operating cell were performed. Finally, one important and often overlooked aspect of on-anode internal reformation, the localized cooling of the fuel cell, was examined in detail to better understand one of the potential challenges of internal reformation. In general, the results obtained in this program demonstrate the feasibility of internal reformation within the stack without significant performance penalty.

7 CONTROL SYSTEM DEVELOPMENT

The control system development was conducted using the "Design for Control" methodology wherein dynamic issues and controllability are addressed at the earliest stage possible in the overall system design effort. The control algorithms and overall strategy are developed and evaluated using dynamic simulation analysis. The output of the analysis provides controllability and operability feedback to different design teams. After the control algorithm is finalized, the control system team transitions the algorithm to software and identifies the appropriate control hardware. The control software is then compiled into real time software and implemented in the hardware controller. The whole control system, including all the software and hardware, needs to pass through a series of tests to ensure its reliability and performance. The control system development is discussed in greater detail in the following sub-sections.

7.1 CONTROLS STRATEGY DEVELOPMENT

The challenge of controlling the SOFC system is the diverse time scales for physical phenomena throughout the system as shown in Figure 7.1. The control strategy must be able to account for fast dynamic behavior in the power electronics and SOFC electrochemistry, slower thermo-fluid response and long-term performance degradation effects. For the residential application, this translates to a design that must handle automated startup, shutdown and normal operation while maintaining the system within its operating constraints when subjected to load changes or disturbances.

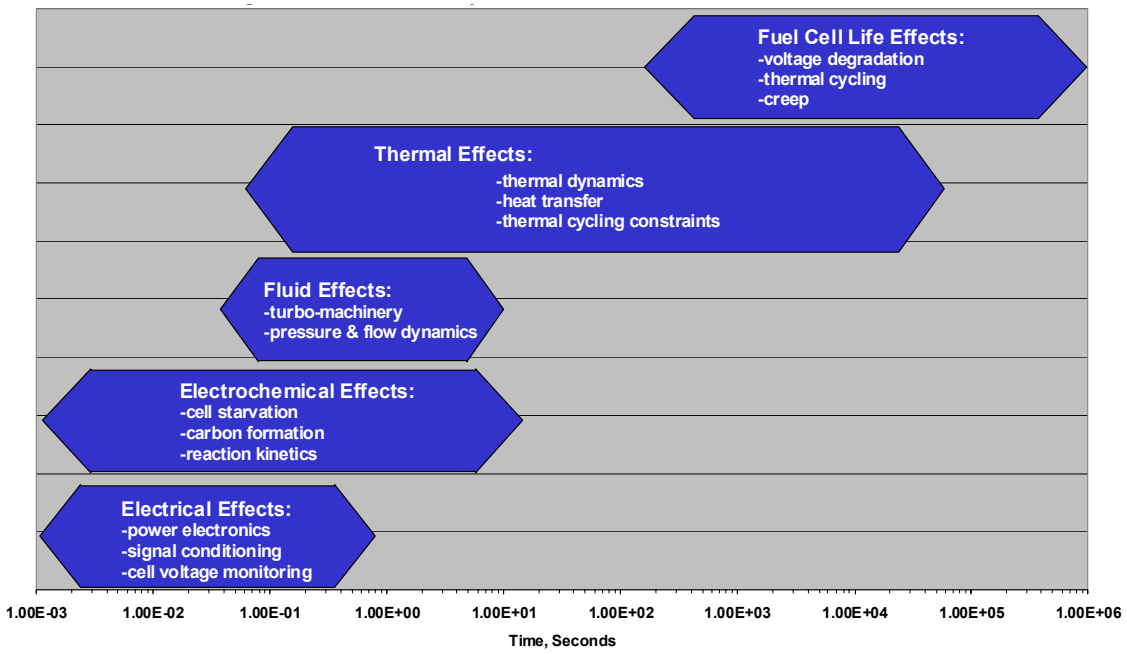

Figure 7.1. Fuel cell system time scales

7.1.1 Dynamic System Modeling and Analysis

A key component of the "Design for Control" methodology is to develop dynamic component, subsystem, and system models early in the design effort. This allows the system's dynamic interactions and transient behaviors to be studied up-front through simulation rather than waiting for the final system integration. These same models can also be used to design the control algorithms that are eventually implemented in the hardware system.

The modeling efforts began with constructing dynamic models for each component in the system. These component models, together with a few commonly used calculation and logic modules, form the proprietary GE Hybrid Power Generation Systems Dynamic Model Library as shown in Figure 7.2.

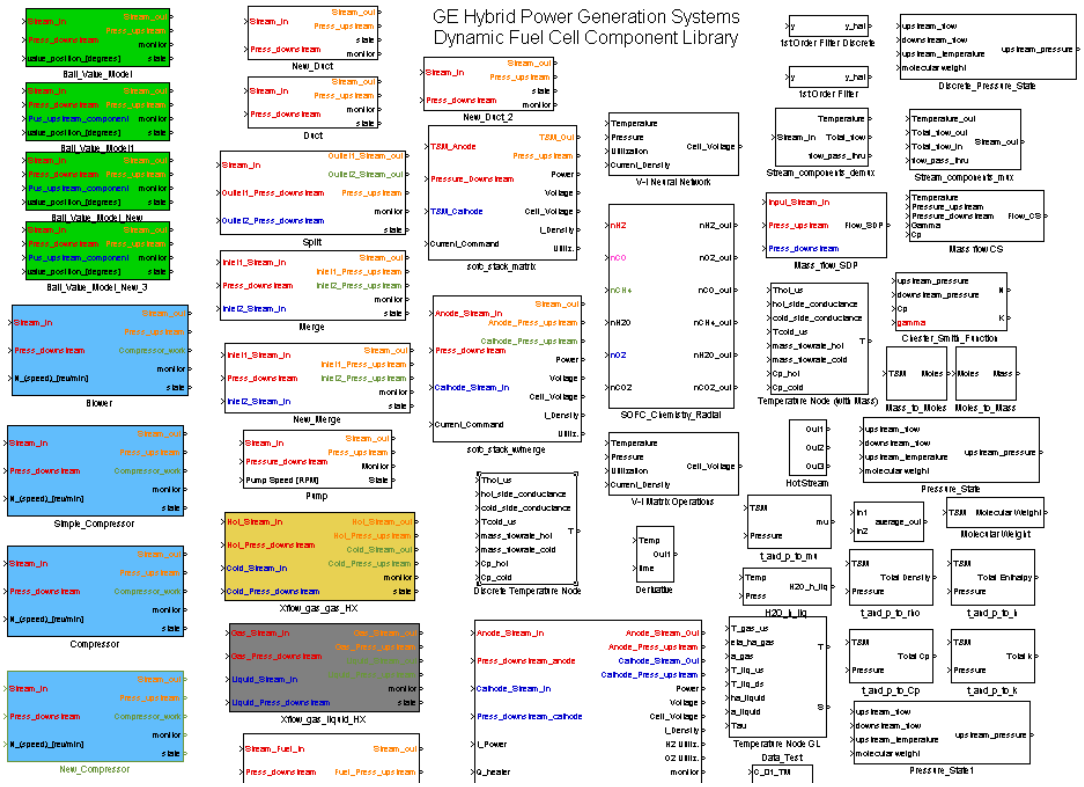

Figure 7.2. GE Hybrid Power Generation Systems dynamic fuel cell component library.

To analyze the dynamics of the system, component, subsystem, and full system dynamic models are built by assembling the modules from the component library. The general modeling structure for analyzing the entire system and designing the controls is shown in Figure 7.3 where the dynamic system model is combined with models of the controls, models of noise in the system, and any disturbances that the system would be expected to see. An expanded view of the dynamic system model is shown in Figure 7.4. Throughout the design process, modeling efforts are focused on tuning system component data parameters as more accurate information becomes available from the various design teams and hardware data. The controls model is refined throughout the design process and eventually will become the control software that is downloaded to the system's hardware controller. This modeling and control design strategy permits the control architecture and detailed algorithms to be exercised in the various operating modes in the simulation environment, greatly reducing the risk and cost associated with hardware integration.

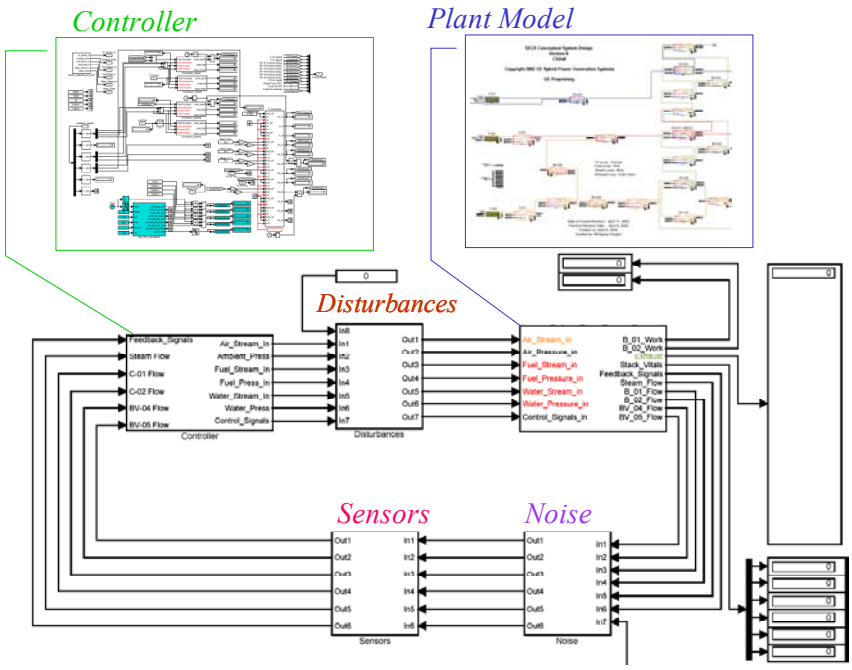

Figure 7.3 General Modeling Strucutre.

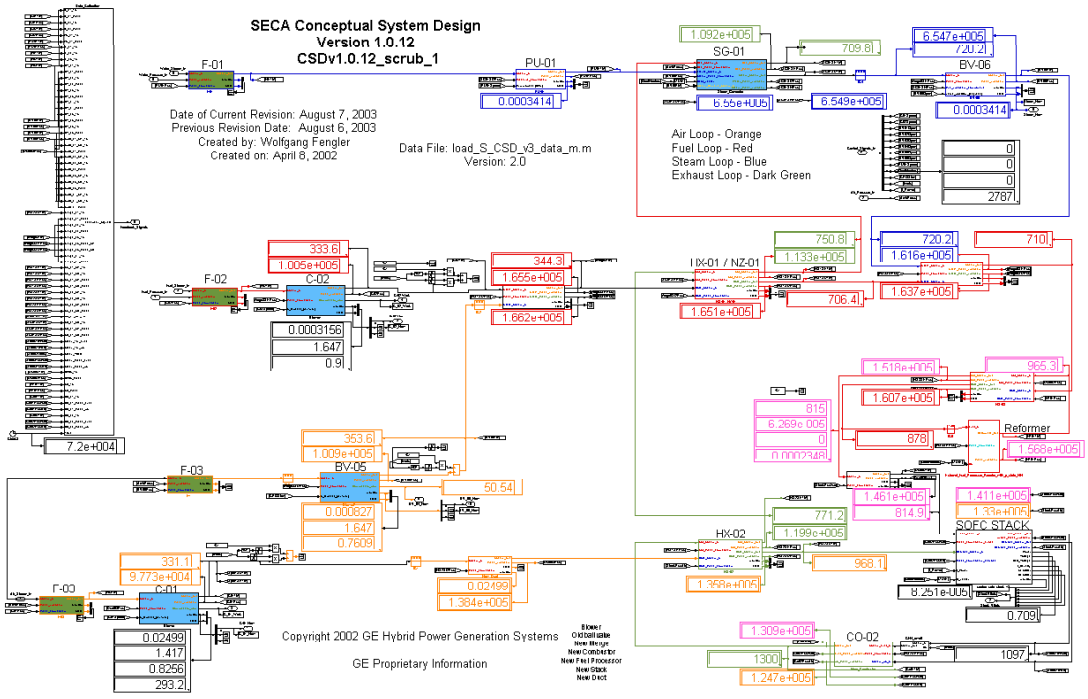

Figure 7.4 Dynamic System Model (Plant Model).

Efforts were undertaken to benchmark the dynamic models' output with the results from steady state analysis in Aspen. Tools were developed to automate this process. The output of this effort was a quantification of the

difference between the steady state and dynamic model results. If the differences between the model results were sufficiently large, the component, subsystem, and system models were updated as appropriate.

7.1.2 General Control System Architecture

A multi-level design was developed to manage the various control system tasks. The general control system architecture for this design consists of top-level supervisory algorithms that determine setpoints based on user settings and system conditions. These setpoints are provided to a set of active controls that handle setpoint tracking and disturbance rejection.

The supervisory controls serve the function of coordinating system operation, providing the structure for the various operating modes of the system, handling the sequencing and transition between operating modes, monitoring the health and safe operation of the system, and optimizing system efficiency.

In the system design there are five key independent variables that govern the operation of the system. These key independent variables are set by the supervisory controls to maximize system efficiency and stability while meeting the required power command. These key variables are then interpreted and driven down to the lower level control loops as individual actuator setpoints. The key independent variables for the system are:

- Output Power
  - User/load prescribes power demand
  - Used to determine gross DC power needed from the fuel cell
- Oxygen-to-Carbon Ratio
  - Controller determines to maintain reformer temperature while maximizing efficiency and stability at setpoint
- Steam-to-Carbon Ratio
  - Controller determines to prevent carbon formation
  - Maintains carbon deposition margin
- System Fuel Utilization
  - Controller determines to maximize efficiency and stability at setpoint
- System Air Utilization
  - Controller determines to maximize efficiency and stability at setpoint

7.1.3 Active Controls

The active controls translate setpoint commands from the supervisory controls into signals that ultimately drive individual actuators throughout the system.

7.1.4 Supervisory Controls

The supervisory controls focus on start-up sequencing, shutdown sequencing, and load transition coordination. The operating modes in the supervisory controls include start-up, idle, normal operation, shutdown, emergency shutdown, and maintenance. The setpoints provided to the lower level active control loops are calculated based on the current operating mode and key system parameters.

A state transition diagram was developed with rules that are used by the supervisory controls to determine what operating mode the system is in and what steps are appropriate to take to change system settings in response to user commands, load changes or disturbances. Additional modes are also included to accommodate maintenance, idle and system power off conditions.

7.1.4.1 Startup

The main focus of the startup design is to control the various key system variables to their setpoints in a manner that does not subject the SOFC to undue thermal stresses or other potentially damaging or unsafe conditions. In doing so, the startup algorithms contribute to promoting the reliability of the SOFC system. The specific performance requirement of start time has an effect not only on availability, but also on the utility of the product to a potential customer and market.

The synthesis of the startup strategy began by the assembling customer requirements and component operating parameter data along with lessons learned from the stack and fuel processing teams. This information was used to brainstorm and evaluate four concepts that were evaluated versus the system requirements of cost, startup time, and general controllability.

7.1.4.2 Normal Operation

During normal operation, the primary tasks of the controller are to hold the stack to its power setpoint while maintaining component constraints, to accommodate load increases and load decreases, and to reject disturbances.

During load transition operation, it was anticipated that all the cell voltages needed to be above a safe operating point to protect the stack. A unique control algorithm was developed to meet all the stack operating requirements.

The operation of the fuel processor also needed to follow a desired sequence to prevent carbon deposition and to improve stack performance. A supervisory control module was implemented to give out the steam, fuel and fuel processor airflow setpoints.

Holding the multiple system variables to their targets was a significant challenge as there were only limited variables available for the controller to adjust. A supervisory control algorithm was designed to meet all the key control system requirements.

7.1.4.3 Shutdown & Emergency Stop

The key focus of the shutdown strategy is to control the stack temperature decrease to prevent damage to the stack and other system components. This requires active control of the system from operating conditions down to a temperature where the anode would be unaffected by being in an oxidizing environment. An additional requirement is to be able to quickly remove fuel from the system in an emergency situation. Where the normal shutdown strategy seeks to protect the stack, fuel processor and other components from damage, the primary consideration of the emergency stop design is to protect people from potentially dangerous situations, even if the stack or system are damaged as a result. Shutdown time is one of the key performance requirements as it impacts system availability. Another key issue is to minimize the capital cost of the shutdown process.

The synthesis of the shutdown strategy began with assembling customer requirements and component operating parameter data along with lessons learned from the stack and fuel processing teams. This information was used to brainstorm and evaluate the four candidate concepts to determine which as the most favorable combination of cost, reliability, and performance.

7.1.4.4 Built-in Test and Health Monitoring

The inherent need for safe and reliable system operation requires that feedback data be used not only for control of actuators, but also for monitoring and diagnostics so that variables throughout the system are maintained within acceptable limits for the current operating mode.

A list of key system constraints was compiled to aid in the control system development and trade studies. These constraints were used as evaluation criteria for various trade studies that were conducted with alternative system and control system designs. As the system and component designs mature, this list of constraints develops into the basis for the built-in test (BIT) that monitors system health.

As noted above, the basis for system health monitoring is the table of system variable constraints. By comparing the measured or derived data returning from the system with the ranges established for each operating mode, the controller is able to determine if the system is operating within acceptable limits. Two limit levels were used for the BIT evaluations. A warning threshold was set at a level that provided a safety margin away from the specification limits. The specification limits themselves set the range for the hazard limit levels. Another factor that affects the establishment of system health is the duration of deviant signals since outside influences may temporarily give false readings. For signals with an out-of-specification value that lasts for a prescribed

period of time, the system reports a warning to the user via the human-machine interface. In most cases, the active controls function to negate the deviation. However, for situations when the warning persists or the error grows and exceeds the maximum threshold level, a hazard signal is displayed and either a normal or emergency shutdown is initiated by the supervisory controls. A sequencer sets the data retrieval schedule for each individual built-in test comparator with more critical data points being sampled at a higher frequency.

7.2 CONTROL SYSTEM IMPLEMENTATION

The control system consisted of software and hardware that were developed. The control software for the SECA system was first developed in the Matlab/Simulink® environment where it was analyzed and debugged. The software was then implemented using dSPACE® hardware and software, which facilitated rapid controller prototyping to simplify software changes and optimization. This relationship is noted in Figure 7.5. The hardware development includes the evaluation of the controller and the identification of the sensors and actuators.

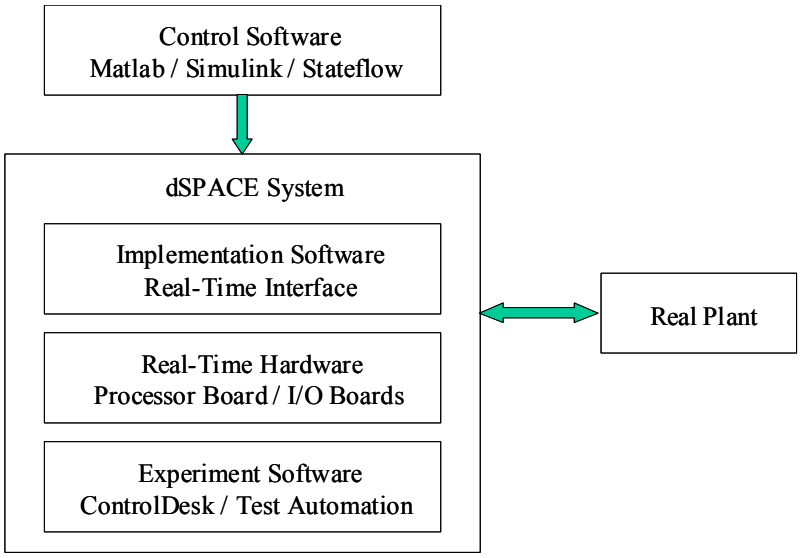

Figure 7.5. Controller structure.

7.2.1 Software Development in Matlab/Simulink®

The goal for the software development was to create a software that was open and met the following criteria:

- Compatible with the plant simulation model
- Downloadable for use with a real-time controller
- Organized into key elements
- Structure readily understood by software development team

- Elements as simple and self-explanatory as is practical

The general control architecture is divided into subgroups as illustrated in Figure 7.6. Where appropriate, additional modularization was enacted within each subgroup. The high degree of modularization facilitated testing of the algorithms and rapid expansion or modification of the code. This ability to adapt the software was considered useful for building subsets of the full code to support component and subsystem testing.

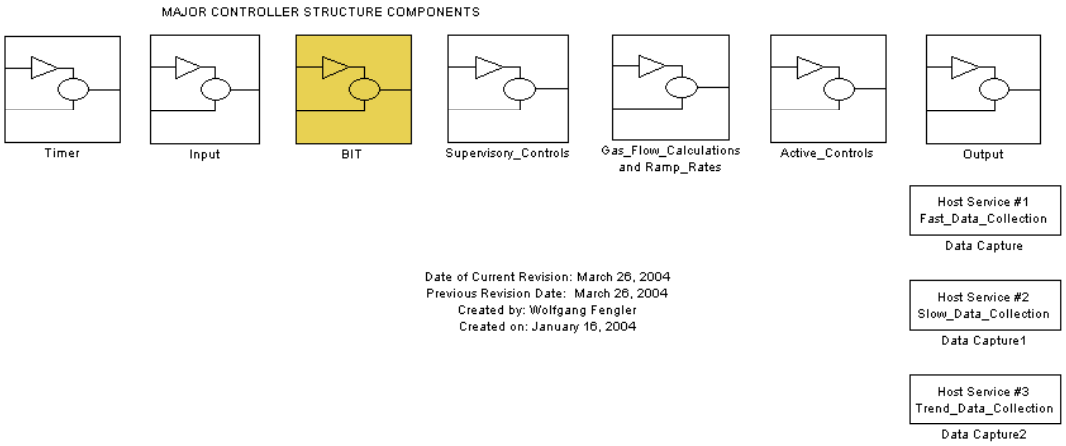

Figure 7.6. Top-level controller modules.

The top-level modules and key sub modules in the control software are as follows:

- Timer Block
  - Running time counter module – set different frequency based on basic sample rate
- Input Block
  - Hardware check module - detect sensor failure and trigger warning
  - Conversion module – convert physical input unit to engineering unit
  - Redundancy selection module - output an appropriate value calculated from all redundant sensor readings
  - RS-232 receiver module – receive inverter status and DAQ data through RS-232 communication
- BIT Block
  - Software BIT module – set upper limit and lower limit for each sensor reading, detect violation of the limits and trigger fault or warning
  - Fault transmission sequencer module – sweep through all the sensors, find the faults and warnings, record them in a fault log

- Supervisory Control Block
    - Operating modes module – determine operating modes and actions of system based on input conditions
    - HMI manual module – password protected manual settings for all the set points, analog and digital outputs, soft limits
- Gas Flow Calculation Block
    - Gas flow calculation module – calculate fuel flow, air flow, and steam flow based on current, fuel utilization, air utilization, O/C ratio, and S/C ratio
    - Stack temperature control module – utilize cathode airflow to control stack temperature and prevent combustor over temperature
    - Power and voltage control module – apply model based voltage setting and use current to regulate voltage
- Active Control Block
- Output Block
    - Conversion module – convert engineering actuator output to digital output
    - RS-232 transmitter module – send controller output command to inverter and backup data to DAQ

The Matlab/Simulink® modeling environment includes several tools that facilitate hardware-in-the-loop (HIL) testing and controller development. The first such tool employed was Stateflow®, which simplifies the coding of sequences and transitions between steps in a process. This feature was particularly useful for organizing the various states needed to capture the progression of the system from an off condition, through startup, normal operation and shutdown.

The primary operating modes provide the basic structure for handling the different conditions and steps associated with automated operation. Details of these modes are provided below:

- Power On Mode
    - Purpose
        - Prepare system to operate in either Maintenance or Startup modes
    - Capabilities
        - Initialize key system parameters (ratios, ramp rates, etc.)
- Maintenance Mode
    - Purpose
        - Allow individual actuators and control loops to be exercised for testing
    - Capabilities
        - Resets Estop flag (prevents direct restart from Power On mode after an Estop incident as a precaution)

        - Estop can be activated at any time
        - Defaults to fully automatic inputs for all setpoints with all control loops on
        - Individual control loops can be turned off
        - Individual setpoints can be manually entered
- Startup Mode
    - Purpose
        - Automatically warm-up the system and prepare it for operation
    - Capabilities
        - Sequence events, e.g. opening of valves, to warm-up system within component constraints
        - Condition driven transitions between steps
        - Alters setpoints according to sequence
        - Shutdown or Estop can be activated at any time
- Idle Mode
    - Purpose
        - Hold system at a zero stack power condition
    - Capabilities
        - Provides a means of holding the system in a “hot standby” state
        - Lowers load and flows when a “nuisance” trip occurs (grid fault, etc.) during Normal Operation
        - Waits for fault to clear or shutdown command
        - Shutdown or Estop can be activated at any time
- Normal Operation Mode
    - Purpose
        - Maintain stable system operation while meeting prescribed load
    - Capabilities
        - Alters flows when load demand changes per schedule. This scheduling provides sufficient reactants to the SOFC to prevent stack damage during load changes.
        - Provide capability to manipulate fuel utilization, steam-to-carbon, oxygen-to-carbon, stack temperature rise, etc., to optimize system efficiency or peak power
        - Can activate heaters as needed to maintain critical temperature constraints
        - Shutdown or Estop can be activated at any time
- Shutdown Mode
    - Purpose
        - De-energize system in a manner which protects the SOFC stack and other components from damage
    - Capabilities
        - Sequence events, e.g. closing of valves, to de-energize and cool-down system while meeting component constraints
        - Condition driven transitions between steps

        - Alters setpoints according to sequence
        - Estop can be activated at any time
        - Returns system to Power On state when completed
- Emergency Shutdown Mode
    - Purpose
        - De-energize system in a manner which protects personnel
    - Capabilities
        - Sequence events, e.g. closing of valves, to de-energize and cool-down system as rapidly as possible
        - Condition driven transitions between steps
        - Alters setpoints according to sequence
        - Returns system to Power On state when completed

Besides the modular design, the software includes a number of features that provide flexibility for both development work and final automated operation. These include:

- Fault codes
    - Separate codes for different failure modes
    - Code also identifies sensor location and type
    - Fault code actions are individualized by sensor and type of fault
- Built-In Test (BIT) for sensor failures
    - Determination of whether a sensor has failed high or low
    - Redundant sensors added for critical control variables
    - A voting algorithm determines which redundant input is valid
    - Fault action for redundant sensors overridden to allow continued operation while at least one input is valid
- BIT for critical variable data ranges
    - Low hazard
    - Low warning
    - High warning
    - High hazard
- Password protected manual override available in all modes
- Grouped active controls
    - Feedforward, feedback and other low-level control logic organized by actuator

7.2.2 Software Deployment in dSPACE®

The Real-Time Workshop® tool allowed compiling software developed graphically in Matlab/Simulink® into code downloadable to a real time controller. The controller selected for this project was produced by dSPACE® and included a processor, data input and output boards and software that works with

Matlab/Simulink® to assure proper translation of generated executable code for use on the dSPACE® controller. The dSPACE® software also included a development tool for creating the graphical user interface (GUI) portion of the human machine interface (HMI). This simplified the transfer of mouse and keyboard inputs to the software running on the controller and the viewing of assorted variables to the user display.

7.2.2.1 dSPACE® System

The requirements for the SECA controller are:

- Real-time operation
- Flexibility
- Robustness
- Reliability

Based on these requirements, a dSPACE® system was chosen due to its known capability as a versatile and dependable development system that helps optimize real time control software design and implementation.

The dSPACE® system was connected to a host PC through Ethernet cable. The host PC was used to download compiled control software to the dSPACE® system, monitor real-time parameter changes using ControlDesk® experiment software, and store real-time captured plant data.

7.2.2.2 Human Machine Interface

ControlDesk® experiment software was used to develop the human machine interface (HMI) for the prototype system. The requirements for the HMI are:

- Robustness
- Reliability
- User friendliness
- Completeness

The HMI structure is depicted in Figure 7.7.

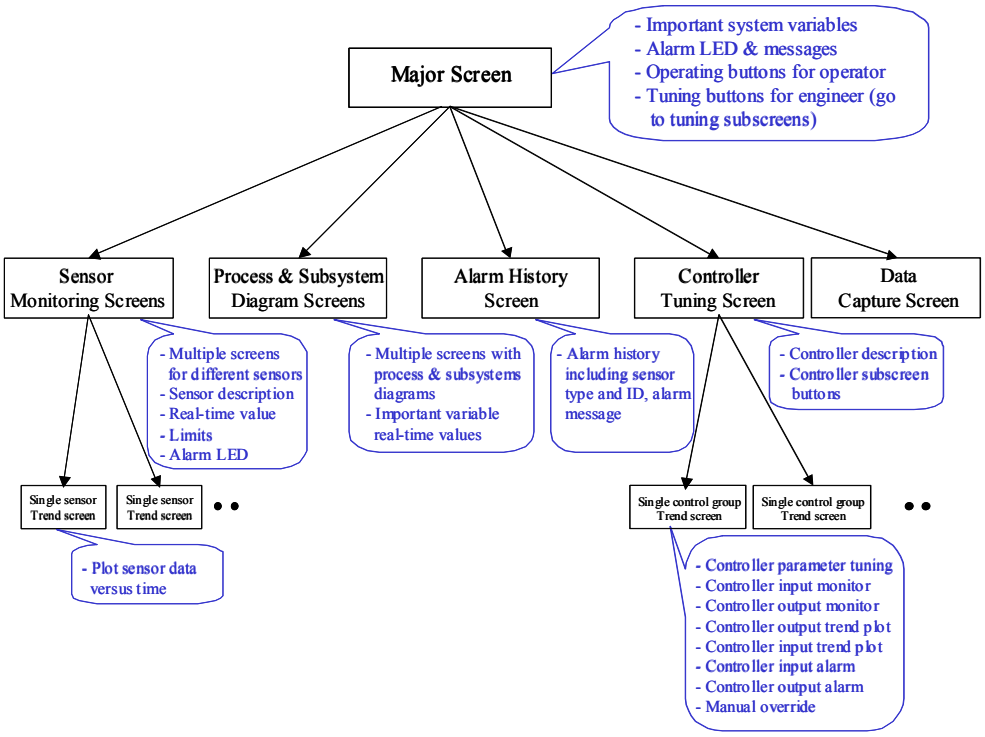

Figure 7.7. HMI layer structure.

Each layout of HMI was built using the ControlDesk® virtual instrumentation tool. At the top of the HMI structure is a primary screen including displays of important system variables, a system alarm indicator, mode selection buttons for the operator (start, stop, maintenance, and emergency stop), and tuning buttons for engineers (sensor calibration, alarm history, data capturing, and controller tuning). The primary HMI screen is shown in Figure 7.8.

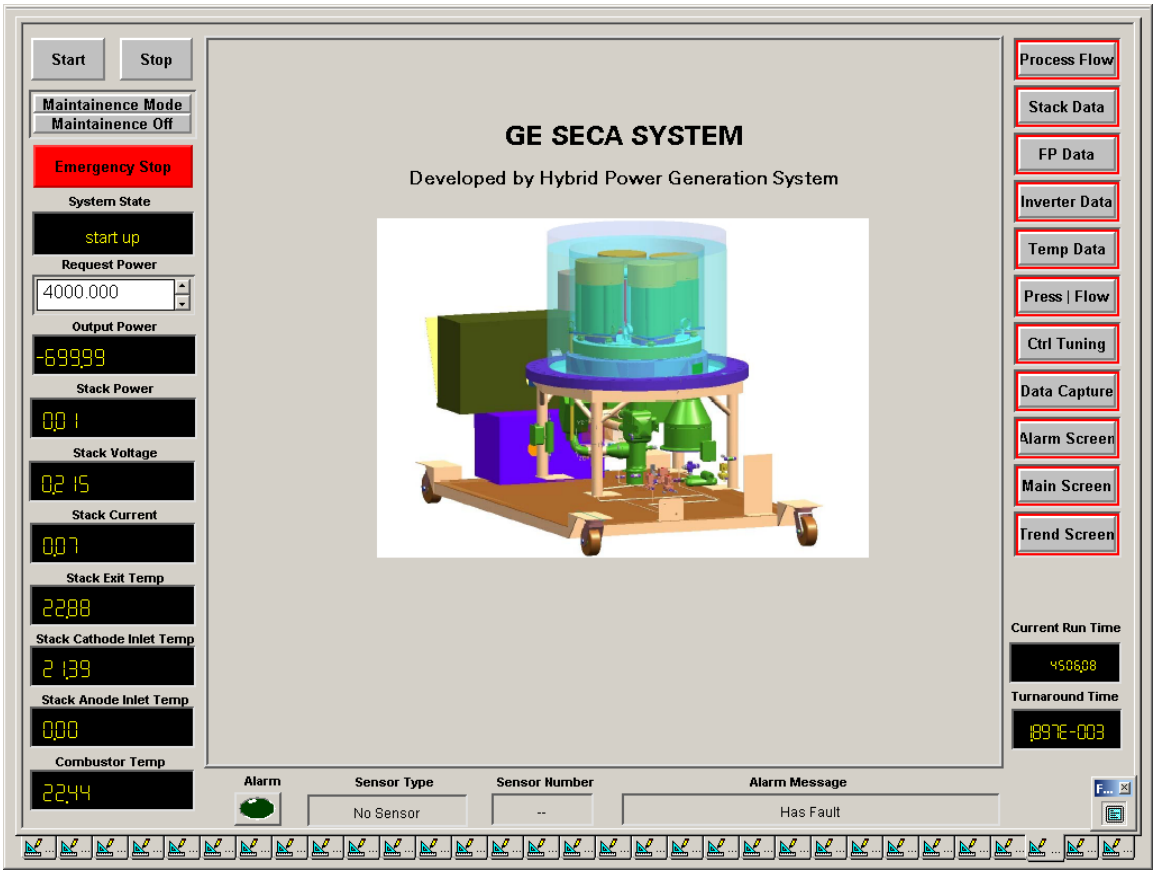

Figure 7.8. Primary HMI screen.

The buttons on the right side of the major screen guide the user to the second layer of HMI. In this layer, there are several sub-screens for monitoring the system and important subsystems. Diagrams are shown in these sub-screens to indicate system, subsystem, and component configurations. Selected critical variables are displayed at proper locations on the diagrams. Also, sub-screens are generated to monitor each sensor including temperature, pressure, flow and other process variables. On these sub-screens, each sensor reading is displayed with its current value, operating limits and an alarm indicator. There is also a trend button for each sensor that opens a real time trend plot. On the control tuning sub-screen, controllers are categorized by actuator or function and each has a corresponding tuning button. Clicking on the tuning button brings up an on-line tuning screen that allows the engineer to adjust controller parameters, monitor controller inputs and outputs, and enter manual inputs. The data capture sub-screen groups the important data into a high frequency group and other data into a lower frequency group. The alarm history sub-screen displays any current alarms and a list of the past 10 alarms triggered. Various HMI sub-screens are shown in Figure 7.9.

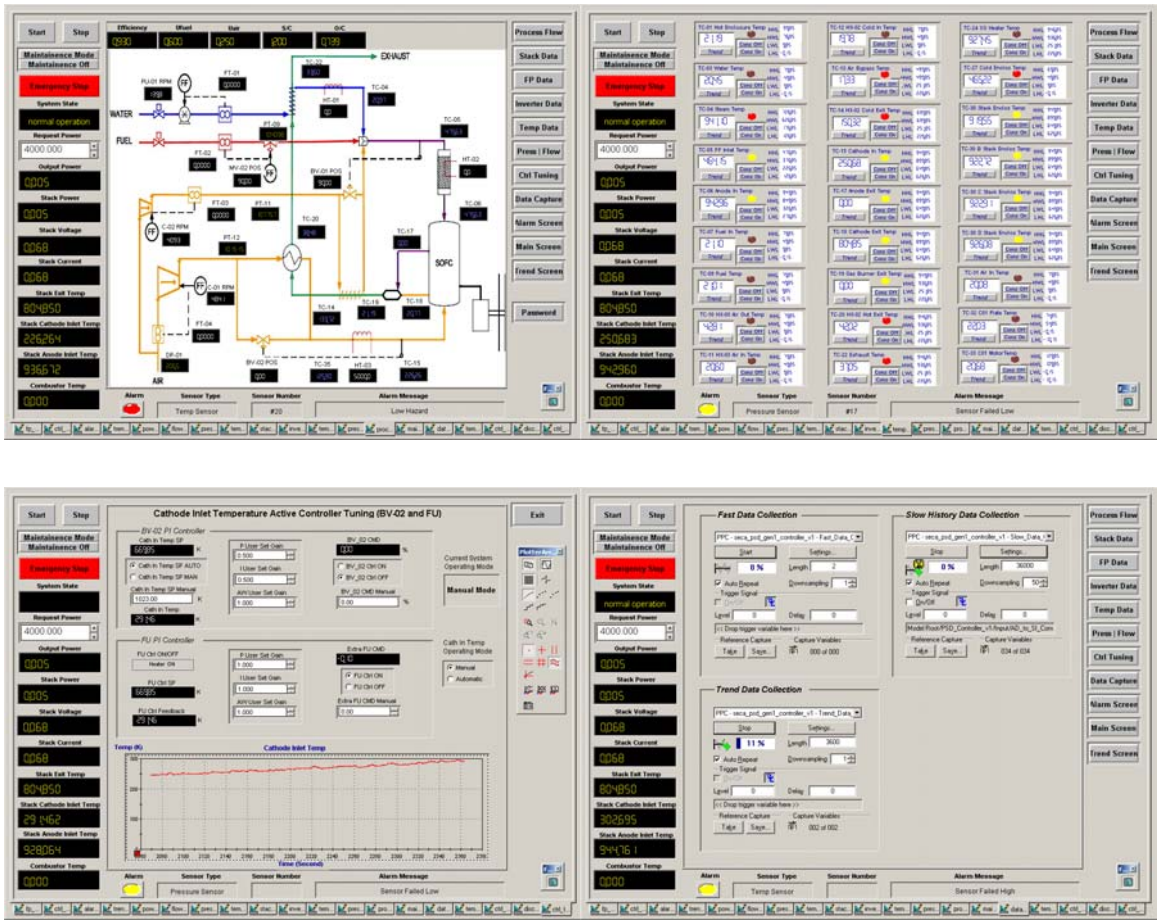

Figure 7.9. HMI sub-screens. Clockwise from the upper left: - process diagram, temperature sensors, controller tuning, and data capture.

7.2.2.3 Software Implementation

The implementation of the control software followed an integrated procedure involving both the dSPACE® Real-time Interface and Matlab/Simulink® Real Time Workshop®. With Real Time Workshop®, the Matlab/Simulink® code was converted to C code. It was then compiled and linked as an executable application for the dSPACE® system. The linked application then was downloaded to the dSPACE® system through ControlDesk®.

Key requirements for the control software are that it executes in real-time and is robust. Testing with all of the input A/D data, BIT check, supervisory controls, active controls, and output D/A showed that the software executes with significant margin to the software update rate.

To verify the robustness of the real-time control software prior to integrated prototype system testing, a series of evaluations were performed:

- Continuously ran the real-time control software for 40 hours with constant A/D data. All the process and subsystem diagrams with variable displays were verified to function correctly. All sensor-monitoring instruments ran

well. Instantaneous alarm display and alarm history were tested using a sequence of pseudo alarm messages. Password protection was validated. Data capture was verified and the projected data storage space for 1500-hour operation was calculated. Real-time data and historical data plotting were tested with constant data.

- Investigate the control system behavior by loading, stopping and reloading the application. The control system execution performance was compared and verified for consistency. All data displays were repeatedly tested and the captured data and associated time stamp were validated.
- Several failure mode investigations were performed. The controller was suddenly switched off to simulate an unexpected power loss. The data was verified to be continuously transmitting to the host PC. All data sent before the power was lost was safely stored in the host PC. Another scenario was to simulate an unexpected power loss of the host PC. In this case, the application kept running on the dSPACE® system with the most recently downloaded parameters. After recovering the power of the host PC, all data before the power outage was confirmed to be safely stored on the controller's hard drive.

7.2.3 Sensors & Actuators Identification

The control system requires sensors and actuators to measure and enact system requirements. Sensors include flowmeters, thermocouples, and pressure transducers. Actuators include valves, both manual and motorized, regulators, and fluid delivery components.

7.3 CONTROL SYSTEM INTEGRATION AND VALIDATION

The control system validation and integration process reduces the risk to the system components as the system is integrated. First, the controller and control software undergo significant stand-alone testing to verify the software and the basic functionality of the code before they are used with hardware in the system. Hardware testing is conducted to verify individual component operation and performance and provides the information needed to further tune the control strategy. Subsystem tests are conducted to verify subsystem operation and performance and provide additional information required to further tune the control strategy. Cold system tests are conducted with all components in the system with the exception of the fuel processor and the SOFC stacks to verify the basic control system functions and operation of the electrical system. Hot system tests with fuel are conducted with the addition of the fuel processor to further verify the control system and to tune the various controller loops. The hot tests are critical to assuring that the control system and other components in the system function properly and therefore minimize the risk to the SOFC stacks when they are introduced to the system. The SOFC integration testing can be conducted with the full set of SOFC stacks or with some subset of the SOFC

stack assembly. These integrated tests are the final verification of the control system, cell monitoring, power electronics, and control loops. Once SOFC integration testing is complete, the system is ready to go through its prescribed test plan. Ideally the integration steps are serial, but generally are iterative and can include parallel testing activities.

7.3.1 Software Testing

As previously mentioned, the control software was first developed in the Matlab/Simulink® environment with a detailed dynamic model of the entire prototype system. The control software was then implemented using dSPACE® hardware and software, which facilitates rapid controller prototyping to simplify software changes and optimization. This dynamic development environment allowed designs to first be validated in the simulation environment prior hardware implementation. Likewise, data generated in the laboratory was then quickly fed back to the simulation environment for further improvement of the dynamic system model and control software.

To ensure control system performance, robustness and reliability, a detailed test plan was developed and implemented. The testing of the control system concentrated on two areas: software evaluation and integration of the software with system hardware. The overall test procedure is depicted graphically in Figure 7.10 and the details are discussed in the following subsections.

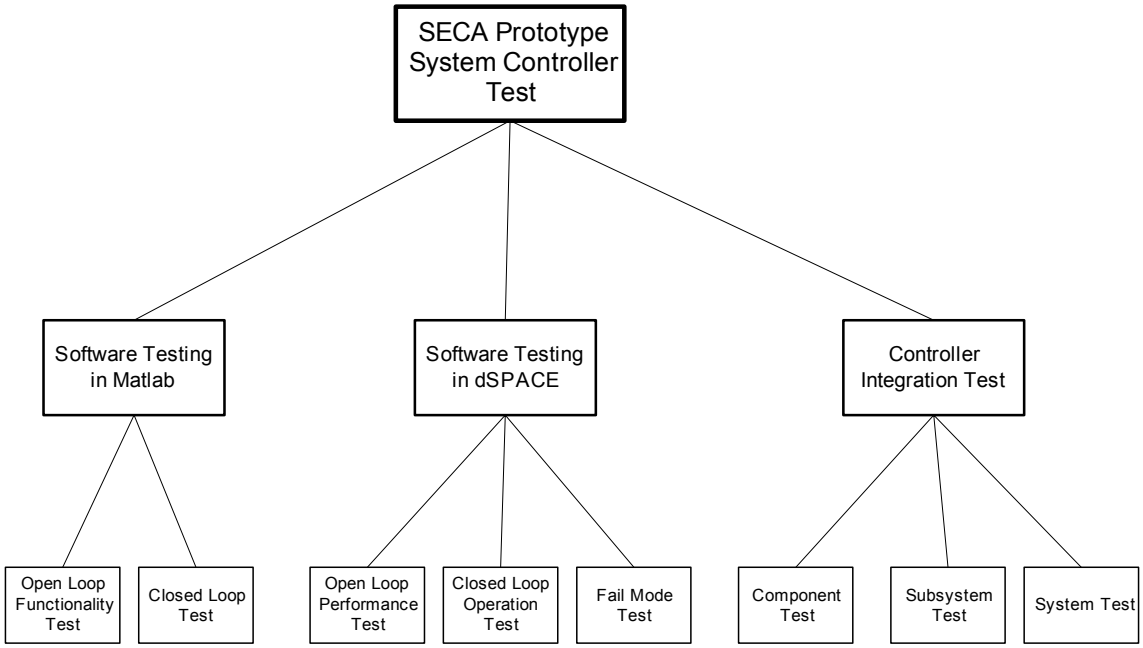

Figure 7.10. Control system test procedure.

Software testing in the Matlab/Simulink® environment was used to prove the effectiveness of the algorithms including input processing, fault detection,

event-driven settings, and control actions. Also, the interactions between different modules, events, and variables were validated. The first step was open loop functionality testing that was used to verify the performance of each control module.

All of the software modules were tested and operated as expected. The open loop functionality tests improved the confidence in the robustness of the algorithms and code, allowing the test to move on to closed loops testing. The closed loop test was comprised of normal and fault detection cases. The normal case of the evaluation covers start-up, normal operation, and shutdown scenarios. The fault detection case test is used to verify the Built-In-Test (BIT) codes. Each input variable of the controller is assigned different warning and hazard limits. During the test, different values are sent to each controller input and the warning and hazard indications confirmed.

Once the software was successfully tested in the Matlab/Simulink® environment, the code was then transferred to the dSPACE® real time environment for further evaluation. This study began with an open loop performance test of the real time version of the control code. This test is used to confirm that control code can meet real time requirements of executing all of the required calculations and functions within the specified frame rate for the software. Within the SOFC system, different reaction requirements exist for different process variables. The fastest time scale in the system concerns the interaction between current and voltage in the electrochemistry of the SOFC stack. This helps determine the upper limit that the real time control code must operate within. During testing, it was confirmed that the controller is able to finish all computations within this limit in the dSPACE® environment. The second evaluation conducted in dSPACE® environment was a closed loop operation test. In this study, two dSPACE® systems were used. The real time version of the control software was loaded onto one and a simplified dynamic system model of the system (referred to as a plant simulator) was downloaded to another. The controller and simulator were connected through analog input/output modules. The test procedure was the same as the closed loop test in Matlab/Simulink® environment noted above. In this testing, the performance of the real time code was validated. Failure mode tests conducted in dSPACE® environment were used to confirm the robustness of the controller to loss of power. This verified that the near-continuous data archiving of the controller assured that no data was lost during an unexpected power outage. In addition, no degradation of code functionality was observed after power was restored to the controller.

7.3.2 Control System Hardware & Software Integration

After the successful control software testing, the software was then integrated with the control hardware in the system. The overall control system includes the system controller, signal-conditioning module, and sensors measuring temperature, pressure, and flow rate, as well as actuators such as valves and blowers (Figure 7.11).

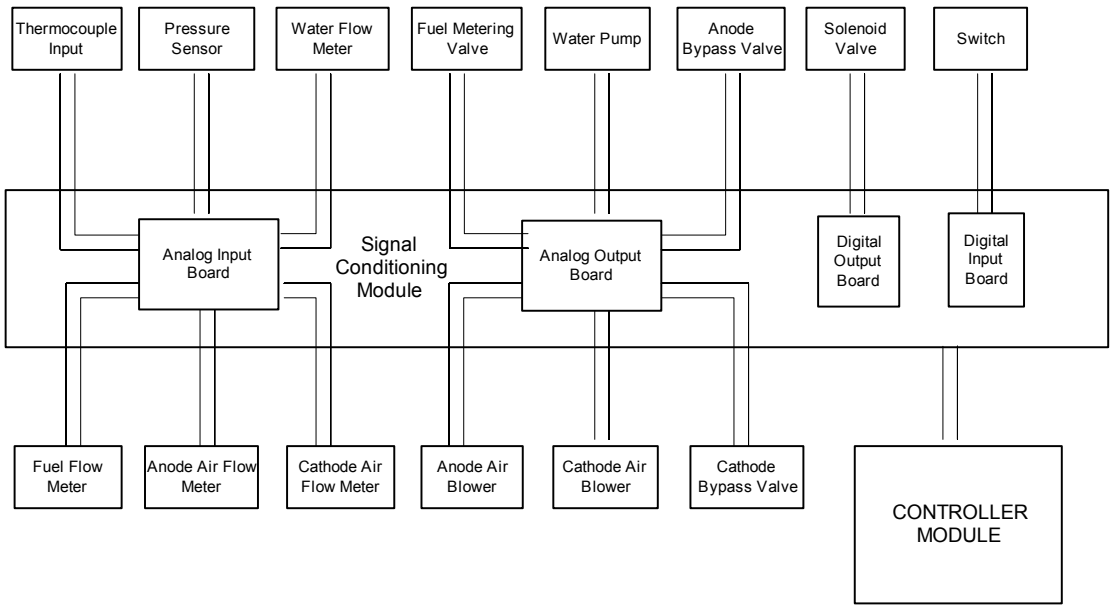

Figure 7.11. Control system diagram.

As mentioned earlier in this report, the system controller in dSPACE® hardware includes process board, analog input/output boards, digital input/output boards, and a communication board (Figure 7.12a). The signal conditioning module (Figure 7.12b) includes five 5B-01 16-channel panels that accept any of the 5B Series isolated signal conditioning blocks. Four 5B-01 panels are assigned to accept analog inputs. Different 5B signal conditioning blocks are selected to convert sensor signals to the appropriate voltage signals for the controller to read. One 5B-01 panel is designated to send out analog outputs to the various system actuators. Voltage outputs from the system controller are converted by appropriate 5B modules to the various signal types needed for actuators such as valves and blowers.

a) b)

Figure 7.12. System controller (a) and signal conditioning module (b).

After establishing connections from the controller and signal conditioning modules to sensors and actuators, component and subsystem tests were conducted. In the open loop component tests, electrical connections from controller to component, component hardware functionality, and component operability were verified for all items noted above.

Following the successful open loop component tests, each reactant delivery subsystem was tested to validate the actuator performance and dynamic characteristics. Based on the test results, it was concluded that each delivery subsystem met the performance and efficiency design requirements. The operation capability of each delivery subsystem was also verified.

7.3.3 Data Acquisition System

Development of the stand-alone data acquisition (DAQ) system was accomplished separately. The DAQ system is tasked with monitoring and recording individual cell voltages along with all other system sensor readings as a backup for the main system controller. The DAQ system also transmits the individual cell voltages to the controller for monitoring and corrective action. DAQ software includes the following modules:

- Controller data receiving and transmission module
- Controller data logging module
- Agilent® data receiving module
- DAQ data analysis module
- DAQ data logging module
- Coordinating module
- Global data structure

The DAQ system is comprised of six multiplexing data acquisition units and one monitoring computer. Since the SECA prototype system has four SOFC stacks, one unit is assigned to read all cell voltages from one stack. An additional two units are used to receive temperature and pressure inputs. The DAQ system graphical interface (Figure 7.13) provides various views to look at the performance of the system and controller. The DAQ software was developed in the LabView's graphical software development environment (Figure 7.14).

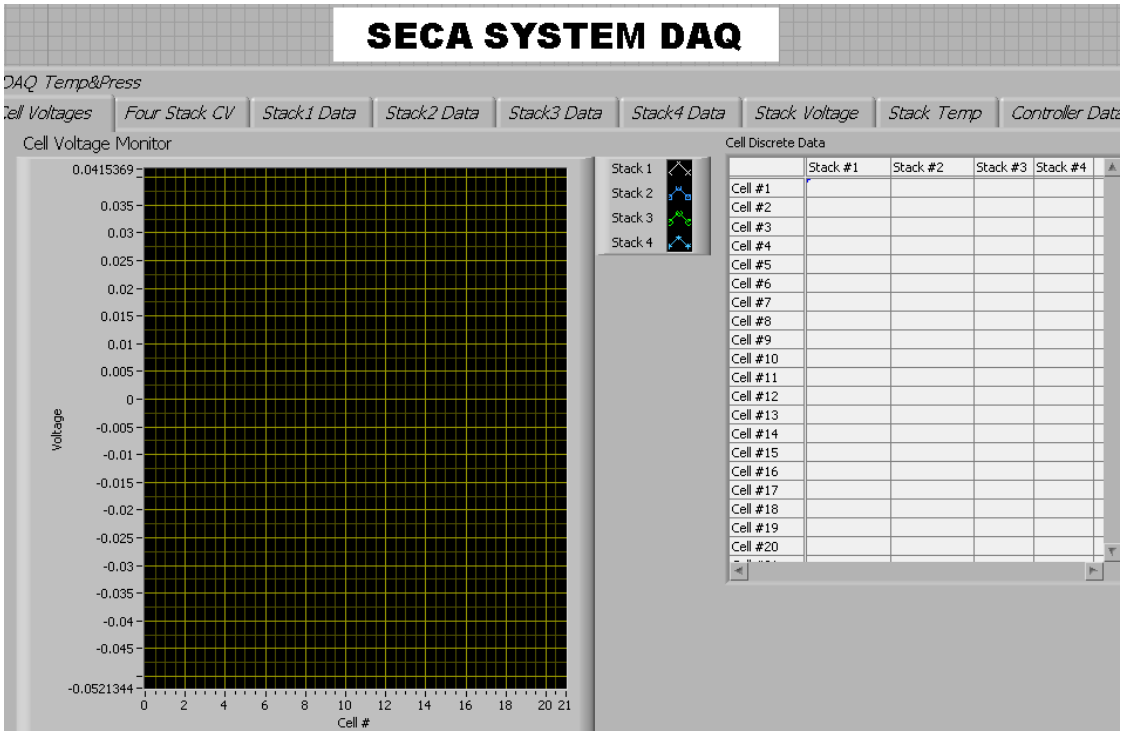

Figure 7.13. DAQ Interface.

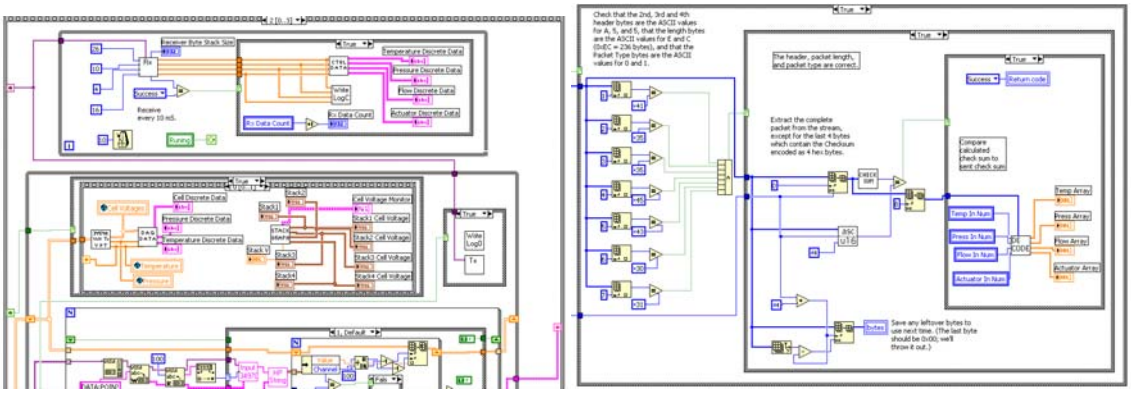

Figure 7.14. DAQ modules: coordinate module (left) controller data receiving module (right).

8 THERMAL MANAGEMENT SUBSYSTEM

The thermal management subsystem is defined as those components downstream of the stack (i.e. burner & heat exchangers) whose primary tasks are to; 1) react any remaining combustibles in the anode exhaust and, 2) to preheat the various streams that eventually find their way to the stack inlet (anode & cathode inlets).

Figure 8.1, highlights (in red) components that make up the thermal management subsystem. The primary components of the system include a combustor, cathode air preheater, steam generator, fuel processor steam superheater, and fuel processor air preheater. The combustor can be either of a catalytic-type or a more conventional, diffusion-type combustor. The cathode air preheater is a very compact, two-stream, plate-fin heat exchanger. The steam generator consists of a serpentine tube placed in the system exhaust duct. Additional superheating of the steam as well as preheating of air for delivery to the fuel processor is provided by running both of these delivery lines alongside the hot, combustor exhaust gas line. These functions are designated as SH (for superheat) and PH (for air preheat) in Figure 8.1. A discussion of the development effort for each of these major components will be presented in the following subsections.

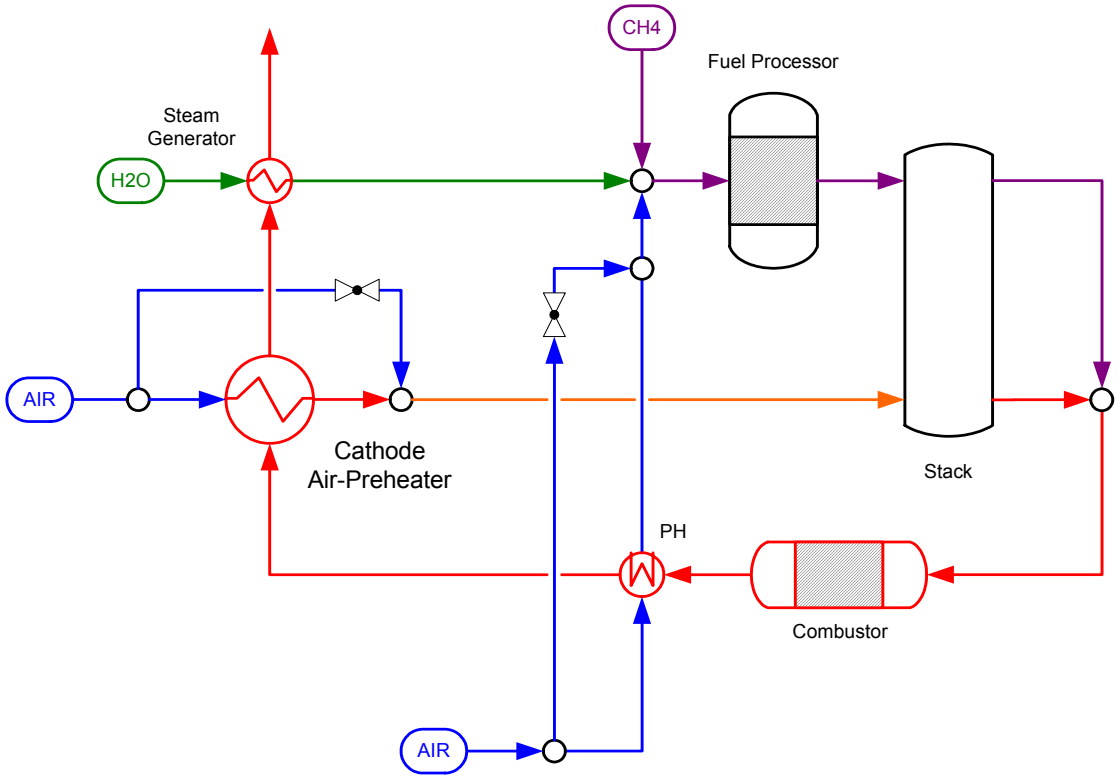

Figure 8.1 Simplified system schematic of thermal management system.

8.1 COMBUSTOR DEVELOPMENT

Combustor development activities focused on determining system design considerations necessary to operate either a catalytic-type burner or a more conventional, diffusion-type burner. The operating conditions that either type of burner would be subjected to is quite unique. For instance, either burner will be expected to operate over a wide range of fuel and oxidant flows; from moderately lean to extremely lean mixtures. Flowrates for each stream may vary by as much

as ten-fold. Operating temperatures are expected to be very high (especially at low stack fuel utilization), with little or no available supplementary cooling air (see Figure 8.2). Furthermore, pressure drop must be kept low, so as to not adversely effect air delivery power requirements and, subsequently, net system efficiency. Because of the uniqueness of this application, investigations into both combustor options were pursued.

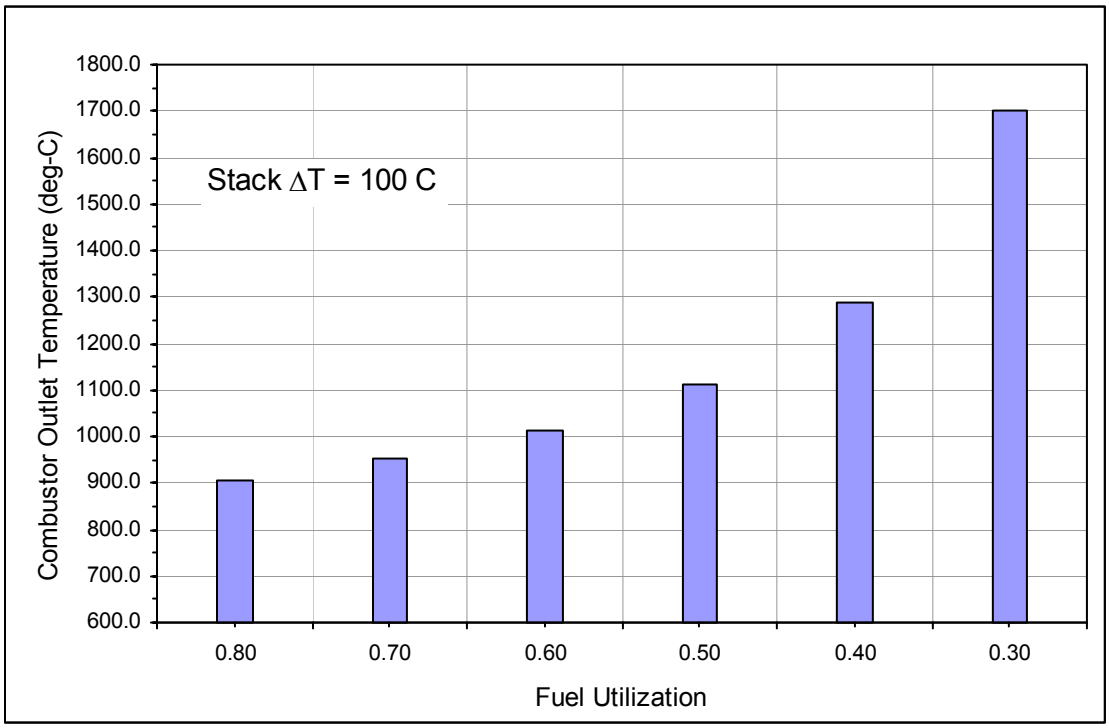

Figure 8.2 Combustor outlet temperature as a function of fuel utilization.

8.1.1 Catatalytic Combustor

Catalytic combustion provides both a number of advantages and disadvantages for use in a SOFC system. One of the primary advantages over a conventional, diffusion-type combustor is the “lack” of a flame and the associated instabilities that may accompany “flame” combustion. Another advantage is the near complete combustion of carbon monoxide (CO) that is found in anode tail-gas. Finally, a fully catalytic approach is the simplest strategy to implement.

Disadvantages of a catalytic approach include the limits imposed on surface temperature and the potential for autoiginition due to mixing of the anode and cathode exhaust streams prior to entering the catalyst bed. High catalyst surface temperatures may lead to sintering and/or vaporization of the catalyst as well as to thermal shock fracture of ceramic supports. Autoignition of the mixture prior to entering the catalyst bed is of concern since it is an “uncontrolled” combustion process. The uncontrolled nature of the combustion process could

lead to localized hot spots within the delivery ducting, with the potential for damaging the pipe wall if appropriate design measures are not taken.

8.1.2 Conventional Turbulent-Diffusion Combustor

A parallel combustor development task was to determine the operational feasibility and subsequent preliminary design of a more conventional, turbulent-diffusion type of combustor. Combustors of this type are commonly used in gas turbines and may more appropriately be referred to as a tubular or can type combustors. A simplified sketch showing basic details of a "typical" combustor is shown in Figure 8.3.

Four "zones" can be distinguished in the combustor; diffuser, primary, secondary, and dilution. The diffuser zone is used to reduce velocity to a value at which combustor pressure loss is tolerable, and to recover as much dynamic pressure as possible. The primary zone mixes the fuel and air, stabilizes the flame and provides sufficient time, temperature, and turbulence to achieve the majority of the combustion within a limited space. The secondary zone introduces additional air to allow unburned fuel oxidation and recombination reactions take place. The dilution zone serves to admit the remaining air and provide an outlet stream. The diffuser zone would be located upstream of the fuel and primary injection ports and is not shown in Figure 8.3.

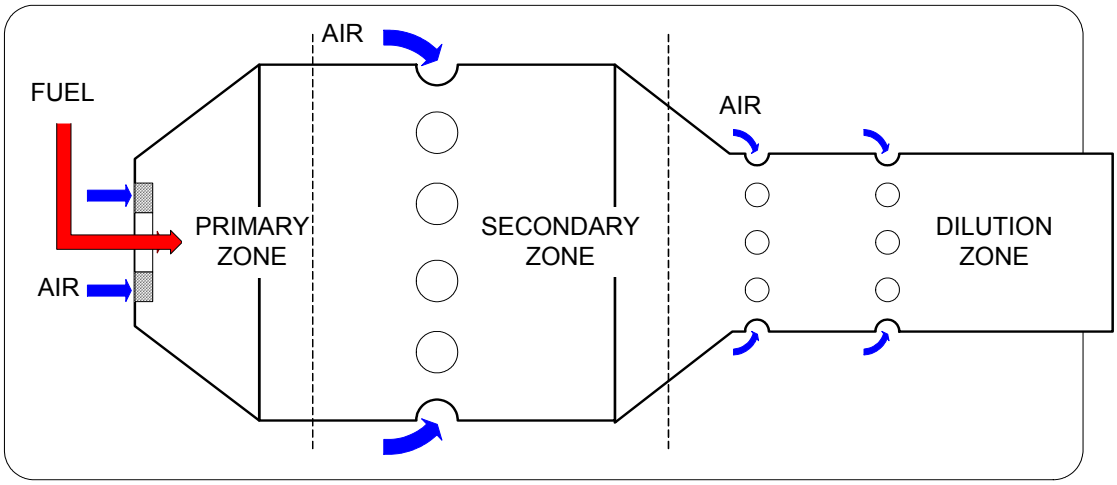

Figure 8.3 Simplified sketch of typical combustor.

For the PSD, development of a successful combustor design represents quite a challenge since the combustor must meet the following criteria;

- Handle inlet/outlet gas stream temperatures in excess of 815°C (1500 ^{o}F),
- Operation at part-load conditions (i.e. reduced flowrates),
- Minimal pressure drop through the combustor

- Aggressively low cost targets
- Accommodate issues related to start-up and shut-down,
- Safety considerations.

Additionally, at start-up, very little fuel will be consumed in the fuel cell. Therefore, the combustor must be able to burn a fuel mixture with significantly higher heat content during these conditions.

The most significant challenge for this combustor design is the lack of "cold" cooling air, such as may be found in a gas-turbine application. The combustion airflow for this burner is provided by the cathode gas exhaust stream, which is on the order of 800-850^{o}C. This is far higher than might be seen in a gas-turbine application, where the airflow temperatures may be on the order of 300 ^{o}C to 400 ^{o}C.

8.1.3 Combustor Down-select

The analysis completed showed that either combustor option represents a viable approach to tail-gas combustion. Based on the difficulties encountered with designing a suitable diffusion flame combustor to meet the wide range of operating conditions and the availability of a catalytic burner that could marginally meet the operability requirements on fuel utilization, it was determined that the catalytic approach would be lower risk for the prototype system. In addition to lower technical and program risk, the purchase of an existing catalytic combustor was an order of magnitude less expensive than completing the development of the diffusion flame combustor. The integration of a catalytic burner into the prototype design was less challenging than a diffusion type burner. It was also felt that the more conventional diffusion-type burner would require a more extensive development effort to fully meet the performance requirements of the system.

The issue of catalyst temperature limits was addressed by selection of a suitable catalyst material. The second issue regarding potential for autoignition prior to entering the catalyst bed has been addressed by careful design of a mixing chamber prior to entering the combustor.

8.2 CATHODE AIR PREHEATER

Activities involved with the cathode air preheater were focused on three areas; 1) determination of heat exchanger sizing methodology to accommodate off-design operation with bypass lines, 2) the procurement of the required heat exchanger, and 3) the characterization of the cathode air preheater performance for inclusion into the Aspen system model.

8.2.1 Cathode Air Preheater Sizing Methodology with Bypass Line

One of the major challenges associated with cathode air preheater development was the determination of a methodology to properly size the heat exchanger when a cold-air bypass line is used for temperature control. To facilitate this work, a simplified system was modeled using Aspen Plus. A schematic of the simplified model is shown in Figure 8.4.

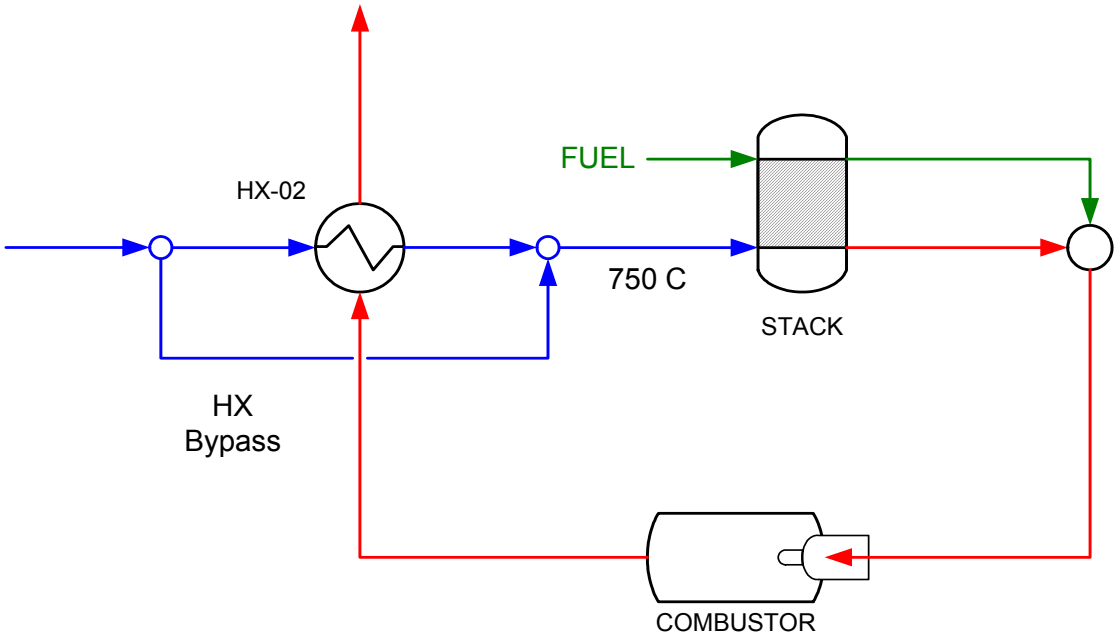

Figure 8.4 Simplified system schematic to determine conditions for HX Sizing.

For this study, the cathode air preheater (HX-02) was sized at a number of different conditions corresponding to different power levels and different HX bypass ratios. Results showing relative HX size are shown below in Figure 8.5. The designations HX-100, HX-90, HX-80, etc. correspond to system design point power levels of 100%, 90%, 80%, etc., respectively.

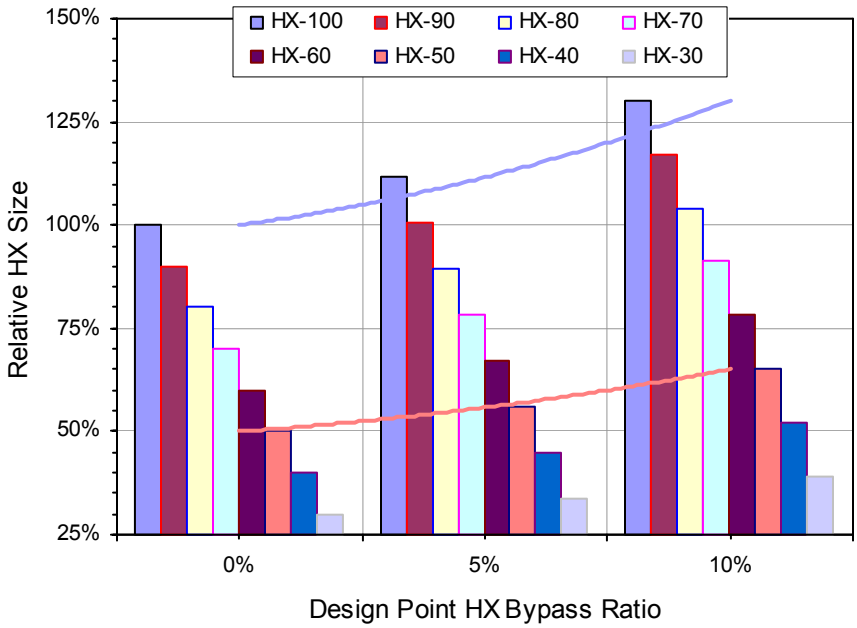

Figure 8.5 Relative HX size as a function of design point.

The reference area used in this plot was for a HX sized at conditions corresponding to 100% net system power, 80% fuel utilization, sufficient cathode air to provide an appropriate temperature rise across the stack, and without the use of HX bypass. If the HX is sized at conditions corresponding to lower power levels, the relative size of the HX decreases due to decreased heat duty requirements. If the HX is sized at conditions corresponding to higher levels of bypass flow, the relative HX size increases due to the reduction in mean temperature difference across the HX.

The selection of the proper design point is essential if temperature control of the cathode inlet gas stream is expected over the widest range of operating conditions. Figure 8.6 shows the net effect on cathode inlet temperature as one moves away from the design point for 4 separately sized HXs. The design point for each heat exchanger is highlighted with larger symbols. The sizing conditions for each HX correspond to 80% fuel utilization and net system power levels of 100%, 80%, 60%, and 40%. For a HX sized at 100% power (without the use of bypass air, e.g. HX-100-0), the cathode air preheater will not be able to maintain the cathode inlet temperatures as system power is decreased. Alternately, if the HX is sized at 40% power (without the use of bypass air, e.g. HX-40-0), cathode inlet temperatures will exceed the required cathode inlet temperature as power level is increased. Although such temperatures can be moderated by initiating cold air bypass, the increase in pressure drop as one moves from low to high power is significant. This is shown in Figure 8.7 a & b, which plot the percentage of bypass air needed to meet the cathode inlet air temperature requirement as well as the pressure drop across the heat exchanger.

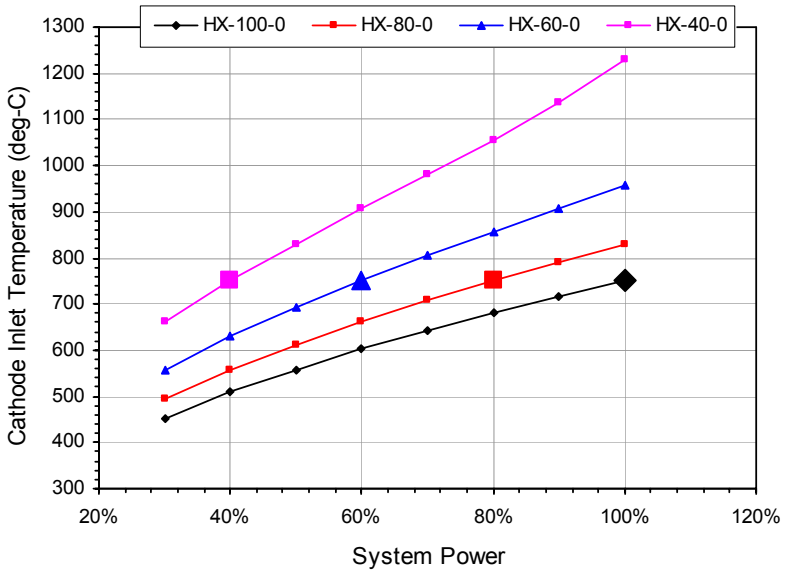

Figure 8.6 Cathode air preheater performance at “off-design” conditions.

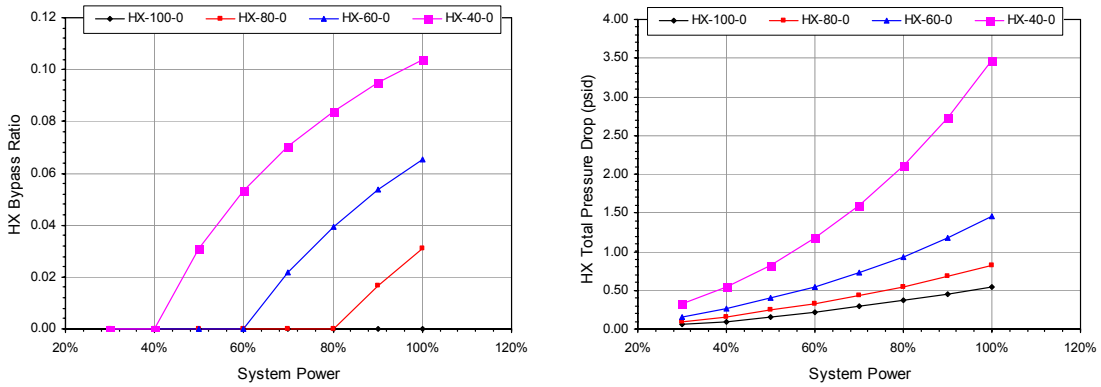

Figure 8.7 a) Bypass air requirements; b) HX total pressure drop.

It is noted that temperature control using bypass air can only be used for conditions in Figure 8.6 where the cathode air preheat temperatures have the potential for exceeding 750 ^{o}C. Loss of temperature control occurs when the bypass air ratios fall to zero.

As is generally the case in system design studies, compromises are made in selecting the design point. To this end, an operating condition corresponding to 80% net system power, with 10% bypass air was chosen for sizing the cathode air preheater. The off-design performance curve for this HX (with constant 10% bypass airflow) is shown in red below (HX-80-10). Using this HX, power levels can be increased or decreased by increasing or decreasing the amount of bypass air flow. This is demonstrated by the curves shown in Figure 8.8 (highlighted in red).

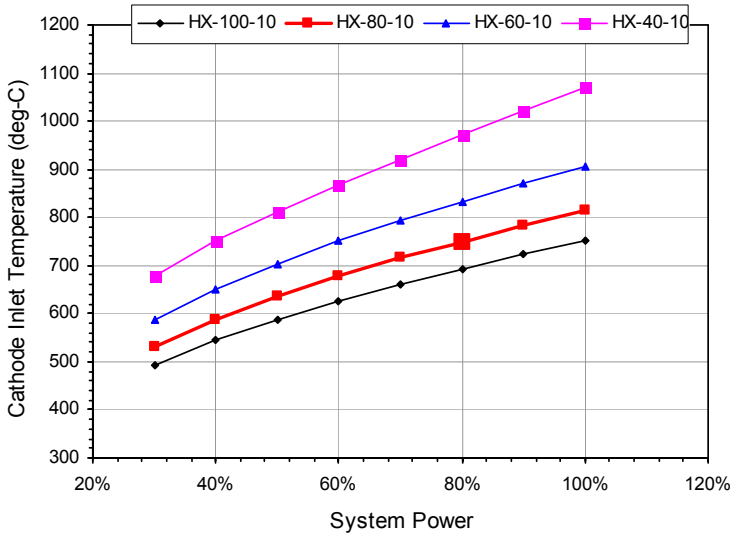

Figure 8.8 Performance at "off-design" conditions with 10% bypass flow.

The practical lower limit of system operation before losing cathode supply air temperature control corresponds to 30% power. Pressure drop requirements using a HX designed at this condition are reasonable over the entire range of expected operation (Figure 8.9).

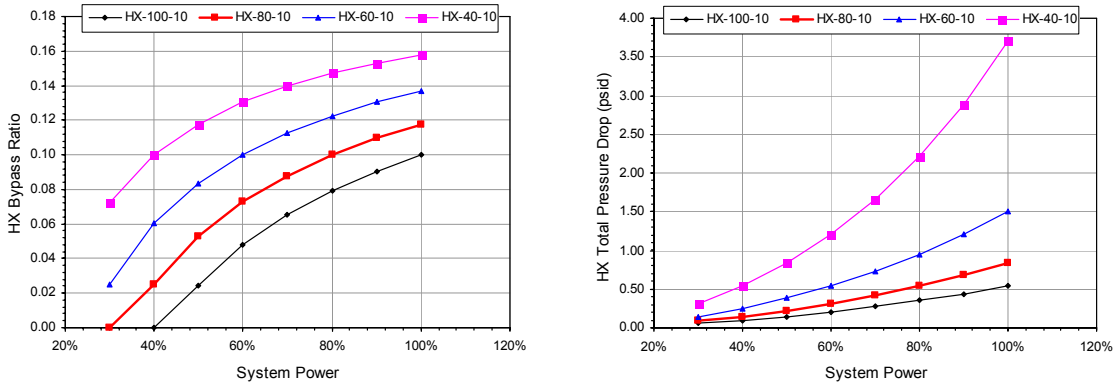

Figure 8.9 Bypass air requirements and total HX pressure drop.

8.2.2 Cathode Air Preheater Procurement

A broad search of high temperature heat exchangers was conducted and a vendor was selected to provide this component. An Inconel 600 plate-fin heat exchanger was designed to meet the problem statement for cathode air preheating. This design was also considered in both Inconel 600 and Inconel 600/SS 347 combination. This dual alloy combination proves cost effective at very high volumes, however, additional fabrication costs outweigh the material savings at low volumes.

Alternative heat exchanger options were evaluated over the course of Phase I, but none of them were cost-effective or reliable enough to displace the compact heat exchanger that was selected. These alternatives will be reconsidered in Phase II as a more mature package design is developed for the system, which could drastically change the requirements for the various heat exchangers in the system.

8.2.3 Performance Characterization

The vendor provided pressure drop and heat transfer performance predictions at a number of different operating conditions. A simple Aspen model was set up to allow correlation of the performance predictions into a form suitable for use within Aspen. The correlated heat exchanger performance model was later integrated into the Aspen system model and serves as the basis for off-design system performance predictions.

8.3 STEAM GENERATOR DESIGN AND DEVELOPMENT

The steam generator design is composed of a compact cylindrical heat exchanger with a helically-coiled,finned-tube, placed in the annulus region of concentric pipes. Such a design is commonly used for recovering waste heat from diesel engine exhaust gases. The design utilizes full counter flow heat transfer for maximum effectiveness. Water will be introduced into the top of the unit and allowed to flow downhill across the hot heat exchanger tubing. The fins were included on the tubing to maximize the gas-side heat transfer surface area within the available space.

8.4 FUEL PROCESSOR AIR PREHEATER

Preheating of the air delivered to the fuel processor was accomplished by routing the air delivery line to a location near the hot exhaust lines from the stack. A simple analysis of the heat transfer rates needed to preheat the air show that the required tube lengths are minimal. The design is very simple and consists of of helically coiled, 3/8” tube, wrapped around the perimeter of the hot exhaust line.

9 ELECTRICAL SYSTEM

The electrical system development effort in Phase I is composed of system requirements development, electrical system design, system assembly, and system verification and operation.

The function of the electrical system is to provide all the power required by the system controller, sensors and actuators, data acquisition system, facility power interface, system operator, safety interlock, and the fuel cell stacks. The electrical system includes three main areas:

- Inverter
- Balance of plant electrical components
- System interfaces

The inverter is the power component that converts the DC power generated by the fuel cell stack to the AC power compatible with the facility power. The balance of plant (BOP) electrical subsystem includes all the electrical components required to provide the electrical power supplied to all system components, excitation power supplied to the instrumentation, command signals to actuators, signals from sensors, and the controller hardware. The system interfaces provide all the wiring, connectors, and necessary hardware to connect all the BOP components within the SECA system and the test facility interface.

9.1 INVERTER DEVELOPMENT

9.1.1 Inverter Requirements

The inverter was developed to have all the functionality required for generating power for residential use. A detailed inverter specification was developed. The following are the key requirements.

9.1.1.1 Operating Modes

The inverter is designed for grid parallel and stand-alone operation. The operational requirements for the two modes are described below. The design supports auto transition between operating modes such that the system can seamlessly switch from grid parallel mode and stand-alone modes. However, this function was not used during Phase 1 testing.

Grid Parallel Operation - Variable DC voltage from the SOFC is converted to a grid-synchronous AC voltage and frequency. Grid synchronization is performed and magnitude and phase of the converter current is controlled based on the controller's DC current commands. Grid Over/under voltage and frequency detection is provided.

Stand-Alone Operation - Variable DC voltage from the SOFC is converted to a constant AC voltage and frequency. A load current exceeding the rated output current causes an inverter shutdown and a retry strategy is used to reconnect. The system also includes a current limit mode to provide motor starting capability. This mode is realized by reducing the converter's output voltage. Transient and steady state over-current protection is provided.

9.1.1.2 Efficiency

The inverter shall meet the minimum efficiency requirements. Efficiency is calculated from DC power input to net AC power output. Inverter efficiencies as high as 94.5 % were measured at 80% to 100% of rated power.

9.1.1.3 Inverter Output Rating

Power:	7.5 kVA continuous
Power Factor:	0.8 lag to 0.8 lead
Nominal Voltage:	120V/240V single phase
Voltage regulation in SA mode:	+/-10% outside current limit mode
Voltage range in grid mode:	-20% to +15% of nominal
Nominal frequency:	60 Hz
Frequency range:	+/- 5% in grid mode
Frequency tolerance:	0.5 % in SA mode
Current/Voltage Quality:	according to standard IEEE 519-1992
DC injection:	<0.5% at continuous full load

9.1.1.4 Inverter Input Rating

The power source is a fuel cell stack delivering a DC voltage.

Voltage Range: 88 to 153 V

Current Range: 0 to 80 A

9.1.1.5 Inverter Protection

The inverter contains circuitry to detect and react to the following abnormal conditions that, if exceeded, may cause human harm or damage to internal/external equipment:

- Output over current
- Output over voltage
- Output under voltage
- Output short circuit fault
- Inverter over temperature
- AC over frequency
- AC under frequency
- DC contactor fail
- System overload
- AC contactor fail
- DC link under voltage
- DC link over voltage

In addition, the inverter shall include hardware/software built-in test to detect internal failures such as:

- Controller fault
- Communication fault
- Sensors fault

9.1.1.6 Output Interface

The output interface includes the contactor, the output transformer, and other protection devices based on the local utility requirements. The output contactor is a switch, which is used to connect the output of the line filter to the main output serving the loads. The contactor is able to handle 60 amps rms at 120 volts rms. The contactor also serves as the connection with the grid. The contactor is not used as a protection device, but solely as a disconnect. External protection is required for connection to loads and/or utility grid. The output transformer primarily provides isolation, but is also used to adjust the output voltage. The output transformer converts the inverter output voltage to the required site voltage.

9.1.1.7 Communication Interface

The inverter includes a RS-232 digital communication for control and monitoring by the system controller. The control/monitor interface includes the following data:

- System configuration data
- System calibration data
- DC current command
- Power factor command
- Fault data from Inverter
- Actual power output
- Actual current output
- AC Output voltage
- DC voltage
- DC link voltage
- DC current

9.1.2 Inverter Design and Vendor Selection

Over 100 inverter companies were reviewed during the inverter selection process and many of them were contacted to understand their technology and ability to supply inverters that met the specification. Several companies were provided with the inverter specification and asked to provide a quote for the

prototype unit. Based on efficiency, fuel cell experience, cost, and delivery time, the vendor was selected to provide the inverter for the SECA prototype system.

The vendor was able to meet the specification and delivered an extremely efficient (~94.5%) inverter since its design includes only a single stage inverter and a high efficiency transformer.

9.1.3 Inverter Integration and Testing

The inverter was tested extensively prior to being integrated with the SECA system. The methods and results of the testing are discussed below.

Efficiency testing was conducted at GE. The following equipment was used for the test:

- Sorensen DHP200-11 power supply
- YOKOGAWA WT2030 power analyzer
- PC with Labview
- Agilent 34970A data acquisition unit
- Load bank 0- 10K 1kW step min
- Small load bank 0 - 1K 100W step min
- Shunt resistor 100A-50mV
- Current transformer 250-5A.

The following data was measured and recorded for each test:

- DC Voltage (VDC)
- DC Current (IDC)
- DC Power (PDC)
- AC Voltage (VAC)
- AC Current (IAC)
- AC Power (PAC)
- AC Volts-Amps (VA AC)
- Battery Voltage (VBAT)
- Battery Current (IBAT)

Overall inverter efficiency was calculated as the total AC power output of the unit divided by the total DC power input. Efficiency curves were generated for multiple DC input voltages. Electronic data recording was also added and the setup was reconfigured to provide a more robust test environment. The inverter data acquisition and control console can be seen in Figure 9.1

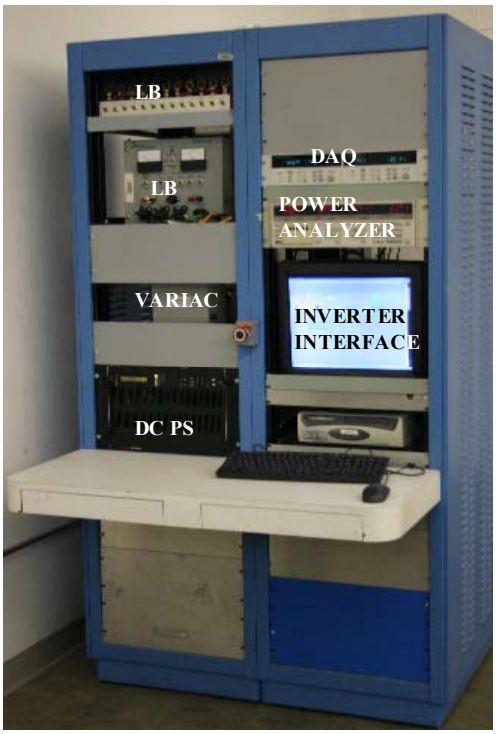

Figure 9.1 Inverter data acquisition and control console.

The inverter unit has undergone extensive testing at the HPGS facility. The following series of tests were conducted:

- Grid-connected performance testing
- Stand-alone performance testing
- Transient testing
- Fault testing

Each of these tests will be discussed in the following subsections.

9.1.3.1 Grid-Connected Performance Testing

The inverter grid-connected performance testing was conducted by setting the inverter in Grid Parallel Mode and commanding the output power in a 500 W step from 0 to 6500 W while keeping the DC voltage constant. Each step resulted in approximately 5A DC current increments. During each power sweep, the inverter limited the DC current to approximately 68A DC. Figure 9.2 shows the fuel cell voltage and current, the utility voltage and current, the overall inverter efficiency, the DC power, and the AC power, with respect to time. The grid voltage varied slightly during the test as function of output power due to AC line impedance. There was no noticeable efficiency difference due to this variation. The overall efficiency of the inverter in grid-connected mode as a function of output power is shown in Figure 9.3. Due to the topology of the

inverter, there was a slight drop in inverter efficiency as the DC voltage increased.

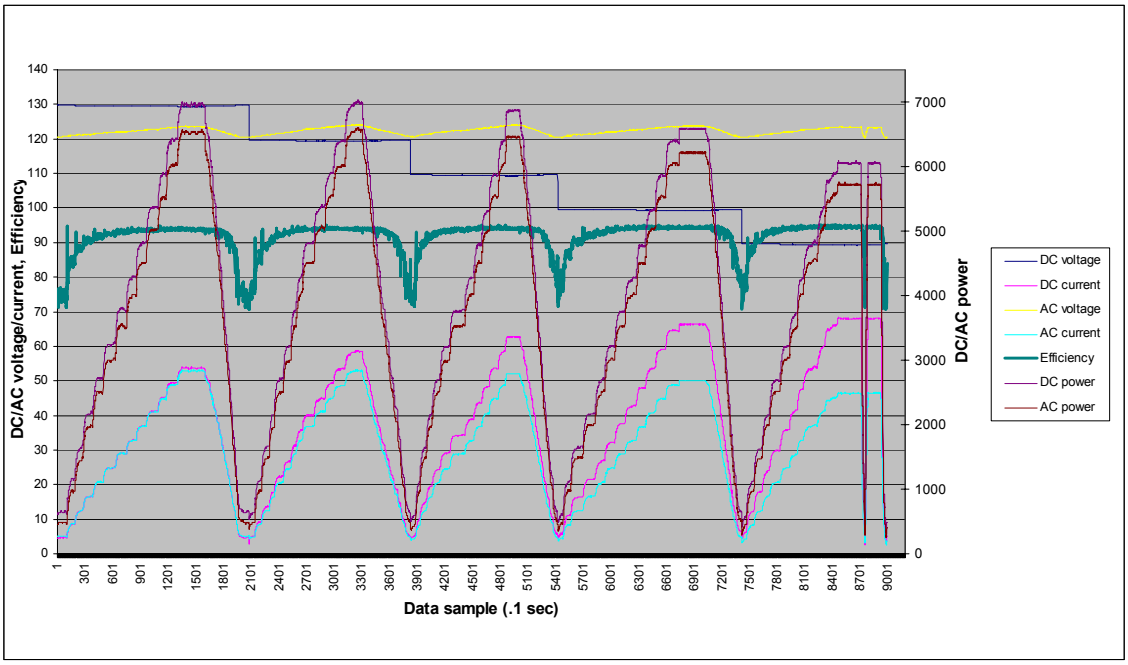

Figure 9.2 Grid-connected performance test data.

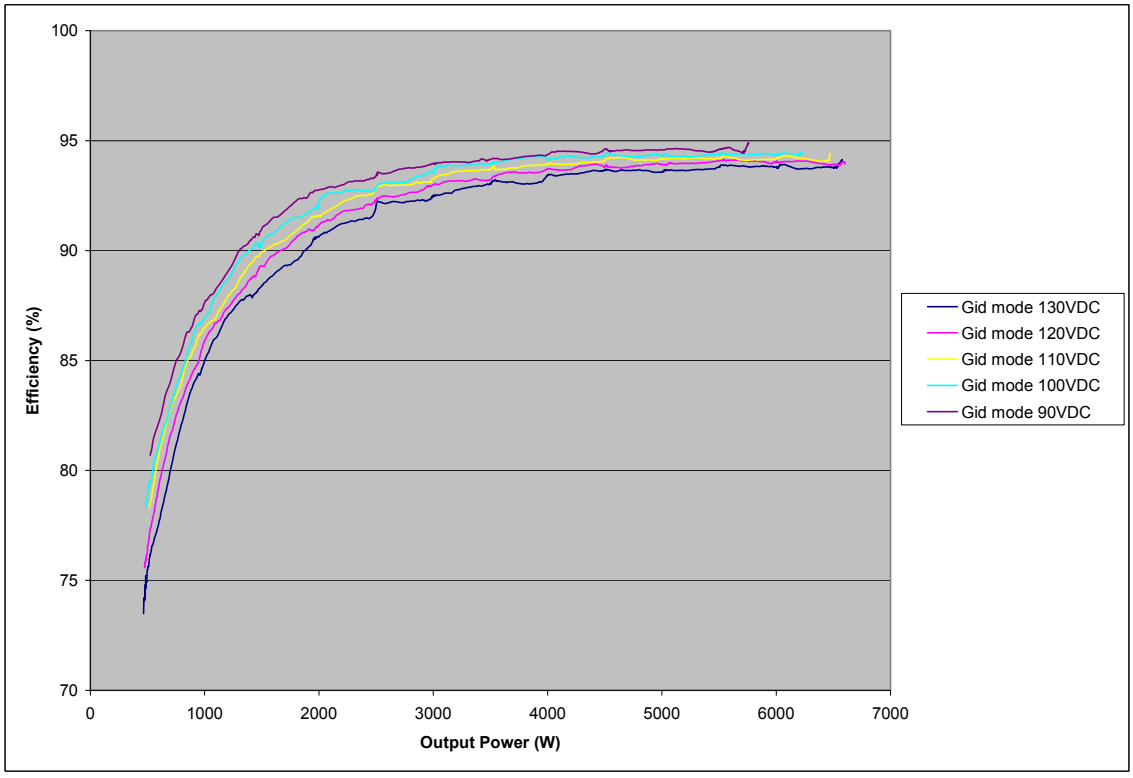

Figure 9.3 Grid-connected efficiency as a function of output power.

9.1.3.2 Stand-Alone Performance Testing

The inverter stand-alone performance testing was conducted by setting the system in Grid Independent Mode and applying the load using load banks. The load was commanded from 0 to 6500 W with each step resulting in approximately 5A DC current increment. The DC voltage remained constant for each of the power sweeps. The inverter responded to load change instantaneously by increasing or decreasing the output current to maintain the output voltage. Figure 9.4 shows the fuel cell voltage and current, the utility voltage and current, the overall inverter efficiency, the DC power, and the AC power, with respect to time. The grid voltage remained constant and therefore independent of output power. The overall efficiency of the inverter in stand-alone mode as a function of output power is shown in Figure 9.5. Similar to the grid-connected data, there was a slight drop in inverter efficiency as the DC voltage increased.

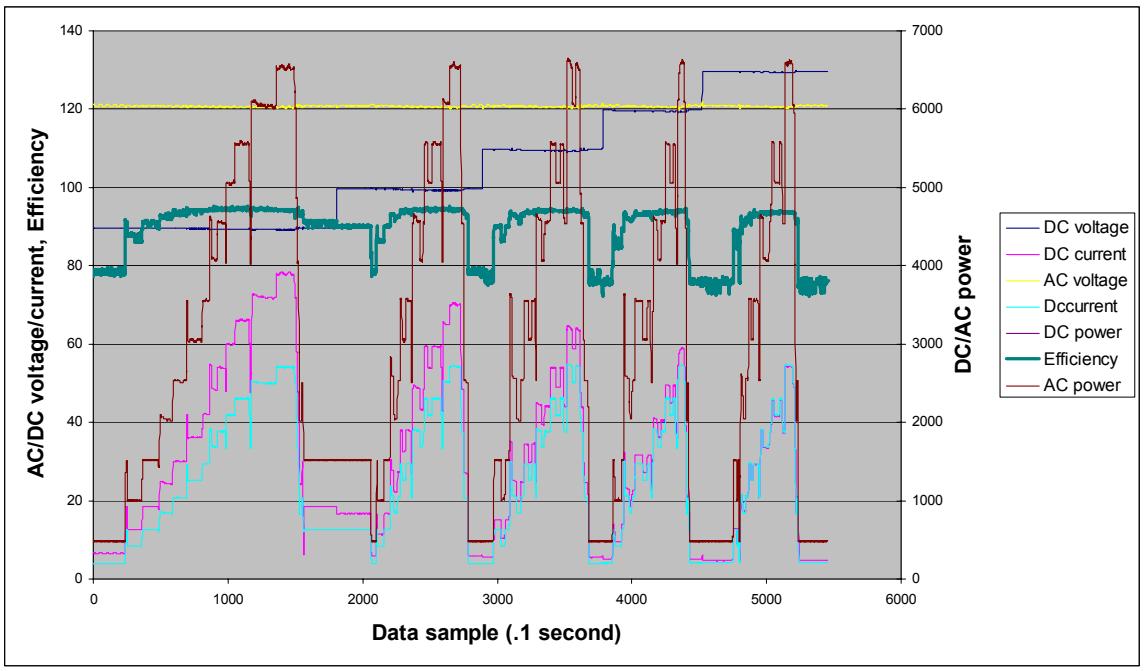

Figure 9.4 Stand-alone performance test data.

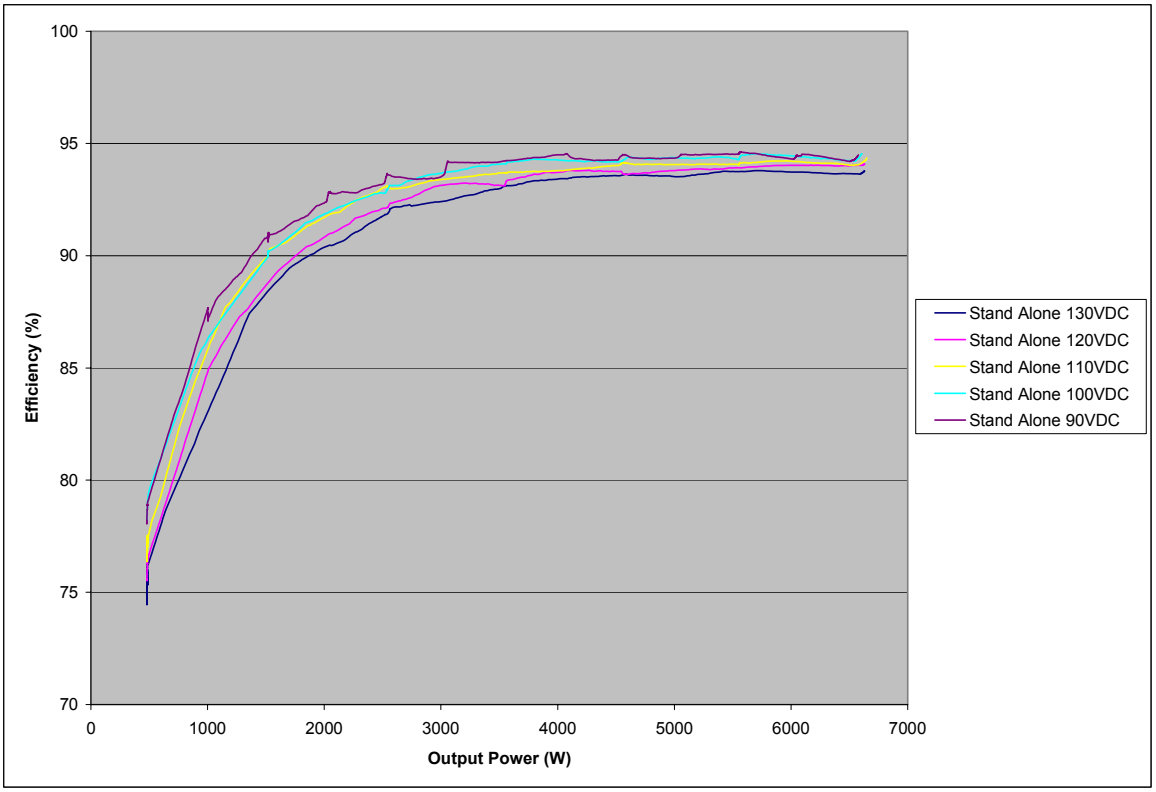

Figure 9.5 Stand-alone efficiency as a function of output power.

9.1.3.3 Inverter Dynamic Response

The dynamic response of the inverter was tested in both grid-connected and stand-alone modes. In Stand-Alone Mode, the inverter supplied the output current to maintain output voltage in response to load change. In Grid Connected Mode, the inverter ramped the current up to close the loop on the power command. Figure 9.6 shows the ramp rate of the inverter in grid-connected mode. The time for power to decrease from full power to 0 power was approximately 8 seconds and the time back to full power was approximately 4 seconds. These ramp rates were sufficient for the testing the prototype system.

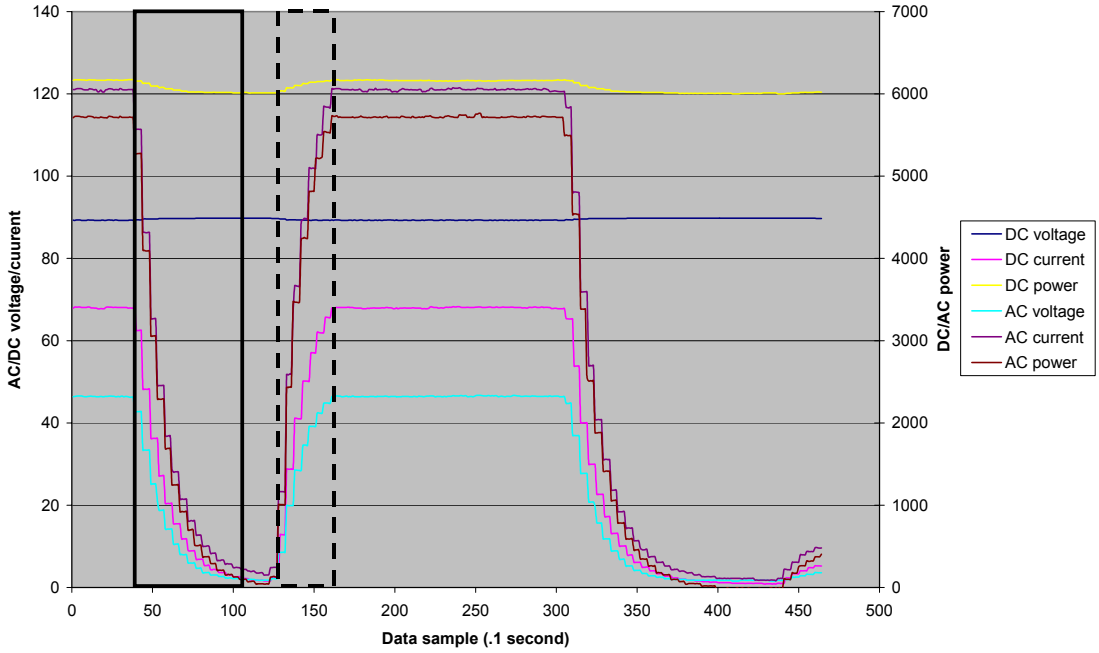

Figure 9.6 Dynamic response inverter data in grid-connected mode.

9.1.3.4 Fault Testing

Inverter fault testing was conducted to verify inverter protection functions. Utility voltage limit faults, fuel cell voltage limit faults, and communication faults were simulated. The inverter protection functions performed as expected.

9.1.3.5 Test Summary

The test data verified the performance and functionality of the inverter for the prototype system. The inverter performance achieved a peak efficiency of 94.5% consistent with the design expectation plotted in Figure 9.7 that shows both grid-connected and stand-alone efficiency as function of output power. There is no noticeable difference in efficiency between grid parallel and grid independent mode.

Figure 9.8 shows the efficiency of the inverter as function of DC current for various DC voltages. The data essentially collapses to a single curve. This shows that the inverter efficiency is primarily a function of DC current as was expected. The system performance model was therefore updated to reflect the data and is shown in Figure 9.9.

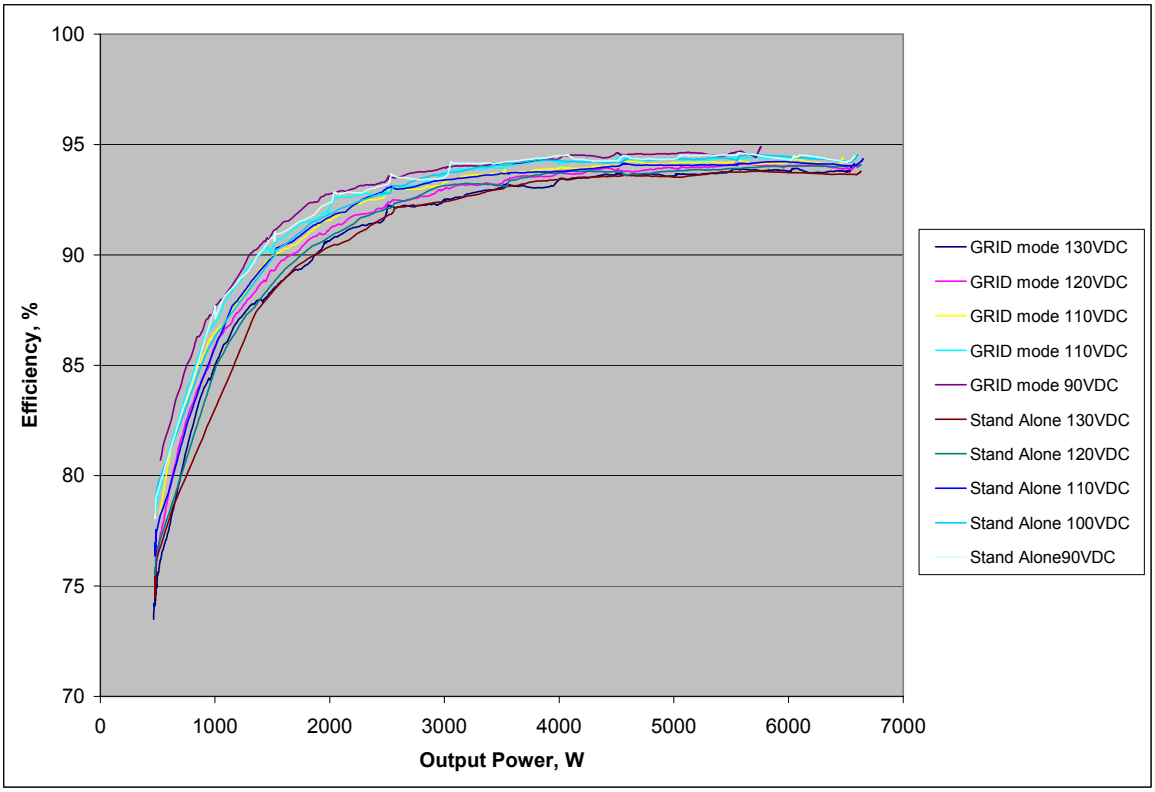

Figure 9.7 Efficiency for grid-connected (G) and stand-alone modes (S).

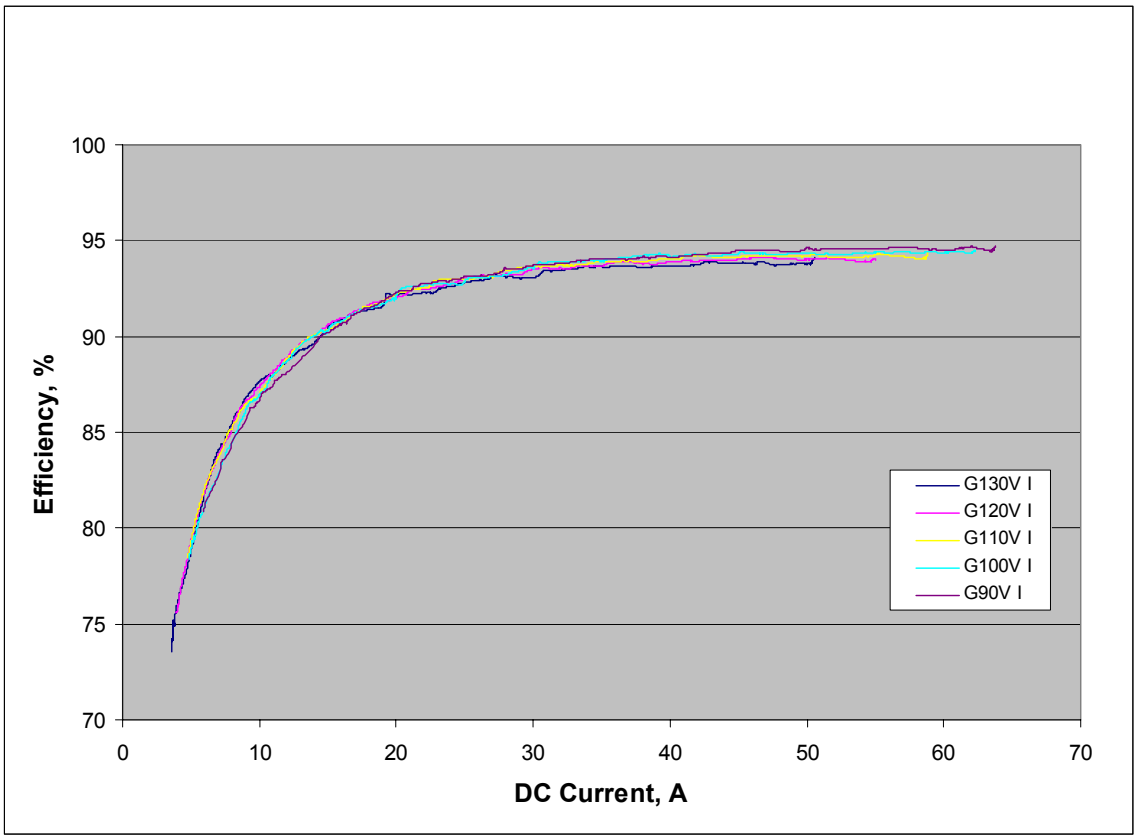

Figure 9.8 Efficiency as a function of DC current.

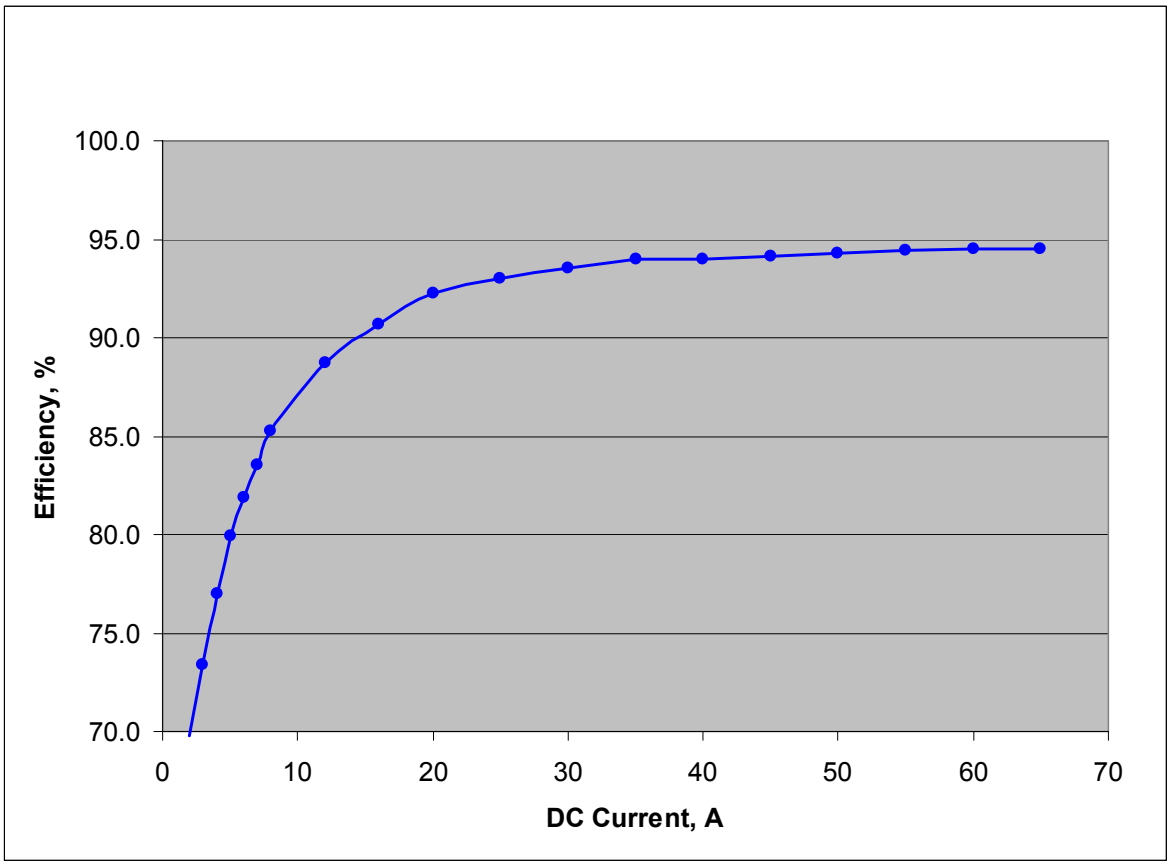

Figure 9.9 Inverter efficiency model for system analysis.

9.2 ELECTRICAL BALANCE OF PLANT (BOP) DEVELOPMENT

9.2.1 Electrical BOP Components Requirements

All components for BOP were designed to have 40000 hours MTBF. Critical components such as control power supplies were designed with fully redundant components to minimize single point failures in the system. All components were designed to ensure a fail-safe operation.

9.2.2 SECA BOP Components Design

The electrical system was designed to facilitate flexibility in support of the prototype testing. The electrical system was designed to maximize its robustness and to allow system design changes to be easily accommodated.

9.3 SYSTEM INTERFACE

The electrical system interface was designed to provide interfaces for the output interface, installation site I/O, and the system control interface. Separate connectors were used for high and low voltage wiring to minimize noise signals

and give maximum flexibility. The prototype system includes the following interfaces:

- Inverter output power
- Backup cathode heater power
- Backup cathode heater control interface
- Cathode heater power
- Cathode heater control interface
- DAQ/sensors interface
- A multi-channel data acquisition interface for CPM
- Stack output power interface
- DAQ/system controller digital interface
- Operator interface
- Manual backup controller interface
- Backup fuel flow controller interface
- Remote emergency power off (EPO)
- Data acquisition monitor interface
- Electronic load
- Site alarm interface

9.4 BOP COMPONENTS ASSEMBLY AND TESTING

During the design phase, testing was conducted to verify the parasite loads for the various components after they were installed in the prototype system to verify that they agreed with the design. The power requirements were measured with the pumps, blowers, and power supplies that were all run under worst-case conditions such as high backpressure and high flow rates on the blower. Based on the worst-case testing, the components all performed as expected. During the Phase I prototype testing, the actual parasite power was measured and the results were consistent with expectations.

10 PROTOTYPE ASSEMBLY

In order to demonstrate system performance as required in the Phase I program objectives, GE constructed a prototype system intended to be flexible and robust to accommodate design changes throughout the entire system integration process. The assembly process began with specifications for various components flowing down from the systems and controls teams via scorecards

so that components could be sourced. A computer model and drawing package of the system geometry was also used to guide construction. Although many items were standard components, a number were developed, modified or designed specifically for the project. Details of key balance-of-plant (BOP) components and the system construction process are outlined below.

10.1 STACK ENCLOSURE

The component with the biggest impact in the system package design was the stack enclosure. This is due to the fact that it needed to be sized to house the 4 40-cell stacks, which represent a large footprint. The remaining balance-of-plant components have been positioned to feed and receive process connections from it. In addition to accommodating the stacks, there were a number of other considerations including heat loss and safety.

A number of design options were studied involving the shape of the enclosure and configuration of the gas manifolds before the current design was arrived at. The downselected stack enclosure features a cylindrical center section with flanged and dished heads on either end. At the bottom of the center section is a flanged joint with o-ring seal that mates the top pieces to the bottom head. This allows the majority of the enclosure to be removed for access to the stacks inside. The lower head has three major nozzle connections that allow fuel, air and exhaust to pass between the enclosure and the rest of the system. A number of other electrically isolated ports in the bottom head allow the power rods and instrumentation connections to the fuel cell stacks to exit the enclosure.

The stack enclosure interior features a gas distribution manifold and the necessary insulation to meet heat loss requirements. The gas distribution manifold provides evenly distributed fuel and air flows between the four stacks.

10.2 CATHODE AIR BLOWER

The cathode air supply for the SOFC stack was a single air blower that provided the required airflow and overcame the system component pressure drops throughout the entire range of prototype system operation. As this is the largest electrical parasite on the system, the blower needed to operate with minimum power consumption in order for the overall system to meet efficiency targets. Additional high-level requirements for the blower were performance, high volume production cost, safety, and reliability.

Early in the search for a suitable blower vendor, it was evident that standard “off-the-shelf” solutions would not meet the efficiency requirement. Several vendors were contacted and provided with the blower specifications. Most vendors who provided data alluded to an overall efficiency baseline (defined as isentropic air pumping power / electrical power) near 30% for standard “off-the-shelf” air blowers in the range of operation required by the prototype system.

Formal proposals were provided by two vendors for a custom designed blower. While the requirements of cost, efficiency, and potential reliability of each development contract was similar, the design was down-selected for its flexibility in meeting the performance requirements over a wide range of system pressure drops. This is advantageous due to uncertainty in the final hardware pressure drops for components such as heat exchangers, valves, stack enclosure, etc.

The contract included the construction of three identical custom blowers. While only one was needed for the prototype system, another operated for a 1000-hour endurance test to help determine reliability. The final unit was used as a spare. The requirement was to provide these units at 57% overall efficiency for the specified design point. A product specification was developed (GE Specification: D50HY0001).

The final mapped performance of the units delivered to GE can be seen in Figure 10.1. The top chart contains the constant speed lines as they relate pressure rise and flow. The bottom chart contains the constant speed lines as they relate overall blower efficiency and flow. The performance of the prototype blower exceeded the 57% efficiency that was specified.

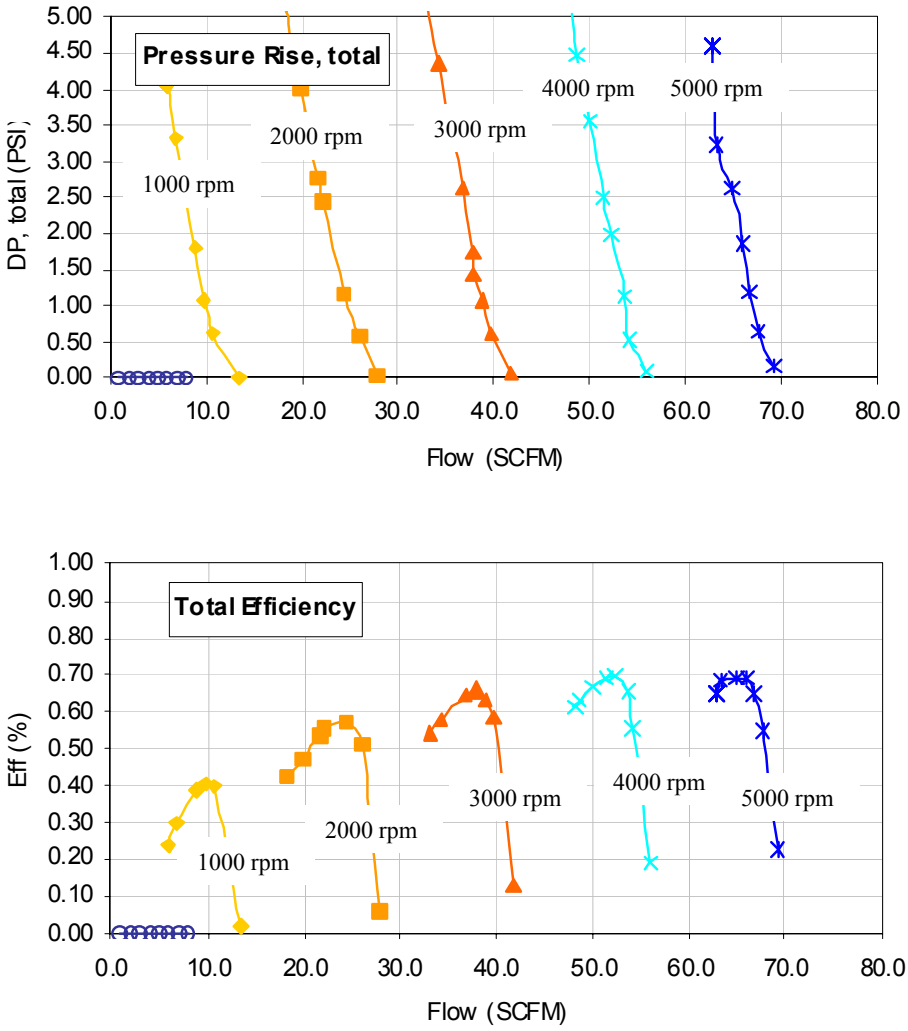

Figure 10.1. Performance maps for cathode air blower.

10.3 WATER METERING

Accurate fluid metering at the small mass flows required by the prototype system is technically challenging. Three products were identified as candidates capable of covering the flow rates anticipated. A key consideration was the need for stable water delivery. Unsteady water delivery has the potential to introduce steam flow oscillations into the fuel processor that could lead to fluctuations in hydrogen production or fuel flow and thus potentially damaging voltage swings in the stack. A loss of steam also could lead to carbon deposition. Each of the three solutions was tested and the water metering device chosen for the prototype system.

10.4 SENSORS AND VALVES

A conceptual analysis was performed to determine the requirements for the SECA prototype critical to control sensors. The required type of sensor, accuracy, and reliability were all determined and appropriate sensors were selected.

10.5 FUEL METERING

Accurate and predictable control of fuel quantity is essential for achieving high overall system efficiency while maintaining an adequate safety margin to prevent excessive combustor temperature. A valve was selected for the system based on the predicted fuel flows and a linear characteristic. During initial trials, it was determined that the optimal control characteristics of the valve and actuator were not well enough aligned, so a slightly different valve was retrofitted and acceptable performance was obtained. The fuel supply system also included block-and-bleed solenoid valves upstream of the fuel control valve as a safety precaution.

10.6 FUEL PROCESSOR AIR BLOWER

Early system designs called for part of the cathode air stream to be diverted to the fuel processor via valving. This arrangement lead to a highly coupled control problem between blower speed and valve position which was determined to increase the risk of being able to adequately control the oxygen-to-carbon ratio. Thus, it was decided to add a separate blower so that a more controlled and de-couple air stream to the fuel processor could be assured.

An appropriately sized blower was selected and procured. Testing at GE included mapping the entire envelope of operation to provide blower performance maps for use in the system steady-state and dynamic models. Figure 10.2 displays constant control voltage input lines as they relate to pressure and airflow delivery. Figure 10.3 shows constant control voltage input lines as they relate to overall efficiency and airflow delivery.

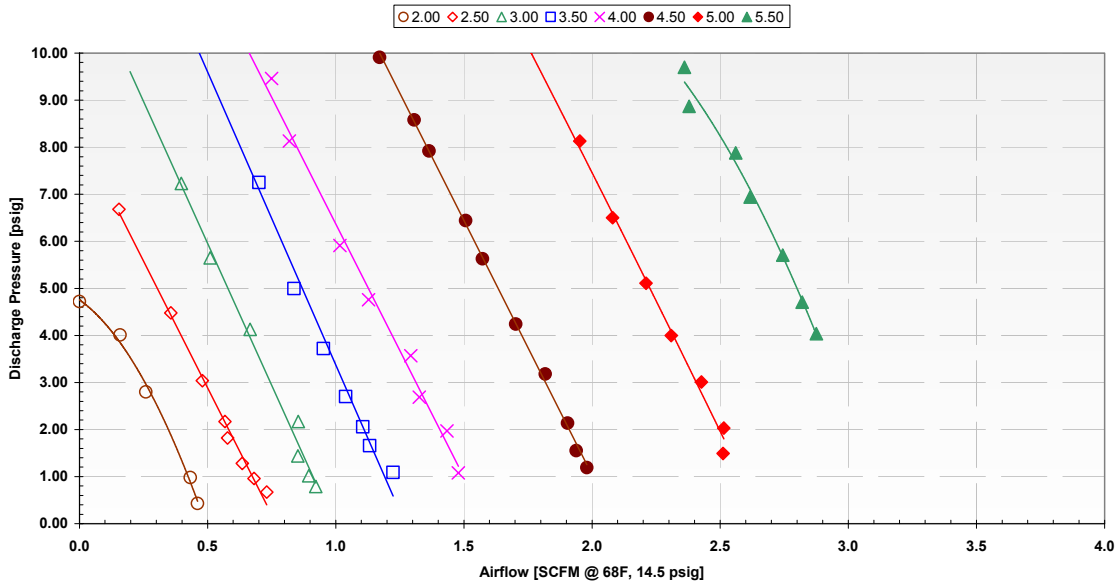

Figure 10.2. Fuel processor air blower pressure versus flow for various control input voltages.

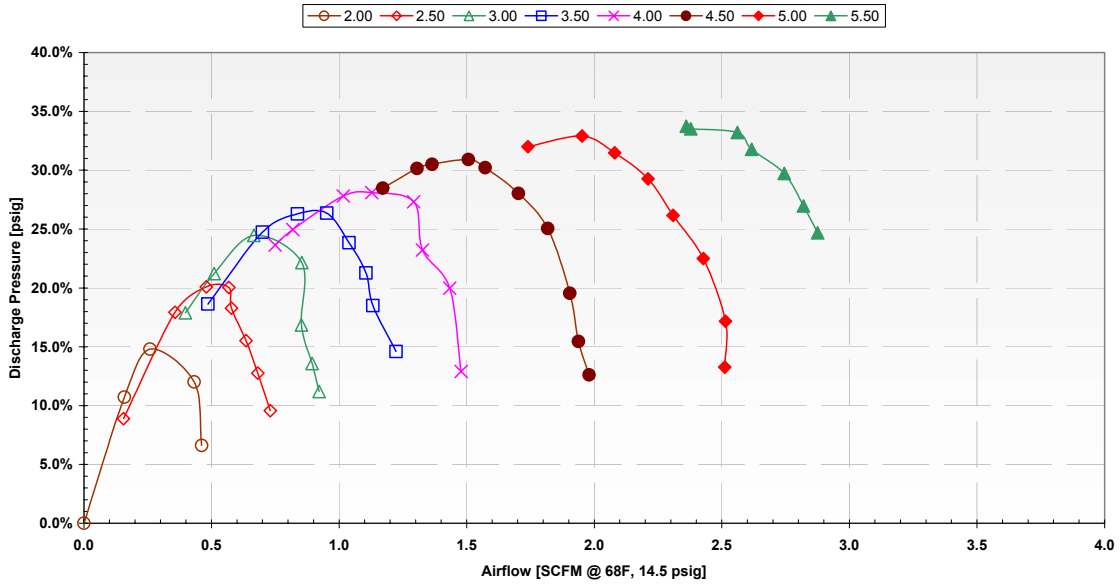

Figure 10.3. Fuel processor air blower efficiency versus flow for various control input voltages.

10.7 FUEL PROCESSOR AIR PREHEATER

Early system designs called for preheating of all streams going to the ATR-type fuel processor; namely fuel, air and steam. A safety concern was raised during a conceptual design review over the plan to warm the fuel stream with an oxygen rich exhaust stream. This safety issue led to a design change

that called for the elimination of fuel preheating. As a result, the temperature of the mixed fuel, air and steam needed to be sufficiently high so as to meet the fuel processor inlet conditions to assure proper reformer operation. After study, it was determined that placing the fuel processor air preheater as a coil around the combustor exhaust would provide sufficiently high quality heat to warm the air to required levels.

10.8 PRODUCT SAFETY AND FAILURE ANALYSIS

The GE Energy product development process includes rigorous product safety and failure mode review procedures that are tied into design reviews. In order to facilitate both of these analyses, the system was parsed into the following subsystems:

- Fuel Delivery
- Power Electronics
- Fuel Processing
- Water Delivery
- Air Delivery
- SOFC Stack and Enclosure
- Thermal Management
- Balance-of-plant
- Controls

10.8.1 Product Safety Review Process

The GE Product Safety Review process consists of three analysis phases; Preliminary Hazard Assessment (PHA), Hazardous Operation (HAZOP) review and Accident Scenario Review.

The PHA is conducted fairly early in the design process and seeks to establish a baseline understanding of potential dangers present in the product. With such knowledge established, the design team was thus able to move forward in their decision making with a more focused view of what areas required particular attention from a safety perspective. This enabled potentially hazardous designs, such as the fuel preheating noted in Section 10.7, to be eliminated where possible or at least moderated before the concepts are fixed.

The HAZOP reviews focused on the dangers to people posed by single point failures or omissions in the design and generated a number of actions for the SECA engineering design team to address. The intent was to systematically step through the subsystems, making use of the failure analysis results, and identify not only the possible hazards, but any existing design features that would mitigate them as well as additional design changes that might be needed to lessen or eliminate any dangers. Most of the actions were items that are

occasionally overlooked such as proper insulation installation and labeling of process flows and components where electrical energy or high temperatures present a potential hazard. Others addressed issues that called for additional inputs to the controller to monitor facility side fuel and purge gas pressures. It was also determined that a discrete flow switch was needed in the system and controller designs to assure that the enclosure ventilation system was working properly. This system is designed to flow fresh air through the system package to keep components, such as sensitive electronic devices, cool and to prevent the buildup of hazardous gasses.

The next review was the Accident Scenario Review, which focused on potential cascading failure affects. During this analysis, the failure modes were linked to their potential of resulting in a potentially injurious situation such as a fire, explosion or electrocution. Each step in moving from a failure to an actual accident was assigned a probability of occurrence. These values were rolled up to give an overall likelihood of a given failure. A few chains resulted in probability scores that were high enough to warrant additional minor changes to the system to reduce the risk of a failure leading to a serious accident.

10.8.2 Failure Analysis

Failure Modes, Effects and Causes Analysis (FMECA) were conducted to determine what the impacts of various subsystem and component failures may have on the ability of the prototype system to operate.

A FMECA review, using a proprietary software tool, was conducted for the conceptual system design and revisited once the detailed design had been completed such that changes to the system made during design revisions were accounted for in terms of their impact on system reliability.

Many of the changes, such as the elimination of the fuel pre-heater and the inclusion of triple-redundant sensors at key locations, resulted in fewer failure modes. A number of action items were generated from the review aimed at improving the reliability of the system. Among the items noted were the need to assure a facility side manual fuel shutoff valve in the event of solenoid valve failure

10.9 SYSTEM INTEGRATION

Assembling of the parts into an integrated whole and thus a working system began with a package design. The intent was to create a robust and flexible platform that could accommodate hardware changes throughout the integration process. A system of u-channel supports and matching hardware formed the main frame to provide a robust and flexible platform for the system components. Parts were assembled as they became available and subsystem tests conducted. Once the final alignment connections were complete and stacks installed, the final components were installed and the system situated in the test room as shown in Figure 10.4.

Figure 10.4. Completed prototype system for hot testing without SOFC stacks (one side panel removed for illustration).

During trial runs, a number of alterations to the system were deemed necessary, several of which were noted in the descriptions of individual components above.

One of the alterations not captured above was the removal of the fuel processor containment. Early trials showed poor fuel processor performance due to overly cool inlet conditions. It was determined that the containment could safely be eliminated by welding the fuel processor to its enclosure connection and eliminating the slip-fit arrangement that had originally been designed. This also allowed a shorter path for the fuel processor air from its preheater, which minimized heat loss and helped to improve fuel processor performance.

Also not noted was the removal of the bypass leg on the fuel processor air supply line. This was originally included to allow finer control over fuel processor temperature. Trial runs indicated that this was ineffective and increased the heat loss of the fuel processor. The bypass valve and leg were removed and this coupled with the shorter path for the heated fuel processor air yielded acceptable fuel processor performance for the duration of the test.

Additional insulation was also installed around the enclosure to minimize heat loss and assure that the enclosure wall was at touch temperature per safety requirements.

Despite some challenges with a few individual components, the integrated system performed well and the flexible architecture of the design proved its worth in accommodating design changes.

11 PROTOTYPE TEST

The prototype system that was tested can be seen in Figure 11.1. There was an extensive system build and integration process leading to the final testing of the unit which was comprised of the following major steps:

- Component Testing
    - Verified basic operation of components in stand-alone testing
    - Developed component performance maps
    - Supported component selection process
- Cold Tests
    - Operated the system with only nitrogen/air and without fuel cell stacks
    - Validated basic operation of components integrated in system
    - Verified plumbing and electrical wiring
- Hot Tests
    - Operated the system on methane without fuel cell stacks
    - Verified and tuned control system hardware and software
    - Verified combustor operation and temperature controls
    - Integrated operation of fuel processor
    - Conducted thermal mapping of system and improved insulation
- Gen 1 System Test
    - Operated integrated system without power electronics due to half-sized stacks
    - Gen 1A – 4x20-cell stacks electrically series
        - Electrical short from base of stack 3 resulted in early termination of test
    - Gen 1B – 3x20-cell stacks electrically parallel
        - Successfully tested stacks in parallel
        - Verified integrated operation of stacks with fuel processor
        - Achieved a peak gross DC power of 2.4 kW on ATR fuel.
        - Achieved a peak gross DC power of 2.6 kW on dilute hydrogen (64% H2/36% N2)

        - Tuned control loops and verified startup and shutdown strategies
    - Gen 1C – 3x20-cell stacks electrically series
        - Verified new method for electrically isolating stacks
    - Operated the system for over 72 hours on ATR fuel with a total test time of over 200 hours.
    - Operated the system in the thermally self-sustaining mode during operation at high current densities.
    - Assessed the heat loss on the system and conducted a thermal survey.
    - Evaluated the pressure drop through the system with the stacks included.
- Gen 2 System Test
    - Integrated system with power electronics
    - 4x40-cell stacks electrically in series
    - Results discussed in detail in the following sections of report

This report will focus on the results of the Gen 2 System Test which is the final prototype test for Phase I. A brief description of the prototype test plan will first be given followed by a detailed analysis of the test results. The results of the test can be seen in summary form in the Phase I prototype system scorecard shown in Table 11.1. It should be noted that the prototype system exceeded all of the SECA minimum requirements with the exception of the transient cycle degradation.

Figure 11.1 SECA Phase I Prototype System

Table 11.1 Phase I Prototype System Scorecard

	CTQ	UOM	LSL	Target	USL	Phase I Perf.	Basis
System	Peak Efficiency	%	35	39	-	40.9	Gen 2 Prototype System Test
	Projected Cost	$/kW	-	720	800	724	Audited, 5.4 kW basis, projected to 50,000 units
	Rated Net Power	kW	3	5	-	5.43	Gen 2 Prototype System Test
	Availability (1500 hrs)	%	80	90	-	80 90	Gen 2 Prototype System Test, ATR operation only Gen 2 Prototype System Test, ATR/1500 hrs
	MTBF	hrs	1000	4500	-	420	Gen 2 Prototype System Test, 9/29
Stack	Fuel Utilization	%	60	80	-	78	Gen 2 Prototype System Test
	Power Density (@0.7V, 80% U_f)	W/cm^2	-	0.300	-	0.172	Gen 2 Prototype System Test (Pre-test Assembly Estimate)
	Projected Cost	$/kW	-	200	-	253	Audited, 5.4 kW basis, projected to 50,000 units
	Steady-state Deg.	%/500 hrs	-	1	2	1.8 1.2	Pre-Transient, Gen 2 Prototype System Test Post-Transient, Gen 2 Prototype System Test
	Cycling Deg.	%/10 cycles	-	1	1	1.8	Gen 2 Prototype System Test

11.1 TEST PLAN

The timeline for the test is shown graphically in Figure 11.2 and detailed out in Table 11.2. Each segment is described in greater detail in the subsections that follow. It should be noted that the exact timing and duration of each segment could be modified during the test as needed to best address the test objectives. A more detailed discussion of each of the test steps is given in the following subsections.

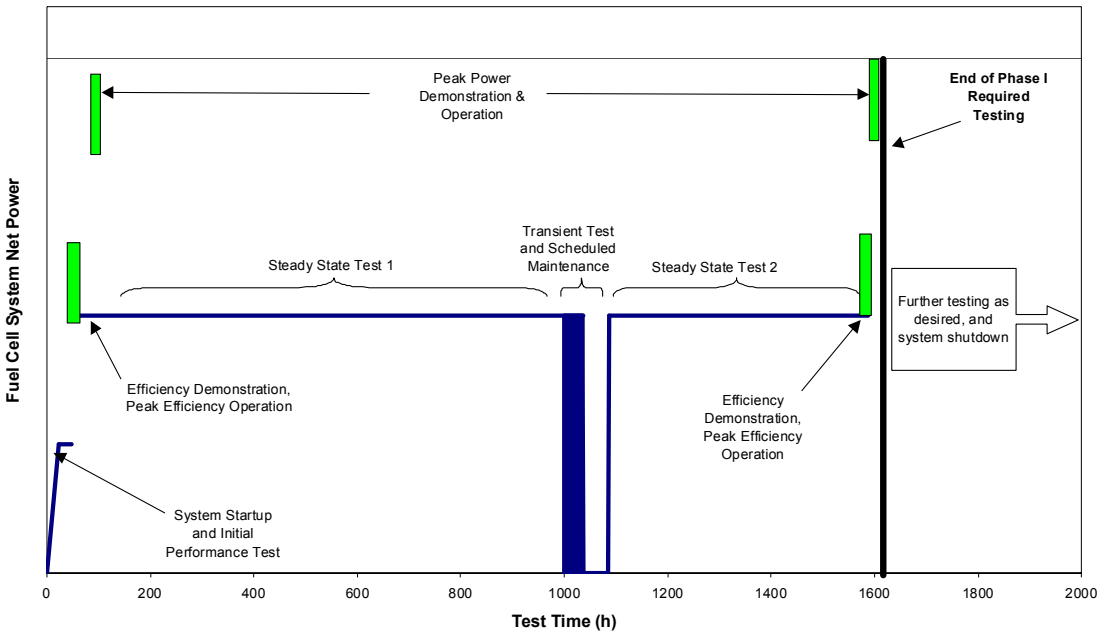

Figure 11.2 Graphical representation of prototype test sequence.

Table 11.2 Test Plan Timeline

Step	Start Time*	Duration*	Procedure	Requirements
1	0	24	A. System Startup	
2	24	48	B. System Check-Out	Confirm stable, safe system operation
3	48	52	C1. Performance Test – Efficiency	Stable operation at peak efficiency for 1 hou
4	52	56	D1. Performance Test – Peak Power	Stable operation at peak power for 1 hour
5	56	1000	E1. Performance Test – Steady-State	NOC, constant current
6	1000	1086	F. Transient Test / Scheduled Maintenance	9 power cycles and 1 thermal cycle
7	1086	1586	E2. Performance Test – Steady-State	NOC, constant current
8	1586	1590	C2. Performance Test – Efficiency	Stable operation at peak efficiency for 1 hou
9	1590	1594	D2. Performance Test – Peak Power	Stable operation at peak power for 1 hour
	Total	**1594**	**Phase I Required Testing Complete**	
10			G. Continuing System Evaluation	Further system testing as desired
11			H. System Shutdown	

*All times and durations are approximate and may be adjusted during the test to better address the test objectives.

11.1.1 Startup (A)

- The standard system startup procedure will be followed, including heat-up, safety checkout, built-in test, and application of a test load.

11.1.2 Initial Performance Testing and System Check-Out (B)

- The system will be operated under pre-determined operating conditions to confirm safe and stable operation.

11.1.3 Performance Demonstration (C1, C2) - Efficiency

- Operating conditions will be adjusted to identify the peak efficiency operating point.
- The system will be operated at the peak efficiency condition for 1 hour.

11.1.4 Performance Demonstration (D1, D2) – Peak Power

- Operating conditions will be adjusted to identify the maximum power that the system can produce.
- The maximum net power output that the system produces in a stable manner for 1-hour period will be considered the system peak power for purposes calculating system factory cost ($/kWe).

- In order to avoid potential damage to the system that may interfere with the required steady-state and transient testing, Performance Demonstration D1 will likely be more conservative in the choice of operating conditions. Consequently, the peak power obtained during Performance Demonstration D2 may be different than that achieved during Performance Demonstration D1.

11.1.5 Steady-State Performance Test (E1, E2)

- The system will be operated at a normal operating condition (NOC) consistent with the targeted application (residential power). The normal operating condition power level must be equal to or greater than 1.5 kWe.
- The system will be operated at constant current.
- The system will be maintained at this operating condition for the durations shown in Table 1 needed to satisfy the SECA Minimum Requirements.
- Steady-state degradation will be evaluated over this time period and reported.

11.1.6 Transient Test and Scheduled Maintenance (F)

- The system will be cycled 9 times between the NOC and a zero net power condition.
- A minimum of one full thermal cycle (to ambient temperature) is required. It may be the first or last of the ten cycles conducted pursuant to the Transient Test.
- The system may be shut down for scheduled maintenance at some point during this transient test. The timing of this maintenance, and details of inspections and replacements to be done during this maintenance, will be determined as testing proceeds.
- If system performance allows, we may choose to forego or delay scheduled maintenance.
- The shutdown before and after scheduled maintenance will be considered one cycle for purposes of the Transient Test.

11.1.7 Continuing System Evaluation (G)

- After the conditions of the required Phase 1 Prototype Testing have been met, we may desire to continue testing the system in order to map performance, understand more fully the system's dynamic response, identify limits of operation, or obtain other information that may prove useful in guiding continued system development under Phase II of the SECA program.

11.2 TEST RESULTS

The results of the prototype system test will be discussed in the following sections in the context of the minimum requirements provided by DOE. The performance of the prototype system exceeded all of the SECA minimum requirements with the exception of the transient/cycle degradation. The time history of key system variables can be seen in Figure 11.3. The various periods of the test plan can be seen with the peak efficiency and peak power demonstrations, 1000 hours of steady operation, transient test, and concluding 500 hours of steady operation.

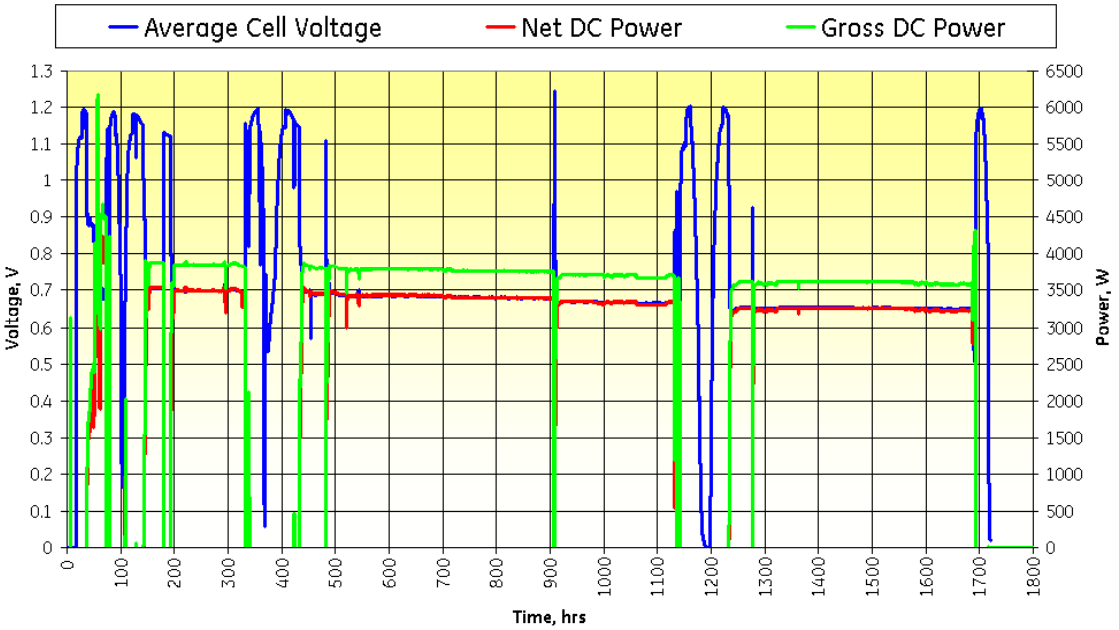

a) Average Cell Voltage, Net DC Power, Gross DC Power

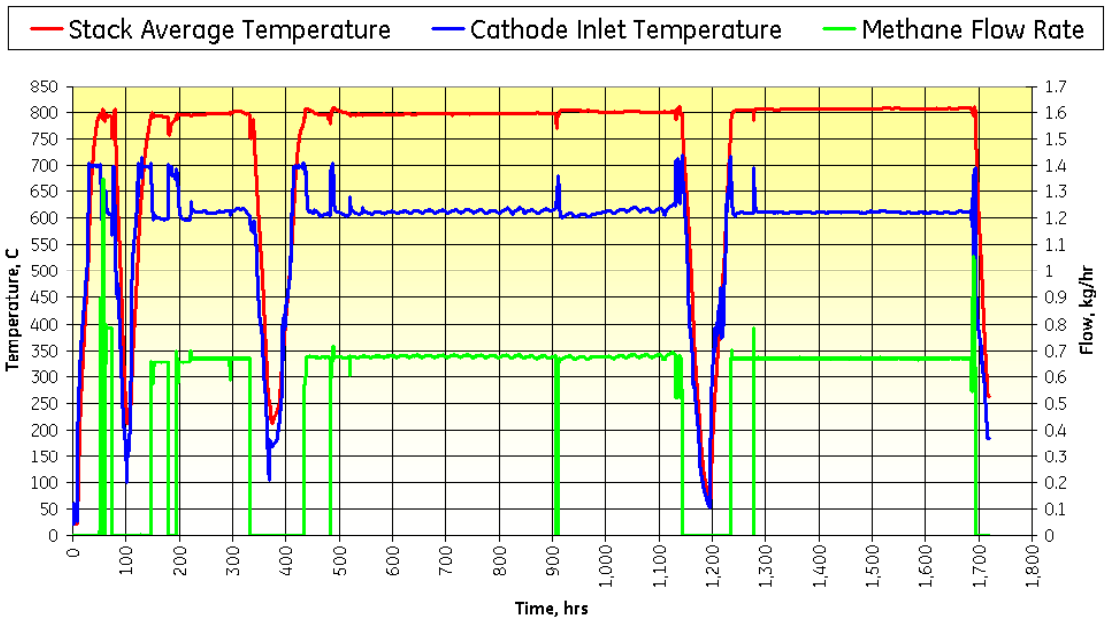

b) Stack average Temperature, Cathode Inlet Temperature, Methane Flow Rate

Figure 11.3 Time history of key system variable for prototype system test.

11.2.1 Beginning of Test Peak Efficiency

The beginning of test peak efficiency was measured over a one-hour steady state period on July 27, 2005. After some exploration in changing various setpoints in the system, the peak efficiency settings were determined and the system was held for the required one hour at this steady state condition. The system achieved a DC efficiency of 40.9% under the following conditions:

- Fuel utilization of 78%
- Air utilization of 26%
- Steam-to-carbon ratio of 1.2
- Oxygen-to-carbon ratio of 0.68
- Current of 31.0 A (218 mA/cm^2)
- Average cell voltage of 0.733 V
- Gross DC power of 3.59 kW (158 mW/cm^2)
- Net DC power of 3.26 kW

The overall system was stable for the entire one-hour period with no abnormalities with the system or the test facility. The individual cell voltages were stable with no sign of fuel distribution issues or cell starvation. The cell voltages for all four SOFC stacks can be seen in Figure 11.4. The typical end effects can be seen on each stack due to temperature distributions within the individual stack. Additionally, Stacks 1 and 3 have significantly lower voltages at the top of the stack. A histogram of all of the cell voltages can be seen in Figure 11.5. The mean voltage is 0.735 V with a standard deviation of 0.047 V. The majority of cells remained above 0.7 V at this test condition, but a small percentage of cells exhibited lower performance.

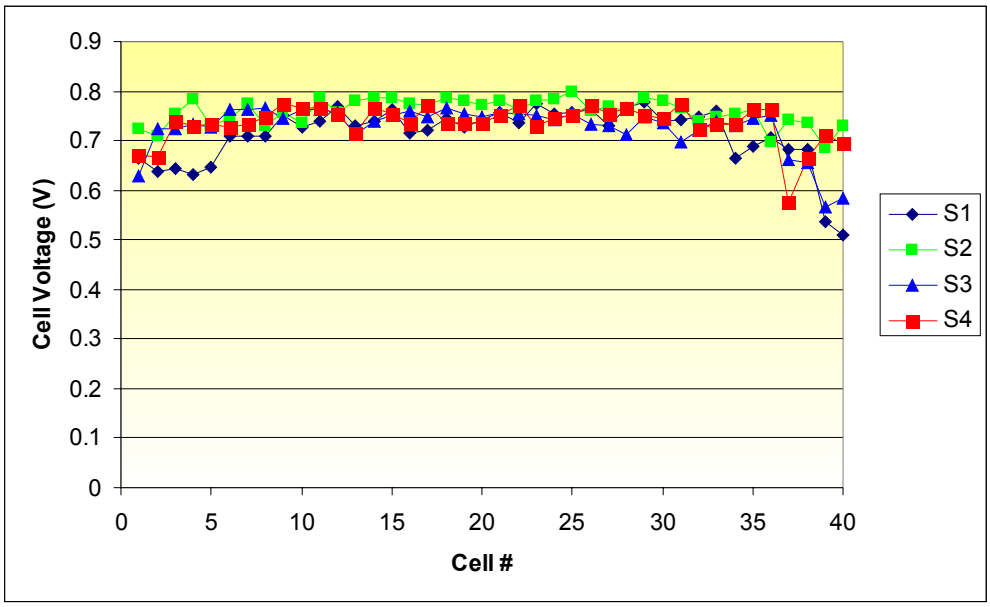

Figure 11.4 Cell Voltages at Peak Efficiency Point.

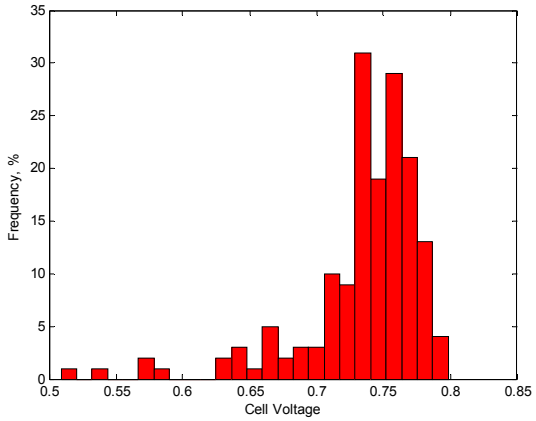

Figure 11.5 Histogram of all Cell Voltages at Peak Efficiency Point.

The temperature distribution within each of the four stacks can be seen in Figure 11.6. The trends show higher temperatures in the center cells of the stack and that the top of the stacks are at a higher temperature than the bottom of the stacks. Stack 1 showed a higher temperature than the other stacks which is likely due to its voltage being lower than the other stacks which results in additional heat generation. The average temperature for the individual stacks and the stack assembly can be seen in Table 11.3. The stack assembly was at an average temperature of 794°C with Stack 1 being at an average temperature of 798°C. In addition to performance differences, the relative placement of the stacks in the stack enclosure relative to the fuel inlet and cathode air inlet to the enclosure also impacted the temperatures of the stacks.

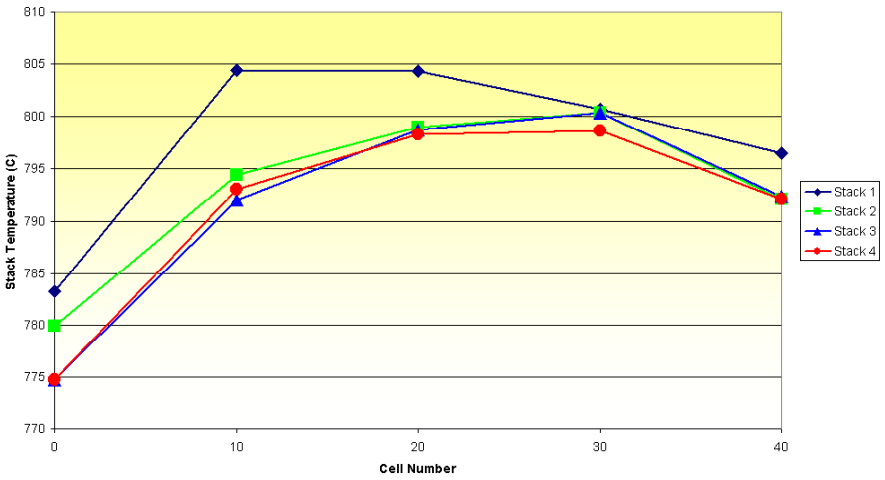

Figure 11.6 Stack Temperature Distributions at Peak Efficiency Point.

Table 11.3 Average STack Temperatures for Peak Efficiency Point

Stack 1	798°C
Stack 2	793°C
Stack 3	792°C
Stack 4	791°C
Stack Assembly	794°C

The process variation seen during the one-hour peak efficiency demonstration can be seen in Figure 11.7. The mean efficiency was 40.9% with a standard deviation of 0.46%. This source of this variation could be electrical noise on instrumentation as well as the slight variation in pressures, flows, and temperatures in the system.

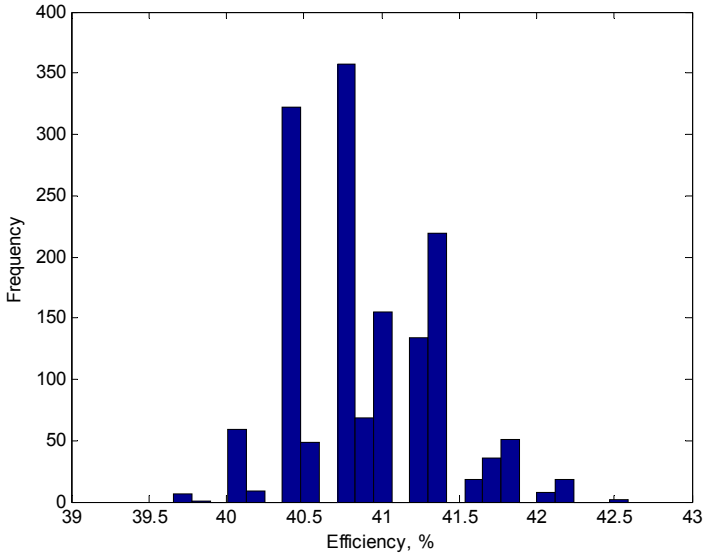

Figure 11.7 Histogram of Efficiency for One-Hour Peak Efficiency Period.

The measurement uncertainty was analyzed and propagated using Crystal Ball. The analysis was performed using the specified measurement uncertainties as well as the pre-test and post-test calibrations. The worst efficiency resulted from the post-test calibration numbers, but even in this case there is a 95% confidence that the system efficiency is between 39.9% and 41.9%.

During the peak efficiency run, the fuel cells output power was being dissipated with an electronic load rather than the inverter due to concerns over the stability of the test stand power infrastructure. Subsequent tests verified stable operation of the inverter in the prototype system with performance matching stand-alone tests of the inverter. Based on stand-alone testing of the inverter, the projected AC performance of the system at the peak efficiency point would have been:

- AC Efficiency of 38.0%
- Net AC power of 3.03 kW

11.2.2 Beginning of Test Peak Power

The beginning of test peak power was measured over a one-hour steady state period on July 23, 2005. After some exploration in changing various setpoints in the system, the peak power settings were determined and the system was held for the required one hour at this steady state condition. The system achieved a net DC power of 5.43 kW under the following conditions:

- Fuel utilization of 67%
- Air utilization of 18%

- Steam-to-carbon ratio of 1.3
- Oxygen-to-carbon ratio of 0.66
- Current of 63.1 A (444 mA/cm^2)
- Average cell voltage of 0.625 V
- Gross DC power of 6.13 kW (269 mW/cm^2)
- DC efficiency of 29.0%

The overall system was stable for the entire one-hour period with no abnormalities with the test facility. During this test period there was an air leak from the startup heater which led to a lower peak power output due to the excess parasite load associated with a higher setpoint on the cathode air blower. The individual cell voltages were stable with no sign of fuel distribution issues or cell starvation. The cell voltages for all four SOFC stacks can be seen in Figure 11.8. The typical end effects can be seen on each stack due to temperature distributions within the individual stack. Additionally, Stacks 1 and 3 have significantly lower voltages at the top of the stack. A histogram of all of the cell voltages can be seen in Figure 11.9. The mean voltage is 0.625 V with a standard deviation of 0.081 V. The cell-to-cell variation at the peak power point is 72% greater than the variation seen at the peak efficiency point. The majority of cells remained above 0.5 V at this test condition, but a small percentage of cells exhibited lower performance.

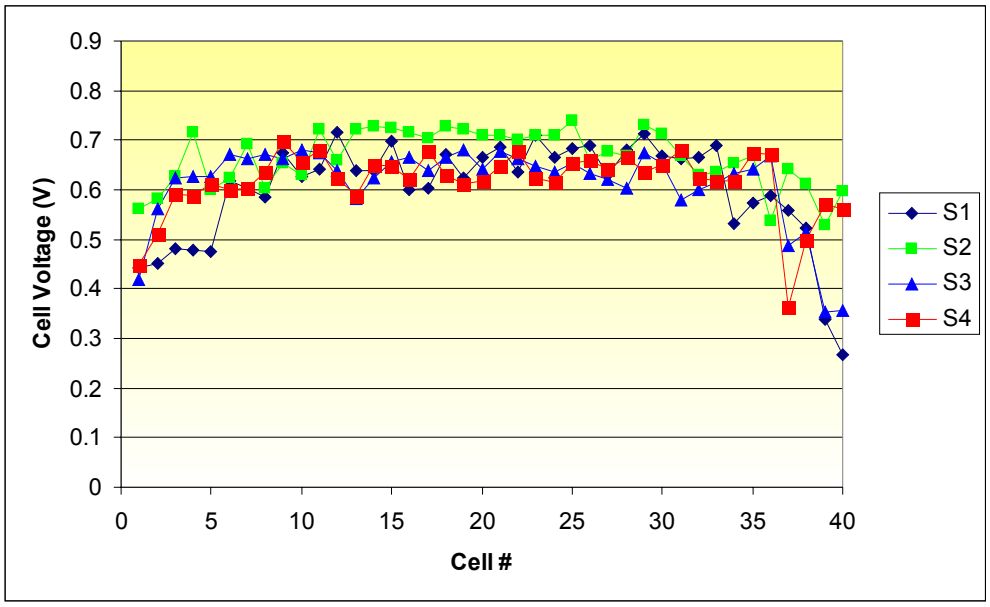

Figure 11.8. Cell Voltages at Peak Power Point.

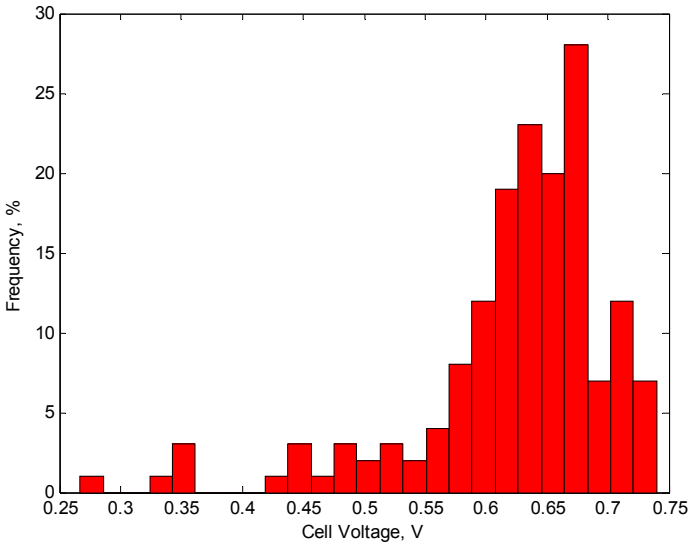

Figure 11.9 Histogram of all Cell Voltages at Peak Power Point.

The temperature distribution within each of the four stacks can be seen in Figure 11.10. The trends are very similar to those seen in the peak efficiency period except that the increased heat generation in the peak power case amplifies the temperature differences within stacks and raises the average stack temperatures. The average temperature for the individual stacks and the stack assembly can be seen in Table 11.4. The stack assembly was at an average temperature of 803°C with Stack 1 being at an average temperature of 811°C.

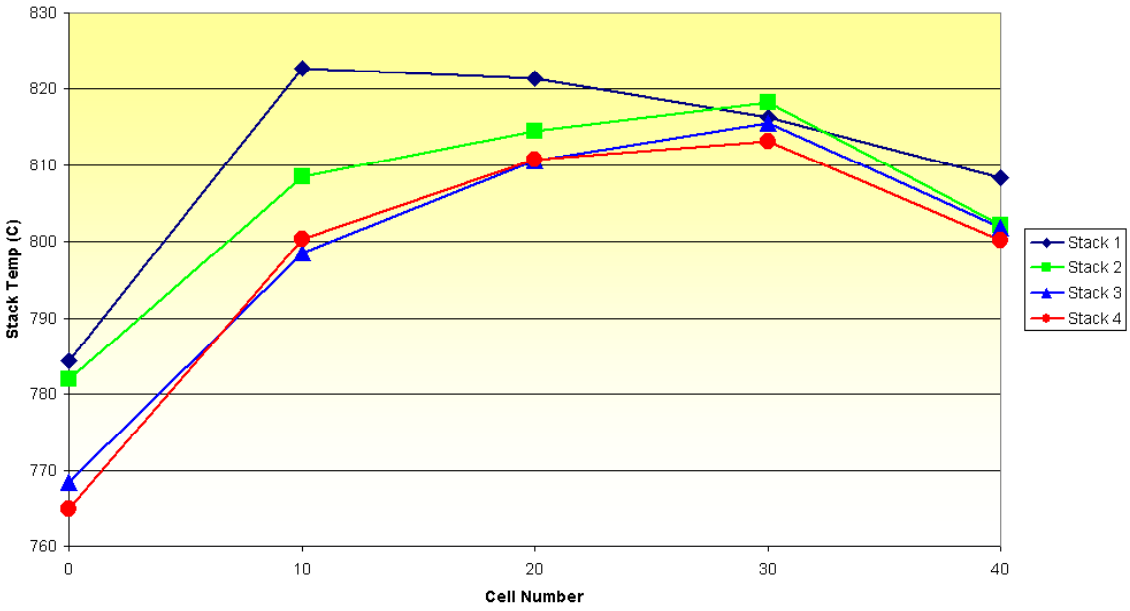

Figure 11.10 Stack Temperature Distributions at Peak Power Point.

Table 11.4 Average STack Temperatures for Peak Power Point

Stack 1	811°C
Stack 2	805°C
Stack 3	799°C
Stack 4	798°C
Stack Assembly	803°C

The process variation seen during the one-hour peak power demonstration can be seen in Figure 11.11. The mean net DC power was 5.43 kW with a standard deviation of 0.06 kW. This source of this variation could be electrical noise on instrumentation as well as the slight variation in pressures, flows, and temperatures in the system.

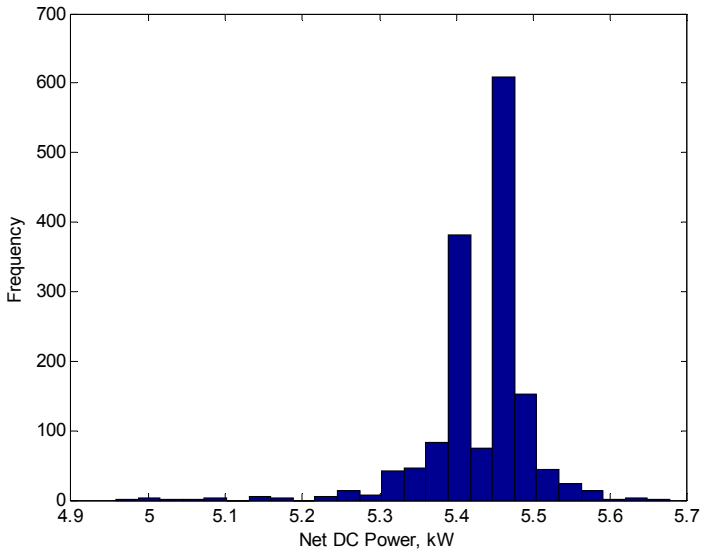

Figure 11.11 Histogram of Net DC Power for One-Hour Peak Power Period.

The measurement uncertainty was analyzed and propagated using Crystal Ball. This analysis was performed using the specified measurement uncertainties as well as the pre-test and post-test calibrations. The worst peak power resulted from the post-test calibration numbers, but even in this case there is a 95% confidence that the system efficiency is between 5328 and 5538 Watts.

During the peak power run, the fuel cells output power was being dissipated with an electronic load rather than the inverter due to concerns over the stability of the test stand power infrastructure. Subsequent integrated tests verified stable operation of the inverter in the prototype system with performance

matching stand-alone tests of the inverter. Based on stand-alone testing of the inverter, the projected AC performance of the system at the peak efficiency point would have been:

- Net AC power of 5.10 kW
- AC Efficiency of 27.2%

11.2.3 Degradation

In order to adequately evaluate voltage degradation within the system, it is necessary to address the issue from three different perspectives. From a top-level perspective, system-level degradation is the most important as it represents the behavior of the system as a whole. Because the system is made up of four individual stacks, it is also of use to analyze stack level degradation so as to assess and understand performance variations between stacks. Lastly, evaluation of cell-level degradation as a function of position within the stack is of use in investigating potential degradation drivers stemming from the stack design.

11.2.3.1 Degradation Calculation Time Period Considerations

Prior to assessing the system, stack, and cell level degradation, it is necessary to define both the time period over which the degradation is to be calculated and the method to be used for carrying out the degradation calculation. As can be seen in Figure 11.12, the system was operated under steady state conditions during several intervals separated by thermal and power cycles. In order to accurately evaluate degradation within the system, it is necessary to select a sufficiently long time period during which overall system operational parameters remain constant and the system is no longer undergoing significant conditioning.

For the purpose of this analysis, two steady state operational time periods were selected as shown in Figure 11.12. The pre-transient interval was selected to occur between days 25.7 and 37.7, and the post transient interval was selected to occur between days 57.2 and 70.2.

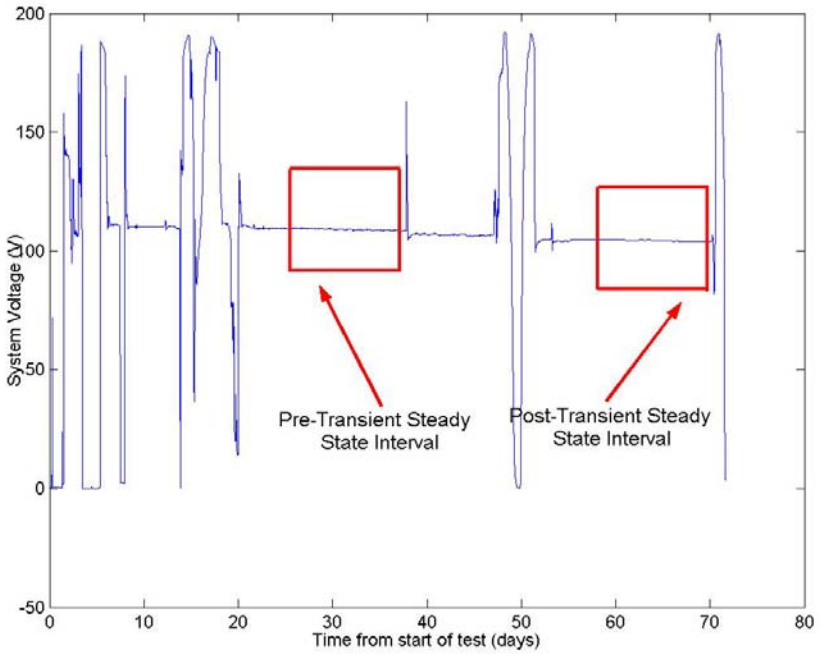

Figure 11.12 - System Voltage Time Series with Steady State Intervals Indicated

It should also be noted that the baseline voltage used to determine the percent voltage degradation for each analyzed time period was calculated using a one-hour windowed average voltage centered around the start time for each of the steady state time intervals

11.2.3.2 Degradation Rate Calculation Methods

In order to evaluate degradation within the SECA system, three different calculation methods were employed. The first method, referred to as the "discrete method," was determined by calculating an average voltage value over a period of one hour at the beginning and end of the desired time interval. A linear curve was then drawn between these two voltages and its slope compared with a reference voltage value in order to determine the voltage degradation as shown in Equation 11.1, where $D_{discrete}$ is the voltage degradation, $\overline{V}$ is the average voltage over the given one hour time span and $\bar{t}$ is the average time within the given time span.

$$D_{discrete} = \frac{\overline{V}_2 - \overline{V}_1}{\bar{t}_2 - \bar{t}_1} \qquad \textbf{(11.1)}$$

The second method, referred to as the "continuous method," was determined using least squares to fit voltage data with a linear curve of the form

shown in Equation 11.2. The slope of this curve was used to determine the voltage degradation value $D_{continuous}$.

$$V = V_0 + D_{continuous}t \quad \textbf{(11.2)}$$

The third method, referred to as the "linear area specific resistance (ASR) method," was determined using least squares to fit ASR data with a linear curve as shown in Equation 11.3. Because ASR is defined as shown in Equation 11.4, where E is the Nernst potential for the operating fuel condition, V_{op} is the operating voltage, and j is the operating current density, it is necessary to convert the ASR slope coefficient M_{ASR} into a voltage degradation coefficient D_{ASR}, as shown in Equation 11.5, where $\bar{j}$ is the average current density over the given steady state interval.

$$ASR = ASR_0 + M_{ASR}t \quad \textbf{(11.3)}$$

$$ASR = \frac{E - \mathrm{V_{op}}}{j} \quad \textbf{(11.4)}$$

$$D_{ASR} = \bar{j}M_{ASR} \quad \textbf{(11.5)}$$

In addition to the considerations of conditioning and steady state operation, it was found that the overall system exhibited ambient temperature induced daily voltage fluctuations. While these fluctuations did not have an effect upon the actual system degradation, their presence was found to have a numerical impact upon the calculation of percent degradation as a function of time. When analyzing degradation within the first steady state interval as indicated in Figure 11.12, it was found that the calculated degradation rate using the "discrete method" varied significantly as a function of the time at which the interval began even though the overall steady state interval ran for a period of 12 days. As can be seen in Figure 11.13, by varying the start time within a period of one day the degradation rate calculated using the "discrete method" was found to vary by a maximum value of 0.29% per 500 hours while the "continuous method" and "ASR method" were found to vary by a maximum value of 0.03% and 0.05% per 500 hours respectively as shown in Table 11.5.

Table 11.5 - Calculated Degradation Rate Variation as a Function of Interval Start Time

	Discrete method	Continuous method	ASR Method
Mean	1.69%	1.65%	1.84%
Sigma	0.109%	0.011%	0.023%
Max Variation	0.290%	0.030%	0.050%

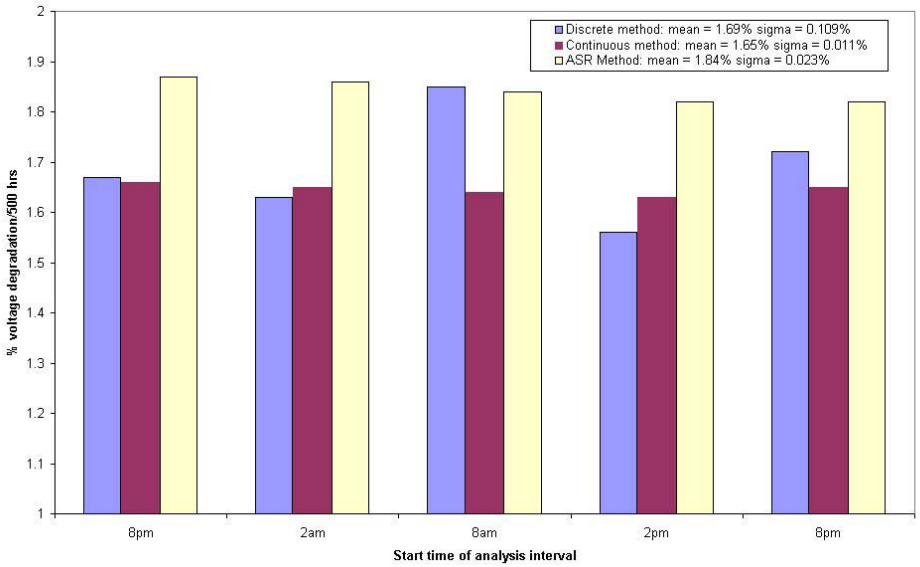

Figure 11.13 - Calculated Degradation Rate as a Function of Interval Start Time

As can be seen in Table 11.5 and Figure 11.13, the “continuous method” and “ASR method” are less sensitive to daily voltage fluctuations present within the system than is the “discrete method.” It can also be shown that the “discrete method” is highly sensitive to slight voltage perturbations occurring within either of the one-hour time spans used to determine the starting and ending voltage values used to carry out the degradation calculation. This behavior may be demonstrated by evaluating the stack level degradation during a period of time in which stack 4 was observed to undergo a brief voltage drop of roughly 3.5 mV per cell, as shown in Figure 11.14. If the one hour window for the initial voltage calculation of the “discrete method” coincides with the voltage drop shown in Figure 11.14, use of the “discrete method” introduces significant error to the degradation calculation. This error is introduced due to the fact that the voltage within the “discrete method” initial voltage calculation window is not representative of the general steady state stack voltage. As can be seen in Figure 11.14, per-cell voltage fluctuations on the order of 3.5mV or greater were not un-common and therefore have the potential to introduce significant variation to the calculated degradation rate when using the “discrete method.” This variation may be quantified by calculating the degradation over the interval shown in Figure 11.14 using both the “discrete method” and “continuous method.” When the degradation rates calculated using the two methods are compared it can be seen that for stacks one through three, where no voltage fluctuation was present, the “discrete method” and “continuous method” yield similar degradation values. In the case of stack four, as shown in Figure 11.15, the calculated degradation rate was found to drop significantly due to the error introduced by the 3.5mV per cell voltage fluctuation present during the initial voltage calculation window.

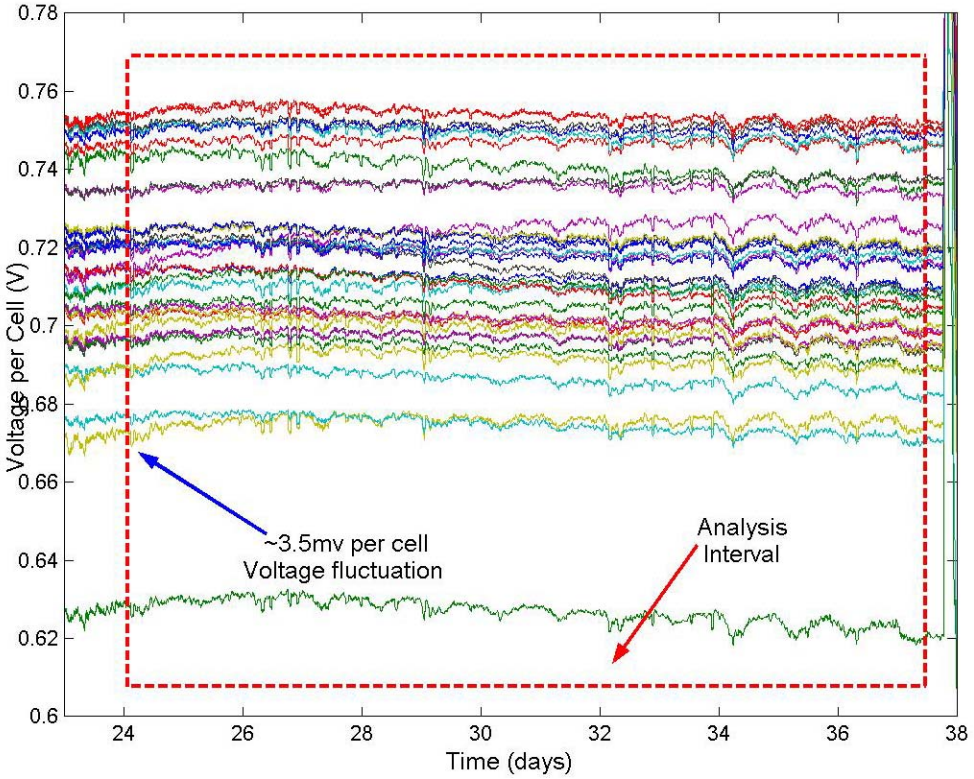

Figure 11.14 - Stack 4 Per Cell Voltage Time Series used in Analysis of 3.5mV per Cell Voltage Fluctuation

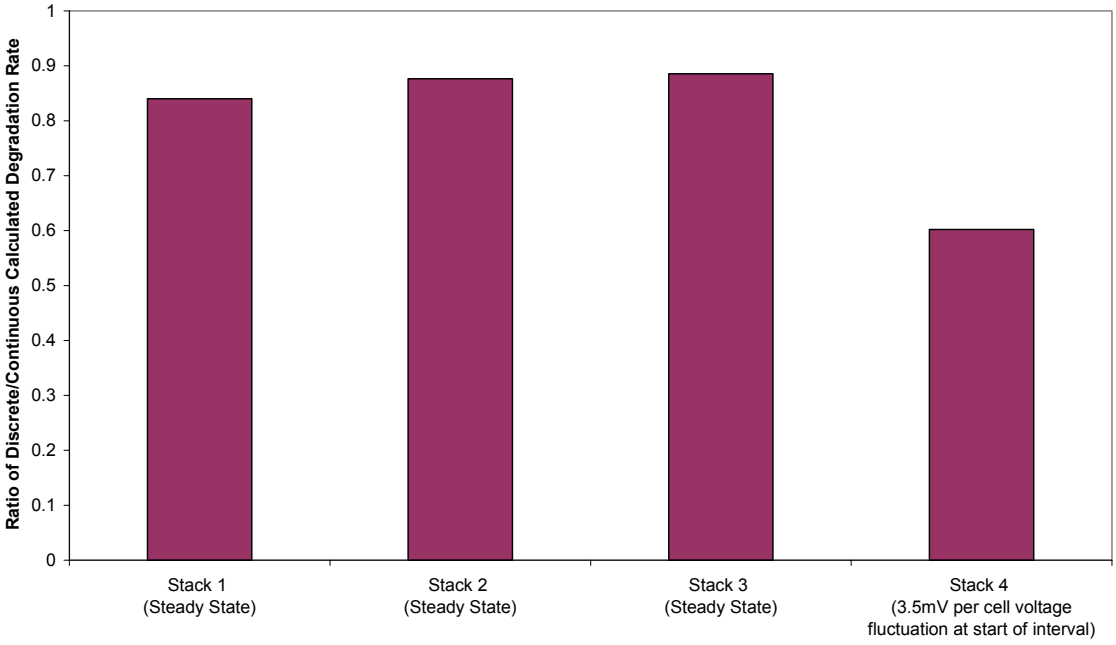

Figure 11.15 – Ratios Showing the Relative Impact of 3.5mV per Cell Voltage Fluctuation Upon "Discrete Method" and "Continuous Method" Degradation Calculations

Of additional concern is the sensitivity of the degradation calculation method to longer time scale voltage trends present within the system. Because the system is designed to operate under real world conditions, such trends will always occur and the selection of a truly steady-state analysis period is critical for determination of an accurate system degradation rate. The way in which the calculated degradation rate can change as a function of the selected analysis interval and selected analysis method is illustrated in Figure 11.16 and Figure 11.17. Although the system voltage time series shown in Figure 11.16 appears to be in steady operation for the entire period indicated in the figure, it can be seen in Figure 11.17 that the calculated degradation rate is heavily dependant upon the selected interval start time. While the degradation rates calculated using the “discrete method” and the “continuous method” vary significantly as a function of the interval start time, the variation of the calculated degradation rate is more than three times greater when using the “discrete method” than it is when using the “continuous method” over the same set of interval start times.

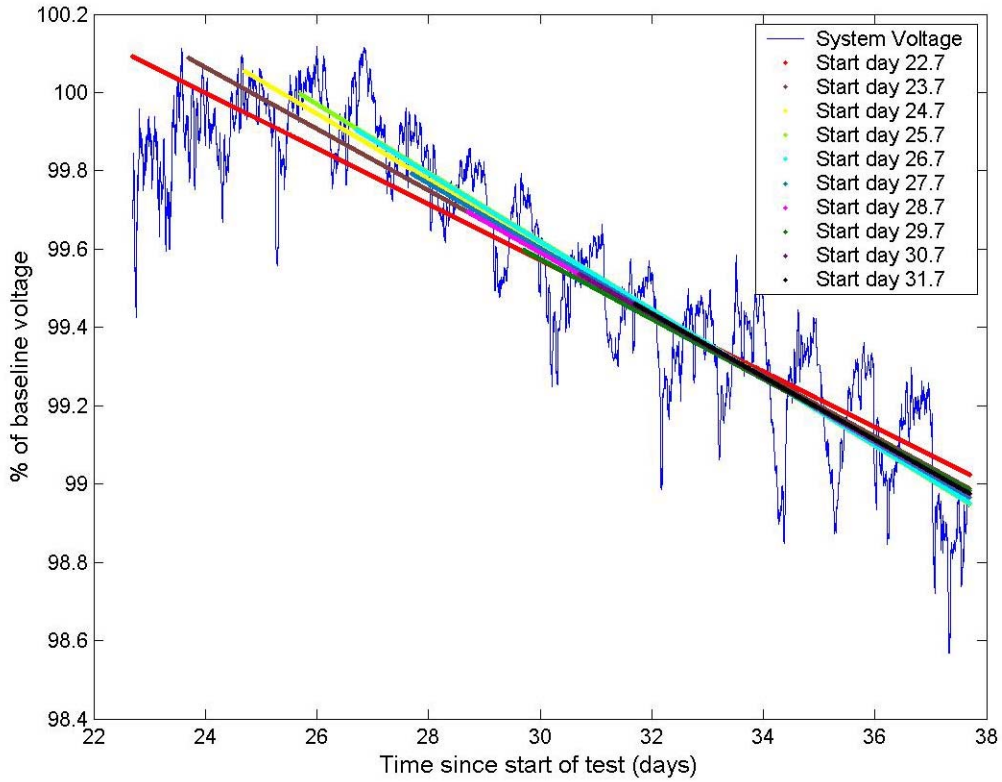

Figure 11.16 - Effect of Analysis Interval Selection upon "Continuous Method" Calculated Degradation Rate

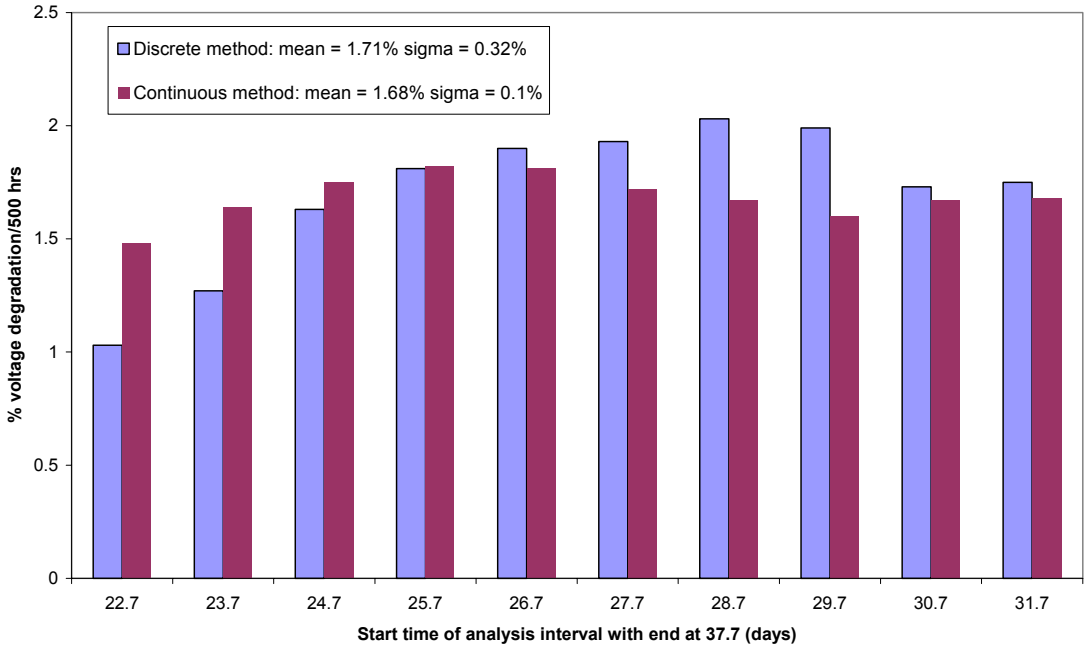

Figure 11.17 - Analysis Interval Start Point Impact on "Discrete Method" and "Continuous Method" Calculated Degradation Rates

It should also be noted that while a linear ASR fit typically provides a better fit than a linear voltage fit, due to the fact that it takes into account variation in current density, some of this additional accuracy is lost because it is necessary to use an average current density when calculating a voltage degradation rate using the "ASR method."

Due to the variation in the "discrete method" calculated degradation rate that can be induced by daily voltage fluctuations, short time scale voltage fluctuations, and longer time scale voltage trends, the more accurate and robust "continuous method" was selected for use in the subsequent degradation analyses presented in this paper.

11.2.3.3 Stack Level Degradation

While voltage degradation is most visible at the system level, it is necessary to evaluate the degradation at the stack level in order to better understand the overall system degradation characteristics. Using the "continuous method," the cell voltage degradation as a function of position within each of the four stacks was found to be as shown in Figure 11.18 and Figure 11.19. The figures represent the degradation behavior of the stacks in the pre and post transient steady state analysis periods, where values of zero correspond to lost voltage leads and negative degradation indicates conditioning.

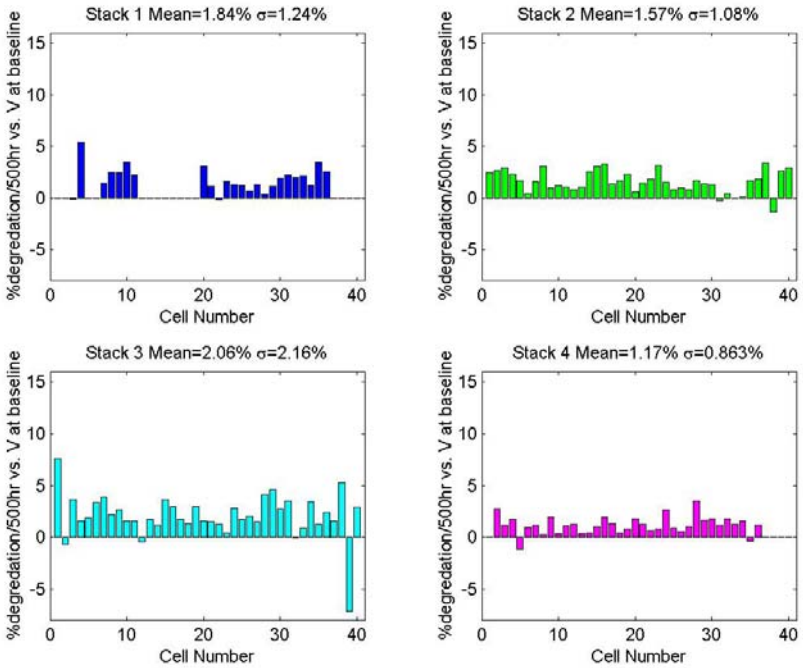

Figure 11.18 - Pre-Transient Cell-Level Degradation Rates by Stack using "Continuous Method"

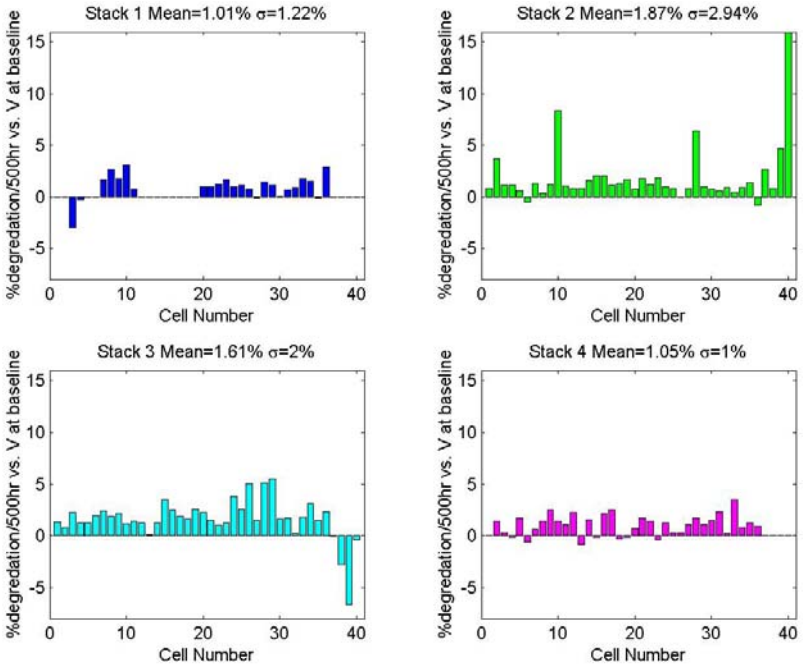

Figure 11.19 - Post-Transient Cell-Level Degradation Rates by Stack using "Continuous Method"

If cell position within the stack is not taken into account, it can be seen that histograms of cell-level degradation rates within each of the four stacks form

similar bell-curve shaped distributions as shown in Figure 11.20 and Figure 11.21, where *pdf* is the probability density function or frequency of observation.

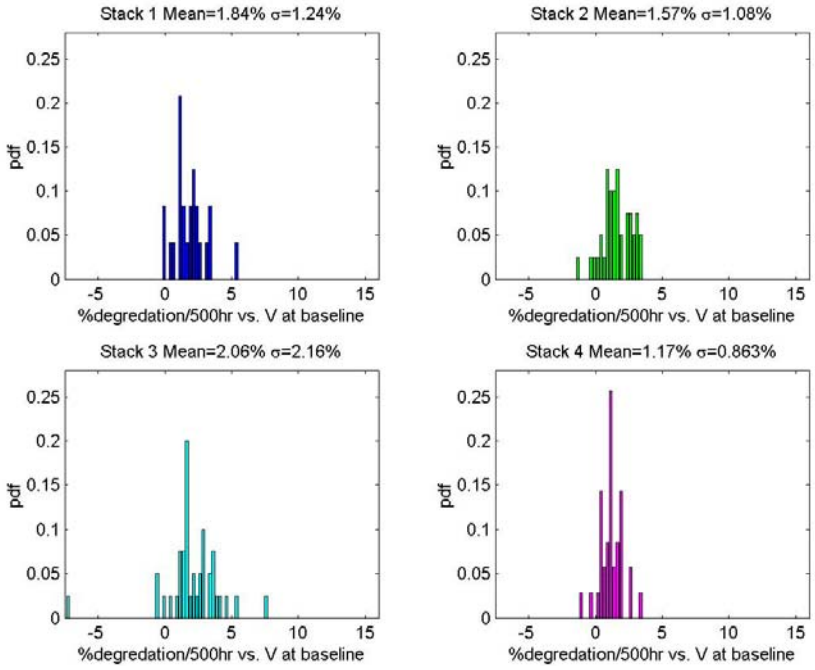

Figure 11.20 - Pre-Transient Cell-Level Degradation Rate Histograms by Stack using "Continuous Method"

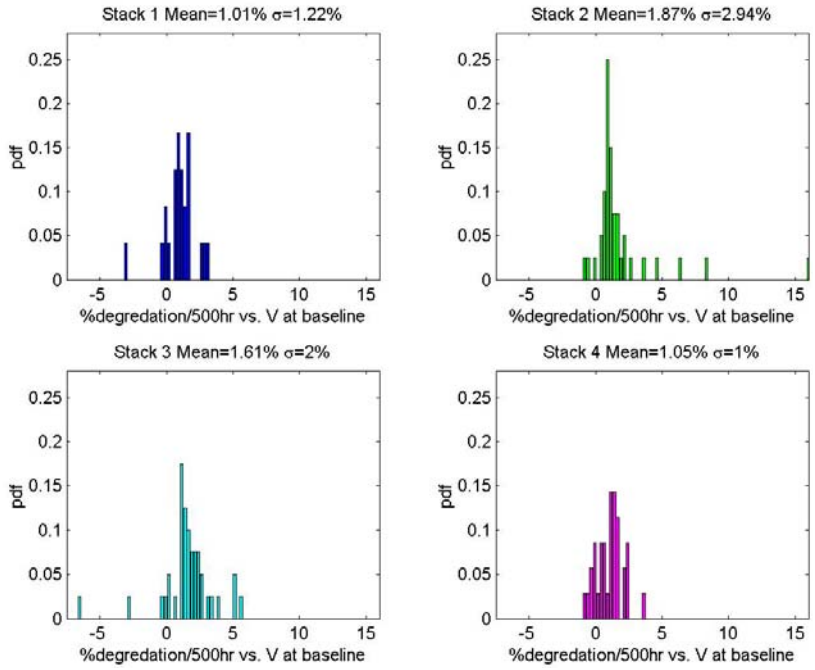

Figure 11.21 - Post-Transient Cell-Level Degradation Rate Histograms by Stack using "Continuous Method"

From analysis of the pre and post transient steady state time intervals, it can be seen that variation in degradation rates exist between each of the four stacks that comprise the system. Overall, this variation was found to be relatively small with no one of the four stacks contributing disproportionately to the overall system voltage degradation.

As shown in Figure 11.22, the mean degradation rate for stacks 1 and 3 was observed to decrease slightly following the transient cycle while rising moderately in stacks 2 and 4. Similarly, the cell-to-cell voltage variation (sigma) was observed to drop slightly for stacks 1 and 3, while rising moderately in stack 4 and significantly in stack 2.

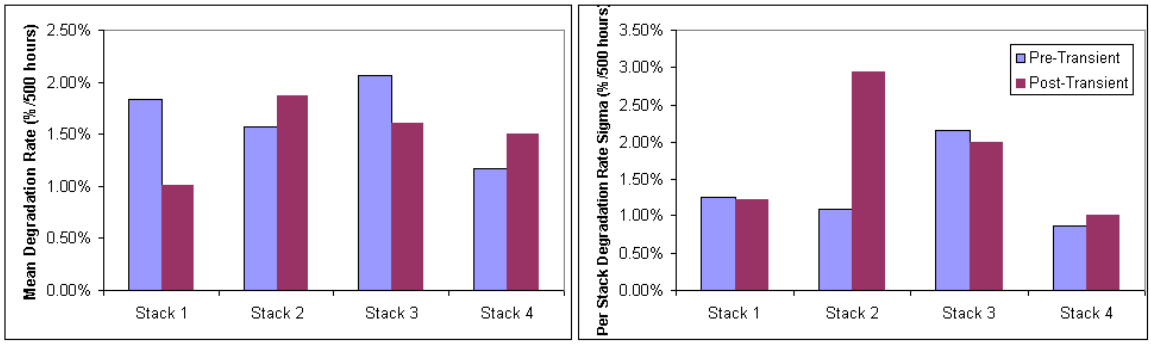

Figure 11.22 - Pre and Post Transient By Stack Degradation Rate Means and Sigmas

11.2.3.4 System Level Degradation

Because the variation in cell-level degradation was found to be relatively small as a function of stack position and cell position within the stack, it is possible to treat the system as a collection of 160 distinct cells. Using this approach, the histograms shown in Figure 11.23 and Figure 11.24 represent the overall pre and post transient degradation characteristics of the system not taking into account the 21 cells for which voltage leads were lost.

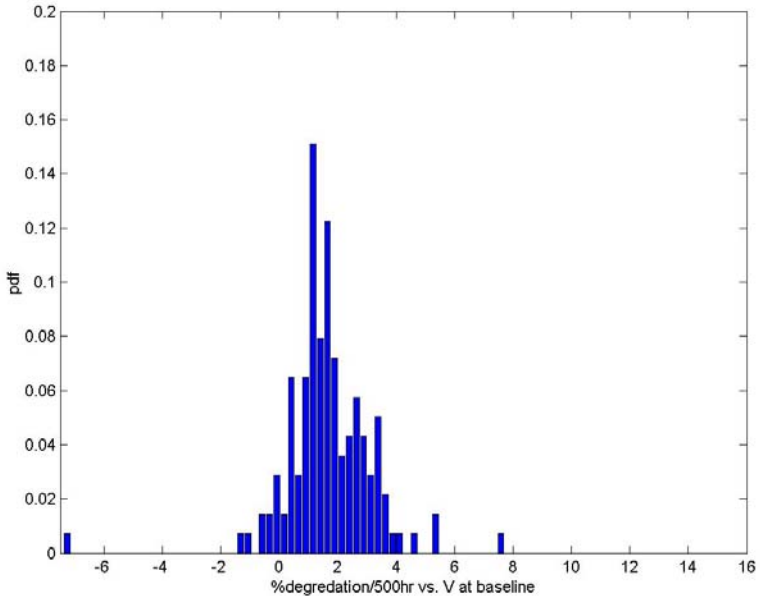

Figure 11.23 - Pre-Transient Cell-Level Degradation for All Cells in System using "Continuous Method"

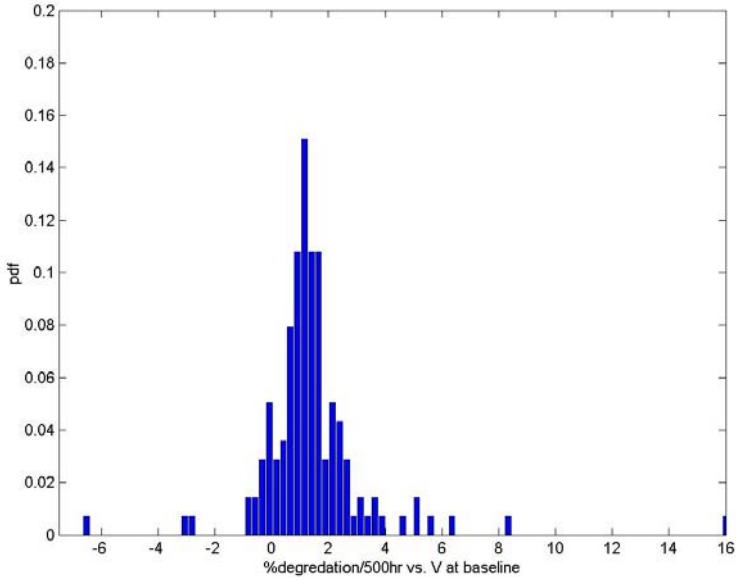

Figure 11.24 - Post-Transient Cell-Level Degradation for All Cells in System using "Continuous Method"

It should be noted that while the distributions shown in Figure 11.23 and Figure 11.24 are shaped similarly to a normal distribution, the data itself is not normal per standard normality tests. It may also be observed that 11 of the pre-transient cells and 17 of the post-transient cells with active voltage leads were observed to undergo conditioning throughout the analyzed steady state intervals.

Although analyses of the cell-level degradation rates are useful for gaining greater understanding of degradation occurring throughout the system, the net system degradation rate for the pre and post transient intervals can best be shown by using the “continuous method” to fit a linear curve to the system output voltage as shown in Figure 11.25.

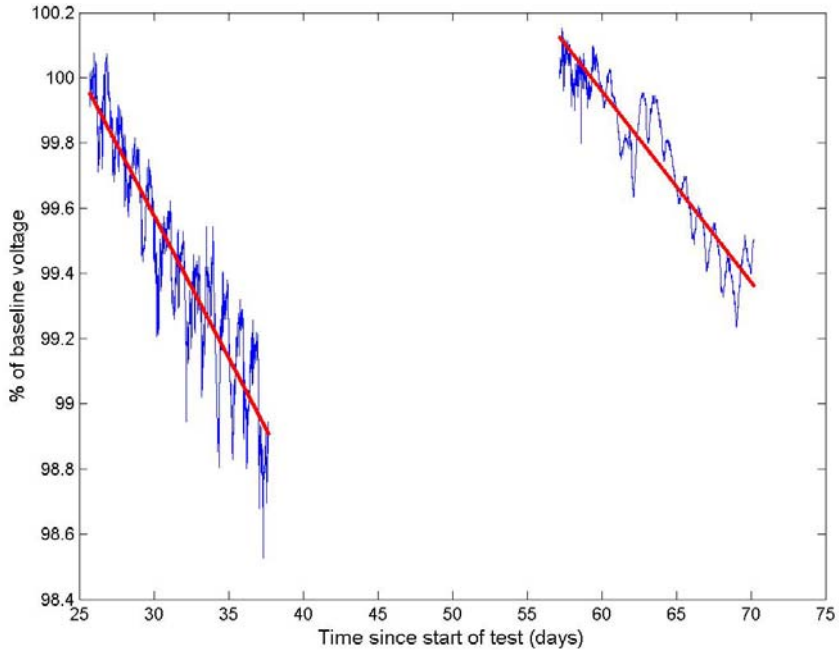

Figure 11.25 - Pre and Post Transient System Level Degradation Linear Curve Fit using "Continuous Method." Percentages taken relative to steady state interval initial voltage

As can be seen in Figure 11.25, the pre and post transient system voltage as a percent of the baseline voltage follows a linear trend when daily voltage fluctuations are not considered. It should be noted that the system level degradation rate can be calculated by taking the mean cell-level degradation rate for all of the cells in the system with active voltage leads, or by calculating the degradation rate of the system output voltage. The results of these two analysis procedures are shown in Table 11.6 and Table 11.7 for continuous and discrete calculations. The difference observed between the system level and cell level degradation is due to the loss of voltage leads from 21 cells and their subsequent exclusion from the cell-level degradation rate calculation.

Table 11.6 - System Level Voltage Continuous Calculation Results Degradation Rate.

	Degradation Rate Intervals (%/500 hours)	
Calculation Method	**Pre-Transient**	**Post-Transient**
System-Level Voltage Degradation	1.82%	1.22%
Mean Cell-Level Voltage Degradation	1.66%	1.44%
Cell-to-Cell Voltage Variation (sigma)	1.48%	2.05%

Table 11.7 - System Level Voltage Discrete Calculation Results for Degradation Rate.

	Degradation Rate Intervals (%/500 hours)	
Calculation Method	**Pre-Transient**	**Post-Transient**
System-Level Voltage Degradation	1.85%	1.28%
Mean Cell-Level Voltage Degradation	1.67%	1.49%
Cell-to-Cell Voltage Variation (sigma)	1.45%	1.94%

11.2.4 Transient Test Degradation

The transient test consisted of 9 power cycles and a thermal cycle down to touch temperature on the SOFC stacks. The power cycles were conducted over the course of a day with each power cycle taking approximately 45 minutes. The thermal cycle followed the normal shutdown and startup procedures for the system and took approximately 2.5 days for the stacks and system to get from operating temperatures to touch temperature and then back to operating temperatures. The degradation due to the transient test period is difficult to quantify due to the post transient conditioning and the various other system variables that can cause the system voltage to vary. The pre and post transient system voltage plot can be seen in Figure 11.26. The pre-transient voltage was determined by averaging the system voltage over a 24-hour period just prior to the transient test. The post-transient voltage was determined by averaging the system voltage over a 24-hour period after the voltage achieved it's maximum voltage under normal operating conditions to take the maximum benefit of post-transient conditioning. The post-transient voltage was 1.8% lower than the pre-transient voltage. The cause for this higher than expected degradation will be investigated further in Phase II of SECA in more controlled experiments where the impact of individual power and thermal cycles can be isolated and analyzed.

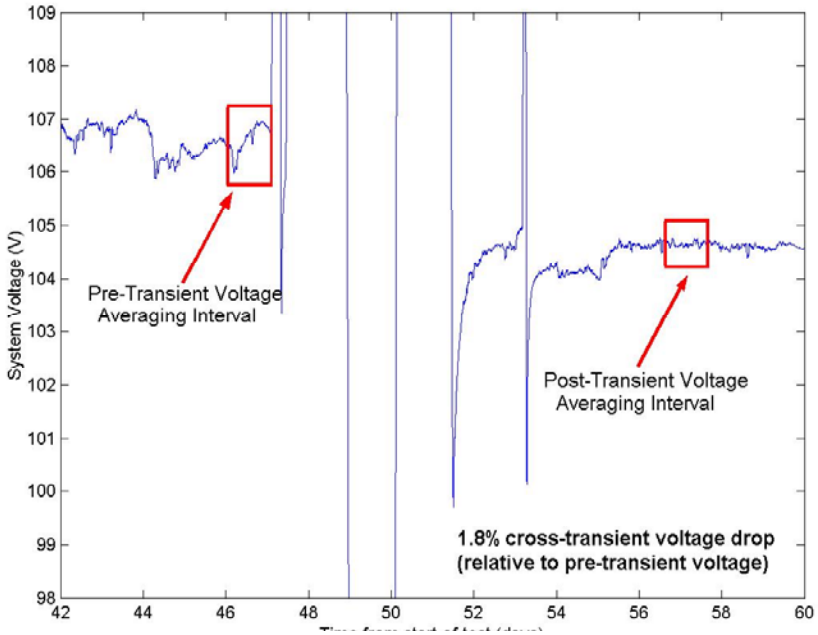

Figure 11.26 Transient Test Degradation Measurement.

11.2.5 End of Test Peak Efficiency

The end of test peak efficiency was measured over a one-hour steady state period on September 29, 2005. After some exploration in changing various setpoints in the system, the peak efficiency settings were determined and the system was held for the required one hour at this steady state condition. The system achieved a DC efficiency of 37.1% under the following conditions:

- Fuel utilization of 77%
- Air utilization of 28%
- Steam-to-carbon ratio of approximately 1.2 (measured 1.3)
- Oxygen-to-carbon ratio of 0.62
- Current of 29.6 A (208 mA/cm^2)
- Average cell voltage of 0.659 V
- Gross DC power of 3.12 kW (137 mW/cm^2)
- Net DC power of 2.79 kW

The overall system was stable for the entire one-hour period with no abnormalities with the system or the test facility. The individual cell voltages were stable, but there was a wider spread in performance when compared with the beginning of test peak efficiency period. The cell voltages for all four SOFC stacks can be seen in Figure 11.27. The end effects can be seen on each stack

due to temperature or possibly flow distributions within the individual stacks. A histogram of all of the cell voltages can be seen in Figure 11.28. The mean voltage is 0.677 V with a standard deviation of 0.084 V. The lower performance and wider variation is likely due to the planned and unplanned thermal and power cycles over the duration of the prototype system test.

Figure 11.27 Cell Voltages at End of Test Peak Efficiency Point.

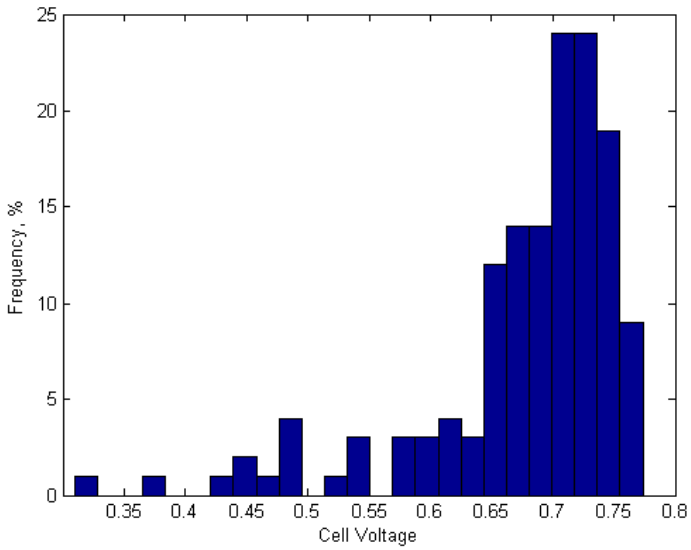

Figure 11.28 Histogram of all Cell Voltages at End of Test Peak Efficiency Point.

The temperature distribution within each of the four stacks can be seen in Figure 11.29. The trends show higher temperatures in the center cells of the stack and that the top of the stacks are at a higher temperature than the bottom

of the stacks. Stack 1 showed a higher temperature than the other stacks which is likely due to its voltage being lower than the other stacks which results in additional heat generation. The average temperature for the individual stacks and the stack assembly can be seen in Table 11.8. The stack assembly was at an average temperature of 801°C with Stack 1 being at an average temperature of 806°C. In addition to performance differences, the relative placement of the stacks in the stack enclosure relative to the fuel inlet and cathode air inlet to the enclosure also impacted the temperatures of the stacks.

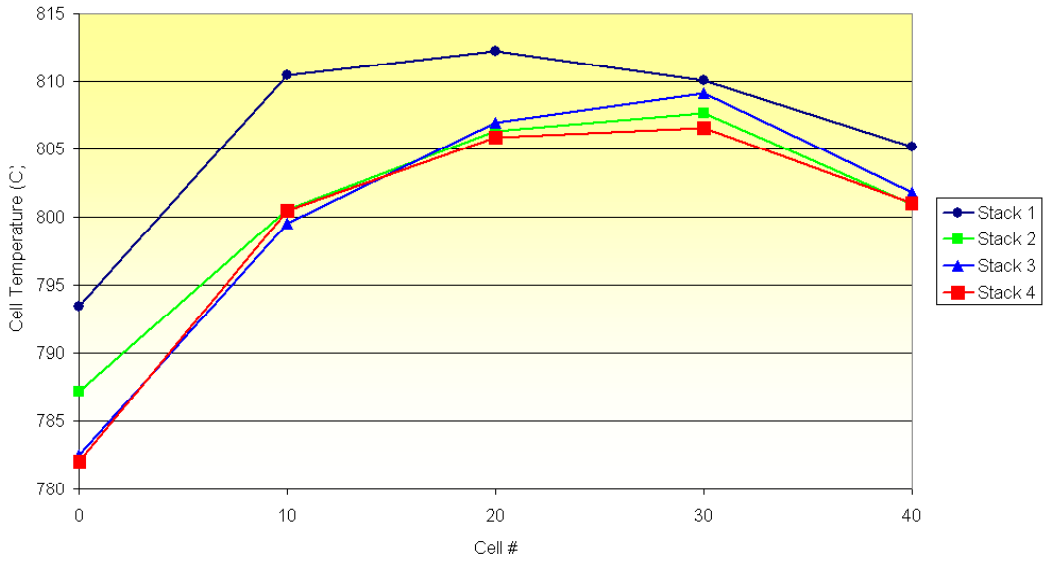

Figure 11.29 Stack Temperature Distributions for End of Test Peak Efficiency Point.

Table 11.8 Average Stack Temperatures for End of Test Peak Efficiency Point

Stack 1	806°C
Stack 2	801°C
Stack 3	800°C
Stack 4	799°C
Stack Assembly	801°C

The measurement uncertainty was analyzed and propagated using Crystal Ball. This analysis was performed using the specified measurement uncertainties as well as the pre-test and post-test calibrations. The worst peak efficiency resulted from the post-test calibration numbers, but even in this case there is a 95% confidence that the system efficiency is between 36.2% and 38%.

During the peak efficiency run, the fuel cells output power was being dissipated with an electronic load rather than the inverter due to concerns over the stability of the test stand power infrastructure. Subsequent tests verified stable operation of the inverter in the prototype system with performance matching stand-alone tests of the inverter. Based on stand-alone testing of the inverter, the projected AC performance of the system at the peak efficiency point would have been:

- AC Efficiency of 34.5%
- Net AC power of 2.59 kW

11.2.6 End of Test Peak Power

The end of test peak power was measured over a one-hour steady state period on September 29, 2005. After some exploration in changing various setpoints in the system, the peak power settings were determined and the system was held for the required one hour at this steady state condition. The system achieved a net DC power of 3.72 kW under the following conditions:

- Fuel utilization of 67%
- Air utilization of 22%
- Steam-to-carbon ratio of approximately 1.1 (measured at 1.2)
- Oxygen-to-carbon ratio of 0.56
- Current of 50.1 A (353 mA/cm^2)
- Average cell voltage of 0.523 V
- Gross DC power of 4.19 kW (185 mW/cm^2)
- DC efficiency of 25.6%

The overall system was stable for the entire one-hour period with no abnormalities with the test facility. The individual cell voltages were stable with a much wider distribution amongst cells than during the beginning of test peak power run. The cell voltages for all four SOFC stacks can be seen in Figure 11.30. The typical end effects can be seen on each stack due to temperature distributions within the individual stacks. A histogram of all of the cell voltages can be seen in Figure 11.31. The mean voltage is 0.553 V with a standard deviation of 0.142 V. The cell-to-cell variation at the peak power point is 69% greater than the variation seen at the peak efficiency point. When compared with the beginning of test peak power point, the variation has increased by 75% over the duration of the prototype system test.

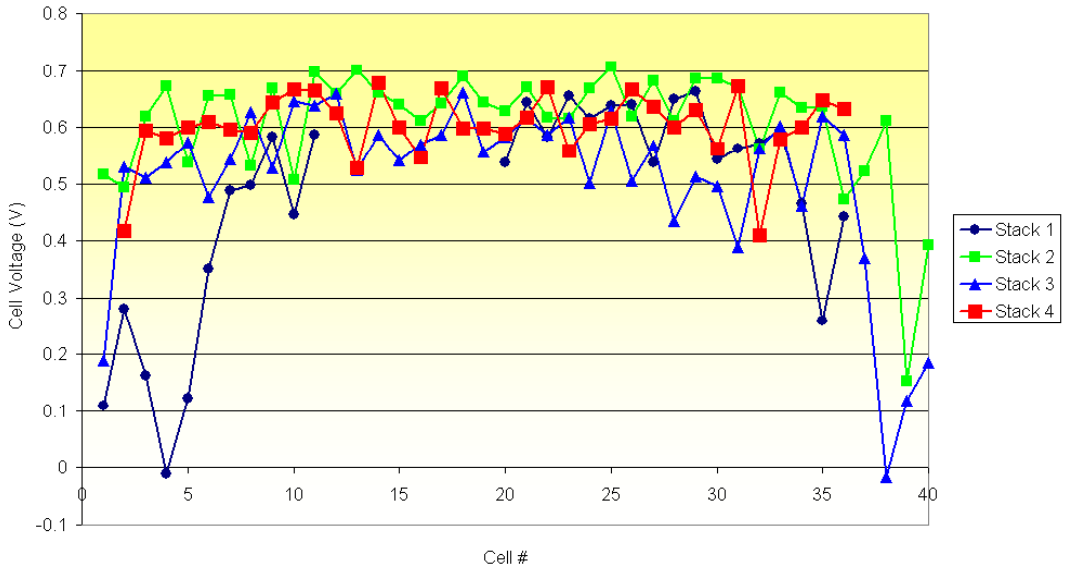

Figure 11.30. Cell Voltages for End of Test Peak Power Point.

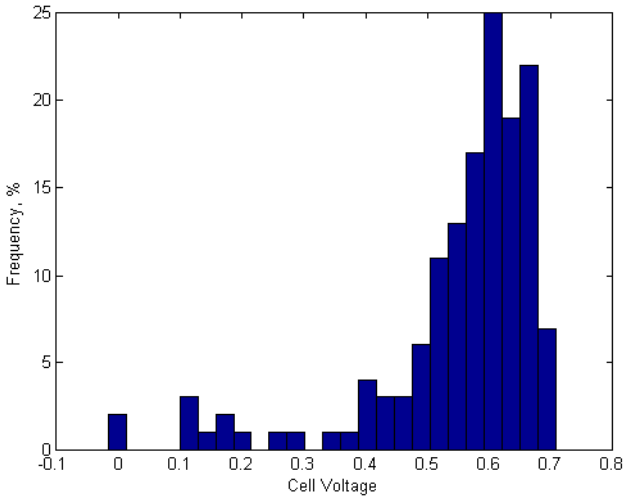

Figure 11.31 Histogram of all Cell Voltages for End of Test Peak Power Point.

The temperature distribution within each of the four stacks can be seen in Figure 11.32. The trends are very similar to those seen in the peak efficiency period except that the increased heat generation in the peak power case amplifies the temperature differences within stacks and raises the average stack temperatures. The average temperature for the individual stacks and the stack assembly can be seen in Table 11.9. The stack assembly was at an average temperature of 803°C with Stack 1 being at an average temperature of 811°C.

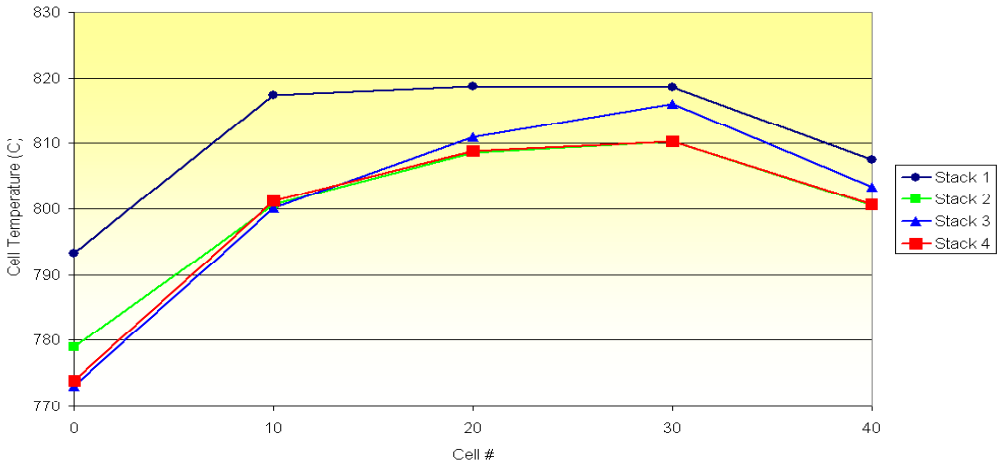

Figure 11.32 Stack Temperature Distributions for End of Test Peak Power Point.

Table 11.9 Average Stack Temperatures for End of Test Peak Power Point

Stack 1	811°C
Stack 2	800°C
Stack 3	801°C
Stack 4	799°C
Stack Assembly	803°C

The measurement uncertainty was analyzed and propagated using Crystal Ball. This analysis was performed using the specified measurement uncertainties as well as the pre-test and post-test calibrations. The worst peak power resulted from the post-test calibration numbers, but even in this case there is a 95% confidence that the system efficiency is between 3646 and 3789 Watts.

During the peak power run, the fuel cells output power was being dissipated with an electronic load rather than the inverter due to concerns over the stability of the test stand power infrastructure. Subsequent integrated tests verified stable operation of the inverter in the prototype system with performance matching stand-alone tests of the inverter. Based on stand-alone testing of the inverter, the projected AC performance of the system at the peak efficiency point would have been:

- Net AC power of 3.48 kW
- AC Efficiency of 24.0%

11.2.7 System Availability

The system availability can vary depending on how the various facility issues and startup times are included in the calculations as unavailable or are removed from the calculations completely.

The most rigorous interpretation of system availability is simply the number of hours the system was under load with reformed fuel divided by the total number of hours of the test. This results in the following:

- Hours under load with reformed fuel: 1358 hrs
- Total hours of test: 1693 hrs
    - Total hours: 1720 hrs
    - Shutdown: -27 hrs
- Availability: 80%

The slightly less rigorous interpretation of system availability is the number of hours the system was under load divided by the total number of hours of the test. This results in the following:

- Hours under load: 1401 hrs
- Total hours of test: 1693 hrs
    - Total hours: 1720 hrs
    - Shutdown: -27 hrs
- Availability: 83%

The first two methods penalize the system for facility issues which were outside of the control of the prototype system and beyond the scope of the program. The next interpretation of system availability is the number of hours the system was under load with reformed fuel divided by the total number of hours with facility issues and planned shutdowns removed. This results in the following:

- Hours under load with reformed fuel: 1358 hrs
- Total hours of test with facility or planned events: 1512
    - Total hours: 1720 hrs
    - 1^{st} facility outage: -74 hrs
    - 2^{nd} facility outage: -16 hrs
    - Transient Test Thermal Cycle: -91 hrs
    - Shutdown: -27 hrs
- Availability: 90%

This method is the most objective of the measures, since it only penalizes the system for the initial startup of the system, the system shutdown to repair the startup heater, and the system controller related interruptions.

The final method is the most aggressive of the calculations in that it does not penalize the system for startup time at either the initial warm-up of the system and after the startup heater was repaired. This results in the following:

- Hours under load with reformed fuel: 1358 hrs
- Total hours of test with facility or planned events: 1395
    - Total hours: 1720 hrs
    - Initial startup of system: -50 hrs
    - 1st facility outage: -74 hrs
    - 2nd facility outage: -16 hrs
    - Startup after heater repair: -67 hrs
    - Transient Test Thermal Cycle: -91 hrs
    - Shutdown: -27 hrs
- Availability: 97%

11.2.8 Pre-Test Comparison

While the prototype system test was successful, it should be noted that significant work is still needed in the area of stack and system reliability to move SOFC technology closer to commercial applications. Cell-to-cell variation in performance had a significant impact on the system test results since the system was limited by its poorest performing cells. This can be seen in Figure 11.33 that compares the average stack performance at peak efficiency and peak power to the pretest predictions. On average the stack performance compared well to pretest predictions. At the peak power point, some cells were significantly below the average voltage and therefore additional current could not be drawn without placing the poor performing cells at risk. If the average performance could have been exhibited on all of the individual cells, an additional 1 to 2 kilowatts of gross power could have been produced with the system. Therefore, reducing cell-to-cell variation should provide better performing stacks that will move the system performance closer to its entitlement.

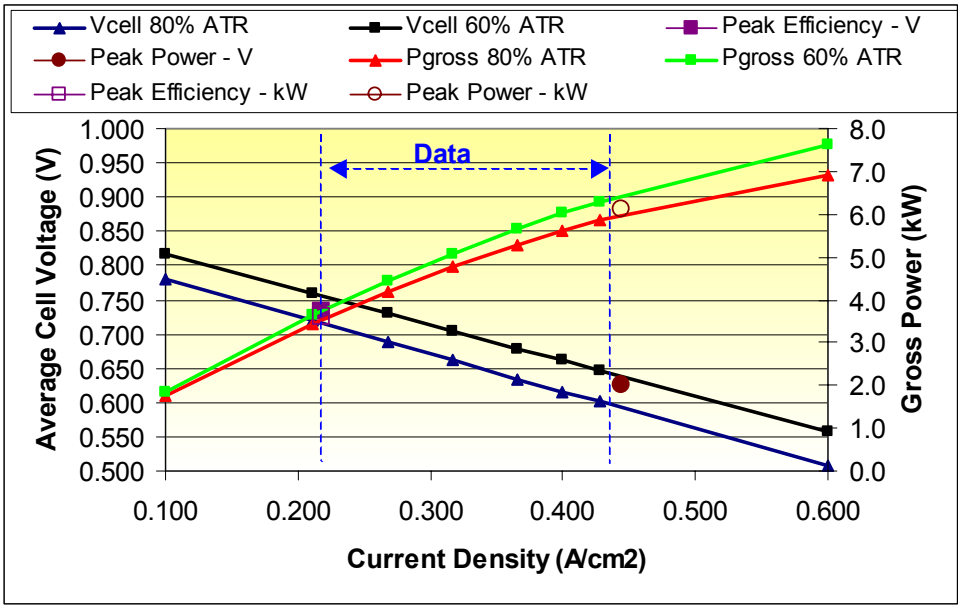

Figure 11.33 Comparison of average stack performance at peak power and peak efficiency with pre-test predictions.

12 NETL PROTOTYPE

12.1 SYSTEM DESIGN AND INTEGRATION

There were four stacks of 6" cells in the SECA Phase I Gen 2 system. With recent progress on cell fabrication scaleup and successful testing of 12" cells, the prototype built for delivery to NETL (referred to as NETL prototype) was designed and assembled with a single 12" cell stack..

Transitioning from four 6"-cell stacks to a single 12"-cell stack reduces the cost by $76/kW in stack material and labor and $84/kW in packaging cost. Moreover, stack testing indicated stack efficiency and peak power are significantly improved with a 12"-cell stack over the 6"-cell stacks used in Gen 2 system. As shown in Figure 12.1 for the same percent of auto thermal reforming and same current density, the average cell voltage of 12" cell increases by approximately 0.03V or 4% compared to 6" cell. Also the gross power of a single 12"-cell stack increases by approximately 0.5 kW compared to the four 6"-cell stacks. Improved performance ultimately drives down stack cost as well. Another advantage of a single stack is to reduce the current collection losses compared to four stacks. The combination of improved cost and performance drove the stack design in the NETL prototype to a single 12"-cell stack.

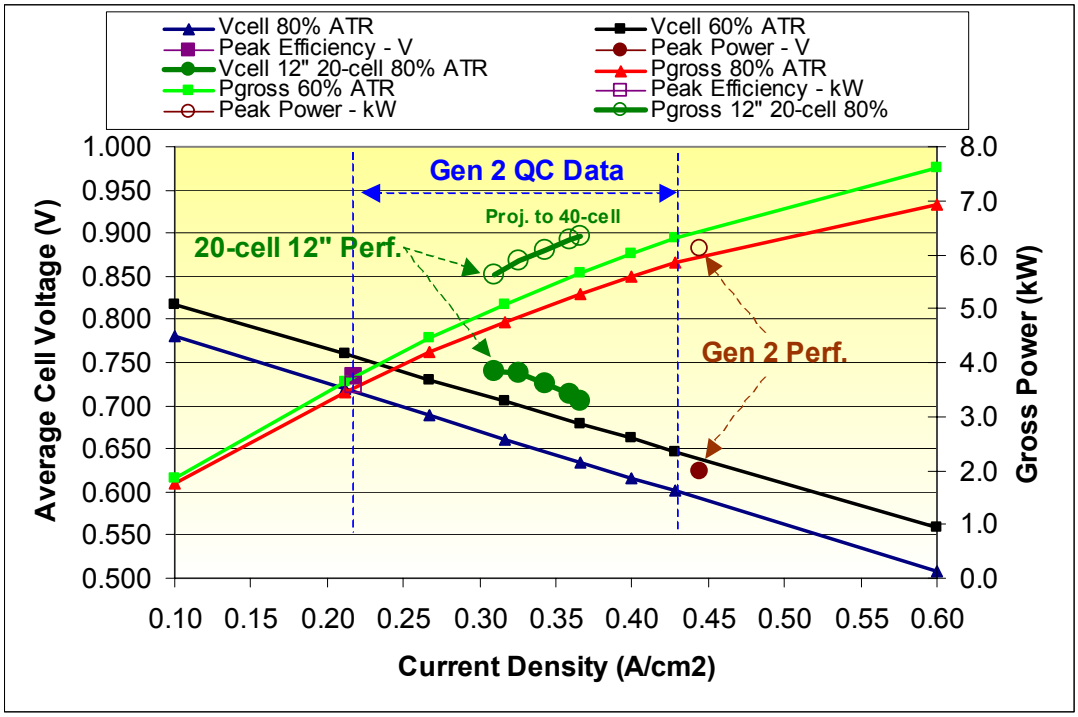

Figure 12.1 Performance Comparison between 6”-Cell Stack and 12”-Cell Stack.

The switch to a single 40-cell stack composed of 12” cells required the design of a new stack enclosure and stack interface. To take advantage of the new stack enclosure design, the balance of plant components were also repackaged. Table 12-1 provides the scorecard for the effort.

Significant effort went into redesigning the new stack enclosure and the new balance-of-plant configuration to meet the system volume reduction and provide a product like appearance. Ultimately the balance-of-plant was housed in the bottom half of the stack enclosure below the stack.

Table 12-1 SECA NETL Prototype Packaging Scorecard.

CTQ	UOM	LSL	Target	USL	Perf.*	Phase I	NETL*
System Volume vs. original	%	-	50	75	25	10 m^3	2.5 m^3
Program cost vs. original	%	-	75	90	-	$100k	-
Heat loss vs. original	%	-	33	75	32	1500 W	483 W
System weight vs. original	%	-	60	75	-	5000 lbs	-
Pressure drop vs. original	%	-	75	90	100†	0.073 psi	0.073 psi
Exterior at touch temperature	°C	-	60	60	-	60 **	60
Pressurized operation	ATM	4	5	-	-	1	9.6
Availability	%	80	90	-	-	80/90	-
MTBF	hrs	800	4500	-	-	420	-
Thermal Cycles	-	10	50	-	-	6	-

*Projections for current design
**Extra insulation applied during testing
†Uncertainty in pressure drop assumptions for Phase I startup heater

With the new BOP configuration design, especially allocating the fuel processor inside the stack enclosure, the NETL system performance is predicted to be significantly higher than the SECA Gen 2 system. As presented in Figure 12.2, the oxygen-to-carbon ratio for the FP is a major driver to improve the system efficiency. With the new packaging design, the fuel processor inside the enclosure could operate with a lower oxygen-to-carbon ratio as compared to that of the SECA Gen 2 system. This helps to improve the NETL system efficiency. Moreover, the new packaging design helps to reduce the total heat loss of the system which also improves the system efficiency.

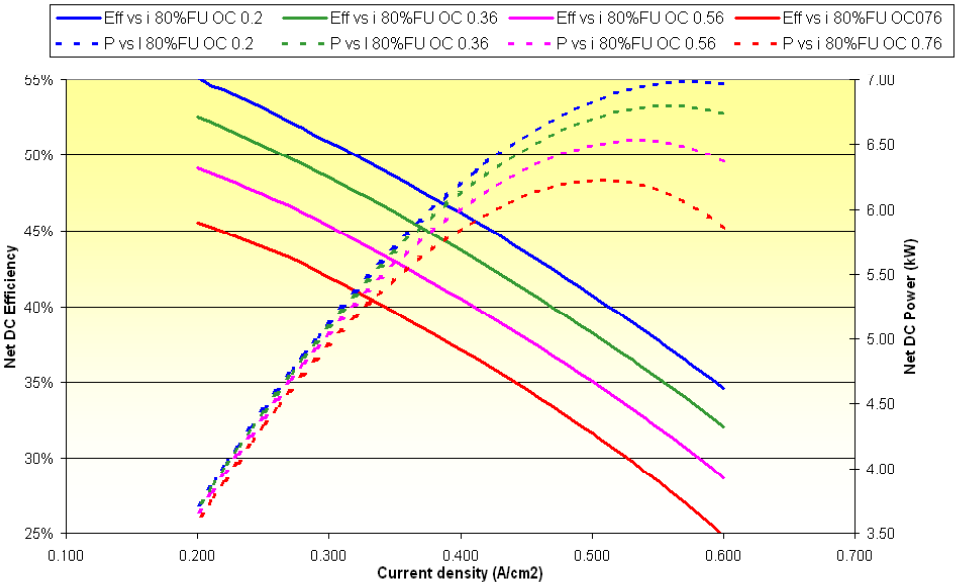

Figure 12.2 NETL Prototype Performance Prediction.

12.1.1 Stack Enclosure

The initial efforts focused on sizing the new stack enclosure. Using the dimensions of the stack, a heat transfer model was developed to determine insulation thickness and the affects of various insulation arrangements. As shown in Figure 12.3, a layer of insulation with a thermal conductivity on the order of 0.30 W/m-K provided good performance. The insulation down-selection process evaluated materials on price, performance, manufacturability and impacts to other system components. For example, a lower performing material might be cheaper, but when weighed against the increased size of the stack enclosure shell, increased heat loss and other factors, the micro-porous insulation proved the best choice. The insulation thickness and stack girth thus determined the stack enclosure shell inside diameter of 30 inches. For comparison, the original prototype was 48 inches in diameter.

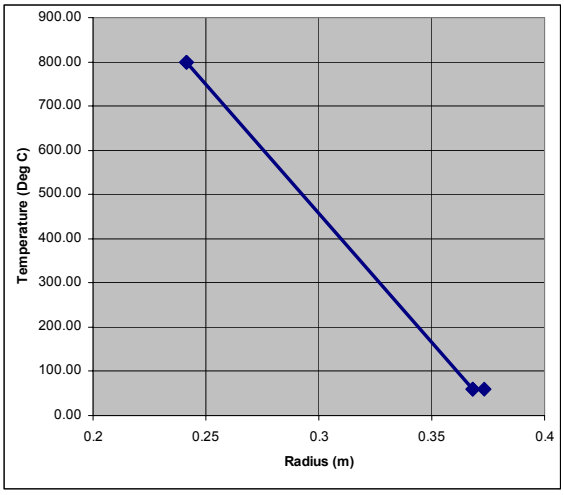

Figure 12.3 Temperature Distribution within Stack Enclosure Insulation.

Other design considerations were the selection of materials for the enclosure shell and the integrity of the shell under failure modes such as a fire or explosion. These were addressed and resolved satisfactorily for this enclosure shell design.

12.1.1 Thermal Management Subsystem

The first prototype design placed the majority of the thermal management subsystem external to the stack enclosure as shown in Figure 12.4. Although this configuration met the functional requirements for the design, it led to a significant amount of exposed hot surface area that proved challenging to insulate. The design also required three hot gas interfaces between the stack enclosure and thermal management subsystem that were prone to leaks.

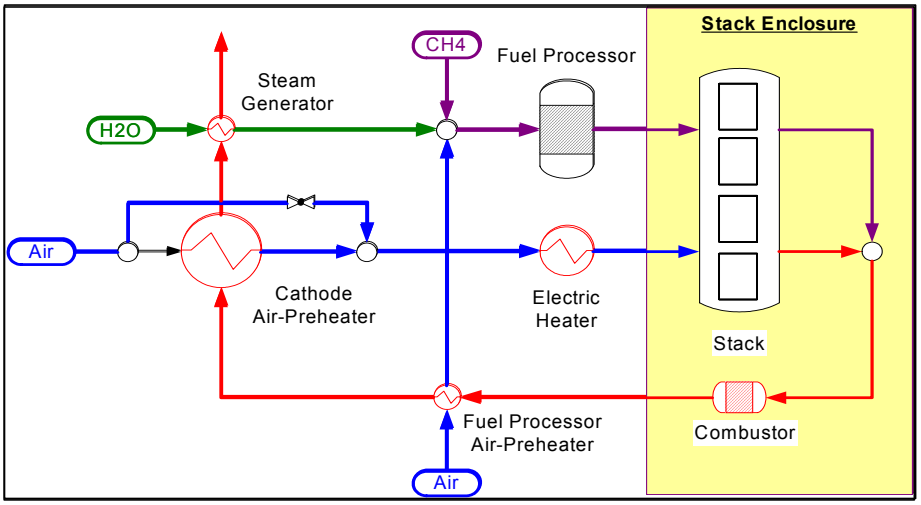

Figure 12.4 SECA Gen 2 Enclosure Boundary

The need to redesign for the single stack presented an opportunity to utilize the same basic thermal management components repositioned inside the stack enclosure as shown in Figure 12.5. This reduced thermal loses, allowed the gas connections to be reconfigured to design around hot gas interfaces.

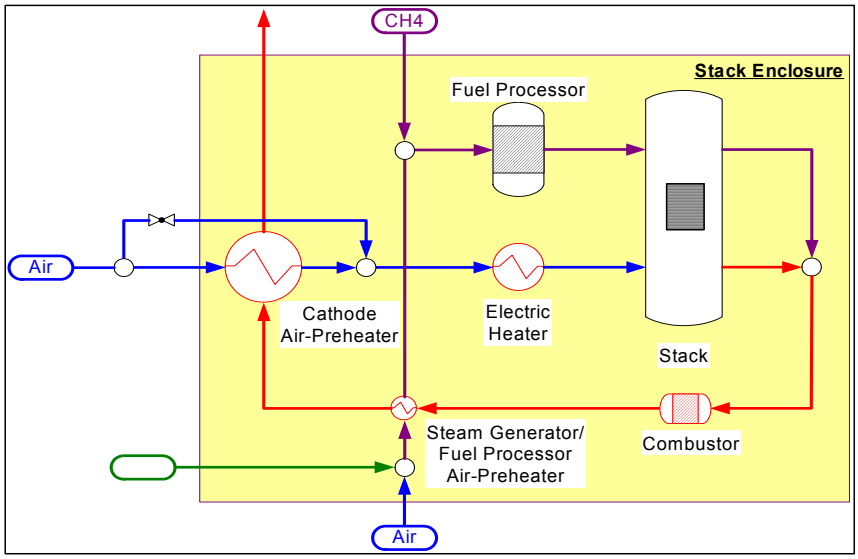

Figure 12.5 SECA NETL Prototype Enclosure Boundary

12.1.2 Stack Interfaces

An additional challenge was the need to connect to the existing twelve-inch cell stack design with a minimum of modifications to the stack while maintaining system pressure drop levels similar to the original prototype.

Various configurations of inlets were then evaluated for flow distribution, pressure drop and mechanical impact on the design of connection hardware and loading on the manifold seals. As shown in Figure12.6, a cathode air inlet configuration was selected and determined to be suitable for the system.

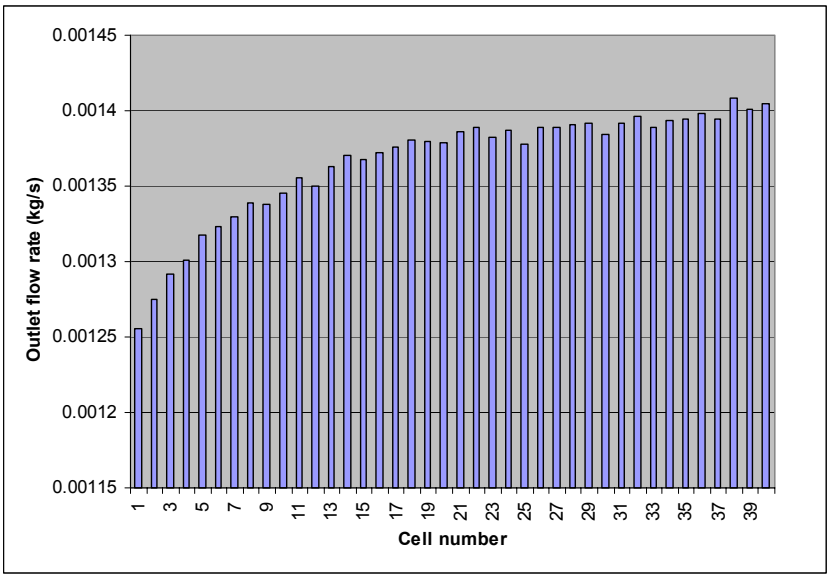

Figure 12.6 Cathode Air Inlet Flow Distribution

It was also necessary to design a framework to support the stack and thermal management subsystem. Computational analysis was used to assure the frame design would withstand rigors of its intended use as depicted in Figure 12.7.

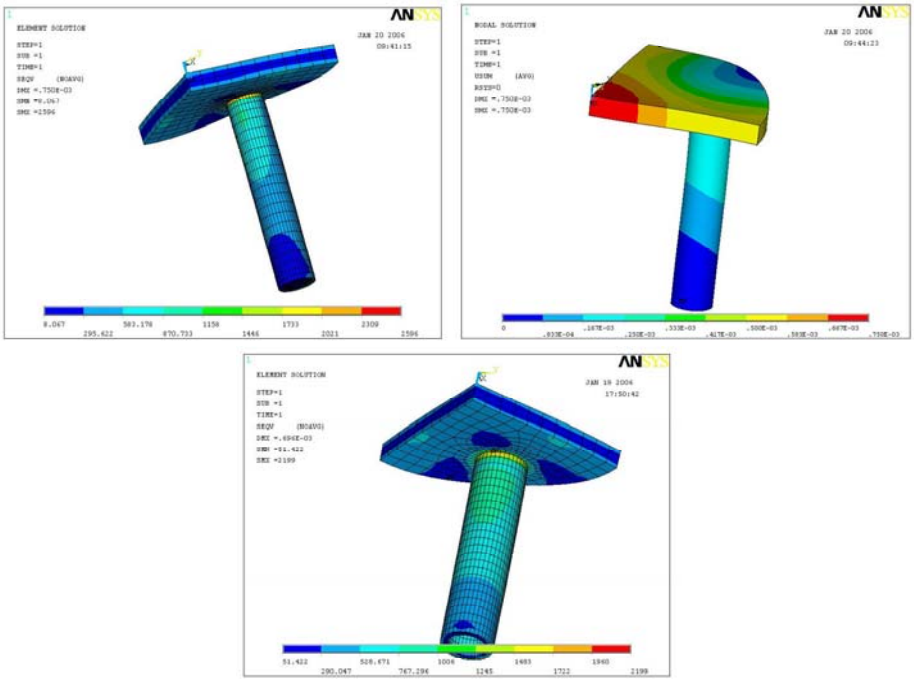

Figure 12.7 Stack Support Frame, Plate and Column Load Analysis

12.1.3 Balance-of-Plant Packaging

The original prototype, the SECA Gen 2 system, was designed with flexibility and accessibility in mind, which led to a package that did not necessarily make the most efficient use of the footprint of the unit. With a smaller stack enclosure and internalized hot gas components, it was possible to significantly reduce the overall volume of the prototype. Specifically, the original unit had a volume of 10 m^3 whereas the new powerplant was expected to fit within about 2.6 m^3. The smaller size and enclosed boundary proved critical when packaging the system for shipping.

Figure 11.18 shows the more product-like aesthetics of the NETL prototype with the outer enclosure. The outer enclosure provided protection to the equipment and instrumentation. Additionally, the outer enclosure enabled restricted access to electrical and thermal hazard areas. The roof had a slanted inner surface that channeled any gases to an exhaust fan and prevented any accumulation. Figure 12.9 shows the prototype ready for delivery to NETL. The delivery packaging included a false base for shock isolation, a vacuum-sealed foil bag with moisture protection and an outer wood crate with shock and tilt instrumentation.

Figure 12.8 SECA NETL Prototype System

Figure 12.9 SECA NETL Prototype System Delivery Packaging

12.2 PROTOTYPE TEST

The prototype system that was tested can be seen in Figure 11.1. Applying the similar approach as integrating the SECA Gen 2 system, there was an extensive system build and integration process leading to the final commissioning testing of the unit which was comprised of the following major steps:

- Component Testing
    - Verified basic operation of components in stand-alone testing
    - Developed component performance maps
    - Supported component selection process if it is a new component
    - Calibrated several key components
- Cold Tests
    - Operated the system with only nitrogen/air and without fuel cell stacks
    - Validated basic operation of components integrated in system
    - Verified plumbing and electrical wiring
- Hot Tests
    - Operated the system on methane and hydrogen without fuel cell stacks
    - Simulated start-up and shut down process
    - Verified and tuned control system hardware and software
    - Verified combustor operation and temperature controls
    - Integrated operation of fuel processor
    - Conducted thermal mapping of system and improved insulation
- Gen 1 System Test
    - Operated integrated system with a 20-cell stack
    - Verified integrated operation of stacks with fuel processor
    - Tuned automatic control loops and verified startup and shutdown strategies
    - Operated the system for over 72 hours on ATR fuel with a total test time of over 200 hours.
    - Operated the system in the thermally self-sustaining mode during operation at high current densities.
    - Assessed the heat loss on the system and conducted a thermal survey.
    - Evaluated the pressure drop through the system with the stacks included.
- Gen 2 System Test
    - Operated the integrated system with a 40-cell stack.

The following discussion focused on the results of the Gen 2 System Test which was the commissioning test for NETL prototype. A brief description of the

prototype test plan will first be given. The calibration of the measurement system is presented next. A detailed analysis of the test results will then be provided. The results of the test can be seen in a summary form in the NETL prototype system scorecard shown in Table 11.1.

Table 12-2 NETL Prototype System Scorecard

	CTQ	UOM	LSL	Target	USL	Perf.	Basis
System	Peak Efficiency	%	40	45	-	49.6	NETL Prototype commissioning test at HPGS
	Projected Cost	$/kW	-	400	600	544	Phase I Cost Report, single stack scaled to 5.6 kW net
	Rated Net Power	kW	3	10	-	5.6	NETL Prototype commissioning test at HPGS
	Availability (1500 hrs)	%	85	95	-	80 90	Gen 2 Prototype System Test, ATR operation only Gen 2 Prototype System Test, ATR/1500 hrs
	Volume	m3	-	3	5	2.5	NETL Prototype measurement
	MTBF	hrs	800	4500	-	420	Phase I Prototype System Test
Stack	Fuel Utilization	%	60	80	-	80	20-cell 12" (S1106) projected to 40-cells
	Power Density (ATR, 0.7V, 80% U_f)	W/cm^2	0.200	0.300	-	0.265	20-cell 12" (S1106) @80% FU
	Number of Cells (12")		35	40	-	40	NETL Prototype commissioning test at HPGS
	Projected Cost	$/kW	-	200	-	244	Phase I Cost Report, single stack scaled to 5.6 kW net
	Steady-state Deg.	%/500 hrs	-	1	2	1.8 1.2	Pre-Transient, Gen 2 Prototype System Test Post-Transient. Gen 2 Prototype System Test
	Cycling Deg.	%/10 cycles	-	0.5	1	1.8	Gen 2 Prototype System Test

12.1.1 Test Plan

The purpose of the commissioning test was to verify the NETL prototype system operation and to get an initial system performance map. The test was a typical thermal cycle of the system including startup, performance testing, and shutdown. Each segment of the test is described in greater detail in the subsections that following the timeline of the test.

- Pre-Startup
  - Confirm reactant supply valves to system are closed
  - Turn on system controller and DAQ
  - Turn on power supplies
  - Begin recording data on DAQ
  - Begin recording data on system controller
  - Confirm that all thermocouples and pressure transducers are working correctly
  - Confirm proper flow transmitter zeroing
  - Cycle all solenoids, control valves
  - Open reactant supply valves
  - Clear test area

- Startup
  - Flow shop air through cathode side of the system
  - Flow purge gas through anode side of the system
  - Turn on the startup heater
  - Ensure stack temperature ramp rate and temperature difference are within the limit
  - Wait for the temperature safety indicator passing the threshold
  - Gradually increase the hydrogen flow and cut the purge gas flow
  - Use thermocouples and laser thermometer to check for heat leaks on canister and BOP components
  - Observe the stack OCV condition
  - Start to draw current from the stack under hydrogen and observe stack cell voltage response
  - Gradually increase current and increase hydrogen and shop air flow correspondingly
  - Transition from shop air to the main air blower
  - Check stack performance and fuel processor temperature and be ready to transition to ATR fuel
- Normal Operation
  - Gradually increase ATR gas reactants and reduce hydrogen and nitrogen flow to zero
  - Turn on automatic temperature control
  - Turn on load control and reactant gas flow control
  - Explore necessary operating parameters and find the peak system efficiency operating point
  - Explore necessary operating parameters and fine the peak power operating point
- Shutdown
  - Decrease the load and reactant gas flow to zero
  - Switch to shop air on cathode side of the system
  - Switch from ATR fuel to hydrogen on anode side of the system
  - Confirm stack temperature ramp rate and temperature difference are within the limit
  - Switch from hydrogen to purge gas on anode side of the system when temperature safety indicator is below the threshold

- Close purge gas and shop air when the stack enclosure temperature is below certain limit
- Close reactant supply valves
- Turnoff power supplies, controller and DAQ.

12.2.1 TEST RESULTS

The results of the 120-hour commissioning test are discussed in the following sections. The peak efficiency and peak power performance of the NETL prototype system exceeded the SECA Gen 2 system, and were well above the SECA minimum requirements. The performance demonstration portion of the test is presented in Figure 12.10.

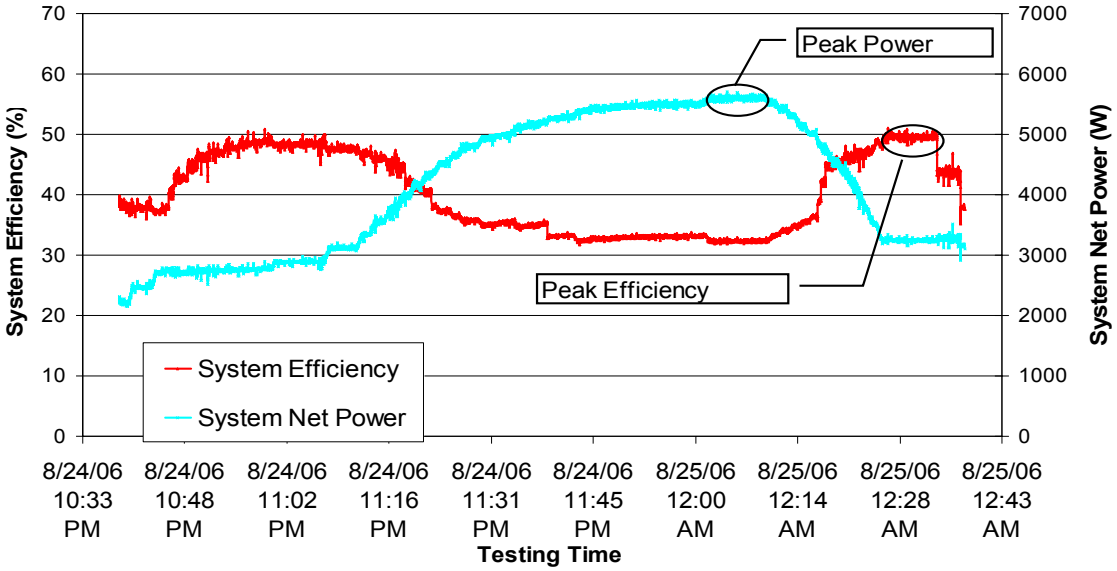

Figure 12.10 NETL Prototype Test Data

12.1.1.1 Peak Efficiency

The peak efficiency was measured over a steady state period on August 25, 2006. After some exploration in changing various setpoints, especially oxygen-to-carbon ratio in the system, the peak efficiency settings were determined. Since this test was a commissioning test, some system operating parameters were not fully explored in order to protect the stack and the system. The system achieved a DC efficiency of 49.6% under the following conditions:

- Fuel utilization of 79.5%
- Steam-to-carbon ratio of 1.5

- Oxygen-to-carbon ratio of 0.4
- Current of 112.6 A (184 mA/cm^2)
- Average cell voltage of 0.783 V
- Gross DC power of 3.52 kW (144 mW/cm^2)
- Net DC power of 3.27 kW

The overall system was stable for the peak efficiency period with no abnormalities with the system or the test facility. The individual cell voltages were stable with no sign of fuel distribution issues or cell starvation. The cell voltages for the SOFC stack can be seen in Figure 11.411. The cell voltage distribution is smooth across the stack. A histogram of all of the cell voltages can be seen in Figure 11.512. The mean voltage was 0.783 V with a standard deviation of 0.0194 V. All of the cells remained above 0.7 V at this test condition.

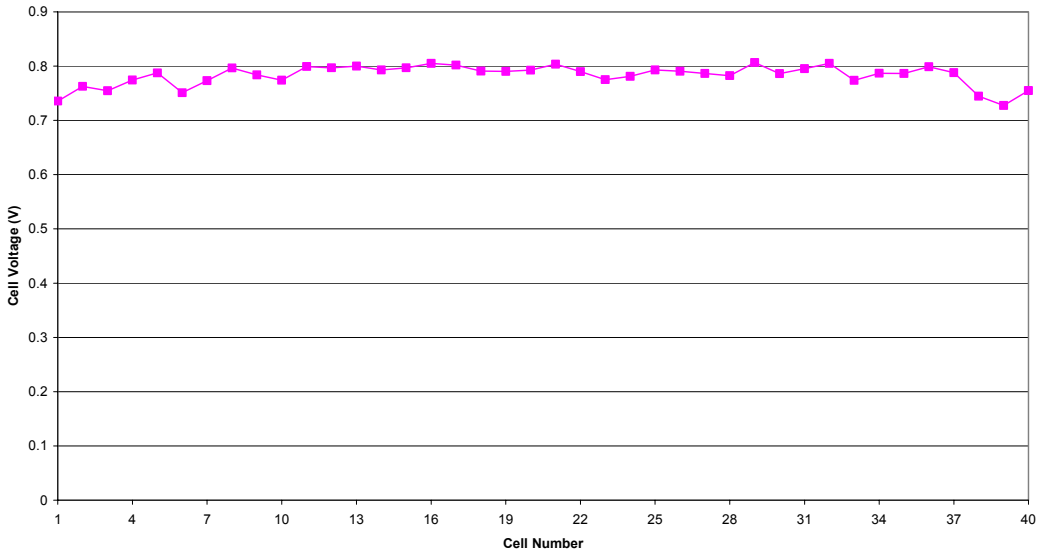

Figure 12.11 Cell Voltages at Peak Efficiency Point.

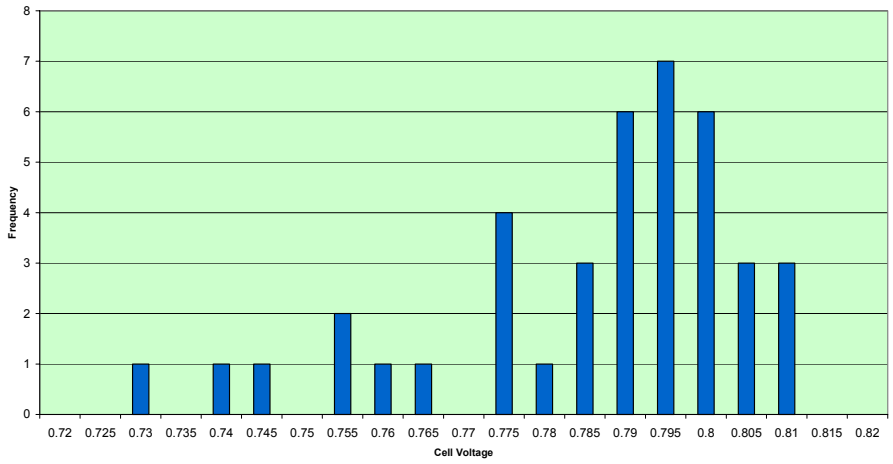

Figure 12.12 Histogram of all Cell Voltages at Peak Efficiency Point.

The temperature distribution within each of the four stacks can be seen in Figure 12.13. The thermocouple for cell 4 was not functional during the test. The trends showed higher temperatures in the center cells of the stack and that the top of the stack was at a higher temperature than the bottom of the stack. The stack assembly was at an average temperature of 808°C.

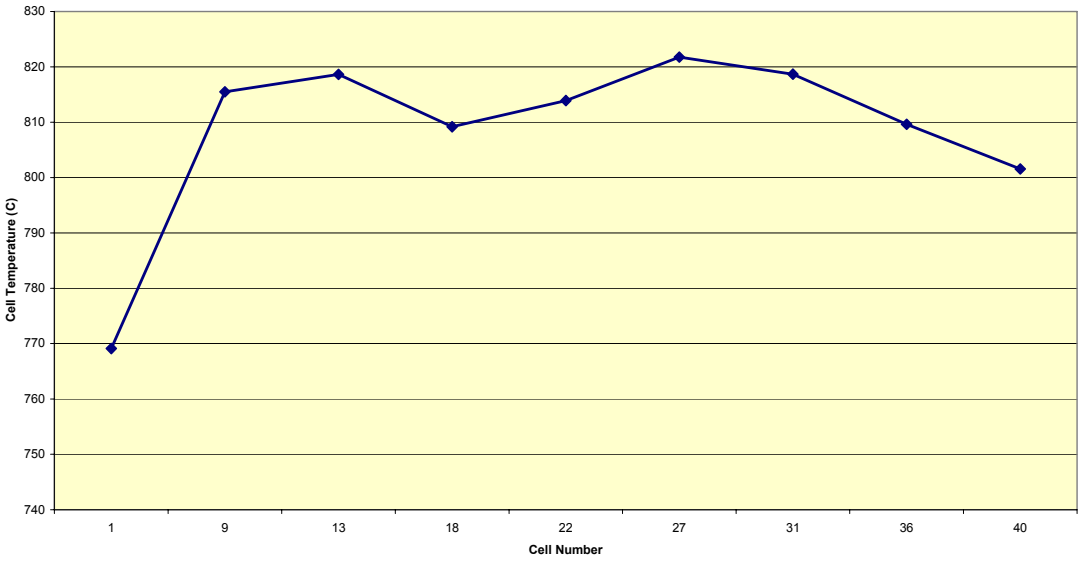

Figure 12.13 Stack Temperature Distributions at Peak Efficiency Point.

12.2.1.1 Peak Power

The peak power was measured over a steady state period on August 25, 2006. After some exploration in changing various setpoints in the system, the peak power settings were determined. Since this was a commissioning test, some system operating parameters were not fully explored in order to protect the stack and the system. The system achieved a net DC power of 5.62 kW under the following conditions:

- Fuel utilization of 63.7%
- Steam-to-carbon ratio of 1.5
- Oxygen-to-carbon ratio of 0.4
- Current of 242.2 A (395 mA/cm^2)
- Average cell voltage of 0.639 V
- Gross DC power of 6.11 kW (249 mW/cm^2)
- DC efficiency of 32.4%

The overall system was stable for the peak power period with no abnormalities with the test facility. The individual cell voltages were stable with no sign of fuel distribution issues or cell starvation. The cell voltages for the SOFC stacks can be seen in Figure 11.814. The typical end effects can be seen on the stack due to temperature distributions within the stack. A histogram of all of the cell voltages can be seen in Figure 11.915. The mean voltage was 0.639 V with a standard deviation of 0.0446 V. The majority of the cells remained above 0.6 V, and only a small percentage of cells were between 0.5 V and 0.6 V.

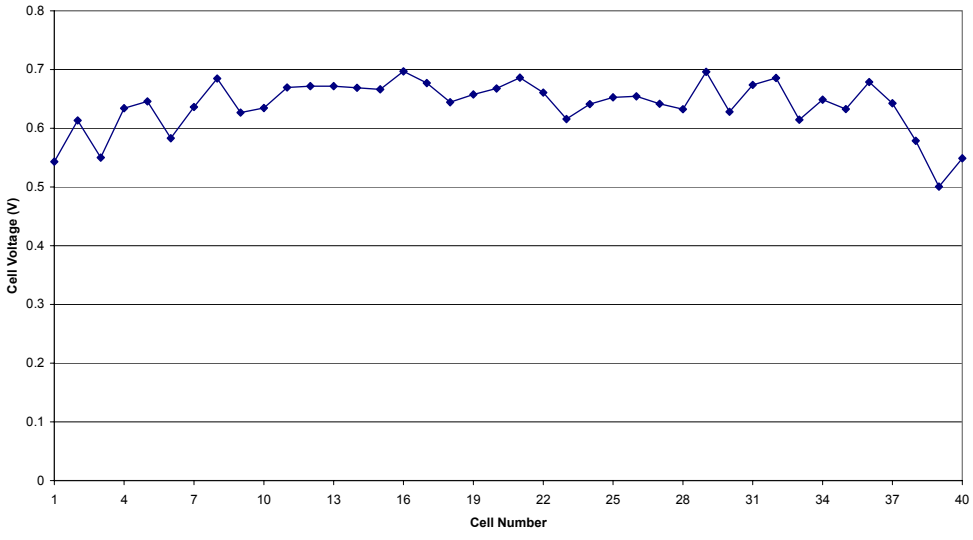

Figure 12.14. Cell Voltages at Peak Power Point.

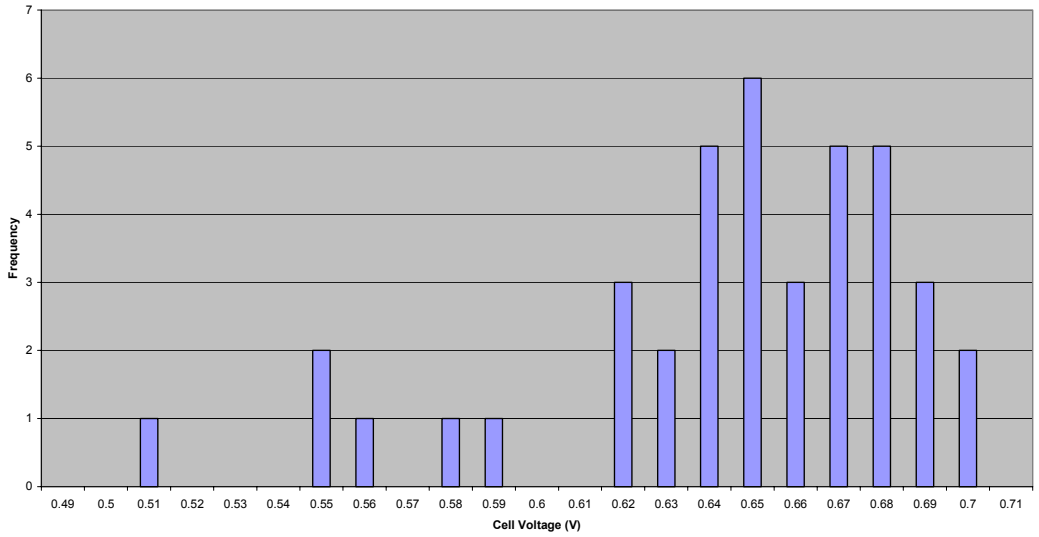

Figure 12.15 Histogram of all Cell Voltages at Peak Power Point.

The temperature distribution within the stack can be seen in Figure 11.1016. The stack assembly was at an average temperature of 815°C.

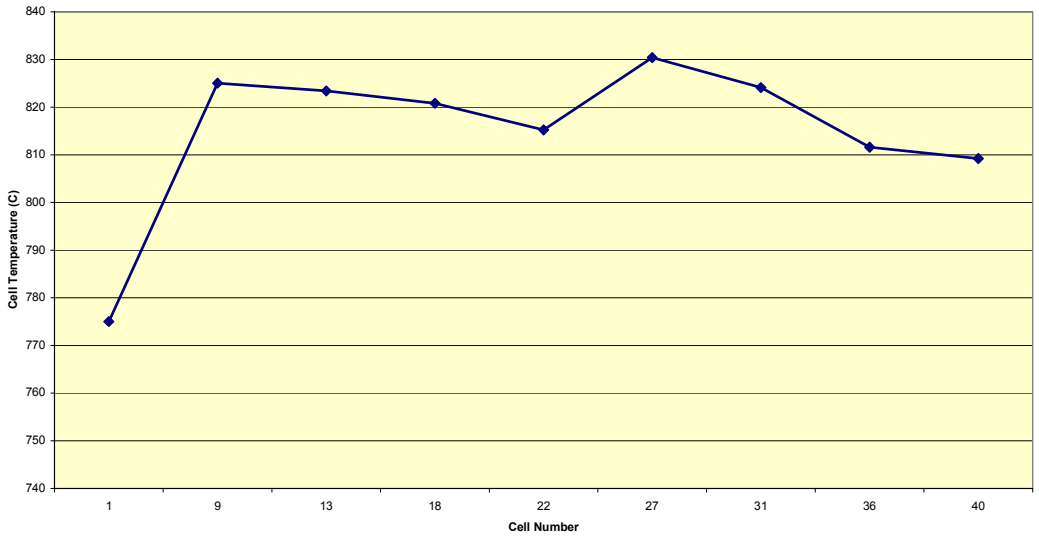

Figure 12.16 Stack Temperature Distributions at Peak Power Point.

13 CONCLUSIONS

In conclusion, Phase I of the SECA program was extremely successful. Major advances in SOFC technology were made in the areas of performance, stack design, manufacturing, and power output. Supporting technology such as fuel processing, controls, power electronics, and thermal management were also matured to meet the unique needs of an SOFC system. Phase I culminated in the system test that tied all of these advances in technology together in a prototype system that was able to exceed all of the SECA minimum requirements except for the transient cycle degradation. The system achieved a peak efficiency of 41% which exceeds even the Phase III requirement for the SECA program. A projected high-volume cost for the system is $724/kW. A summary of the results versus the SECA Phase I minimum requirements is given in Table 13.1.

Table 13.1 Summary of Prototype Results Versus SECA Phase I Minimum Requirements

PERFORMANCE PARAMETER	REQUIREMENTS	RESULTS
DC Efficiency	35%	41%
Estimated Cost	<$800/kW	$724/kW
DC Peak Power	3-10 kW	5.4 kW
Steady State Degradation	<2% per 500 hrs	1.8% per 500 hrs
Thermal cycle	1	3
Power Cycle	9	15
Cycle Degradation	<1%	1.8%
Availability	80%	90%
Test Time	1500 hrs	1720 hrs

With progress on cell fabrication scaleup and successful demonstration of operation of large-area cells, a more product like prototype incorporating a 12” cell stack was designed, built, and delivered to NETL at the end of the program This so-called NETL prototype achieved an extraordinary peak efficiency of 49.6% with a net DC power output of 3.27 kW.